CURVATURE ANALYSIS OF AEROMAGNETIC DATA

CURVATURE ANALYSIS OF AEROMAGNETIC DATA FOR GEOLOGICAL INTERPRETATION AND QUALITY CONTROL

By MADELINE DANA LEE, B.Sc., M.Sc.

A Thesis Submitted to the School of Graduate Studies in Partial Fulfillment of the Requirements for

the Degree Doctorate of Philosophy

McMaster University DOCTORATE OF PHILOSOPHY (2012) Hamilton, Ontario

TITLE: Curvature Analysis of Aeromagnetic Data: Application of Statistics and Lineament Extraction
AUTHOR: Madeline Dana Lee, B.Sc. (McMaster University), M.Sc. (McMaster University)
SUPERVISOR: Dr. William A. Morris
NUMBER OF PAGES: xii, 187

Abstract

Fundamentally the amplitude, sign, and frequency of a magnetic signal are inherently linked to curvature. This thesis employs curvature analysis as a semi-automated tool for source signal extraction from a magnetic field surface represented by a grid. The first step is to compute the full, profile, and plan curvatures from the magnetic grid. These values are used in two approaches to curvature analysis: statistical and lineament. The descriptive statistics mean, standard deviation, kurtosis, and skew are computed for quantitative analysis. Mean is used in conjunction with kurtosis and skew to assess frequency content of the signal, magnetization and source dip. Standard deviation characterizes low, moderate, and extreme curvatures. A rapid technique to statistical analysis is applied using a graphical approach with histograms and scatterplots. Histograms display frequency distribution and scatterplots display the relationship between different curvatures. Curvature in the maximum dip direction is used to systematically identify surficial lineaments characterized as continuous troughs or ridges. These lineaments may represent geological sources or remanent acquisition artefacts. Lineaments representing faults and dykes are used in conjunction with *a priori* knowledge to determine mineralization vectors since many ore deposits are structurally controlled. Quality control of the aeromagnetic grid levelling application may be assessed using spatial correlation of flight lines and magnetic lineaments. In this work curvature analysis is applied to simple synthetic models and two Canadian aeromagnetic data sets. Curvature analysis was applied to magnetic data from the Wopmay Orogen to identify bedrock contacts, fault configurations, and dyke swarms. The data was also used to show lineaments displayed as rose diagrams may be used as an alternative to standard Fourier power spectrums for assessment of levelling. Magnetic survey data from Southern Ontario was used to show a statistical approach to identify regional dip, dominant magnetization, and interference in anomalies.

Acknowledgements

Thank you to all my family, friends, and colleagues for the support throughout the years.

Sarah, for delivering homemade meals so I wouldn't forget to eat. April and Trish, for girl's nights at le Nordik. Janina, for sanity tea breaks. Kenny, for always living life for the moment. Vicki, for SlicVic and MadDog's 'Cheeseburger in a Bag'. 111 Gary Girls, for days of doing absolutely 'nothing'; all 15 volumes. Renée, for being my best friend of 25 years and proof-reading my thesis. Wendy, for being the coolest older sister I could have ever asked for.

Val and Louise's field camps, for the invaluable field experience. You taught this geophysicist a few things about geology.

Sue Webb, Dayspring School participants and Geoscientists *Without* Borders®, for selflessly showing the importance of non-exploration geophysics and giving me the opportunity to see how special Africa is.

Jeff, for your positive attitude throughout this process. You also play a mean set of drums. And George, my other drummer. The 2 years at FRL will never be forgotten. Returning to Ottawa was one of the best decisions for me and my thesis.

Fellow graduate students, for understanding that a thesis is more than just 'words'; it is a manifestation of blood, sweat, and tears. We chose to put many aspects of life on hold to dedicate years to research. This meant sleepless nights, filling plates full of free conference food, and shopping in our parent's cupboards.

Bill Dog. Bill-I-Am. I remember when Dickie first said, "Maddy you should talk to Bill Morris". Little did I realize how my life would be impacted by this meeting. You guided me through my B.Sc., M.Sc., and finally my Ph.D. It has been a pleasure to have you as a supervisor. I have learned so much about geophysics – from the fundamentals to the business. I hope you know the positive influence you have had on so many students.

Pedro. I proved your impression of geophysicists wrong that first day in the field when we were dropped 11 kilometres from the traverse. You have been my rock. Your endless patience and quiet demeanour have kept me grounded. You always reminded me that I was good enough to be here.

My parents. I could not have done it without your continuous support and encouraging words. You have always been there, at any time of day. I am who I am because of the two of you.

Table of Contents

List of Figures

List of Tables

1.0 Introduction

1.1 Fundamentals of potential field interpretation

Potential field theory involves the study of magnetics and gravity, which are the oldest of the geophysical methods. The geometry of a potential field surface will be a function of the causative source's shape, size, depth, and physical property contrast (e.g. magnetic susceptibility for magnetics and density for gravity).This thesis focuses strictly on magnetic field theory for locating subsurface magnetic sources.

The identification of a magnetic source begins with the acquisition of magnetic field measurements across a defined survey area. The acquisition is carried out either on the ground with a hand-held magnetometer or from the air with a magnetometer being carried by either a fixed- or rotor-winged aircraft. Individual measurements may be collected in a spatially random fashion or collected along a pre-determined path at systematic intervals. These measurements may then be interpreted as individual 2D profiles or they may be used to generate a 3D interpolated surface.

From the computed 3D potential field surface (i.e. grid) it is possible to derive pseudo-gradient data over a 2D profile. A number of authors have published semi-automated interpretation routines such as Euler Deconvolution and Sluth (Reid et al, 1990; Blakely and Simpson, 1986; Smith et al., 2012). All of these methods depend on gradients of the magnetic field computed from a grid rather than a profile. The topology of this grid surface will reflect variations in the magnetic field defined by causative magnetic sources. Therefore construction and interpretation of this grid plays a critical role in the final outcome. It has been common practice to use Fourier transform procedures in the analysis of the grid surface. Fourier analysis is able to deconstruct data on the basis of signal wavelength. This means the method treats each point within a grid as a summation of signals with varying wavelengths (1/frequency). Fourier analysis operates under the assumption that any signal may be constructed through the summation of harmonic sine waves with distinct wavelengths and amplitudes. An alternative to the Fourier method is to examine the curvature of the signal at individual points within a grid. Curvature is a characteristic that indirectly describes local frequency content of a magnetic signal. Since the grid is 3D there are numerous directions along which curvature may be calculated. Each directional measurement results in a different curvature attribute. Possible curvature attributes include but are not limited to: Gaussian; mean; maximum and minimum; profile; and planform. The application of curvature has been previously addressed in a variety of geoscientific fields prior to completion of this thesis: Topography (Evans, 1972; Zevenbergen and Thorne, 1987); Seismic (Roberts, 2000; Chopra and Marfurt,

2007); Potential Fields (Cooper and Cowan, 2006; Phillips et al., 2007; Cooper and Cowan, 2008; Cooper, 2009; Cooper, 2010).

1.2 Issues in the domain of magnetic field interpretation

Magnetic field interpretation suffers from a fundamental limitation in potential field analysis – the principle of non-uniqueness. This means an endless number of subsurface source configurations may generate the magnetic anomaly being analyzed. These configurations include changing the source-sensor separation, source geometry, and the source's magnetic susceptibility. Further adding to the issue is that interpretation becomes complicated when the geological environment is not ideal. A non-ideal situation could mean an inclined ambient magnetic field, a dipping source, or interference of anomalies. Ideally *a priori* geologic information curtails some of these issues however sufficient in-situ observations are often not available and indirect methods are necessitated. No current geophysical interpretation method entirely solves for these complicated conditions but many methods aim to mitigate their effects. Reduction-to-pole (Baranov, 1957) is the optimal method for sources in an inclined magnetic field (i.e. mid-latitudes). Reduction-to-pole shifts the maximum amplitude back over the source by simulating the geometry of the anomaly in a vertical ambient field at the pole. This method preserves physical property information such as dip. Alternative methods used at low-latitudes are either reduction-to-equator (Aina, 1986; Roy and Aina, 1986) or analytic signal (Nabighian, 1972; Rajagopalan, 2003). Many geophysical interpretation methods incorporate the fundamental expression of a dipping magnetic source (Bhattacharyya, 1964) to address the asymmetry of the associated anomaly (Reid et al., 1990). Regional-residual separation attempts to address the interference of anomalies through frequency thresholding operations. The method separates near-surface sources from deep-seated or extensive sources by subtracting low frequency content from the original signal (Spector and Grant, 1970; Gupta and Ramani, 1980). Regional-residual separation is a necessary component in any magnetic interpretation when the International Geomagnetic Reference Field is to be removed (Reford, 1980).

A fundamental discussion in geophysical interpretation is the definition of 'signal' and 'noise'. Signal is the portion of the signal the interpreter is interested in and noise is the remainder. This thesis defines signal as any anomaly generated by a magnetic source below surface in an induced field (Leblanc and Morris, 2001) and noise as all other anomalies. Signal needs to be further refined for interpretation purposes. The main objective is to specifically locate geologic features and to identify what type of geology they represent. This means distinguishing between structural (e.g. fault) or lithological (e.g. volcanic intrusion) features. Prior to interpretation, specific physical properties

associated with geologic features needs to be addressed to aid in differentiating between. signal and noise.

This thesis treats acquisition and gridding artfefacts as noise. Many magnetic surveys are carried out as systematic airborne surveys since the aim is to be both cost- and time effective. There are numerous methods to efficiently minimize levelling and other line-to-line variations (Minty, 1991; Nelson, 1994; Luyendyk, 1997; Mauring et al., 2002; Mauring and Kihle, 2006; Beiki et al., 2010). Sometimes the interpreter does not receive precursory information on the method and degree of levelling. This may result in errors due to insufficient levelling misinterpreted as geologic features. How the original point data is projected onto a grid will dictate the shape of the magnetic anomalies and ultimately influence the interpretation. The grid's projection should strive to be an accurate representation of the original data. This requires a fundamental understanding of the data; otherwise gridding artefacts will be generated and misinterpreted as signal. The data type and spatial distribution should be carefully considered prior to projection. This consideration helps determine what the ideal projection / interpolation algorithm should be and what grid cell size should be used to avoid aliasing (El Albass et al., 1990; Xiong and Götze, 1999; Pilkington and Keating, 2004).

1.3 Curvature analysis

This thesis is focused on surficial curvature analysis as a tool in magnetic field interpretation and how it may be used to alleviate potential field issues. The curvature analysis method is shown in Figure 1.1. along with the general data processing work flow. The first step in curvature analysis is the computation of all required curvature attributes. There are then two ways to apply curvature analysis - a lineament approach and a statistical approach. The lineament approach uses an automated lineament extraction algorithm based on the curvature of a magnetic grid. These lineaments are then analyzed using rose diagrams, degree of linearity, and intersection locations. The statistical approach computes the quantitative characteristics. These include mean, standard deviation, kurtosis, and skew. The statistics are also analyzed qualitatively in the form of probability plots, histograms, and scatterplots. Both steps of the curvature analysis are initially applied to assess the quality of the magnetic data and the lineaments themselves. If the data is deemed 'clean' by the user then curvature analysis is applied for the purpose of identifying geological features. The second application of curvature analysis includes both the lineament and statistical approaches. The objective of curvature analysis is to have the final interpretation used as a raster or vector layer for a geologic or natural resource map.

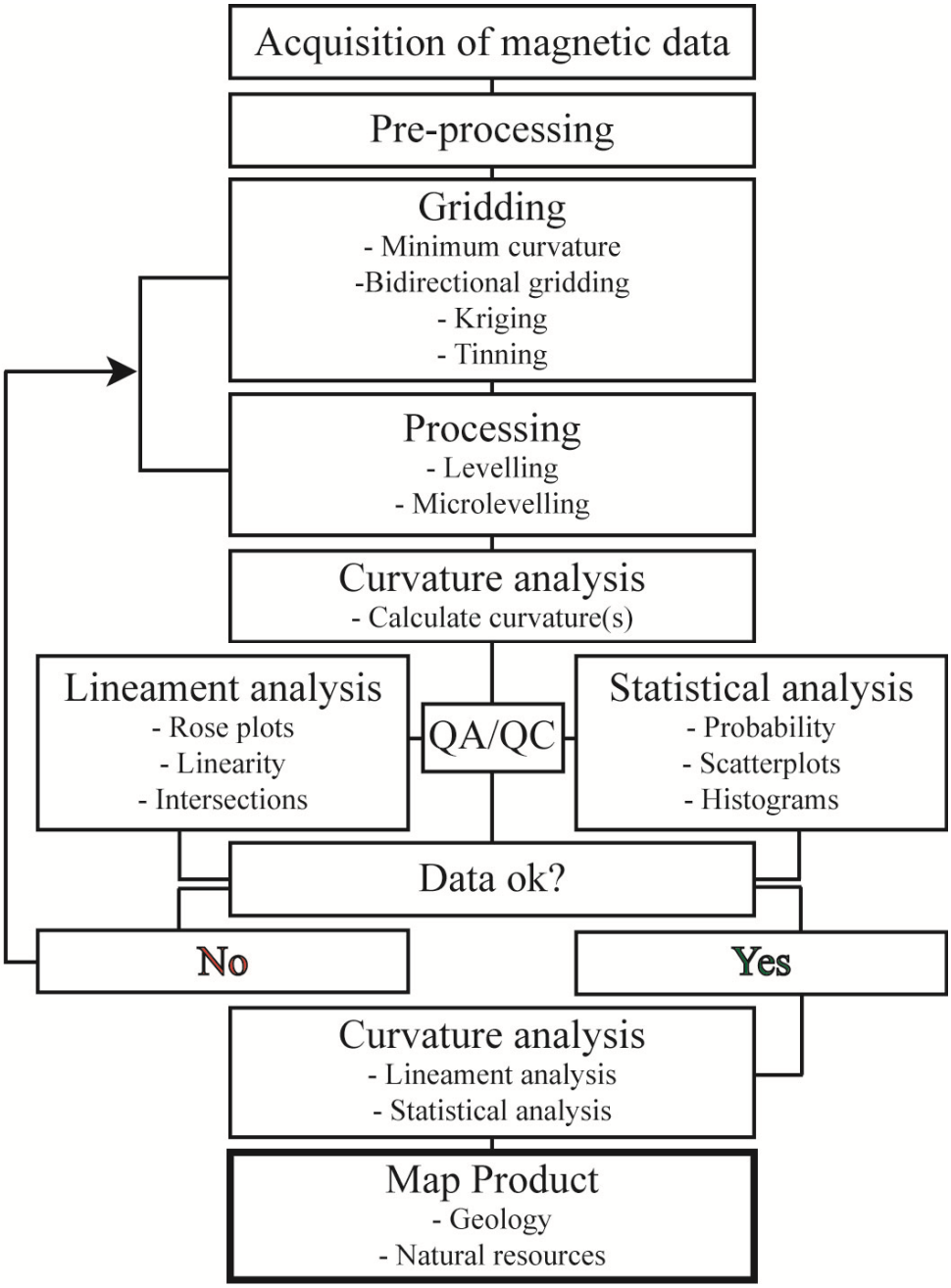

Figure 1.1 Curvature analysis process.

1.4 Significance of study areas

Two aeromagnetic data sets were selected for the real world analyses. The first data set is from the Paleoproterozoic Wopmay Orogen, Northwest Territories, Canada (NTGO, 2008). The aeromagnetic database and preliminary grids are publicly available through Natural Resources Canada's online Geoscientific Data Repository (NRCan, http, 2012). The aeromagnetic survey was flown in accordance with specifications outlined by Geo-Mapping for Energy and Minerals initiative for Natural Resources Canada. This area was of interest for the primary purpose of bedrock mapping and secondary for mineral resource assessment. One hundred and eight (108) rock samples were collected in-situ in 2009 and 2010. These samples underwent magnetic, electrical, and radiometric rock property measurements. These physical rock properties do not directly influence the content of the thesis; however are supplementary and will be used for future work as *a priori* data. The rock property database has been included in this thesis on DVD and initial figures and tables are included in appendix B. The second data set is from Southern Ontario, Canada collected in 1998 and 1999 through collaboration between the Geological Survey of Canada, Ontario Power Generation and the Multi-Disciplinary Center for Earthquake Engineering Research. The purpose of this data set was to assess local fault reactivation within crystalline rocks and Precambrian geologic domains overlaid by a relatively magnetically transparent sedimentary cover. These two aeromagnetic data sets were used due to their high survey resolution and similarity in acquisition specifications but over different geological environments.

1.5 Contribution to thesis

This thesis includes seven chapters in addition to the introduction and conclusion. The thesis chapters do not follow the flowchart in Figure 1.1 exactly to maintain readability. Figure 1.2 shows where each chapter falls into the curvature analysis process discussion. Chapter 2 introduces the definition of curvature and sets the foundation with previous work. The chapter discusses the many curvature attributes which may be calculated with the focus on profile and plan curvature. A statistical approach is briefly introduced in Chapter 2 and is used to differentiate geologic sources from a real world curvature data set. In Chapter 3 statistical analysis is further developed by discussing the link between frequency and amplitude content of a signal with the sign, magnitude, and distribution of curvature. Chapter 4 focuses on profile and plan curvature and how they are used to determine the physical properties of a magnetic source. These first three chapters implement simple synthetic models and then apply them to a real world data set. Chapter 5 introduces a semi-automated method to find surficial lineaments. These lineaments are continuous ridges and troughs along a grid and have specific curvature attributes. The method undergoes initial tests using three synthetic models mimicking real world

geology. The lineaments may represent geological features such as fault systems and dyke swarms. They may also represent signal associated with data acquisition such as survey lines. The application of lineament extraction for the purpose of geologic features is the focus of Chapter 6 where the method is applied to a real world data set. Differentiation between acquisition lineaments and geoscientific lineaments is important and is addressed in Chapters 7 and 8. These chapters focus on quality control of data; this includes magnetic data set and the lineaments themselves. Quality control of lineaments is influenced by gridding artefacts and a brief investigation is conducted to evaluate if the gridding algorithm impacts the production of these automatic lineaments.

Each chapter represents a published, accepted, or submitted manuscript. Some material is repeated since each chapter is an individual manuscript. This includes background, method and real world survey data specifications. Chapters 2, 5 and 6 were published in Geophysical Prospecting (Lee et al., 2012c), The Leading Edge (Lee et al., 2012a), and Exploration Geophysics (Lee et al., 2012b) respectively. Chapter 7 is in press with Exploration Geophysics (Lee and Morris, 2013). Chapters 3 and 8 are undergoing revisions with Mathematical Geosciences and Pure and Applied Geophysics respectively. Chapter 4 is undergoing internal revision with intended submission to Interpretation spring 2013.

All manuscripts were written by the student Madeline D. Lee[1,2] along with one to three co-authors. The student wrote all manuscripts and completed the data processing, figures, and graphs. Each manuscript underwent subsequent revisions by all co-authors. The secondary author is the student's supervisor Dr. William A. Morris[1] who provided research guidance and technical input. The tertiary authors Dr. George Leblanc[2] and Dr. Jeff Harris[3] are directly involved with the real world data sets discussed in 1.4 and provided technical input.

[1] McMaster Applied Geophysical and Geological Imagine Center, Hamilton, Ontario, Canada
[2] National Research Council of Canada, Ottawa, Ontario, Canada
[3] Natural Resources Canada, Ottawa, Ontario Canada

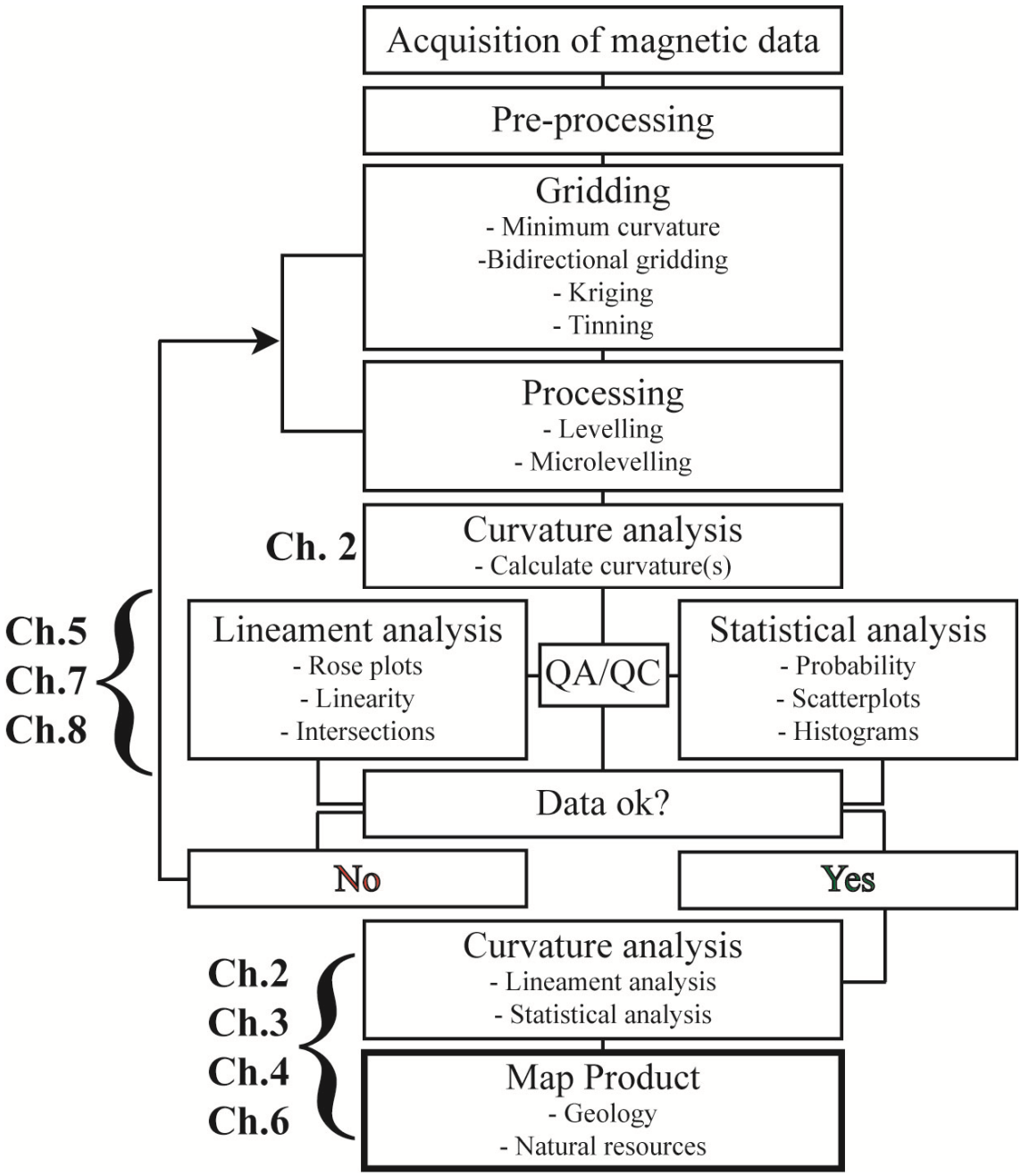

Figure 1.2 Curvature analysis process with relative chapters.

1.6 Presentations

Lee, M.D., Morris, W.A., Harris, J., Jackson, V., and Corriveau, L., 2009, Geophysical interpretation of the South Wopmay, Northwest Territories, Canada: *37th Yellowknife Geoscience Forum*, Yellowknife, November 17-19, 2009, Abstract (Poster Presentation).

Lee, M.D., and Morris, W.A., 2010, Lineament analysis tool for hydrocarbon and mineral exploration a Canadian case study: *CMOS-CGU Congress*, Ottawa, June 1, 2012, Abstract (Oral Presentation).

Lee, M.D., and Morris, W.A., 2010, Lineament analysis as a tool for hydrocarbon and mineral exploration: a Canadian case study: *21st Australian Society of Exploration Geophysicists International Geophysical Conference and Exhibition*, Sydney, August 22-26, 2010, 1–5, Extended Abstract (Poster Presentation).

Lee, M.D., Morris, W.A., Harris, J., Jackson, V., and Corriveau, L., 2010, Geophysics of the Great Bear Magmatic Zone – Northwest Territories: *38th Yellowknife Geoscience Forum*, Yellowknife, November 16-18, 2010, Abstract (Oral Presentation).

Lee, M.D., Morris, W.A., Harris, J., and Leblanc, G., 2012, Remote Predictive Mapping: geophysical applications for geological mapping and mineral exploration of the Wopmay Orogen, N.T., Canada: *33rd Canadian Symposium on Remote Sensing*, Ottawa, June 11-14, 2012, Abstract (Oral Presentation).

Lee, M.D., 2012, Curvature analysis of aeromagnetic data for geologic mapping, natural resource exploration, and data quality control: Application to an aeromagnetic survey from the Wopmay Orogen, Northwest Territories, Canada: *Canadian Exploration Geophysical Society Monthly Meeting*, Ottawa, March 20, 2012, Abstract (Oral Presentation).

Lee, M.D., Morris, W.A., Leblanc, G., and Harris, J., 2012, Curvature analysis for geological mapping and mineral resource assessment: *Society of Exploration Geophysicists 82nd Annual Meeting*, Las Vegas, November 4-9, 2012, Extended Abstract (Oral Presentation).

1.7 References

Aina, A., 1986, Reduction to equator, reduction to pole and orthogonal reduction of magnetic profiles: *Exploration Geophysics*, 17 (3), 141-145, DOI: 10.1071/EG986141.

Baranov, V., 1957, A new method for interpretation of aeromagnetic maps: Pseudo-gravimetric anomalies: *Geophysics*, 22, 359-383, DOI: 10.1190/1.1438369.

Beiki, M., Bastani, M., and Pederson, L.B., 2010, Levelling HEM and aeromagnetic data using differential polynomial fitting: *Geophysics*, 75 (1), L13-L23, DOI: 10.1190/1.3279792.

Bhattacharyya, B.K., 1964, Magnetic anomalies due to prism-shaped bodies with arbitrary polarization: *Geophysics*, 29 (4), 517-531, DOI: 10.1190/1.1439386.

Bhattacharyya, B.K., 1969, Bicubic spline interpolation as a method for treatment of potential field data: *Geophysics*, 34, 402-423, DOI: 10.1190/1.1440019.

Blakely, R., and Simpson, R., 1986, Approximating edges of source bodies from magnetic or gravity anomalies: *Geophysics*, 51, 1494–1498, DOI:10.1190/1.1442197.

Chopra, S., and Marfurt, K., 2007, Curvature attribute applications to 3D surface seismic data: *The Leading Edge*, 26 (4), 404-414, DOI: 10.1190/1.2723201.

Cooper, G.R.J., 2009, Balancing images of potential-field data: *Geophysics*, 74 (3), L17-L20, DOI: 10.1190/1.3096615.

Cooper, G.R.J. 2010. Enhancing ridges in potential field data: *Exploration Geophysics*, 41, 170-173, DOI: 10.1071/EG09038.

Cooper, G.R.J., and Cowan, D.R., 2008, Edge enhancement of potential field data using normalised statistics: *Geophysics*, 71 (3), H1-H4, DOI: 10.1190/1.2837309.

El Abbass, T., Jallouli, C., Albouy, Y., and Diament, M., 1990, A comparison of surface fitting algorithms for geophysical data: *Terra Nova*, 2 (5), 467-475, DOI: 10.1111/j.1365-3121.1990.tb00104.x.

Evans, I.S., 1972, General geomorphometry, derivatives of altitude and descriptive statistics: In Chorley, R. J. (Ed.), *Spatial Analysis in Geomorphology*, p.36, Methuen, London.

Leblanc, G.E., and Morris, W.A., 2001, Denoising of aeromagnetic data via the wavelet transform: *Geophysics*, 66 (6), 1793-1804, DOI: 10.1190/1.1487121.

Lee, M.D., W.A. Morris, J. Harris, and Leblanc, G., 2012a, An automatic network extraction algorithm applied to magnetic survey data for the identification and extraction of geologic lineaments: *The Leading Edge*, 31, 26-32, DOI:10.1190/1.3679324.

Lee, M.D., W.A. Morris, J. Harris, and Leblanc, G., 2012b, A network extraction tool for mineral exploration: a case study from the Wopmay Orogen, Northwest Territories, Canada: *Exploration Geophysics*, 43, 116-124, DOI: 10.1071/EG11045.

Lee, M.D., Morris, W.A., Leblanc, G., and Harris, J., 2012c, Curvature analysis to differentiate magnetic sources for geologic mapping: *Geophysical Prospecting*, DOI: 10.1111/j.1365-2478.2012.01111.x.

Lee, M.D., and Morris, W.A., 2013, Quality assurance of aeromagnetic data using lineament analysis: *Exploration Geophysics*, DOI: 10.1071/EG12034.

Li, X., and Götze, H., 1999, Comparison of some gridding methods: *The Leading Edge*, 18, 898-900, DOI: 10.1190/1.1438401.

Luyendyk, A.P., 1997, Processing of airborne magnetic data: *Journal of Australian Geology and Geophysics*, 17 (2), 31-38.

Mauring, E., and Kihle, O., 2006, Levelling aerogeophysical data using a moving differential median filter: *Geophysics*, 71 (1), L5-L11, DOI: 10.1190/1.2163912.

Mauring, E., Beard, L.P., Kihle, O., and Smethurst, M.A., 2002, A comparison of aeromagnetic levelling techniques with an introduction to median levelling: *Geophysical Prospecting*, 50 (1), 43-54, DOI: 10.1046/j.1365-2478.2002.00300.

Minty, B.R., 1991, Simple micro-levelling for aeromagnetic data: *Exploration Geophysics*, 22, 591-592, DOI: 10.1071/EG991591.

Nabighian, M.N., 1972, The analytic signal of two-dimensional magnetic bodies with polygonal cross-section: its properties and use for automated anomaly interpretation: *Geophysics*, 1972, 507-517, DOI: 10.1190/1.1440276.

Natural Resources Canada (NRCan), 2012, Geoscience Data Repository (GDR), available online: http://www.nrcan.gc.ca/earth-sciences/products-services/geoscience-data-repository/11818, May 14, 2012.

Nelson, B., 1994, Levelling total-field aeromagnetic data with measured horizontal gradients: *Geophysics*, 59 (8), 1166-1170, DOI: 10.1190/1.1443673.

Phillips, J.D., Hansen, R.O., and Blakely, R.J., 2007, The use of curvature in potential field interpretation: *Exploration Geophysics*, 38, 111-119, DOI: 10.1071/EG07014.

Pilkington, M. and Keating, P., 2004, Contact mapping from gridded magnetic data – comparison of techniques: *Exploration Geophysics,* 35, 306-311, DOI: 10.1071/EG04306.

Reid, A., Allsop, J., Granser, H., Millett, A., and Somerton, I., 1990, Magnetic interpretation in three dimensions using Euler deconvolution: *Geophysics,* 55, 80-91, DOI: 10.1190/1.1442774.

Reford, M.S., 1980, Magnetic method: *Geophysics*, 45 (11), 1640-1658, DOI: 10.1190/1.1441055.

Roberts, A., 2001, Curvature attributes and their application to 3D interpreted horizons: *First Break*, 19.2, 85-100.

Roy, A., and Aina, A., 1986, Some new magnetic transformations: *Geophysical Prospecting*, 34, 1219-1232, DOI: 10.1111/j.1365-2478.1986.tb00525.x.

Smith, R.S, Thurston, J.B., Salem, A., and Reid, A.B., 2012, A grid implementation of the SLUTH algorithm for visualizing the depth and structural index of magnetic sources: *Computers and Geosciences*, 44, 100-108, DOI: 10.1016. /j.cageo.2012.03.004.

Xiong, L., and Götze, H., 1999, Comparison of some gridding methods: *The Leading Edge*, 18 (8), 898-900

Zevenbergen, L.W., and Thorne, C.R., 1987, Quantitative analysis of land surface topography: *Earth surface processes and landforms*, 12 (1), 47-56, DOI: 10.1002/esp.3290120107.

2.0 Curvature analysis to differentiate magnetic sources for geologic mapping

Lee, M.D., Morris, W.A., Leblanc, G., and Harris, J., 2012, Curvature analysis to differentiate magnetic sources for geologic mapping: *Geophysical Prospecting*, DOI: 10.1111/j.1365-2478.2012.01111.x

2.1 Abstract

Curvature of a surface is typically applied in seismic data interpretation; however this work outlines its application to a potential field, specifically aeromagnetic data. The curvature of a magnetic grid (from point data) is calculated by fitting a quadratic surface within a moving window at each grid node. The overall and directional curvatures calculated within this window provide insight into the geometry of the magnetic grid surface and causative sources. Curvature analysis is an in-depth study of both qualitative (graphically) and quantitative (statistically) approaches. This analysis involved the calculation of full, profile and plan curvatures. The magnitude, sign, and relative ratios enable the user to define source location and geometry and also discriminate source type; for example, differentiation between a fault and normal polarity dyke. The reliability of the analysis is refined when a priori geological knowledge is available and basic statistics are considered. By allotting a weighting scheme to various statistical populations (e.g. standard deviation), increased detail is extracted on the different lithologies and structures represented by the data set. Furthermore, the curvature's behaviour is analogous to derivative calculation (vertical, horizontal, and tilt) by producing a zero value at the source edge and either a local maxima or minima over the source. Finally, application prior to semi-automated methods may help identify correct indices necessary for identification of magnetic sources. Curvature analysis is successfully applied to an aeromagnetic data set over the 2.6 to 1.85 Ga Paleoproterozoic Wopmay Orogen, Northwest Territories, Canada. This area has undergone regional and local-scale faulting and is host to multiple generations of dyke swarms. As the area has been extensively mapped, this data set proved to be an ideal test site.

2.2 Introduction

The objective identification and mapping of geologic structures from geophysical data, particularly magnetic, is an important activity in producing a bedrock geology map for mineral and energy exploration endeavors. Aeromagnetic survey data are often interpolated to generate a continuous magnetic surface (grid) for processing and interpretation. Quantitative methods may be applied to this magnetic surface to determine magnetic source properties, which include location, depth, dip direction, and magnetic susceptibility (Spector and Grant, 1970). The quantitative method (in conjunction with a qualitative aspect) developed and applied in this paper is curvature analysis. Although the common use of curvature analysis in seismic interpretation and drainage basin analysis has been well-documented, it has rarely been applied to a magnetic data set. In seismic interpretation, curvature analysis is applied to a cross-section (depth plot) or 3D horizon-based (Hilterman, 1975; Roberts, 2001; Sigismondi and Soldo, 2003; Chopra and Marfurt, 2007); Whereas in drainage basin calculation, the curvature analysis is applied to a topographic surface (Evans, 1972; Zevenbergen and Thorne, 1987; Moore, Burch, and Mackenzie, 1988; Moore, Grayson, and Landson, 1991). The curvature analysis we undertake in this paper is more similar to the topographic/drainage basin analysis as calculations are carried out on a surface. The surface is a magnetic grid comprising various curved segments originating from each data point.

Identification of magnetic source location is critical in geological mapping and for mineral and hydrocarbon exploration. The manual identification and mapping of geologic structures, whether it is on geophysical data or other various types of remotely sensed-imagery, is often laborious, subjective, and costly. This has led to the development of quantitative (and therefore objective) methods for identifying geological features on remotely sensed-data including aerial photographs, satellite imagery, and airborne geophysical data. Various map products highlighting potentially significant geologic structures can be produced using these quantitative techniques and aid in geological mapping. Various types of mineral deposits (e.g. lode gold, volcanogenic massive sulfide, diamonds) are often controlled by fault and fracture systems (O'Driscoll, 1980; Lalor, 1987; Woodall, 1994; Chernicoff, Richards, and Zappettini, 2002, Crafford and Grauch, 2002; Twidale, 2007; Woodall, 2007), which act as conduits for mineral-bearing hydrothermal and magmatic fluids (ore) or as structural control mechanisms for diamonds, oil and gas. Therefore, identification of these geologic structures from magnetic data greatly assists natural resource exploration.

Identification of source type is also an important aspect in the quantitative processing of geophysical (magnetic) data. Some semi-automated depth-estimators such as Euler deconvolution (Reid et al., 1990), employ a coefficient (or structural index) linked to the magnetic source's geometry (analogous to a point, line, or prism/sphere). The method of Euler deconvolution and more specifically the calculation of an appropriate structural index (indirectly source type), has been refined through subsequent formulations (Barbosa et al., 1999; Fitzgerald et al., 2004; Gerovska and Araúzo-Bravo, 2006). Curvature computation aids in a similar fashion, where completion of curvature analysis prior to semi-automated routines will help refine the selection of an appropriate coefficient (acts as *a priori* knowledge).

In this paper we apply curvature analysis to an aeromagnetic data set over the Great Bear magmatic zone, Northwest Territories, Canada to differentiate between faults and dykes based on the magnitude and sign of computed surficial (magnetic grid) curvature attributes. Properties of these faults and dykes (e.g. location and extent) are further refined through statistical analysis of their curvature attributes. A final product is generated that may be integrated as a vector layer in any geological or exploration map.

2.3 Method

The geometry of the magnetic surface at each data point may be approximated by computing a quadratic surface using a least squares approach to the eight grid nodes (3 x 3 matrix) surrounding the central data point, P_0 (x, y) (Evans, 1972):

$$z = ax^2 + by^2 + cxy + dx + ey + f \quad (1)$$

Where z is the vertical component and a, b, c, d, e, and f are coefficients along different directional gradients determined from the 3 x 3 matrix. However, the quadratic equation may have difficulty intersecting all nine grid nodes and therefore may represent the data set inaccurately. Accordingly, Zevenbergen and Thorne (1987) introduced a modified equation (1) indicating it is more appropriate to use the partial quartic equation:

$$z = ax^2y^2 + bx^2y + cxy + dx^2 + ey^2 + fxy + gx + hy + i \quad (2)$$

Where a, b, c, d, e, f, g, h, and i are coefficients along different directional gradients from the 3 x 3 matrix and every point must be intercepted by the surface. The addition of i forces the surface to intercept P_0.

Many data processing and Geographic Information System software packages implement curvature computation, each in a different manner. For example Encom Discover[1] implements equation (1), ArcMap[2] implements equation (2), and INTREPID[3] uses a modified curvature algorithm based on Collatz (1960). For this work, curvature was calculated in the ArcGIS environment using equation (2).

At every origin P_0, the slope (m) of z from either equations (1) or (2) is (Zevenbergen and Thorne, 1987):

$$m = \frac{\partial z}{\partial S} = g\cos\theta + h\sin\theta \tag{3}$$

Where S is in the direction of maximum slope, also known as aspect (θ) (Figure 2.1) and g and h are coefficients perpendicular and parallel to maximum slope respectively. To simplify the computation of slope, equation (3) is revised (Zevenbergen and Thorne, 1987):

$$m = -\sqrt{(g^2 + h^2)} \tag{4}$$

The principal or full curvature (FC) in any direction (ϕ) at the grid point P_0 is computed using the directional gradient coefficients from equation (2) and represents the derivative of the slope (Zevenbergen and Thorne, 1987):

$$FC = \frac{\partial^2 z}{\partial S^2} = 2(d\cos^2\phi + e\sin^2\phi + f\cos\phi\sin\phi) \tag{5}$$

Where d is the gradient in x direction, e is in y direction, and f is the overall gradient of the surface. The units for curvature can vary depending on how curvature is calculated. When slope is calculated according to equation (3), the units are radians/L unit where L is the number of units between *x* and *y* and should be the same as z (often some unit of length, such as metres). When slope is calculated according to equation (4) the units are 1/L unit. In this work the latter is applied. In the case of potential field interpretation the units for L and z are not the same. Accordingly L will be in units of metres while z will be in units of nanotesla. Typically a z-factor may be introduced to convert between different vertical and horizontal units (e.g. conversion between feet and metres); however since metre is a unit of length and nanotesla is a unit of magnetic flux density, no such z-factor exists. Therefore curvature may be considered as 1/nT/m.

[1] Encom Technology, Encom Discover
[2] ArcGIS®, ArcGIS Desktop, ArcMap
[3] INTREPID Geophysics, INTREPID

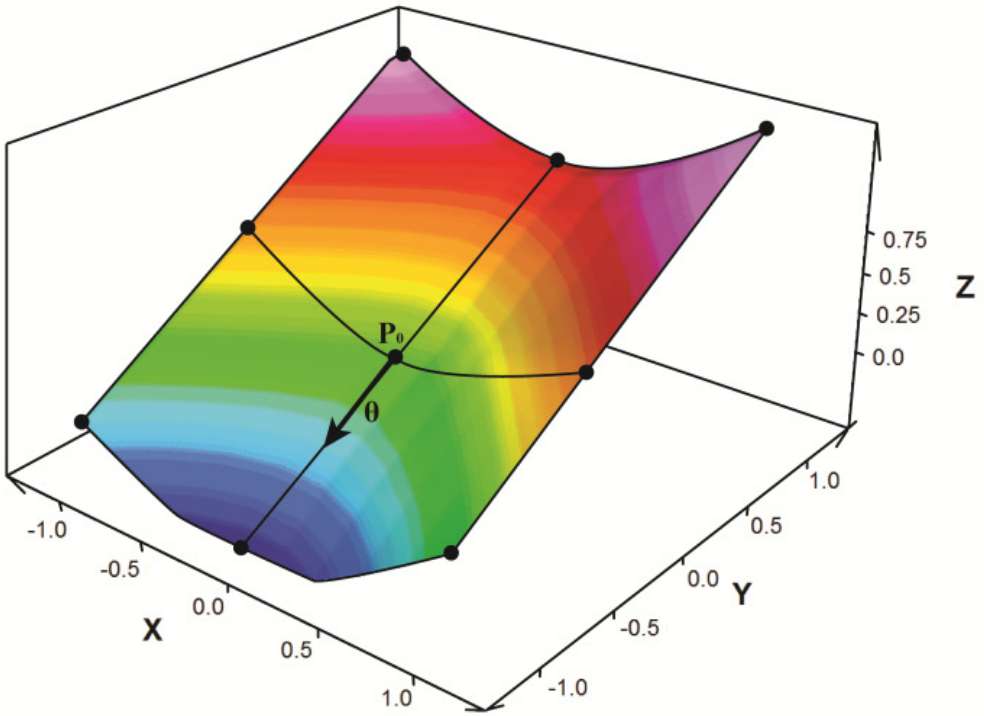

Figure 2.1. A quadratic surface fitted to the surrounding eight grid nodes of P_0. Direction of maximum slope, θ, is in the negative Y direction and perpendicular to the X axis (black arrow).

A range of curvatures may be calculated, many of which are summarized in Roberts (2001), Hansen and deRidder (2006), Phillips et al. (2007), and Cooper (2010). These curvatures include but are not limited to Gaussian, profile, plan, mean, maximum, and minimum. We focus on profile (PrC) and plan (PlC) curvatures which are computed from FC. These curvatures emphasize different magnetic sources depending on the magnitude of their curvature segment at point P_0. According to Wood (1996) and Roberts (2001) PrC is the rate of change in the maximum dip direction ($\phi = \theta$), also known as dip curvature. This can be calculated using the coefficients from equation (2) (Zevenbergen and Thorne, 1987).

$$\mathrm{PrC} = -2(\mathrm{d}\cos^2\theta + \mathrm{e}\sin^2\theta + \mathrm{f}\cos\theta\sin\theta) \qquad (6)$$

Application of PrC to a potential field data set was shown in Cooper and Cowan (2006; 2008), where they use the association of zero PrC in their potential field terracing algorithm.

Normal to PrC is PlC ($\phi = \theta + \pi/2$), which is also known as the strike or tangential curvature (Wood, 1996; Roberts, 2001). PlC is also calculated using the coefficients from equation (2).

$$\mathrm{PlC} = -2(\mathrm{d}\sin^2\theta + \mathrm{e}\cos^2\theta - \mathrm{f}\sin\theta\cos\theta) \tag{7}$$

Cooper (2010) showed PlC was an effective locator for potential field data set ridges. Cooper's method involved the calculation of PlC where all solutions undergo a threshold so all peaks have the same amplitude and similarly for all troughs. Cooper (2010) also showed PlC was not overly sensitive to noise, however recommended the potential field data set be smoothed prior to calculation of PlC.

PrC and PlC may be computed to be 1/L unit rather than degree/L unit, and equations (6) and (7) respectively become (Zevenbergen and Thorne, 1987):

$$\mathrm{PrC} = -2(\mathrm{dg}^2 + \mathrm{eh}^2 + \mathrm{fgh})/(\mathrm{g}^2 + \mathrm{h}^2) \tag{8}$$

$$\mathrm{PlC} = -2(\mathrm{dg}^2 + \mathrm{eh}^2 - \mathrm{fgh})/(\mathrm{g}^2 + \mathrm{h}^2) \tag{9}$$

Since PrC and PlC are orthogonal to one another the average of the two will produce the mean curvature of a surface. How the geometry of a surface will vary depending on PrC and PlC is summarized in Figure 2.2.

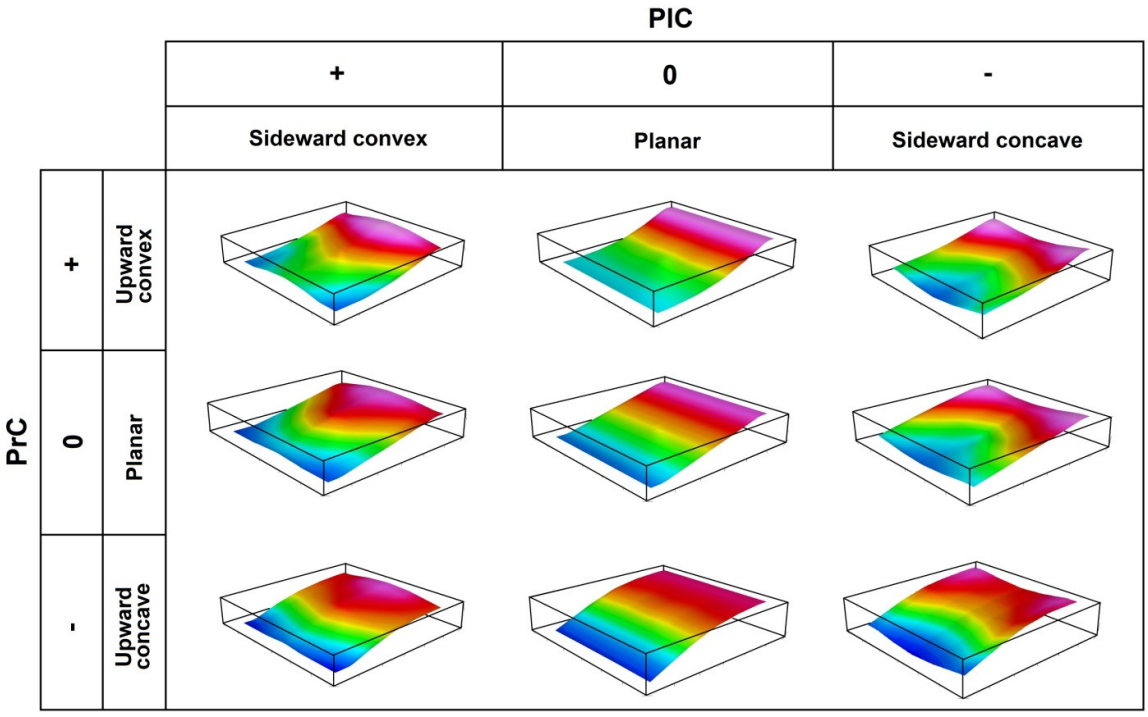

Figure 2.2. Comparison of positive, negative and zero PrC and PlC with respect to P_0 using a simplified surface.

2.3.1 Curvature sign

With respect to the sign of curvature (positive or negative) PrC will have the opposite sign to FC, while PlC will have the same sign as FC. This is because FC and PrC are in the same direction ($\phi = \theta$), but multiplied by -2 (equation 6); while FC and PlC are orthogonal in direction ($\phi = \theta + \pi/2$), but multiplied by -2 (equation 7).

Based on Figure 2.2, a positive magnetic anomaly will produce a negative PrC over the source, a positive PrC outside the source, and zero at the source edges. This is applicable in the high inclination or pole-reduced case for normally magnetized dykes or batholiths intruding into a host rock of lower magnetic susceptibility. The contrary would hold true and would be applicable if magnetism of the dykes were dominated by reversely polarized remanent magnetization.

The sign of PlC of a magnetic anomaly will depend on the geometry of the magnetic source. A fault is typically linear in plan view and therefore should produce a PlC near zero. Dykes typically follow the path of least regional stress, which means they will travel along local fault and fracture configuration systems. Accordingly, dykes will exhibit a similar PlC and azimuth to local faults. On the other hand, a batholith may exhibit both positive and negative PlC at different locations along the source boundary since batholiths often have irregular shapes steeply juxtaposed to the host rocks. Much will depend on the size of the batholiths; most large scale intrusions are big enough their contacts can be interpreted as linear in plan view. Small horizontal scale and large vertical scale intrusions such as kimberlites will have a strongly defined PlC.

2.3.2 Curvature magnitude

With respect to the magnitude of curvature, the amplitude of PrC is very similar to FC, while the amplitude of PlC is independent of FC. PrC and FC are both computed in the same way (equations 5 and 6) and along identical directions.

The magnitude of PrC is directly linked to composition and depth of the source body (Cooper and Cowan, 2006; Cooper and Cowan, 2008; Phillips et al., 2007). PrC will depend on the size of the source relative to the sample spacing, which impacts the resultant anomaly. The typical high magnetic latitude anomaly produced by a magnetic profile perpendicular to a (normal polarity) dyke's strike is narrow and strongly positive due to enhanced magnetite content of the diabase. Likewise, a magnetic profile across a fault is generally associated with a narrow low created by the absence of magnetite through oxidation, the percolation of oxygen-rich fluids (Lee et al., 2010). Such a contact-oxidation anomaly would be superposed on the overall fault anomaly, which could take various forms. In both instances the width of the anomaly is relatively small and as a consequence PrC associated with these types of features would be large. In contrast a batholith is geometrically a large regional scale feature composed of intermediate to felsic coarse-grained rock (e.g. granite, granodiorite) of variable magnetic composition depending on the source of the magmatic fluids. In most instances magnetic anomalies associated with batholiths are characterised by broad relatively uniform anomalies with minor internal variations. Transposed into PrC, this would mean batholiths should generally be associated with low relatively uniform PrC values. The contacts of the batholith are associated with higher PrC values, but due to the large batholith's dimensions PrC associated with these contacts will be smaller than those associated with near surface dykes and faults.

Geologic sources and their associated curvature attributes are summarized in Figure 2.3 and Table 2.1. Hence following a quantitative analysis of the variations of FC, PrC and PlC of the magnetic field it is possible to discriminate between different types of geological sources. Figures 2.3A and 2.3B show curvature analysis works well under the ideal conditions of a non-dipping body in a near vertical field. As with other processing tools (vertical, horizontal, and the arctangent of the vertical to horizontal component, tilt-derivative) the results become convoluted when the source is dipping or a mid-latitude ambient field is introduced since the maximum amplitude of the resultant magnetic field moves away from the location over the source (Figures 2.3C and 2.3D). For curvature analysis to work ideally the magnetic field and sources should be to be near-vertical in orientation. This requires the application of reduction-to-pole prior to computation in cases where the ambient magnetic field is inclined.

	FC	**PrC**	**PlC**
Fault	-	+	0 - small
Normal dyke	+	-	0 - small
Remanent dyke	-	+	0 - small
Homogeneous batholith	+	-	variable

Table 2.1. Summary table of associated curvature characteristics for various geologic sources (calculated from an observation point over the source). Units are 1/100 nT/m.

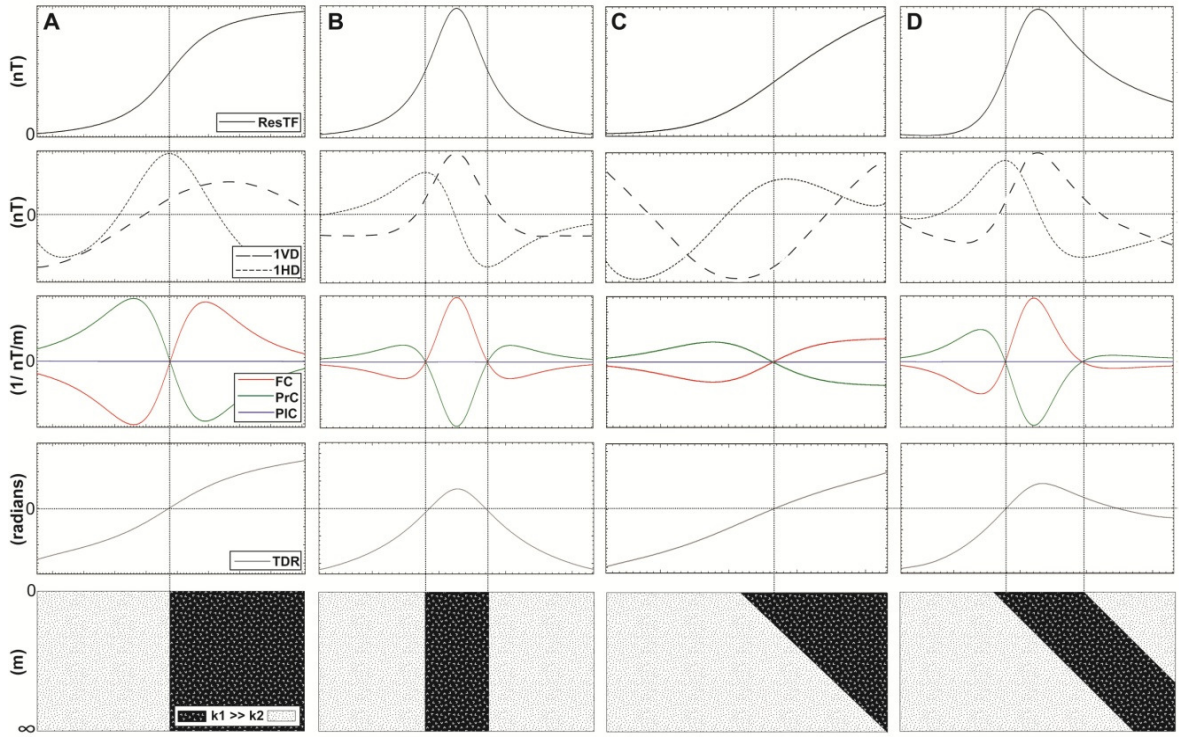

Figure 2.3. Comparison of resultant ResTF, derivatives and curvatures over a fault (A, C) and normal polarity dyke (B, D). FC and PrC have similar anomaly geometry but differ in sign. FC and PlC have similar sign but differ in magnitude (PlC is insignificant relative to FC). The most reliable results are produced under ideal conditions (non-dipping and vertical ambient field). The curvature cross-over locations are coincident with the zero values of the horizontal derivative and tilt-derivative, the maxima of the vertical derivative (fault) and the point of inflection of the ResTF.

2.4 Application

2.4.1 Field data

Curvature analysis was applied to a 2007 high resolution aeromagnetic data set from the Wopmay Orogen, Northwest Territories, Canada. The total field magnetic data (along with radiometrics) set was commissioned by the Northwest Territories Geoscience Office for the purposes of geological mapping and mineral potential assessment (Figure 2.4A). The flight lines were flown east-west at 400 m intervals along a terrain-draped surface with an elevation of 150 m ± 22.8 (NTGO, 2008).

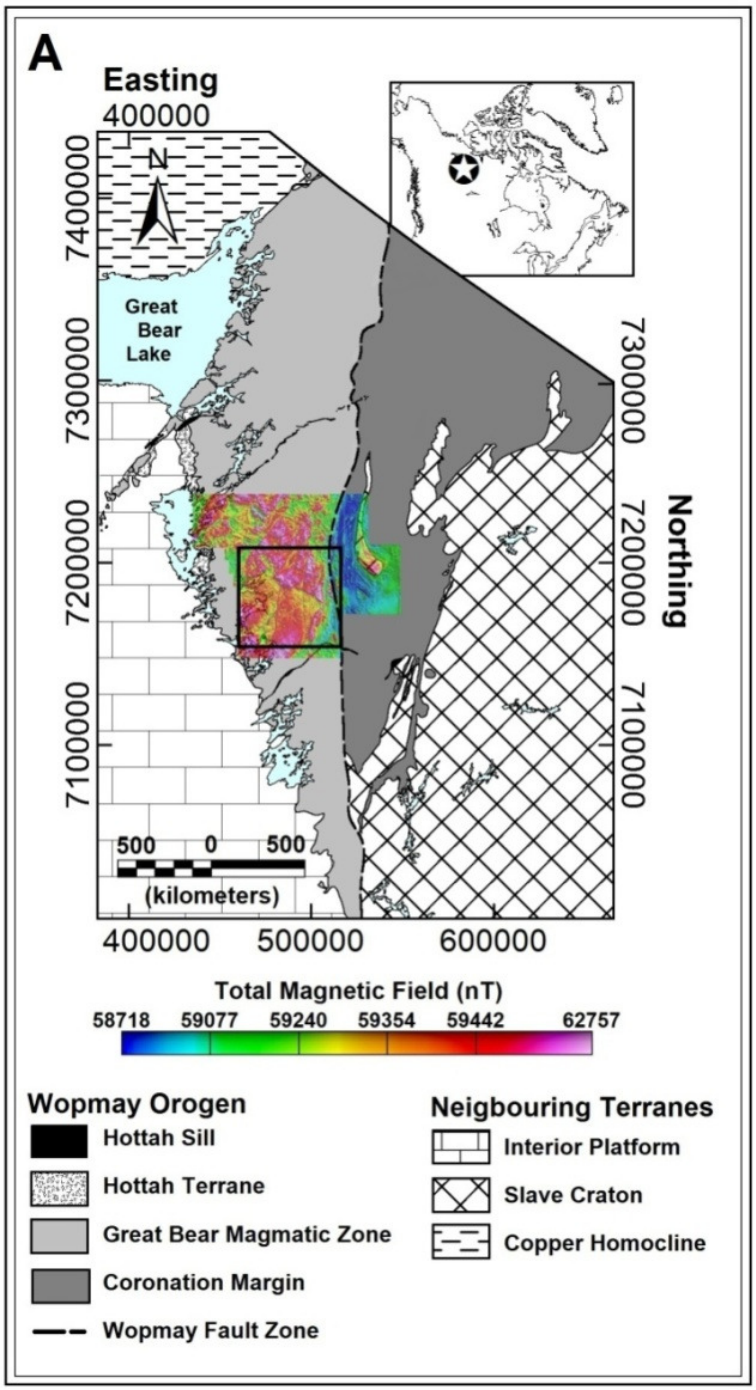

Figure 2.4A. Geologic setting of the Wopmay Orogen (after Hoffman and Hall, 1993) and its location in northwestern Canada (top right inset map). The study area is indicated by the black box and partly coincides with the footprint of a combined radiometric and total magnetic field airborne survey flown in 2007.

2.4.2 Brief geology

The Wopmay Orogen is a 2.6 to 1.85 Ga Paleoproterozoic orogenic belt composed of four geologic domains: Coronation margin (Archean and Paleoproterozoic metasedimentary rocks and plutons); the 1.87 to 1.85 Great Bear magmatic zone; the Wopmay fault zone (divisional fault between Coronation margin and Great Bear magmatic zone); and the >1.89 Ga Hottah terrane which extends eastward as the basement for much of the Great Bear magmatic zone. Field mapped geology over the study area is shown in Figure 2.4B. This region has been identified for its mineral potential; more specifically iron ore copper-gold deposits (Mumin, 2002; Corriveau et al., 2007a; Corriveau, 2007b; Mumin et al., 2007; Corriveau et al., 2009; Mumin et al., 2009; Corriveau and Mumin, 2010a; Corriveau et al., 2010b). Accordingly, significant exploration and geologic mapping has been carried out on the area (Hildebrand et al., 1987; Gandhi, 1994; and Gandhi et al., 2001).

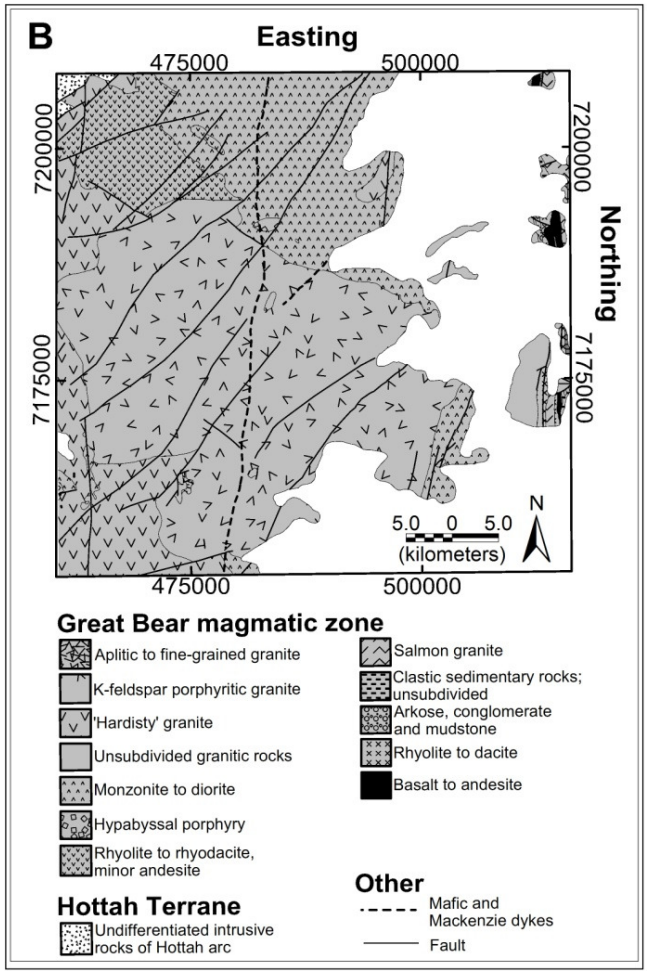

Figure 2.4B. Mapped geology over the study area (after Jackson and Ootes, 2011).

2.5 Results

The total field magnetic data underwent levelling and correction to the International Geomagnetic Reference Field. FC, PrC, and PlC were computed on this residual total field (ResTF) aeromagnetic data set (Figure 2.5A). As per Cooper (2010) the data also underwent smoothing prior to calculation of PlC, which was done using a Butterworth low-pass filter. At the time of acquisition, the magnetic field declination and inclination over this study area was 23° and 82° respectively as per the 2005 International Geomagnetic Reference Field. Reduction-to-pole was not applied to this data set due to the high-latitude location and the magnetic field inclination being sub-vertical. The curvature computations were compared with known mapped geology (Figure 2.4B and overlaid in 2.5B, 2.5C, and 2.5D) (Hoffman and Hall, 1993; Jackson and Ootes, 2011) which included lithological contacts (dotted white lines), dykes (dashed white lines), and faults (solid white lines).

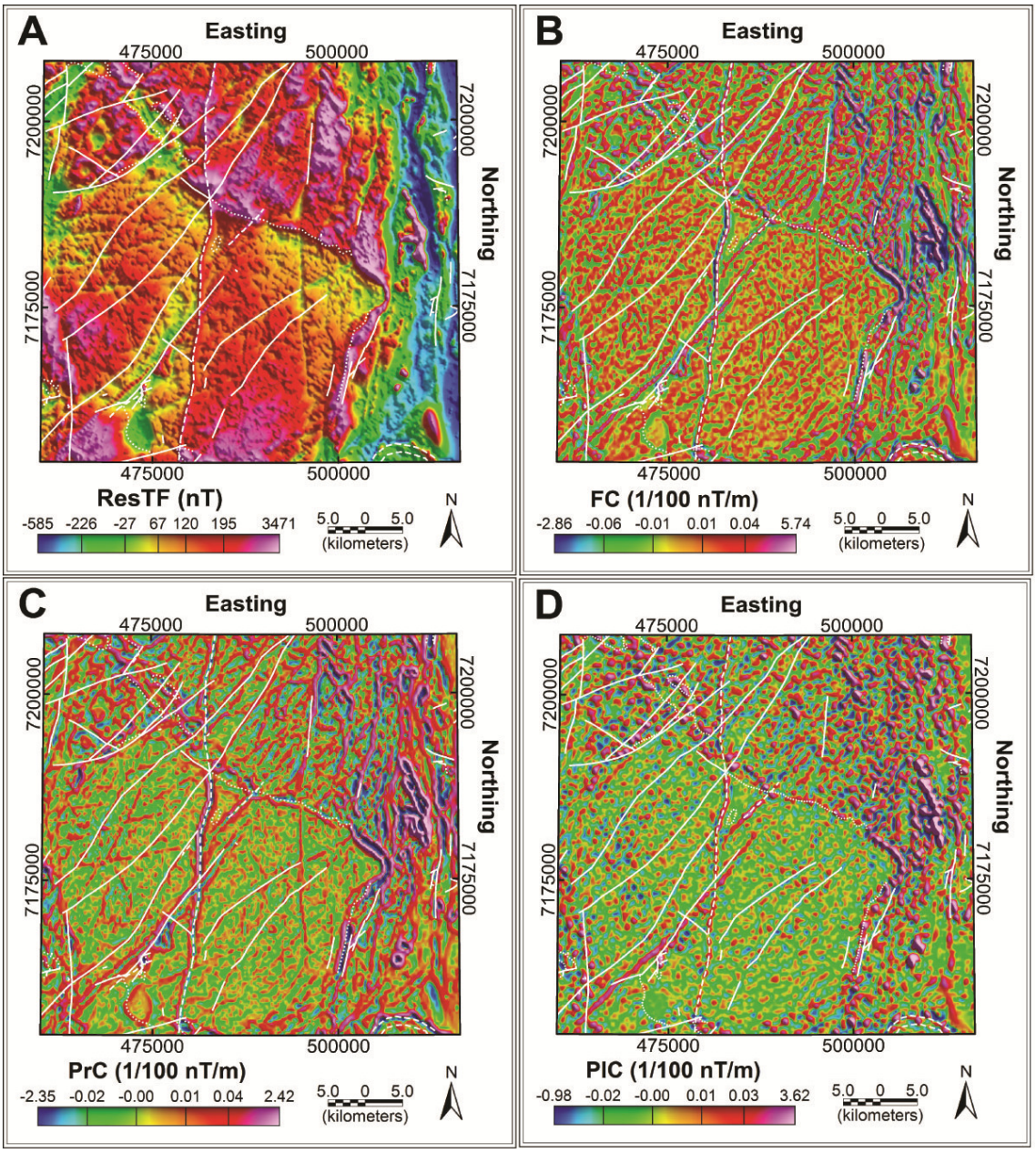

Figure 2.5. Curvature analysis applied to ResTF (A) which produced outputs for FC (B), PrC (C), and PlC (D). The locations of mapped contacts, dykes, and faults have been indicated with a white dotted, dashed, and solid line respectively (Hoffman and Hall, 1993; Jackson and Ootes, 2011).

Curvature analysis produced results analogous to other source detection techniques such as vertical and horizontal derivatives (Pilkington and Keating, 2004), worming (Archibald et al., 1999) and skeletonization (Eaton and Vasudevan, 2004). Standard practice in processing magnetic data to delineate sources is to calculate the first vertical and horizontal derivatives. Methods such as local wavenumber which utilize high-order vertical and horizontal derivatives (Phillips et al., 2007; Keating, 2009) may be more susceptible to noise and interference effects; however these issues are mitigated somewhat with high-resolution surveying and pre-processing (i.e. smoothing). The calculation of curvature extracts additional information over derivatives alone by generating more than one map product. In Figure 2.5 we have provided one primary map product (FC) and two secondary map products (PrC and PlC) computed from ResTF. Curvature analysis allows the user to calculate multiple curvatures all of which provide different information on the features being imaged. FC and PlC are best used for dyke and lithological contact identification while PrC is best used for fault identification.

The Great Bear magmatic zone is clearly defined through curvature analysis due to an overall composition of Paleoproterozoic volcanic and plutonic rocks which have undergone little deformation or metamorphism, but have multiple generations of faults, fractures, and dykes. Since the Great Bear magmatic zone host rocks (granite, monzonite, and diorite) are relatively homogeneous with respect to overall magnetite content, curvature analysis can easily identify these multi-generational linear features. The Wopmay fault zone is also well defined by the curvature analysis. Since the Wopmay fault zone represents the collisional boundary between the Hottah terrane and the Slave craton during the Wopmay Orogen, this N-S boundary is associated with extensive deformation and metamorphism. This tectonic activity has resulted in the presence of shearing, faulting, fracturing, and the emplacement of dykes. The presence of hydrothermal / metamorphic magnetite causes the Wopmay fault zone to be a prominent feature on regional and local high resolution magnetic datasets.

Closer analysis along two profiles A-A’ and B-B’ in Figure 2.6 and displayed in Figure 2.7 within the study area, shows results similar to the standard set of guidelines outlined in Figure 2.3 and Table 2.1. The large scale (500 km wide and 2100 km long) radiating Proterozoic Mackenzie dyke swarm cuts the study area along a north-south trend over this portion of the Canadian Shield. The Mackenzie dykes are mafic in composition and exhibit a magnetic texture due to late-crystallizing magnetite distributed along the pre-existing rock fabric (Ernst and Baragar, 1992). There are also moderate to small scale intermediate and mafic intrusions of monzonite, diorite, and aplitic granite intruding the k-feldspar porphyritic granite of the Great Bear magmatic zone along pre-existing faults.

These various-scaled intermediate and mafic intrusions are identified by their unique curvature geometry of a single point +FC and +PlC anomaly, coincident with a single point -PrC anomaly. The lithological boundary between the k-feldspar porphyritic granite and monzonite/diorite located further east within the study area (Figure 2.7A). The boundary is identified by a curvature anomaly with the geometry of a second derivative Gaussian function. This anomaly is coincident with a -PrC anomaly of similar yet converse geometry of the +FC anomaly. The Great Bear magmatic zone is cross-cut by various faults and fractures pre-dating the Mackenzie dyke swarm (Ernst and Baragar, 1992). These lineaments are identified by coincident -FC and +PrC anomalies. The lineaments have negligible PlC indicating a high degree of linearity in plan view. One of the principal host rocks of the Great Bear magmatic zone k-feldspar porphyritic granite, shows a consistent curvature background of -0.5 to 0.5 1/100 nT/m.

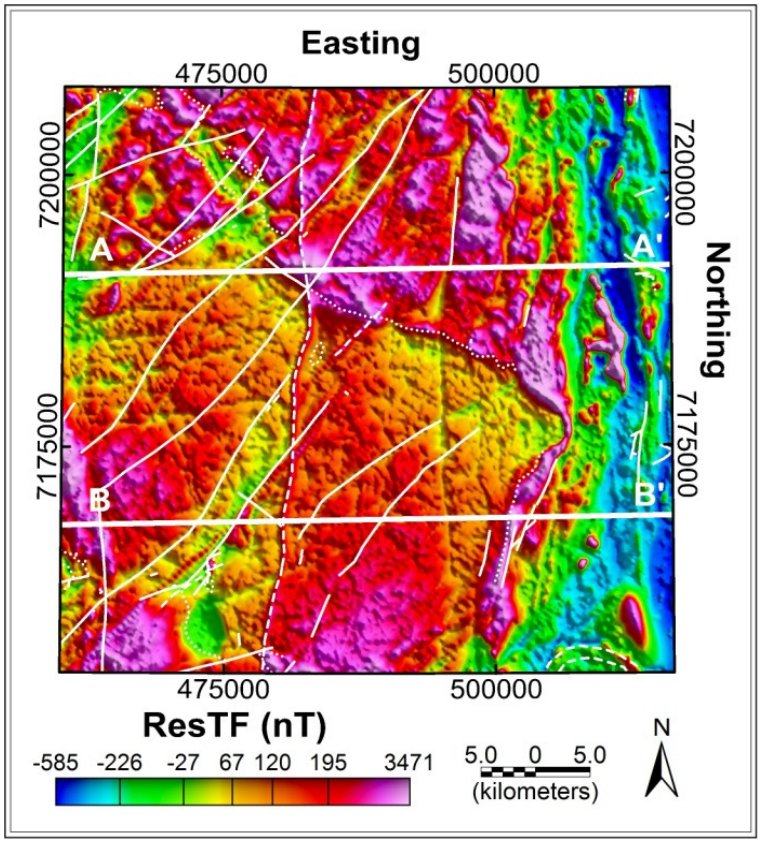

Figure 2.6. ResTF with location of curvature analysis profiles A-A' and B-B' indicated in white. These profiles were chosen to be orthogonal to dominant geologic trend and intersect some key mapped geology and structure (Figure 2.4B).

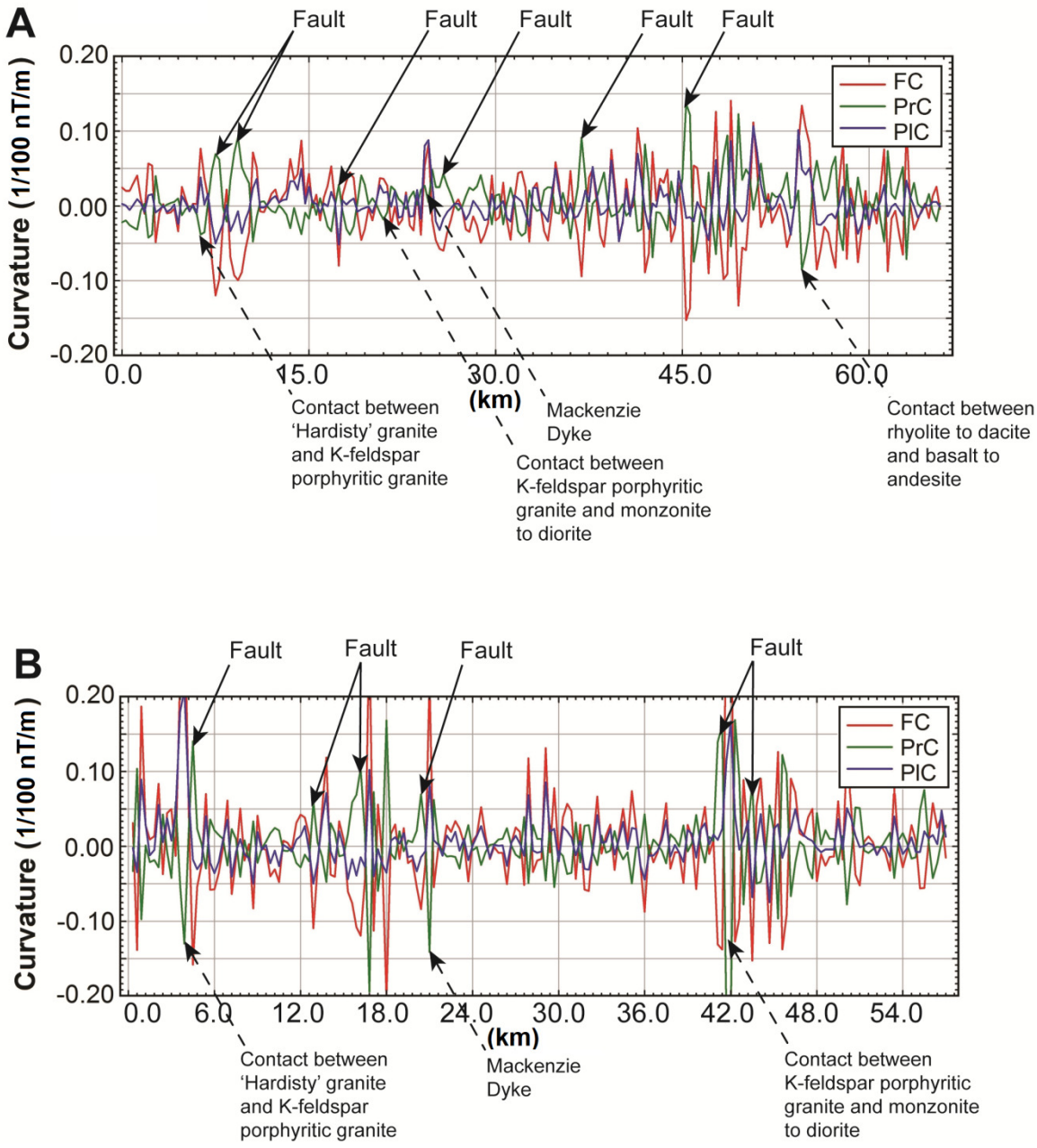

Figure 2.7. Curvature analysis along A-A' (A) and B-B' (B). The location of key mapped geology and structure (Figure 4B) are indicated by arrows. Faults are solid black arrows while dykes and lithological contacts are dashed black arrows. Based on the curvature attributes of mapped features other potential unmapped faults and dykes may be identified along the profiles.

Taking this a step further analysis can move from profile to grid format. However, to choose appropriate curvature cut-offs we need to consider the statistics of the curvature data set (Table 2.2). Statistical analysis allows the user to set cut-offs to define a 'fault' or 'dyke' as each feature may show up as a separate population when looking at the histogram or Q-Q (quantile-quantile) plot analysis. The former displays the distribution based on number of occurrences and latter is the graphical representation of the comparison between two probability distributions. The histogram (Figure 2.8) and Q-Q plots (Figure 2.9) show the data have a high degree of kurtosis (243.6, 128.0, and 215.1 for FC, PrC, and PlC respectively) indicating the maximum and minimum curvatures occur at a greater frequency than a normal distribution (kurtosis of 0).

	FC	**PrC**	**PlC**
Mean	0.000±0.191	0.010±0.123	0.010±0.109
Maximum	12.525	4.432	6.076
Minimum	-6.695	-6.449	-2.959

Table 2.2. Descriptive statistics of the curvature analysis data set. Units are 1/100 nT/m.

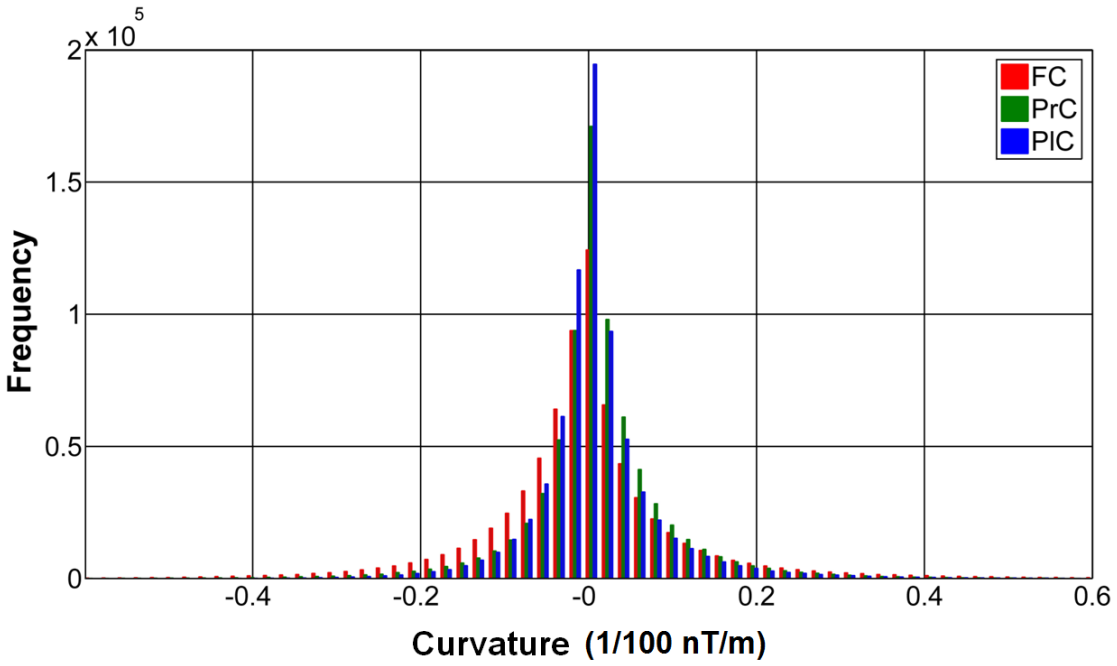

Figure 2.8. Histogram analysis of FC, PrC, and PlC. Data displays a non-Gaussian distribution since the highest concentration of values is centered at the mean for each curvature data set.

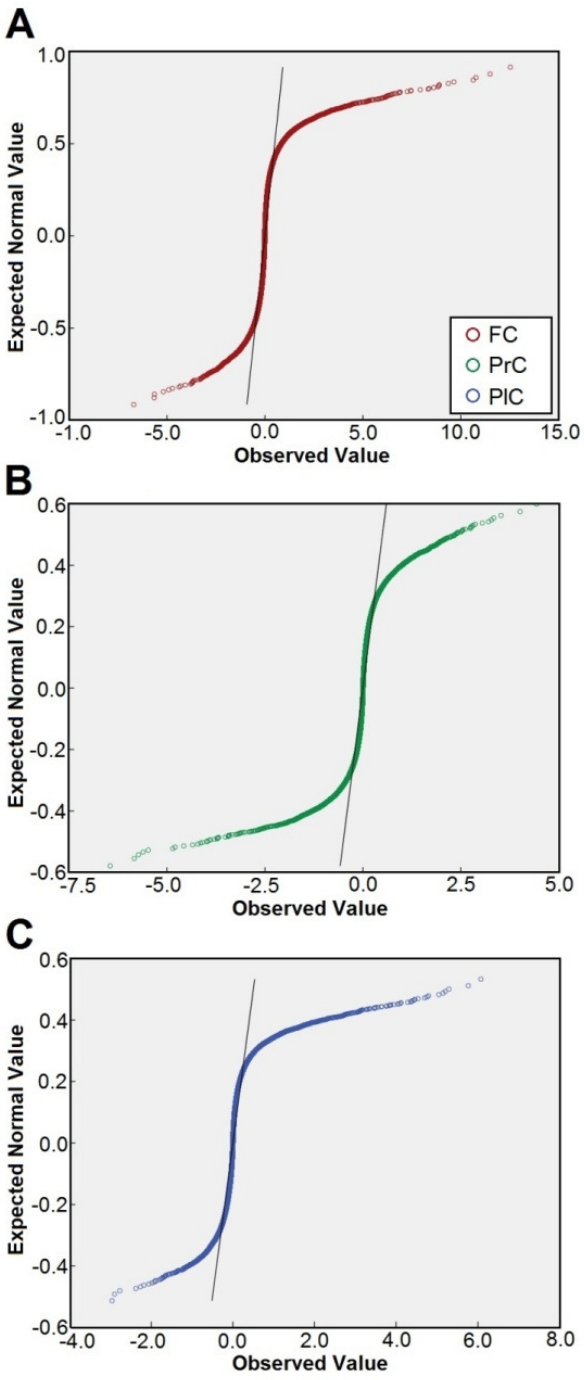

Figure 2.9. Q-Q plot analysis of FC (A), PrC (B), and PlC (C) showing the high degree of kurtosis (leptokurtic). The data exhibits a heavy-tailed population and a high concentration of values around the mean (relative to a standard normal distribution).

Standard curvature analysis applied to terrain surfaces for drainage basin analysis classifies 'moderate relief' as curvatures -0.5 to 0.5 and 'extreme relief' as curvatures -4 to 4 (Zevenbergen and Thorne, 1987). As mentioned earlier, when curvature analysis is applied to a magnetic surface the definition of low, moderate, and extreme relief is defined by the statistics. We assign low, moderate, and extreme relief to be within 1σ, 2σ, and 3σ of the mean value for each curvature type (Table 2.3).

	FC	**PrC**	**PlC**
Low (1σ)	-0.191 to 0.191	-0.113 to 0.223	-0.099 to 0.119
Moderate (2σ)	-0.382 to -0.191 0.191 to 0.382	-0.236 to -0.113 0.223 to 0.256	-0.208 to -0.099 0.119 to 0.228
Extreme (3σ)	-0.573 to -0.382 0.382 to 0.573	-0.359 to -0.236 0.256 to 0.379	-0.317 to -0.208 0.228 to 0.337

Table 2.3. Data set defined low, moderate, and extreme relief. Units are 1/100 nT/m.

Based on observations from profiles A-A' and B-B' in Figure 2.7 and the statistics in Tables 2.2 and 2.3 faults were identified as those having a FC less than 0.191 nT/m, a PrC greater than 0.0223 nT/m, and a PlC between 0 nT/m and -0.099 nT/m (Figure 2.10A and 2.10B). These values are appropriate considering a fault will be a magnetic low and nearly linear in map view. Dykes and magmatic lithology contacts had a PlC and FC combined value greater than 0.31 nT/m (0.191 nT/m + 0.119 nT/m) and a PrC less than zero (Figure 2.10C and 2.10D). The specific cut-off magnitudes for each curvature were chosen to capture the greatest number of curvature anomalies (1σ or 68% about the mean). For comparative purposes Figure 2.11 exhibits the solutions for low, moderate, and extreme curvatures in blue, green, and red respectively.

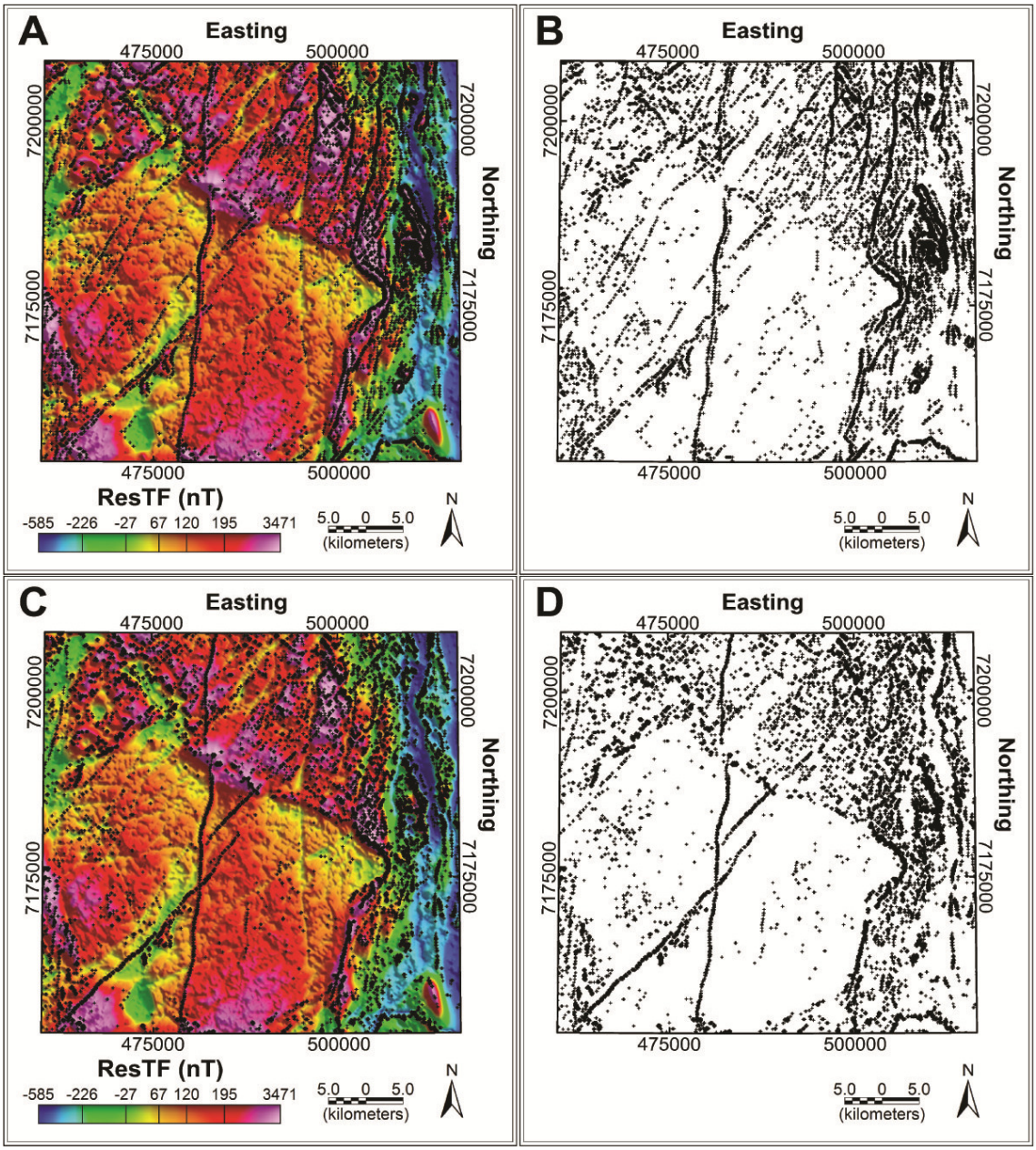

Figure 2.10. Curvature analysis with faults (A, B) and dykes (C, D) are identified by black +, based on their combined (FC, PrC, PlC) curvature statistics. Curvatures associated with either low or high magnetic relief are identified on the ResTF to show coincidence with apparent magnetic lows (A) or highs (C). The faults (B) and dykes / lithological contacts (D) become even more apparent when the curvatures are shown independent of ResTF.

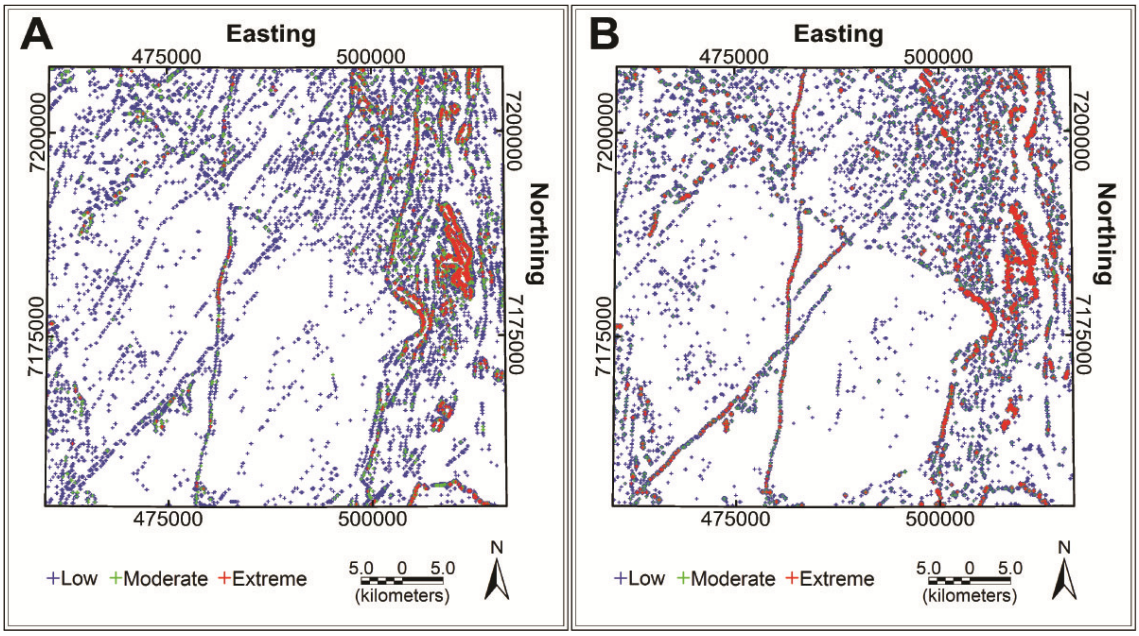

Figure 2.11. Low, moderate, and extreme faults (A) and dykes (B) – as defined by the curvature statistics in Table 2.3. The extreme and moderate relief have less detail than the low relief solutions; however they indicate some major geology and structure including the mafic and Mackenzie dykes and phase boundary between the k-feldspar porphyritic granite and monzonite/diorite.

Combining Figures 2.10B and 2.10D allows for quick identification of the source type (Figure 2.12A). The original curvature grids (Figure 2.5B, 2.5C, and 2.5D) are reclassified to binary values based on the above 1σ statistics to make the curvature analysis outputs more useful for field mapping. This causes all positive and negative 'low' relief anomalies to be of value 1, while non-'low' anomalies are 0. A 'thinning' algorithm (ArcMap[1]) is then applied to the reclassified binary grid to create vector lineaments. Thinning is the process where all grid cells with a value of 1 are combined along the spatial median to form a polyline so long as a specified thickness of *t* is met Cells with a value of 0 are considered null and therefore not included in the thinning output.. A thickness of 1000 or 2.5 times the flight line spacing was selected to avoid possible Nyquist effects. The polylines representing dykes and faults seen in Figure 2.10B are a vector file that can be included as an independent GIS layer and included as a valuable structural component in any digital geologic map.

[1] ArcGIS®, ArcGIS Desktop, ArcMap

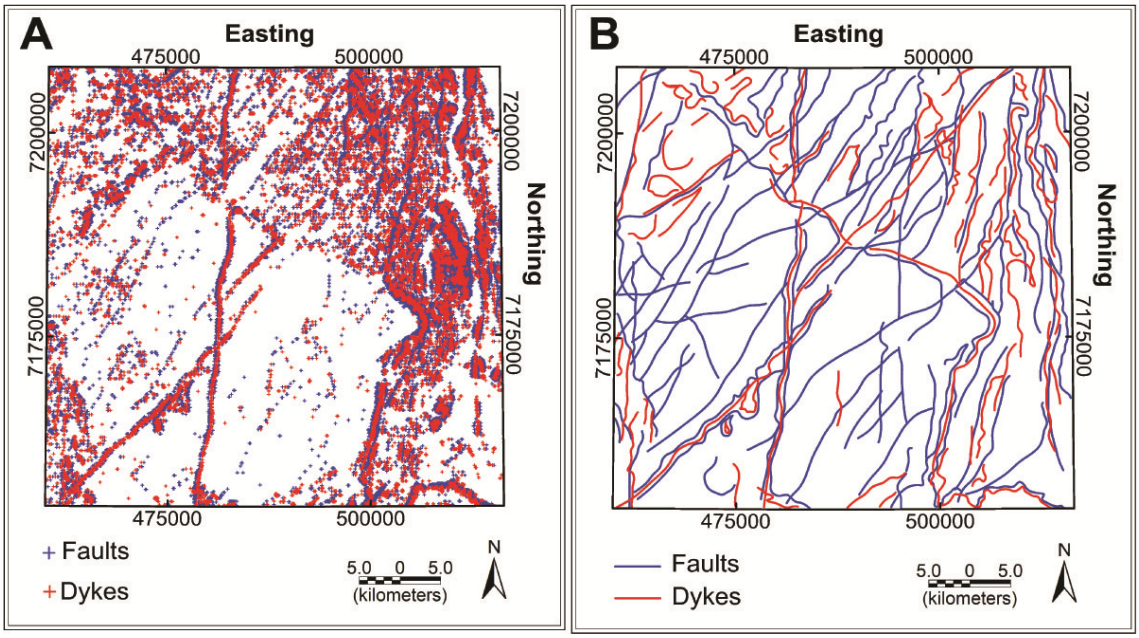

Figure 2.12. The combined curvature analysis derived from Figure 2.10 with dykes in red and faults in blue (A). The original curvature data can be reclassified in grid format (Figure 2.4B,2. 4C, 2.4D) to produce an easy to read polyline file (B) applicable as an additional layer to most digital geologic maps.

2.6 Conclusion

Curvature analysis allows the user to discriminate the location and type of a magnetic source based on the degree of curvature of the resultant magnetic field anomaly. The method is implemented by calculating the full, profile and plan curvatures of magnetic data. This is followed by statistical analysis to identify specific magnetic source populations representing different structural and intrusive features. The statistics are used to generate a series of raster images outlining different severities of curvature. The raster images may be vectorized using a GIS thinning algorithm to produce polylines representing geological lineaments.

Curvature analysis was applied to a high resolution aeromagnetic data set over the Wopmay Orogen, Northwest Territories, Canada. The curvature method presented here isolated numerous and separate populations of dykes and faults in a broad range of bedrock lithologies. These automatically and objectively derived structures comprise a very useful component of a bedrock geology map and can be included as a separate and integral part of a geologic database within a Geographic Information System. These structures identified through curvature analysis are very useful for mineral exploration studies as faults, dykes and lithological contacts play a significant role as vectors to mineralization in many mineral deposit types.

Curvature analysis conducts feature identification on an automated basis through numerous map products. In this study, we only presented curvature and two secondary map products, profile and plan curvature; however, curvature analysis may produce numerous curvature map outputs, each of which accentuate different features. Curvature analysis also allows the more experienced user to isolate specific features based on the statistics and geometry of curvature anomalies.

2.7 Acknowledgements

The authors wish to thank V. Jackson, L. Ootes from the Northwest Territories Geoscience Office and L. Corriveau of the Geological Survey of Canada for their support and assistance on bedrock geology, petrology, and helpful discussion of the manuscript. This work was in part funded by numerous programs: the IOCG-Great Bear (00410) and Remote Predictive Mapping (GKM005) projects of the Geomapping for Energy and Minerals program through Natural Resources Canada; the South Wopmay Bedrock Mapping project of the Northwest Territories Geoscience Office through Aboriginal Affairs and Northern Development Canada; and the Polar Continental Shelf Program (50709). The project was conducted through various collaborative agreements between Natural Resources Canada, the Northwest Territories Geoscience Office, the Community Government of Gamètì, and Fortune Minerals Limited. The authors would also like to acknowledge the contribution by the Editor, Associated Editor, and Reviewers for their recommended revisions.

2.8 References

Archibald, N., Gow P., and Boschetti, F., 1999, Multiscale edge analysis of potential field data: *Exploration Geophysics*, 30, 38-44.

Barbosa, V.C.F., Silva, J.B.C., and Medeiros, W.E., 1999, Stability analysis and improvement of sturctural index estimation in Euler deconvolution: *Geophysics*, 64 (1), 48-60, DOI: 10.1190/1.1444529.

Chernicoff, C., Richards, J., and Zappettini, E., 2002, Crustal lineament control on magmatism and mineralization in northwestern Argentina: geological, geophysical, and remote sensing evidence: *Ore Geology Reviews*, 21 (3-4), 127-155, DOI: 10.1016/S0169-1368(02)00087-2.

Crafford, A., and Grauch, V., 2002, Geologic and geophysical evidence for the influence of deep crustal structures on Paleozoic tectonics and the alignment of world-class desposits, north-central Nevada, USA: *Ore Geology Reviews*, 21 (3-4), 157-184, DOI: 10.1016/S0169-1368(02)00088-4.

Chopra, S., and Marfurt, K., 2007, Curvature attribute applications to 3D surface seismic data: *The Leading Edge*, 26 (4), 404-414, DOI: 10.1190/1.2723201.

Collatz, L., 1960, Numerical Treatment of Differential Equations (Third ed.). Springer Verlag, pg. 542, stencil 2.

Cooper, G.R.J., 2010, Enhancing ridges in potential field data: *Exploration Geophysics*, 41, 170-173.

Cooper, G.R.J., and Cowan, D.R., 2006, Enhancing potential field data using filters based on the local phase: *Computers and Geosciences*, 32 (10), 1585-1591.

Cooper, G.R.J., and Cowan, D.R., 2008, Edge enhancement of potential field data using normalised statistics: *Geophysics*, 71 (3), H1-H4.

Corriveau, L., Ootes, L., Mumin, H., Jackson, V., Bennett, V., Cremer, J.F., Revard, B, McMartin, I., and Beaudoin, G., 2007a, Alteration vectoring to IOCG(U) deposits in frontier volcanic-plutonic terrains, Canada. In: *'Proceedings of Exploration 07: Fifth International Conference on Mineral Exploration*, Milkereit, B. (Ed.) p.. 1171-1177.

Corriveau, L., 2007b. Iron oxide-copper-gold deposits: a Canadian perspective. In: Goodfellow, W.D. (Ed.) *Mineral deposits of Canada: a synthesis of major deposit-types, district metallogeny, the evolution of geological provinces and exploration methods*.

Geological Association of Canada, Mineral Deposits Division, Special Publication 5: pp 307–328

Corriveau, L., Brouillette, M.I., Bleeker, W., Jackson, V.A., Montreuil, J.F., Mumin, H., Harvey, B., Kiss, F., Carson, J., 2009, The IOCG/Multiple Metals - Great Bear Region (NWT) project, Geomapping for Energy and Minerals Program: Field results, status and progress: In Jackson, V. & Palmer, E. (compilers), *37th Annual Yellowknife Geoscience forum Abstracts*. Northwest Territories Geoscience Office, Yellowknife, NT, YKGSF Abstracts Volume 2009, p. 9.

Corriveau, L, and Mumin, A.H., 2010a, Exploring for iron oxide copper-gold deposits: the need for case studies, classifications and exploration vectors: In Corriveau, L., Mumin A.H. (Eds.), *Exploring for iron oxide copper-gold deposits: Canada and global analogues*, Geological Association of Canada, Short Course Notes 20: pp 1–12.

Corriveau, L., Williams, P.J., Mumin, A.H., 2010b, Alteration vectors to IOCG mineralization from uncharted terranes to deposits: In Corriveau, L., Mumin, A.H. (Eds.), *Exploring for iron oxide copper-gold deposits: Canada and global analogues*, Geological Association of Canada, Short Course Notes 20: pp 89–110.

Eaton, D., and Vasudevan, K., 2004, Skeletonization of aeromagnetic data: *Geophysics*, 69 (2), 478-488.

Ernst, R., and Baragar, W., 1992, Evidence from magnetic fabric for the flow pattern of magma in the Mackenzie giant radiating dyke swarm: *Nature*, 356, 511-513.

Evans, I.S., 1972, General geomorphometry, derivatives of altitude and descriptive statistics: In Chorley, R.J. (Ed.), *Spatial Analysis in Geomorphology*, p.36, Methuen, London.

Fitzgerald, D., Reid, A., and McInerney, P., 2004, New discrimination techniques for Euler deconvolution: *Computers and Geosciences*, 30, 461-469.

Gandhi, S.S., 1994, Geological setting and genetic aspects of mineral occurrences in the southern Great Bear magmatic zone, Northwest Territories: *Geological Survey of Canada Bulletin*, 475, 63-96.

Gandhi, S.S., Mortensen, J.K., Prasad, N., and van Breeman, O., 2001, Magmatic evolution of the southern Great Bear continetal arc, northwestern Canadian Shield: Geochronological constraints: *Canadian Journal of Earth Sciences*, 38, 767-785.

Gerovska, D., and Araúzo-Bravo, M.J., 2006, Calculation of magnitude magnetic transforms with high centricity and low dependence on the magnetization vector direction: *Geophysics*, 71 (5), 121-130.

Hansen, R.O., and deRidder, E., 2006, Linear feature analysis for aeromagnetic data: *Geophysics*, 71 (6), L61-L67.

Hildebrand, R., Hoffman, P. and Bowring, S., 1987, Tectono-magmatic evolution of the 1.9-Ga Great Bear magmatic zone, Wopmay Orogen, northwestern Canada: *Journal of Volcanology and Geothermal Research*, 32, 99-118.

Hilterman, F.J., 1975, Amplitudes of seismic waves – A quick look: *Geophysics*, 40, 745.

Hoffman, P.F., and Hall, L., 1993, Geology, Slave craton and environs, District of Mackenzie, Northwest Territories: *Geological Survey of Canada Open File 2559*, 1 map scale 1:1,000,000.

Jackson, V.A., 2008, Preliminary geologic map of part of the Southern Wopmay Orogen (parts of NTS 86B and 86C; 2007 updates); Northwest Territories Geoscience Office, *NWT Open Report 2008-007*. 1 map, scale 1:100,000, and accompanying report, 51 p.

Jackson, V.A., and Ootes, L., 2011, Preliminary Geologic Map of the South-Central Wopmay Orogen (parts of NTS 86B, 86C, and 86D); results from 2009 and 2010; Northwest Territories Geoscience Office, *NWT Open Report 2011-007*. 1 map, scale 1:100,000, and accompanying report, 41 p.

Keating, P., 2009, Improved use of the local wavenumber in potential-field interpretation: *Geophysics*, 74 (6), L75-L85.

Lalor, J., 1987, The Olympic Dam copper-uranium-gold-silver deposit, South Australia. 4th Circum-Pacific Energy and Mineral Resources Conference (pp. 561-567). Singapore: Horn, MK (Ed.).

Lee, M.D., Morris, W.A., and Ugalde, H., 2010, A rationale for applying magnetic terrain corrections: A case study from the Eye – Dashwa lakes pluton, Atikokan, Ontario: *Geophysics,* 75 (3), B147-B156.

Moore, I.D., Burch, G.J. and Mackenzie, D.H., 1988, Topographic effects on the distribution of surface soil, water, and the location of Ephemeral gullies: *American Society of Agricultural and Biological Engineers*, 31 (4), 1098-1107.

Moore, I.D., Grayson, R.B. and Landson, A.R., 1991, Digital Terrain Modeling: A Review of Hydrological, Geomorphological, and Biological Applications: *Hydrological Processes,* 5, 3-30.

Mumin, A.H., 2002, Scoping study for hydrothermal iron-oxide copper-gold deposits (Olympic Dam–type), *Manitoba. Report of Activities 2002*, Manitoba Industry, Trade and Mines, Manitoba Geological Survey, 303-308.

Mumin, A.H., Corriveau, L., Somarin, A.K., and Ootes, L., 2007, Iron Oxide Copper-Gold-type Polymetallic Mineralization in the Contact Lake Belt, Great Bear Magmatic Zone, Northwest Terriories, Canada: *Exploration and Mining Geology*, 16 (3-4), 187-208.

Mumin, A.H., Somarin, A.K., Jones, B., Corriveau, L., Ootes, L., and Camier, J., 2009, The IOCG-porphyry-epithermal continuum of deposits types in the Great Bear Magmatic Zone, Northwest Territories, Canada, Exploring for iron oxide copper-gold deposits: Canada and global analogues: *Geological Association of Canada, Short Course Notes 20*, 59-78.

NTGO. 2008, Airborne Magnetic and Gamma-ray Spectrometric Survey of the Southwestern Wopmay Orogen, Northwest Territories, parts of NTS 86C, 86E and 86F; Northwest Territories Geoscience Office. *NWT Open File 2008-02*; Geological Survey of Canada, Open File 5821 to Open File 5827; 70 maps and digital data.

O'Driscoll, E.S.T., 1980, The double helix in global tectonics: *Tectonophysics*, 63, 397-417.

Phillips, J., Hansen, R. and Blakely, R., 2007, The use of curvature in potential-field interpretation: *Exploration Geophysics*, 38, 111-119.

Pilkington, M., and Keating, P., 2004, Contact mapping from gridded magnetic data – comparison of techniques: *Exploration Geophysics*, 35, 306-311.

Reid, A., Allsop, J., Granser, H., Millett, A. and Somerton, I., 1990, Magnetic interpretation in three dimensions using Euler deconvolution: *Geophysics*, 55, 80-91.

Roberts, A., 2001, Curvature attributes and their application to 3D interpreted horizons: *First Break*, 19.2, 85-100.

Sigismondi, M.E., and Soldo, J.C., 2003, Curvature attributes and seismic interpretation: *The Leading Edge*, 22, 1122-1126.

Spector, A. and Grant, F.S., 1970, Statistical models for interpreting magnetic data: *Geophysics*, 35 (2), 293-302.

Twidale, C.R., 2007, E.S.T. O'Driscoll, Lineaments and ring structures: In Bourne J. A. and Twidale C.R. (Ed), *Crustal Structures and Mineral Deposits*, pp.208, Rosenburg, Australia.

Wood, J.D., 1996, The geomorphological characterization of digital elevation models: *PhD Thesis*, University of Leicester, UK.

Woodall, R., 1994, Empiricism and concept in successful mineral exploration: *Australian Journal of Earth Sciences*, 41 (1), 1-10.

Woodall, R., 2007, From Broken Hill to Olympic Dam: E.S.T. O'Driscoll's lifelong study of the structural setting of mineral deposits: In Bourne J.A. and Twidale C. R. (Ed), *Crustal Structures and Mineral Deposits*, pp.208, Rosenburg, Australia.

Zevenbergen, L.W., and Thorne, C. R., 1987, Quantitative analysis of land surface topography: *Earth surface processes and landforms*, 12, 47-56.

3.0 Statistical significance of curvature analysis: Application to aeromagnetic data

Lee, M.D., Morris, W.A., and Leblanc, G., 2012, Statistical significance of curvature analysis: Application to aeromagnetic data: *Mathematical Geosciences*, Submitted

3.1 Abstract

The computation of a magnetic grid's surficial curvature is a tool to assist in the identification of a causative magnetic source. Previous studies show full curvature and the derived attributes in profile and plan form can be used to recognize source location, edges, and differentiation of source type (e.g. dyke, fault). Statistical analysis of the curvature data set provides insight into magnetic susceptibility and dip of a source. The analysis includes the graphical construction of histograms and scatterplots. The distribution shown by these graphical outputs allows for quick analysis of frequency content and relative magnetization. Statistical analysis is quantitatively achieved with the computation of the descriptive statistics, kurtosis and skew. Skew of the curvature dataset describes the symmetry of the magnetic anomaly. Skew specifically reports the proportion of positive to negative curvature values. This provides an estimate on the magnetization of the source and whether the source is dipping. Kurtosis of the curvature dataset describes the frequency content of a magnetic signal when assessed in conjunction with the mean curvature. For example, if the mean is in proximity of zero curvature and the kurtosis is a value significantly larger than zero then the data is predominantly low-frequency sources. The statistical analysis approach is corroborated using synthetic models including single vertical source, multiple vertical sources and a dipping source. The curvature statistics for two high-resolution aeromagnetic surveys from Canada show robust analyses may be conducted simply from the histograms and scatterplots.

3.2 Background

Curvature analysis of a potential field surface (grid) may be used as a tool for locating and describe the geometry of causative sources. Curvature of a geophysical surface with emphasis on magnetics has been discussed by various authors (Roberts, 2001; Cooper and Cowan, 2006; Phillips et al., 2007; Cooper and Cowan, 2008; Cooper, 2009; Cooper, 2010; Lee et al., 2012) and applied to both synthetic and real world data sets. Roberts (2001) examines the fundamentals of curvature of a seismic surface. Phillips et al. (2007) utilize curvature as a depth-estimator. Cooper (2009, 2010) uses curvature as a tool for edge enhancement. A normalized statistics approach was shown in Cooper and Cowan (2006; 2008) where they use the association of zero curvature with the identification of steps in their potential field terracing algorithm. Lee et al. (2012) also presented the statistical significance of a curvature data set with the intention to separate dykes from faults. Here we investigate how the histogram and multivariate scatterplot analysis provide insight into the magnitude, sign and frequency content of a signal.

3.3 Theory

Curvature implements a 3 x 3 moving window computing coefficients (a through i) (Zevenbergen and Thorne, 1987) along nine different window directions. Full discussion on surficial curvature and the coefficients as used here is outlined in a geomorphology context by Evans (1972) and Zevenbergen and Thorne (1987); in a seismic context by Roberts (2001); and in a potential field context by Lee et al. (2012). Full (FC) curvature is computed using the surficial curvature equation defined by Zevenbergen and Thorne (1987) in their topographic analysis work:

$$FC = \frac{\partial^2 z}{\partial S^2} = 2(d\cos^2\phi + e\sin^2\phi + f\cos\phi\sin\phi) \quad (1)$$

Where z is in the vertical direction, S is in the maximum dip direction ϕ, and d, e and f are three directional coefficients. Profile curvature (PrC) and Plan curvature (PlC) are derived from the same coefficients:

$$PrC = -2(dg^2 + eh^2 + fgh)/(g^2 + h^2) \quad (2)$$

$$PlC = -2(dg^2 + eh^2 - fgh)/(g^2 + h^2) \quad (3)$$

Where the units are 1/nT/m and g and h are directional coefficients.

Figure 3.1 shows a simplified vector diagram of a positive magnetic anomaly field grid generated by a source whose magnetic susceptibility is greater than the host rock. Under ideal conditions FC and PlC will have similar signs while FC and PrC will have similar magnitudes.

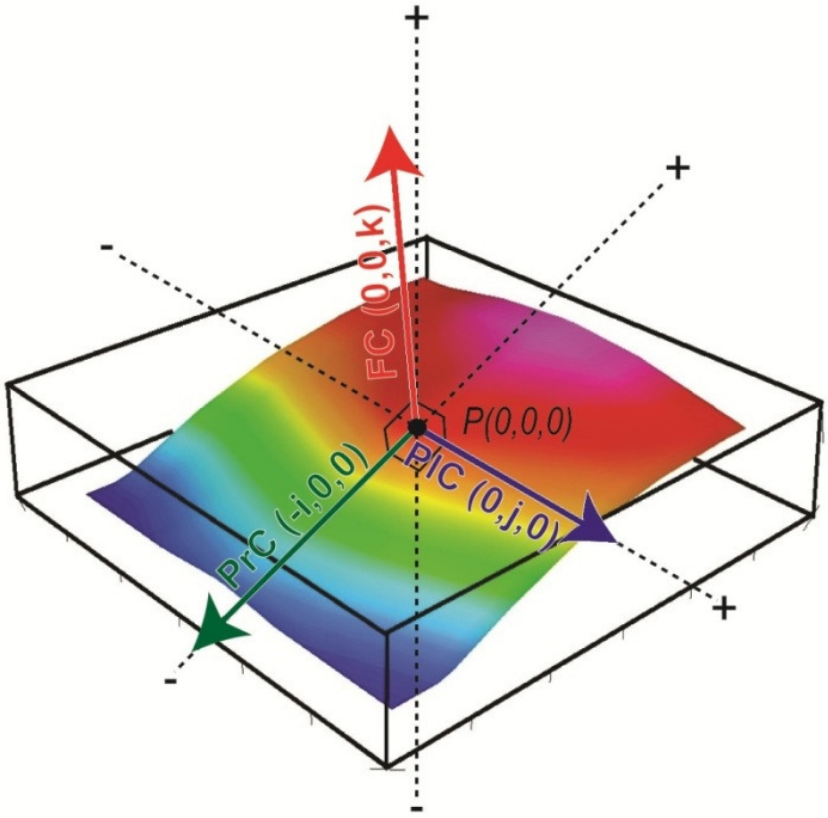

Figure 3.1. A vector diagram of curvature over a positive magnetic anomaly at point P(0,0,0). The magnetic field is positive as is FC and PlC ($j = k$ in sign). The magnitude of FC and PrC are the same but opposite in sign ($|i| = |k|$). The only exception is immediately over the source (pink shaded area on the grid surface) where $j = k$ in both sign and magnitude.

FC is the summation of PrC and PlC since PrC and PlC are orthogonal to each other. When we consider their relationships in its simplest form the conditions of curvature are:

$$\mathrm{FC} = \mathrm{PlC} - \mathrm{PrC} \quad (4)$$

$$\mathrm{PrC} = -\mathrm{FC} + \mathrm{PlC} \quad (5)$$

$$\mathrm{PlC} = \mathrm{FC} + \mathrm{PrC} \quad (6)$$

FC, PrC, and PlC ≠ 0 over and outside the source and FC, PrC, and PlC = 0 along the edge boundaries of a single, isolated anomaly. Equations (4) – (6) are demonstrated when looking at their statistical distributions and are shown in the scatterplot of Figure 3.2. If we consider a tabular, non-dipping magnetic source (κ_1) within a host rock (κ_2) PrC and FC will be inversely proportional, PlC and FC will be linearly proportional, and PlC and PrC will be inversely proportional.

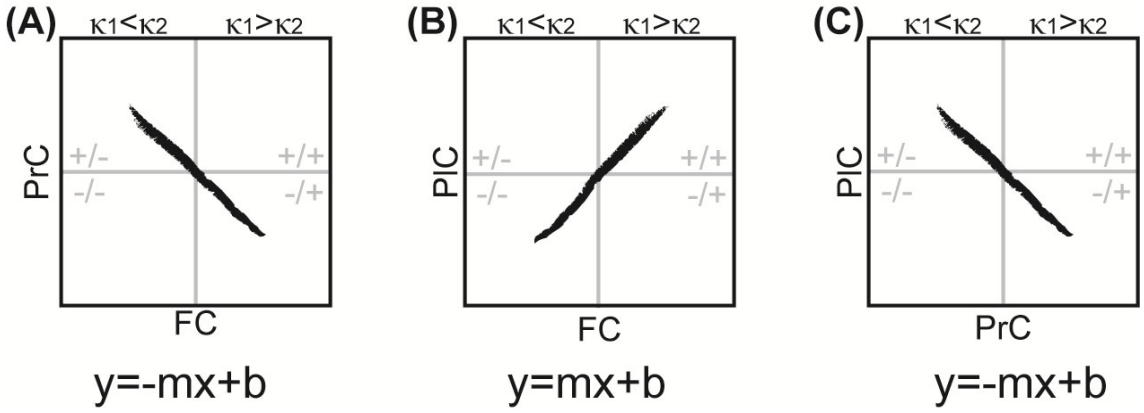

Figure 3.2. The distribution of curvatures based on equations (4) through (6) where κ_1 is the magnetic source and κ_2 is the host rock. The y axis intercept b, will be zero under ideal conditions as this represents the edge of any magnetic source.

The sign and magnitude of FC is directly related to the total field anomaly generated by a source in an applied magnetic field. A positive magnetic anomaly is generated when $\kappa_1 > \kappa_2$ such as a strongly magnetic dyke cross-cutting a weakly magnetic sediment. This results in a positive FC, a negative PrC, and a positive PlC. The converse is true where $\kappa_1 < \kappa_2$ (Lee et al., 2012).

The frequency (*f*) of a magnetic signal is intuitively related to curvature (Figure 3.3). High frequency means a large curvature value. Conversely low frequency means a small curvature value. By knowing the proportion of large and small curvature values and their sign a rapid assessment of the magnitude and frequency content of the total field is obtained. This is achieved quantitatively using the descriptive statistics kurtosis and skew. The qualitative way is generating histograms and scatterplots.

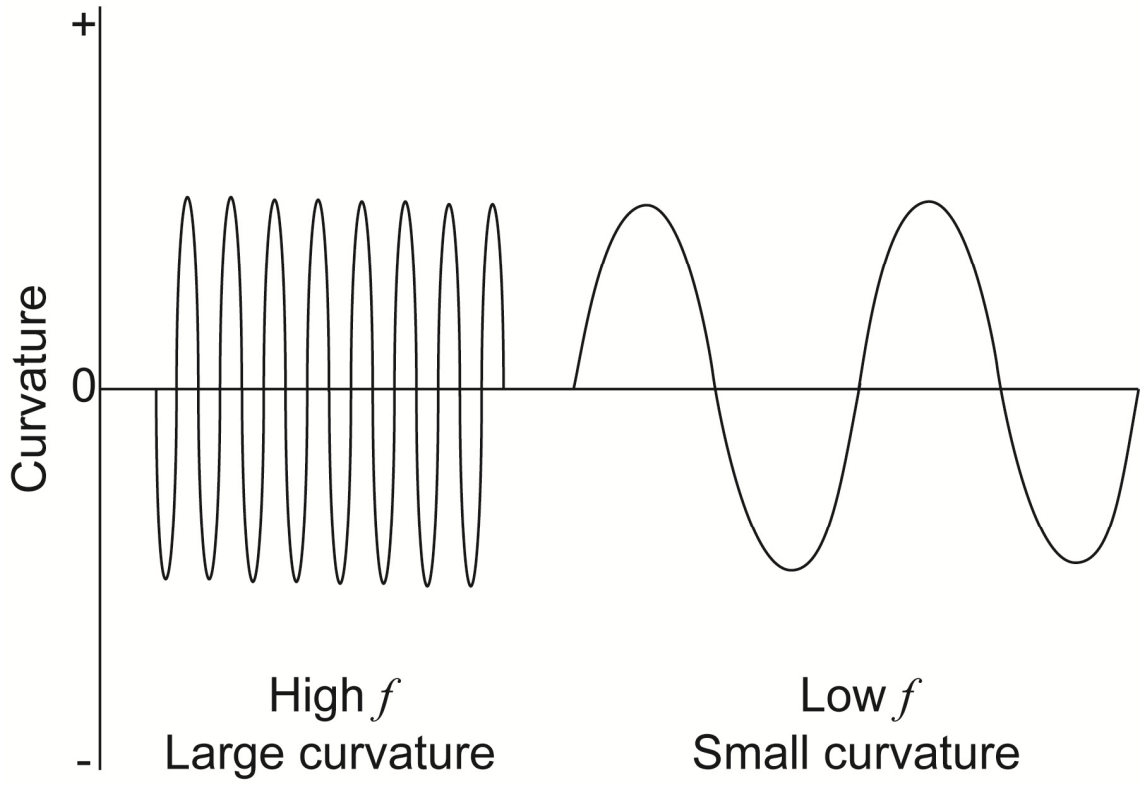

Figure 3.3. High frequencies represent large curvature values and low frequencies represent small curvature values.

Kurtosis ($\mathcal{k}$) indicates how many values are within near proximity of the mean and described as peakedness. Under ideal situations the mean of a curvature data set will be zero. The kurtosis is negative ($\mathcal{k} < 0$) if the distribution of the curvature data set is near flat (Figure 3.4A). A kurtosis of 0 identifies a normal distribution (Figure 3.4B). The data is highly peaked around the mean with fewer outliers if the data exhibits a large kurtosis ($\mathcal{k} > 0$) such as Figure 3.4C. Kurtosis provides insight into the frequency content of a signal dictated by the size, depth, and magnetic susceptibility of the source. To properly assess frequency content requires calculation of the curvature data set's mean ($\bar{x}$) as it is a marker for mean frequency. The user may quickly assess the maximum and minimum frequency content of a signal by identifying maximum and minimum curvatures.

Skew (γ) summarizes the distribution of grid values about the mean in a normal distribution. It describes the number of grid values having a positive value relative to the number having a negative value. For an ideal potential field data set of infinite extent the summation will equal zero as all positive magnetic field signal amplitudes equal all negative amplitudes. Survey grids of limited spatial extent rarely meet this criterion due to the truncation of anomalies along survey edges. It may be necessary to apply a base level shift to ensure the potential field is as close to ideal as possible. Skew provides a measure of the symmetry of the magnetic anomaly. When viewed in a vertical magnetic field a vertical-sided body will produce a symmetrical anomaly; an inclined body produces an asymmetrical anomaly. If *a priori* knowledge is available then we can assess whether the asymmetry of a histogram is due to the ratio of positive to negative magnetic anomalies or dip.

Working with a true potential field then every causative source will have equal positive and negative lobes and integrate to 0. This generates the symmetrical histogram ($\gamma = 0, \bar{x} = 0$) in Figure 3.4B. If we know the sources are vertical to sub-vertically dipping, then a skewed histogram ($\gamma \neq 0, \bar{x} \in \mathbb{R}$), such as those in Figure 3.4A and 3.4C will indicate the proportion of positive to negative magnetic field values. These principles would also be valid for a data set having undergone reduction-to-pole (RTP). The purpose of RTP is to translate the anomaly maxima directly over the source in cases where the source is located in an inclined magnetic field (Baranov, 1957). RTP results in more symmetrical anomalies producing symmetrical histograms (γ closer to 0).

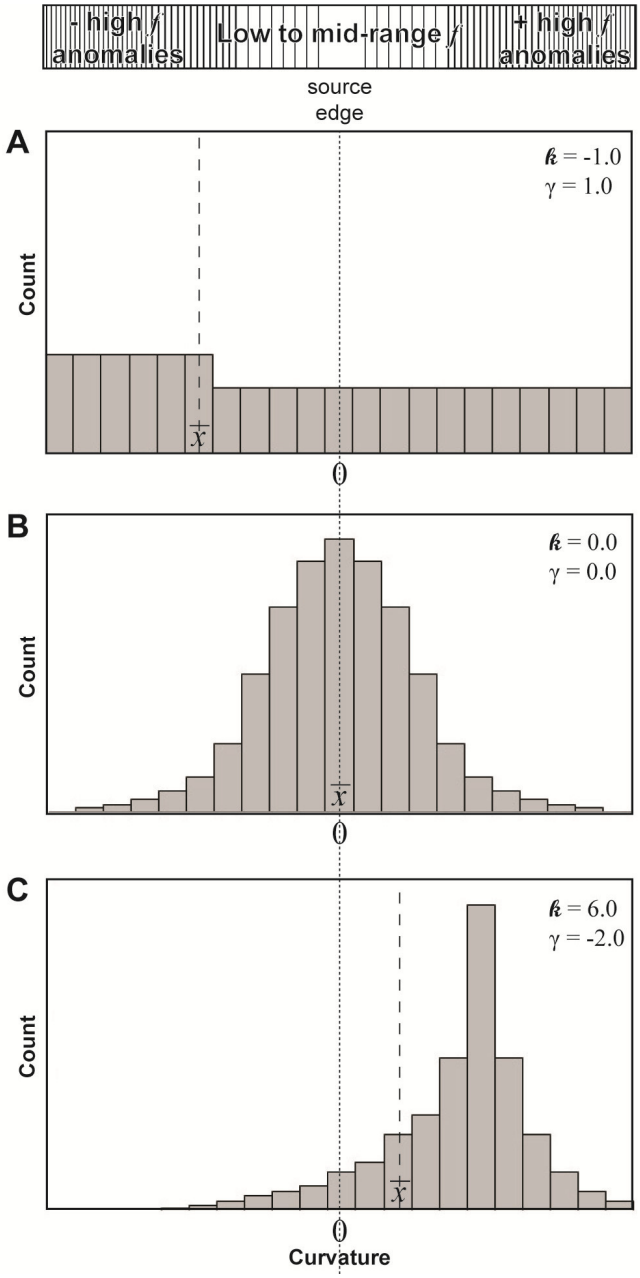

Figure 3.4. The kurtosis and skew of a curvature analysis histogram reveals information about the signal content of an aeromagnetic data set. (A) The curvature data set has a small kurtosis and positive skew. (B) The curvature data set has a kurtosis and skew of zero. These values represent a normal distribution. (C) The curvature data set has a large kurtosis and negative skew. These values represent an exponential distribution. Maximum negative or positive curvature values represent high frequency anomalies. Small curvature values represent low to mid-range frequency anomalies.

A simple, synthetic model is devised to demonstrate these properties. The model contains a north-south trending non-dipping tabular body with a magnetic susceptibility of 0.04SI, and a width, length, and depth of 50m, 2000m, and 2000m respectively. The ambient magnetic field is vertical and a magnitude of 59 000nT. The resultant curvature along profile is shown in Figure 3.5A. A statistical analysis conducted along one line orthogonal to the source's strike includes the computation of histograms and multivariate scatterplots. The scatterplots resemble the ideal distributions in Figure 3.2 and the histograms indicate the data is strongly peaked and skewed (Figure 3.5B). Most measurements are in proximity of the source edge and positive FC. This results in a large kurtosis around zero and asymmetry

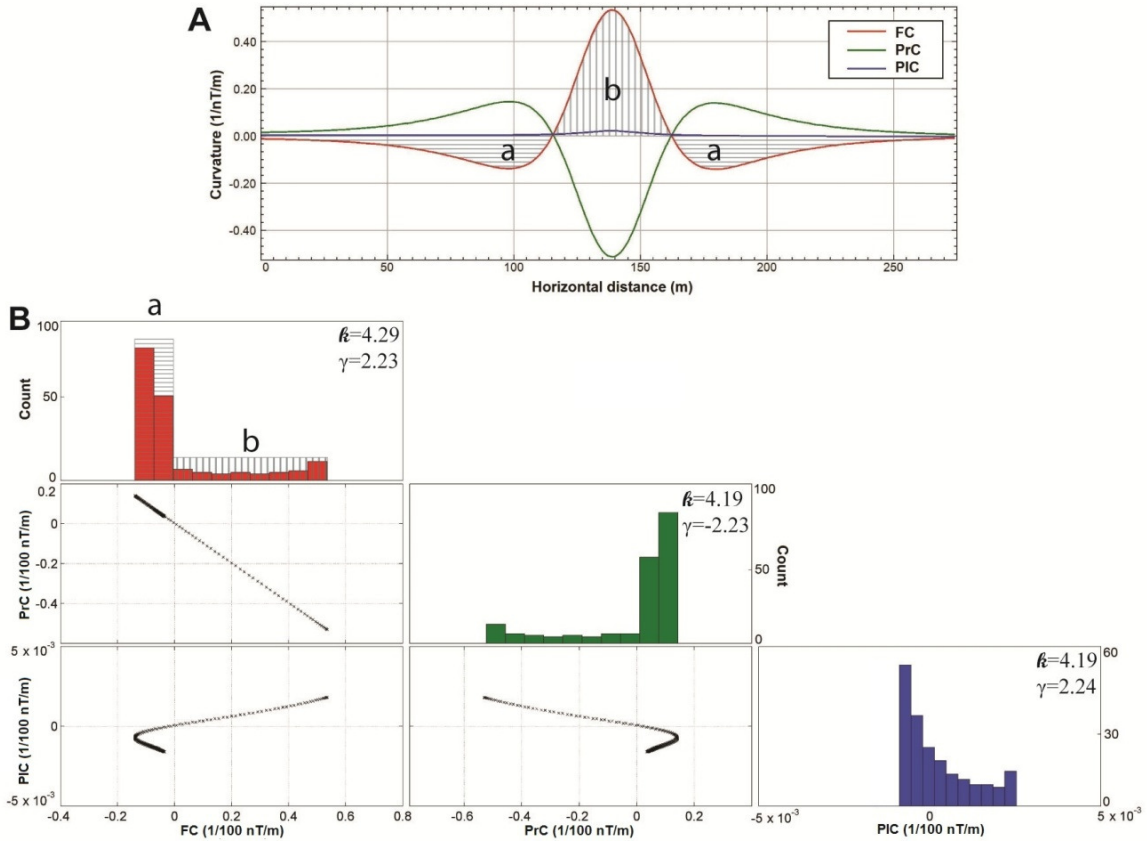

Figure 3.5. A non-dipping tabular body in a vertical magnetic field will produce the curvature profile seen in (A). The statistical analysis along one line orthogonal to strike produces the distributions in (B). The data has a kurtosis >0 and is strongly skewed. The high count of small negative FC (a) corresponds with the low frequency lobes outside the source. The low count of both small and large positive FC (b) corresponds with the high frequency peak over the source. PrC distribution is the inverse of FC and PlC distribution is nearly similar to FC.

Dipping the same tabular body 45° towards the east shows FC and PrC remains inversely proportional to PrC (Figure 3.6B). The distribution of PlC has significantly changed from Figure 3.5B. It is important to note PlC has a very small range with a mean around zero because the modelled source is tabular. A tabular source should produce a PlC of zero, however non-zero curvature values are obtained due to inherent gridding artefacts. As dip increases the data has a lower kurtosis and is less skewed.

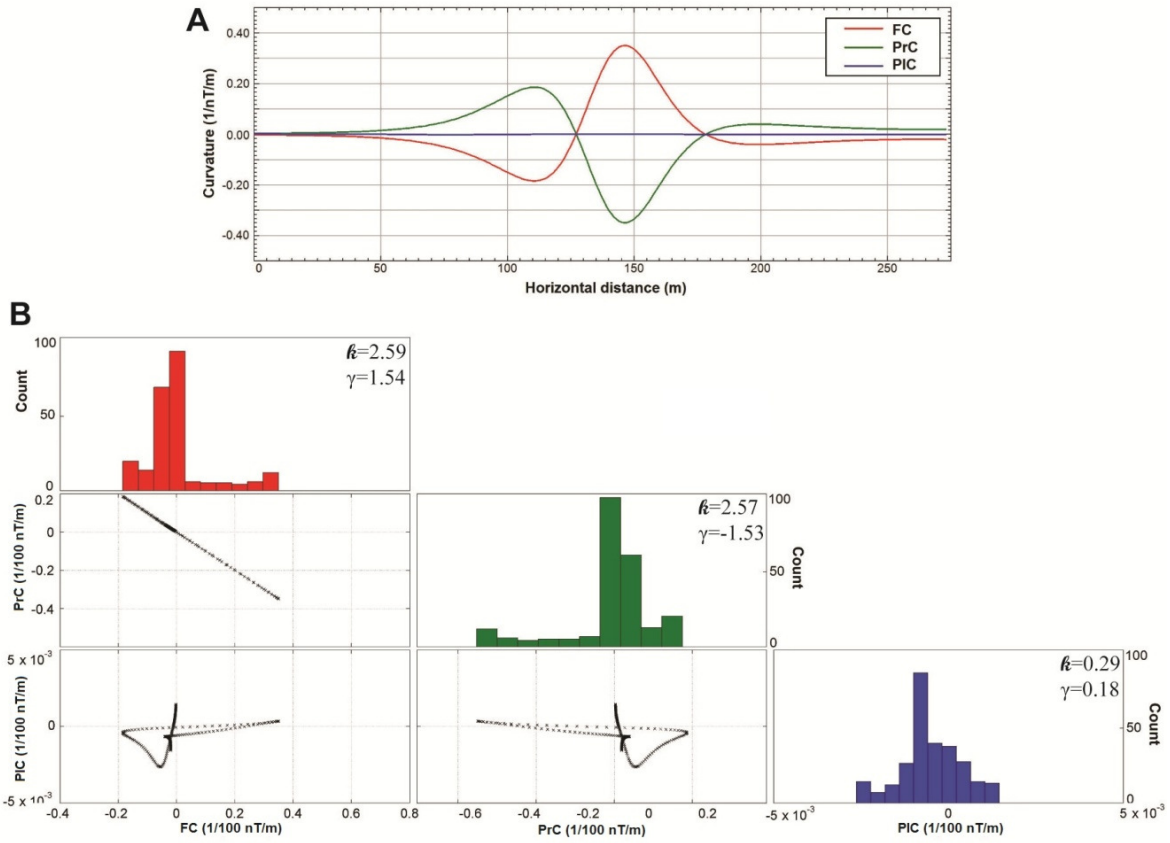

Figure 3.6. A tabular body dipping 45° eastward in a vertical magnetic field will produce the curvature profile in (A). Statistical analysis along one line orthogonal to strike produces the distributions in (B). The data is highly peaked around zero due to signal proximal to source edges. The curvature distribution is asymmetrical since the source is dipping. We can assess the distribution as we did for Figure 3.5. The high count of small negative FC corresponds to the western negative lobe outside the source. The low count of small and large positive curvatures corresponds to the eastern peak over the source.

As the symmetry of the magnetic anomaly increases so does the curvature data's distribution. Two identical non-dipping tabular bodies with inverse susceptibilities (0.04SI and -0.04SI) produce reciprocal anomalies (Figure 3.7A). There are equal occurrences of positive and negative curvature values which results in FC, PrC, and PlC to be nearly symmetrical about $\bar{x}$. This results in a skew of about zero. FC and PrC show a high count for small curvature values which represent the lobes outside the source. The small count of large curvature values represents the peaks over the source. PlC is highly peaked around the mean of 0. These results are reasonable considering the edge in plan view is straight.

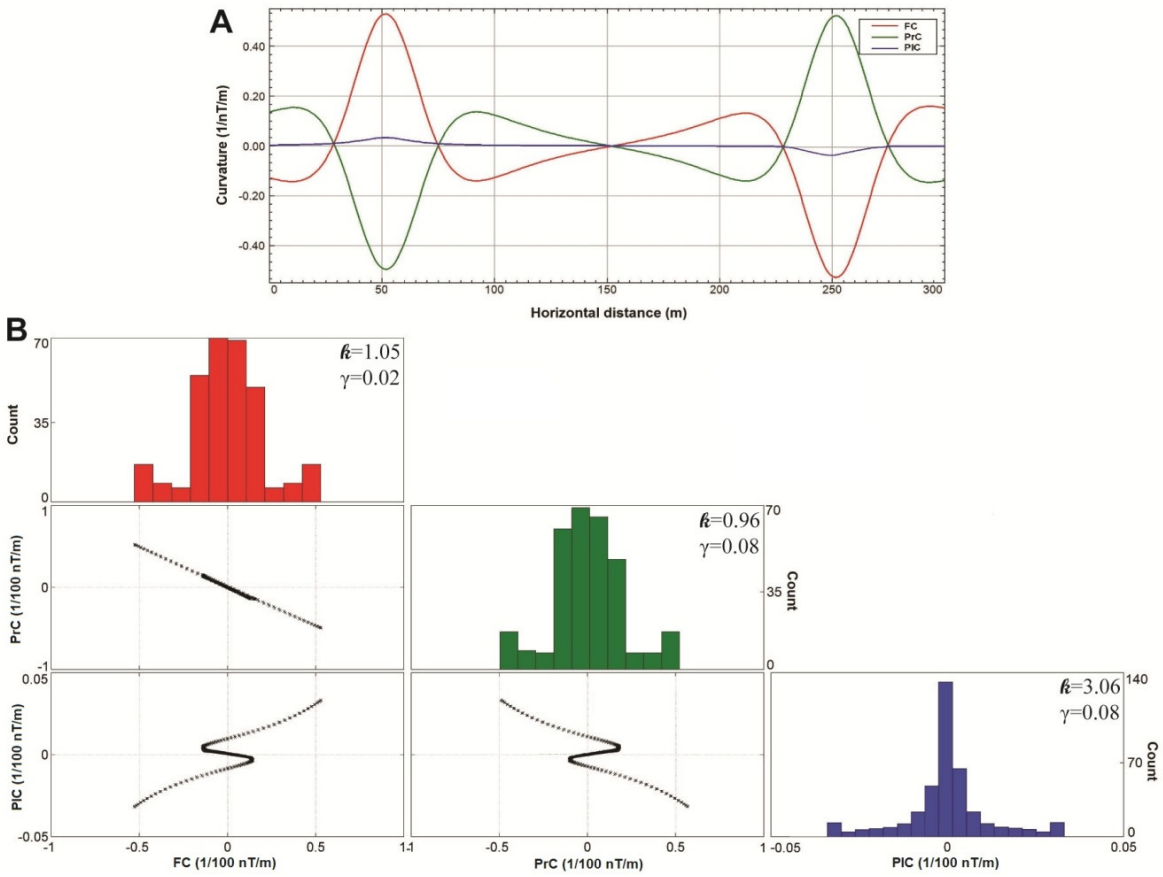

Figure 3.7. Two non-dipping tabular bodies of opposite susceptibilities in a vertical magnetic field will produce the curvature profile seen in (A). The statistical analysis along one line orthogonal to strike produces the distributions in (B). The FC and PrC data has a near-normal distribution and is symmetrical about zero. PlC is highly peaked since a tabular source is straight.

Statistical analysis was computed for three geometrically-identical, non-dipping tabular bodies of susceptibility 0.4SI, 0.04SI, and 0.004SI to evaluate the effect of varying magnetization. Figure 3.8 shows the curvature histograms for the three tabular bodies of varying magnetization and their associated kurtosis and skew. Skew remains the same regardless of magnetization because the geometry of the magnetic anomaly does not change. Kurtosis does change with magnetization and decreases by 0.1 with each decreasing order of magnetization. This is because curvature range increases with increasing amplitude and ultimately frequency.

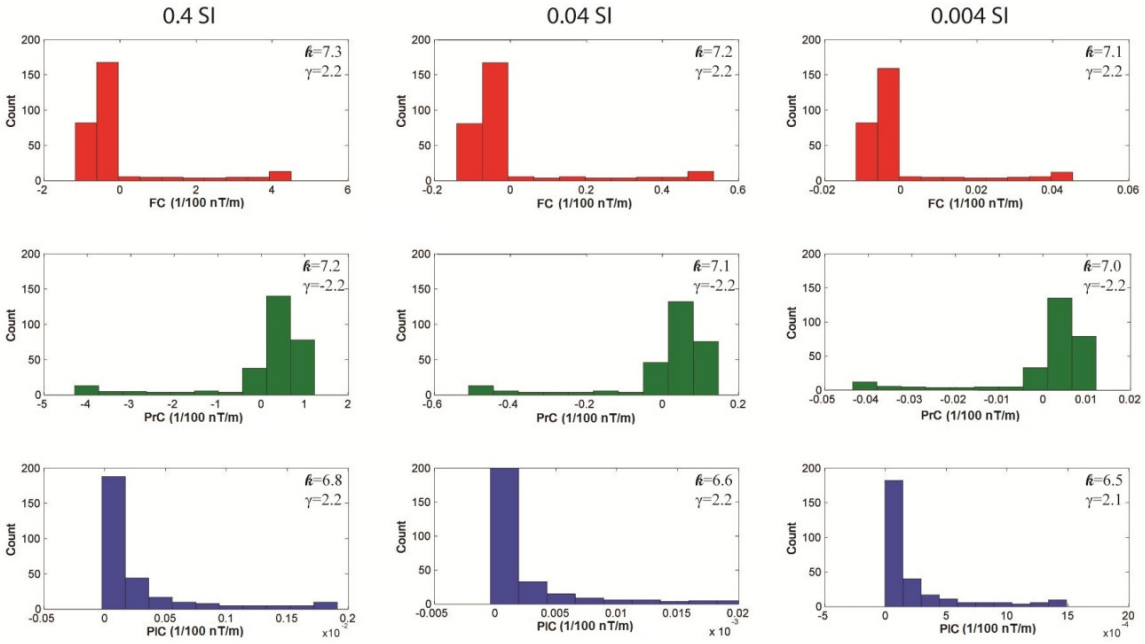

Figure 3.8. Comparison of histograms for FC (top), PrC (middle), PlC (bottom) of three identical tabular sources of different magnetic susceptibility: 0.4SI (left), 0.04SI (middle), 0.004SI (right). The range of curvature values along the Y axis changes by an order proportional to changes in magnetic susceptibility. The skew remains identical as the geometry of the anomaly does not change with varying susceptibility. The kurtosis decreases slightly with decreasing magnetic susceptibility. This is caused by an increase in low frequency content.

3.4 Survey specifications

Two real world data aeromagnetic sets have been compared by assessing the statistics of their computed curvatures (Figure 3.9). The first data set is a 2007 high resolution aeromagnetic data set from the southern portion of the Paleoproterozoic Wopmay Orogen, Northwest Territories, Canada (NTGO, 2008). The second data set is a total field aeromagnetic survey flown over the southern portion of Ontario, Canada in 1998 and 1999. The aeromagnetic survey is over crystalline rocks and Precambrian geologic domains which are overlaid by relatively magnetically transparent sedimentary cover.

The flight lines for both surveys were flown east-west at 400m intervals along a terrain-draped surface with an elevation of 150m.

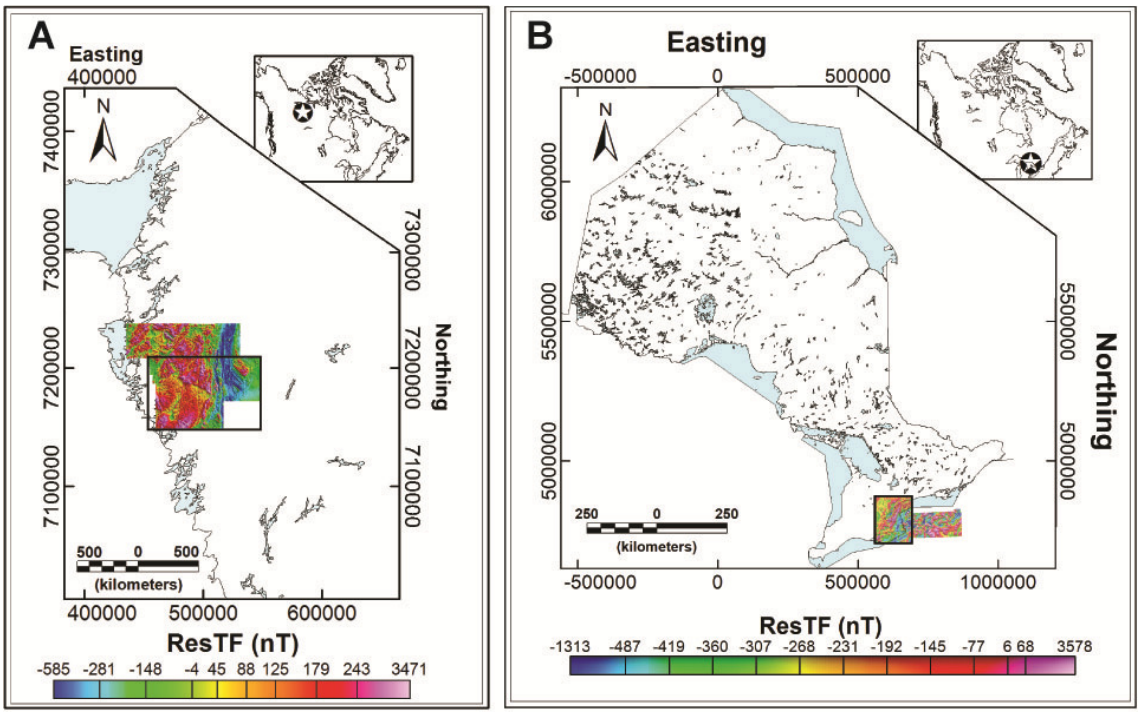

Figure 3.9. Location of the Wopmay Orogen (A) and Southern Ontario (B) aeromagnetic surveys and study area (bold black rectangle) in Canada (✪).

3.5 Results

The scatterplots of all curvatures for the Southern Wopmay and Southern Ontario data sets (Figure 3.10) abide equations (4) through (6) and Figure 3.2. The R^2 value for FC versus PrC is closest to the perfect-fit value of 1 indicating the strongest linear relationship. FC and PlC also show an R^2 value indicating a preferential linear alignment. The R^2 value for PrC versus PlC is not a strong linear relationship because they are normal to each other and their values are independent of each other. Outliers visible in each scatterplot are attributed to gridding effects and truncated anomalies along survey perimeters.

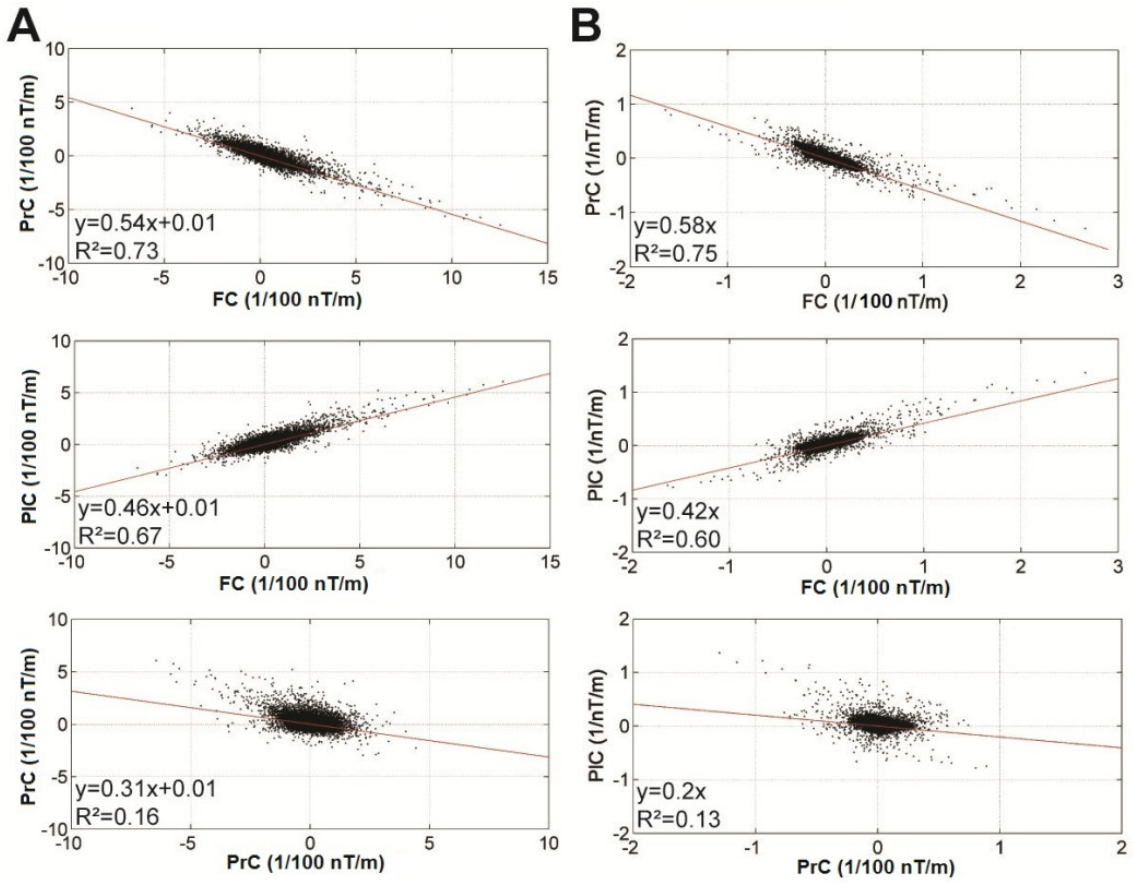

Figure 3.10. Multivariate scatterplot analysis for Southern Wopmay (A) and Southern Ontario (B) data sets. The linear trend is indicated with a red line along with its equation and R^2. Distribution of data complies with equations (4)-(6) and Figure 3.2. The y intercept of 0 remains the same for PrC vs. FC and PlC vs. FC since the source is tabular.

Histogram analysis (Figure 3.11) permits insight into the nature of the data. Both data sets have a large kurtosis ($\mathcal{k} \gg 0$), a slight skew and the mean is centered near zero. These descriptive statistics of curvature have been shown in previous studies for the Southern Wopmay aeromagnetic data set (Lee et al., 2012). A mean of 0 indicates the curvature around the boundary of all magnetic sources. The bulk frequency content in Figure 3.11A represents the host rocks which are massive granitoids of the Great Bear Magmatic Zone. The Southern Ontario data (Figure 3.11B) has a smaller range of curvature values than the Southern Wopmay data but the highest count around the mean of 0. This results in a larger kurtosis value. These results indicate more low frequency magnetic anomalies resulting from an increase in source-sensor separation due to the thick sequence of paleosediments overlying Southern Ontario. Due to the high kurtosis values only a subset of 20 of the 1000 calculated bins are displayed in Figure 3.11.

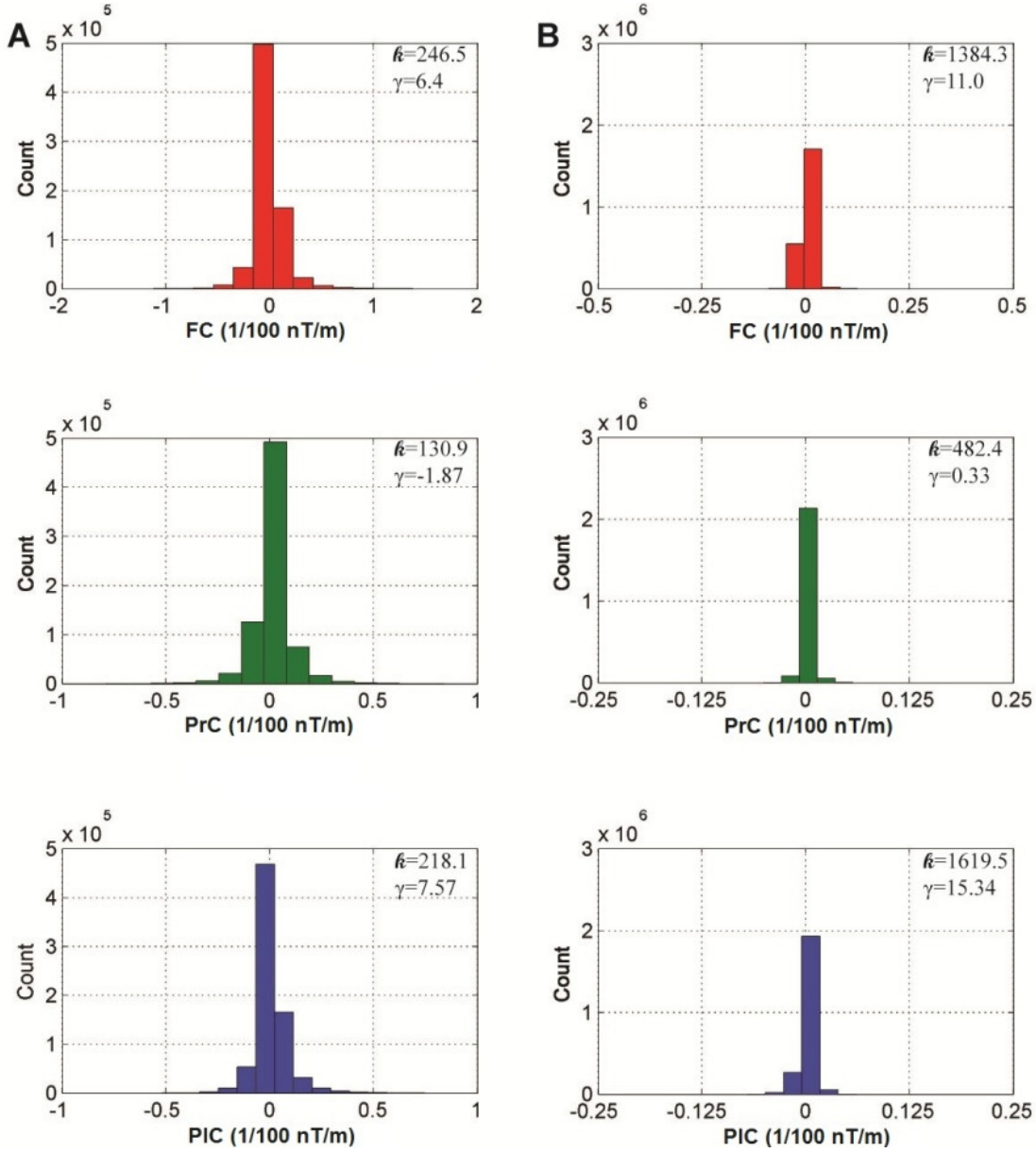

Figure 3.11. Histograms of curvature data sets from Southern Wopmay (A) and Southern Ontario (B). All kurtosis and skew values indicate the data is strongly peaked ($k \gg 0$) with varying symmetry. Due to the high kurtosis value, only a subset of the bins is shown although the histogram is divided into 1000 bins. These descriptive statistics show the data sets are dominated by small curvature values and indirectly the data sets are dominated by low to mid-range frequency magnetic anomalies. These anomalies represent host rocks dominating the spatial extent of the survey areas.

If we consider three east-west lines of data from Southern Ontario (Figure 3.12) their respective histograms (Figure 3.13) will vary depending on the shape and magnitude of the anomalies intersected. Line 1 (Figure 3.13A) shows a skew to the right for FC and to the left for PrC indicating more positive magnetic anomalies. The signal content along Line 1 is dominated by the positive magnetic north-south trending Central Metasedimentary Belt Boundary Zone (CMBBZ) and the Central Gneiss Belt (CGB). The former is a steeply dipping shear zone composed of carbonate rocks causing a strong positive magnetic contrast with surrounding iron-rich rocks (Forsyth et al., 1994). The latter is principally quartzofeldspathic gneisses which have undergone metamorphism and consequently are moderately magnetic. Line 2 (Figure 3.13B) exhibits a near-symmetrical distribution for FC and PrC about a mean of zero. This indicates a similar occurrence of positive and negative anomalies. This line crosses the CGB and CMBBZ as well as the Central Metasedimentary Belt (CMB), which is composed of non-magnetic marbles, quartzites, and pelites (Easton and Carter, 1995; Hildebrand and Easton, 1995). There is an outlier in the maximum positive FC range associated with the highly magnetic intrusions of the CMB along the eastern perimeter. Line 3 (Figure 3.13C) shows the data is less-kurtic and is asymmetrical. This is due to a wider range of frequencies from all three geologic terranes and results in an overall positive magnetic range. The data in Figure 7.13 appears to be more random than the scatterplots produced in Figure 3.10 but the distributions still abide by the linear trends presented in Figure 3.2.

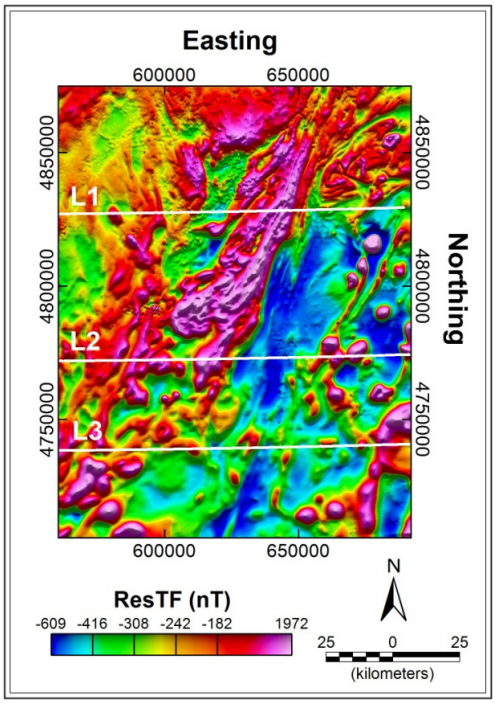

Figure 3.12. Location of lines L1, L2, and L3 within the Southern Ontario data set.

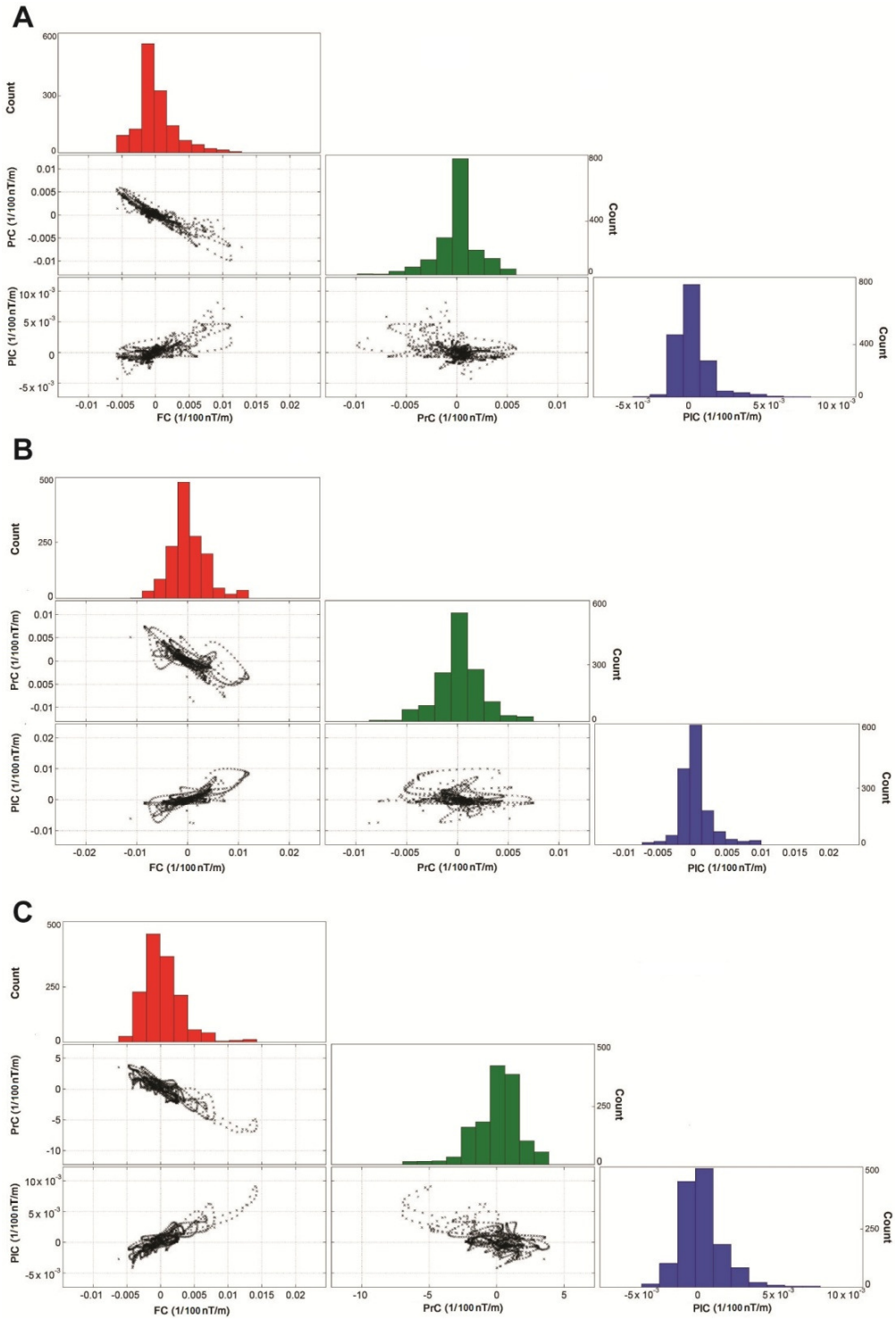

Figure 3.13. Histogram and multivariate scatterplot analysis of lines L1 (A), L2 (B), and L3 (C). The scatterplots exhibit similar trends as Figure 3.10. The histograms vary in kurtosis and skew depending on the signal content along line.

3.6 Conclusion

A magnetic signal is inherently linked to curvature. A high frequency signal will have a large curvature value and a low frequency signal will have a small curvature value. This relationship allows the user to apply statistical studies to derive additional information about a magnetic data set. The statistical descriptors kurtosis and skew provide quantitative information not only on the distribution of curvature data but also on the geometry of a magnetic signal. The kurtosis provides information on the frequency content while skew provides information on the sign and magnitude content. Magnetic susceptibility has a direct relationship with kurtosis since the frequency will vary with magnetization. Skew reflects if a source is dipping. In the case of a vertical source skew indicates the sign (positive or negative) of the magnetization. These characteristics of a magnetic signal may also be represented visually in the form of histograms and scattergrams. The user may also qualitatively assess the distribution of the curvature data to determine relative magnetization, potential dip or inclined field, and bulk frequency content. These applications are shown on various synthetic models as well as two real world data sets from the Southern Wopmay and Southern Ontario, Canada. This statistical approach is a development on previous work addressing the use of curvature statistics to differentiate source type such as a fault versus a dyke.

3.7 References

Baranov, V., 1957. A new method for interpretation of aeromagnetic maps: Pseudo-gravimetric anomalies: *Geophysics*, 22, 359-383, DOI: 10.1190/1.1438369.

Cooper, G.R.J., 2009, Balancing images of potential-field data: *Geophysics*, 74 (3), L17-L20.

Cooper, G.R.J., 2010, Enhancing ridges in potential field data: *Exploration Geophysics,* 41, 170-173.

Cooper, G.R.J., and Cowan, D.R., 2006, Enhancing potential field data using filters based on the local phase: *Computers and Geosciences*, 32 (10), 1585-1591.

Cooper, G.R.J., and Cowan, D.R., 2008, Edge enhancement of potential field data using normalised statistics: *Geophysics*, 71 (3), H1-H4.

Easton, R.M., and Carter, T.R., 1995, Geology of the Precambrian basement beneath the paleozoic of southwestern Ontario: In Ojakanjas, R.W. (Ed.), *Basement Tectonics*, 10, 221-264.

Evans I.S., 1972, General geomorphometry, derivatives of altitude and descriptive statistics: In Chorley, R. J. (Ed.), *Spatial Analysis in Geomorphology*, p.36, Methuen, London.

Forsyth, D.A., Milkereit, B., Davidson, A., and Hanmer, S., 1994, Seismic images of a tectonic subdivision of the Grenville orogen beneath lakes Ontario and Erie: *Canadian Journal of Earth Sciences*, 31, 229-242.

Hanmer, S., 1988, Ductile thrusting at mid-crustal level, south-western Grenville Province: *Canadian Journal of Earth Sciences*, 25, 1049-1059.

Hanmer, S., Corrigan, D., Pehrson, S., and Nadeau, L., 2000, SW Grenville Province, Canada: the case against post-1.4 Ga accretionary tectonics: *Tectonophysics,* 39, 33-51.

Hildebrand, R.S., and Easton, R.M., 1995, An 1161 Ma suture in the Frontenac terrane, Ontario segment of the Grenville orogen: *Geology*, 23 (1), 917-920.

Lee, M.D., Morris, W.A., Leblanc, G. and Harris, J., 2012, Curvature analysis to differentiate magnetic sources for geologic mapping: *Geophysical Prospecting* , DOI: 10.1111/j.1365-2478.2012.01111.x.

Roberts, A., 2001, Curvature attributes and their application to 3D interpreted horizons: *First Break*,19.2, 85-100.

Phillips, J., Hansen, R., and Blakely, R., 2007, The use of curvature in potential-field interpretation: *Exploration Geophysics*, 38, 111-119.

Zevenbergen, L.W., and Thorne, C.R., 1987, Quantitative analysis of land surface topography: *Earth surface processes and landforms*, 12, 47-56.

4.0 Geometry of the magnetic field derived from profile and plan curvature

Lee, M.D. and Morris, W.A., 2012, Geometry of the magnetic field derived from profile and plan curvature: *Interpretation*, To be submitted spring 2013

4.1 Abstract

Profile and plan curvature describe the properties of a magnetic source. Under ideal conditions these properties include source location and edges. These are defined by full curvature amplitude maxima and coincident zero contours respectively. This assumes a vertical ambient field, non-dipping, singular homogenous source. When these ideal conditions are not met most geophysical tools are unable to reliably locate the source considering the amplitude maximum is shifted away from directly over the source. Profile and plan curvature aid in the identification of dipping sources and interference of anomalies through the application of curvature analysis to synthetic models. Plan curvature indicates the dip direction and dip degree through an asymmetrical dipole anomaly. Profile curvature anomaly remains a singular anomaly for a dipping source. Maximum negative profile curvature and maximum positive plan curvature are capable of locating the position and width of a source. These maximums are respectively represented by either the bottom negative or top positive 1/8 of the curvature data. This method is shown on a synthetic model encompassing two intersecting tabular sheets and on a real world data set from Southern Ontario, Canada. These maximum curvature values are compared with the edge detection methods of tilt derivative and Blakely peak detection when the latter is computed from the horizontal gradient. The comparison shows curvature maximum analysis works reliably for delineating sheet-like structures. The Blakely peak is also computed directly on the PrC and PlC grids and the results support PrC as an indicator for source edges and PlC as an indicator for source location. Detailed analysis along one survey line from the Southern Ontario data exhibits the ability of profile and plan curvature as edge and peak detectors.

4.1 Introduction

Geometrical attributes of a potential field surface (i.e. grid) may be defined through the calculation of curvature along different spatial planes. Full curvature defines the overall curvature of the surface from which secondary attributes are calculated. Profile curvature is in the direction of the surface's maximum dip and plan curvature is orthogonal to profile curvature. The use of curvature in potential field theory has been discussed by various authors. Phillips et al. (2007) described the use of special functions to compute curvature-based depth estimation and use curvature as defined by Roberts (2001). Cooper (2010) uses the maxima and minima of the balanced plan curvature to identify ridges and troughs within a potential field surface. Lee et al. (2012b) use the statistics of full, profile, and plan curvature to differentiate between faults and dykes. Here we focus on how profile and plan curvature describe the magnetic field defined by a buried source and apply these conditions to two synthetic models and an aeromagnetic data set from Southern Ontario, Canada.

4.2 Method

Curvature values are calculated on grids generated by the application of an interpolation algorithm to the acquired magnetic point data. The selection of which interpolation algorithm to use will have an effect on curvature and should be carefully considered. The authors refer to Briggs (1974), El Albass et al. (1990), Cordell (1992), Xiong and Hans-Jürgen Götze (1999), Billings et al., (2002) and Smith and O'Connell (2005) for descriptions of different gridding methods.

A 3 x 3 moving window centered at P_0 (x, y) computes curvature using coefficients (a through i) along nine different window directions. Full discussion on surficial curvature and the coefficients as used here is outlined in a geomorphology context by Evans (1972), Zevenbergen and Thorne (1987), in a seismic context by Roberts (2001), and in a potential field context by Lee et al. (2012b). Full (FC) curvature is computed using the equation defined by Zevenbergen and Thorne (1987):

$$FC = \frac{\partial^2 z}{\partial S^2} = 2(d\cos^2\phi + e\sin^2\phi + f\cos\phi\sin\phi) \quad (1)$$

Where z is in the vertical direction, S is in the maximum dip direction, or ϕ and d, e, and f are coefficients in the directions of x, y (both intersect P_0 (x, y)), and overall gradient respectively.

Profile curvature (PrC) and Plan (PlC) curvature are derived from the same coefficients:

$$\mathrm{PrC} = -2(\mathrm{dg}^2 + \mathrm{eh}^2 + \mathrm{fgh})/(\mathrm{g}^2 + \mathrm{h}^2) \quad (2)$$

$$\mathrm{PlC} = -2(\mathrm{dg}^2 + \mathrm{eh}^2 - \mathrm{fgh})/(\mathrm{g}^2 + \mathrm{h}^2) \quad (3)$$

Where the units are 1/z unit/horizontal unit, which for a potential field are 1/nT/m. The coefficients g and h are also in the directions of x and y however they do not intersect P_0 (x, y) like d or e. The response of curvature grids or profiles with respect to different simplified sources is outlined in Lee et al. (2012b). For a sheet-like source (e.g. fault, fracture, or lithological contact) PrC and PlC is represented by a spike. The spike is a sharp, single point anomaly. Both the PrC and PlC spikes will have similar geometry but be separated by a DC shift equivalent to the magnitude of FC. PrC will assume a negative value and PlC will assume a positive value when the magnetic susceptibility (κ) of the sheet-like source is greater than the host rock. The contrary case would generate opposite results. For a broad source (e.g. volcanic intrusions) PrC exhibits a dipole effect while PlC exhibits a monopole. The width of the PlC anomaly may be used to indicate the edge of the source. Where κ of the broad source is greater than the host rock then PrC will be negative and PlC will be positive.

Equations (2) and (3) were designed for topographic data analysis. PrC describes the acceleration and deceleration of flow; while PlC describes the dispersion of flow. Changing the application of equations (2) and (3) to potential fields means PrC describes the gradient of the anomaly; while PlC describes width of the anomaly. PrC is dictated by the κ contrast and its depth and PlC is dictated by 2D planar versus 3D point sources (Mikhailov et al., 2007).

The topology of any magnetic anomaly is a function of the source geometry and its interaction with the inducing Earth's magnetic field. The curvature properties will vary for a constant source body as the resulting magnetic anomaly pattern depends on the Earth's field orientation, which depends on the location at Earth's surface. To best define source geometry the maxima of a magnetic anomaly should reside over the top of the source and be symmetrical on either side. Curvature calculations should be applied to reduced-to-pole data and to sources assumed to be singular (no interference), non-dipping, and near-infinite depth. It is important to have a firm understanding about whether an anomaly is singular or due to interference when any semi-automated processing routine is applied. Should anomalies not be identified as singular, then there is no reliability in the interpretation results. Many semi-automated routines are black boxes

as they do not discriminate whether an anomaly is singular or not (Fairhead et al., 1994). However, PrC and PlC may provide insight into whether a source is dipping and whether the anomaly is singular or is a composite resulting from interference.

We generate two synthetic models to assess the impact of a dipping source and anomaly interference on the calculation of curvature. All models are computed using a vertical ambient field with a strength of 59 000nT. Flight line spacing in 10m and sample spacing is 10m. These specifications were selected based on software limitations and do not reflect the standard airborne survey grid that exhibits in a higher density of samples along-line relative to across-line.

Model A is designed to assess the effect of a dipping body. It contains a single tabular body 50m thick, 2km long, and 1.5km deep with a magnetic susceptibility of 0.04SI. This tabular body starts in a complete vertical position relative to the horizontal plane and then undergoes dipping at 60°, 45°, and 30° relative to the horizontal. Model B is designed to assess the effect of anomaly interference and is identical to the model used by Lee et al. (2012a). The model includes two vertical tabular bodies intersecting at a 45° angle to demonstrate complete interference. The tabular bodies continue along trend and have no influence over each other's magnetic field geometry. This results in each body having a singular anomaly.

It is also appropriate to compare with the standard geophysical tool tilt-derivative (TDR) considering we are using curvature analysis to locate the source edges (Miller and Singh, 1990). Tilt-derivative is an edge detector routine implementing the ratio of vertical to horizontal gradient and producing a zero value at the edge of an anomaly and a positive value over the source. Blakely peak detection (Blakely and Simpson, 1986) is an edge detection routine when computed from the horizontal gradient of the magnetic field.

4.3 Synthetic results

Model A (Figure 4.1) indicates the magnetic field over a non-dipping tabular body will generate a symmetrical anomaly overtop of the source and the source edges are defined by 0 curvature (FC, PrC, PlC) and 0 TDR. For PrC, PlC, and TDR, as the tabular body dips the location of the maximum amplitude migrates from overtop of the source in the direction of dip (by the same horizontal distance). The PlC anomaly becomes a dipole as soon as the source begins to dip. PrC and PlC amplitudes decrease with increasing dip and TDR maintains the same amplitude ($\pi/2$). The source is likely dipping if a TDR peak is associated with an asymmetrical PrC and dipolar PlC.

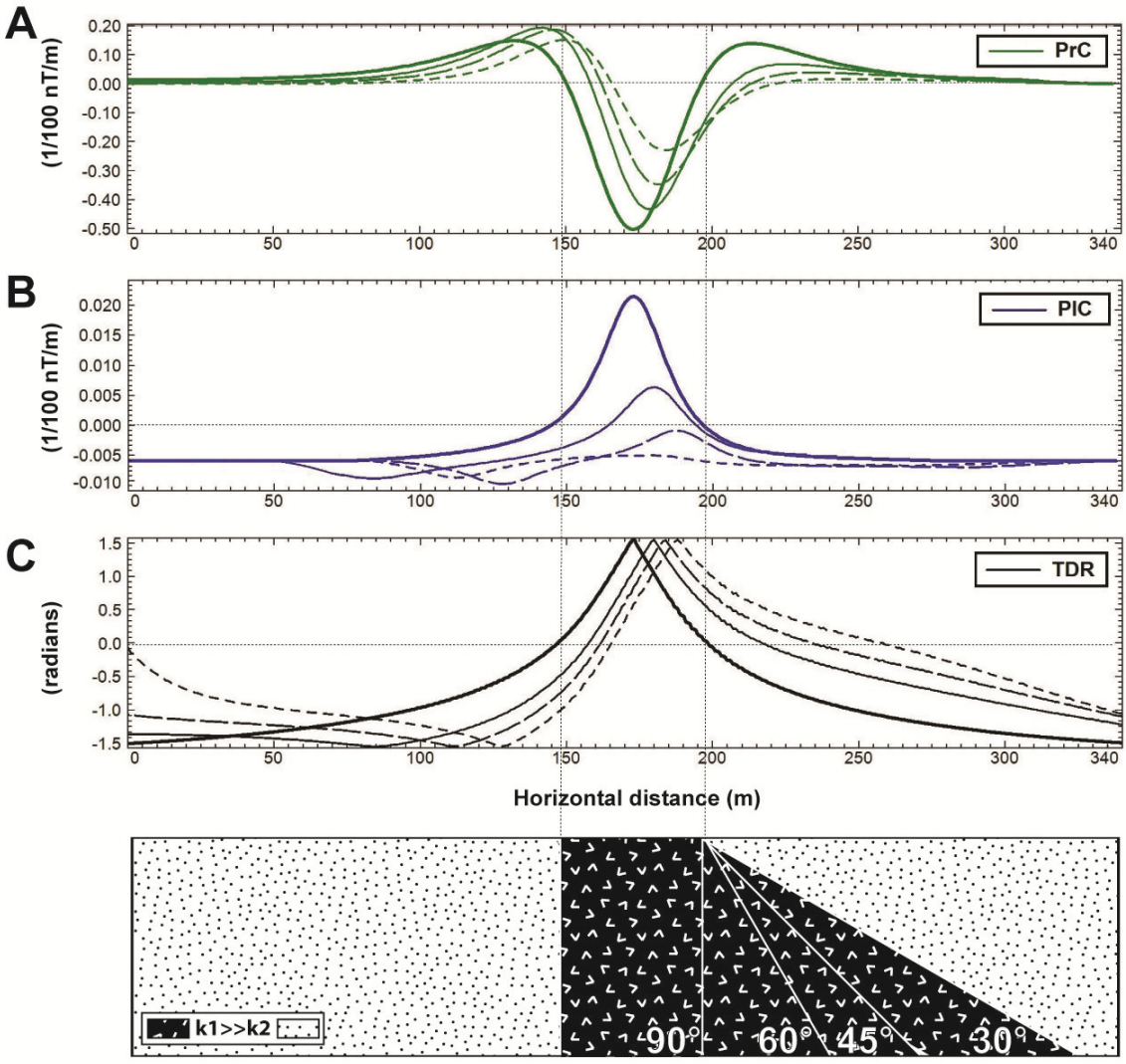

Figure 4.1. The resultant PrC (A), PlC (B), and TDR (C) generated by magnetic tabular source dipping 90° (bold line), 60° (thin line), 45° (long dash line), and 30° (short dash line). A dipping body results in an asymmetrical negative PrC anomaly, a PlC dipole anomaly and the peak of TDR migrates in the dip direction from overtop of the source with increasing dip angle.

Model B (Figure 4.2) indicates the magnetic field over two intersecting tabular sheets will generate a symmetrical anomaly at the point of intersection (Line A); however the source edges are not clearly defined by 0 1/100 nT/m curvature and 0° TDR. This is because the interference of the individual anomaly convolutes the original signal (constructive interference) generating a stronger anomaly over the intersection location. As the sources separate (Line B) the maximum amplitudes are still located over the source. As the anomalies spread further apart their influence over each other is minimized and the results look more similar to those in the ideal non-dipping scenario from Figure 4.1 (Line C).

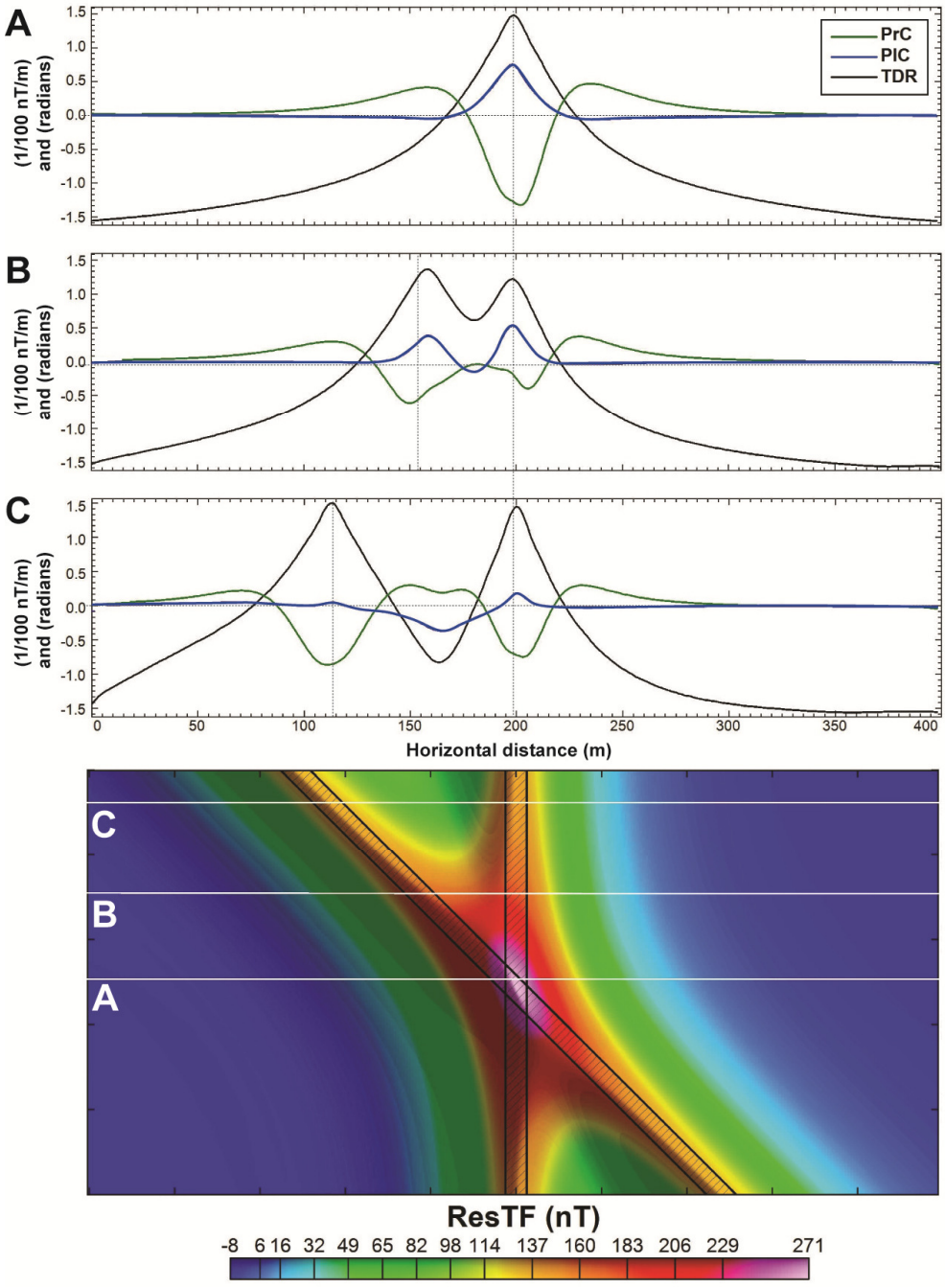

Figure 4.2. The resultant PrC, PlC, and TDR generated by two intersecting tabular sources. Due to anomaly interference, the edge of the source is ambiguously defined by all three measurements (0 contours do not coincide).

The maximum negative PrC and maximum positive PlC suggest the area directly over the source (maximum magnetic amplitude). This method is comparable to Blakely peaks (Blakely and Simpson, 1986) which identifies source location but not continuous ridges. The maximum 1/4 of a normal distribution coincides with TDR contours and represents the peak of an anomaly. Conversely the minimum would represent the trough of an anomaly. Figure 4.3 shows maximum values of PrC and PlC are able to reliably locate intersecting tabular sheets. Regions of no interference are defined by uniform curvature of constant value while dipping or interfering anomalies vary.

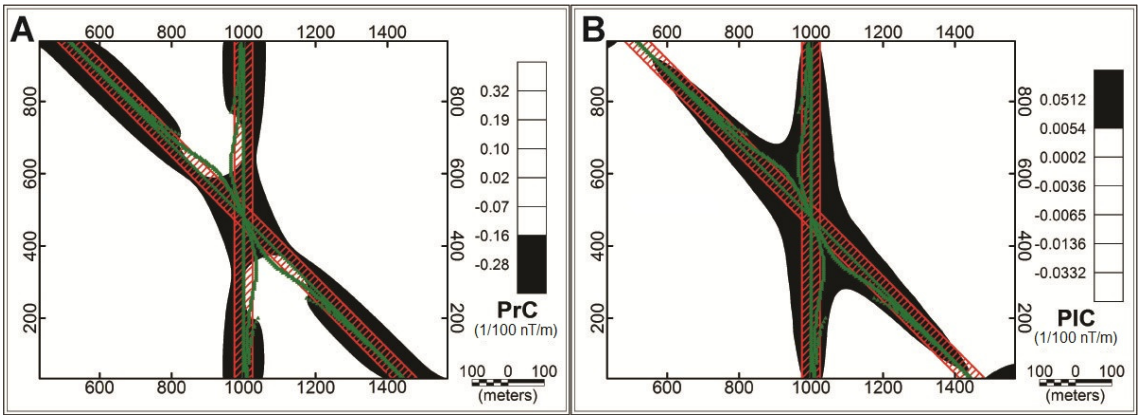

Figure 4.3. Maximum negative PrC (A) and maximum positive PlC (B) over two intersecting tabular sources. Maximum values (black) indicate the area over the source. The sources are outlined in red and Blakely peaks are green +.

4.6 Case study

The total field magnetic survey of the western end of Lake Ontario and the eastern end of Lake Erie was collected from November 28, 1998 until April 26, 1999 (Figure 4.4). Flying was conducted along a constant mean terrain clearance of 150m. Line spacing was 400m along 90° and control lines were flown every 5000m along 0°. The magnetometer was an optically pumped cesium vapour. The total intensity of the magnetic field vector is 55542 nT with a declination and inclination of -10.269° and 70.437° respectively; these values were used to conduct reduction-to-pole. The aeromagnetic survey covers crystalline rocks and Precambrian geologic domains which are overlaid by relatively magnetically transparent sedimentary cover. These domains include the Central Gneissic Belt (CGB), Central Metasedimentary Belt (CMB), and the Central Metasedimentary Belt Boundary Zone (CMBBZ). Based on borehole data, the sedimentary cover thickens from 300m to 3000m towards the southeast (Sanford et al., 1985). The magnetic signal will be dominated by the Precambrian basement while high frequency anomalies will be produced by near surface features and the sedimentary cover.

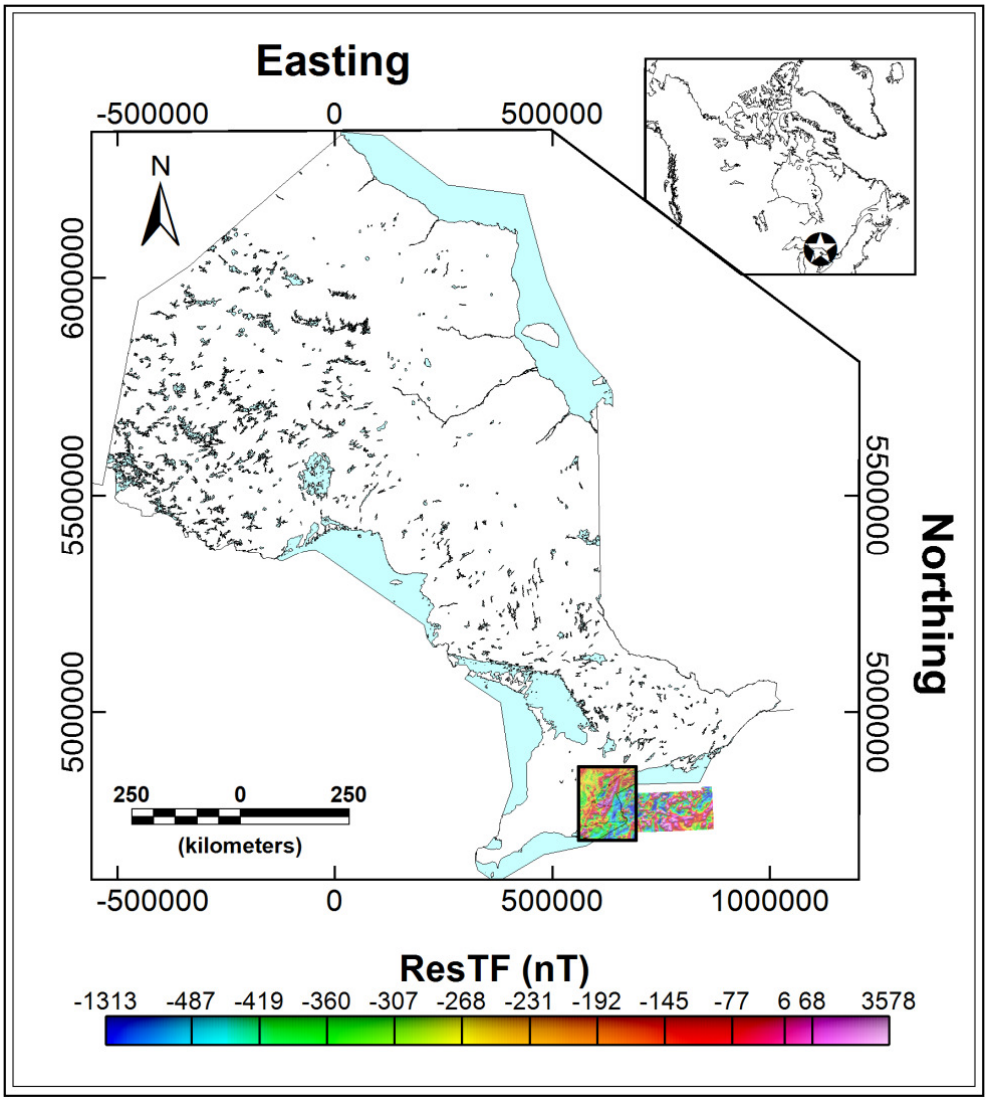

Figure 4.4. Location of aeromagnetic survey and study area (black rectangle) in Ontario and Canada (✪).

The data underwent initial processing including levelling and removal of cultural effects. Interpretation was conducted on the Residual Total Field (ResTF) since the data was corrected for the regional magnetic field. The flight and control lines were gridded using the minimum curvature interpolation algorithm at ¼ the line spacing (100m). Microlevelling was performed using two applications of a Butterworth filter and a directional cosine. Upward continuation was computed at 800m to minimize any residual high frequency artefacts and emphasize the subsurface bedrock. This is important as the bedrock is overlain with a sedimentary cover with a variable thickness of 300m to 1000m. An increment level of 800m was selected as it is equivalent to twice the flight spacing and

approximates the maximum thickness of the sedimentary cover over the study area. Upward continuation also minimizes the sensitivity to instrumental noise, which is generally high frequency and low amplitude (Cooper, 2010). The final leveled and upward continued ResTF map is shown in Figure 4.5A. Curvature analysis was carried out on the southern Ontario dataset where FC, PrC, and PlC were computed (Figure 4.5B-4.5D).

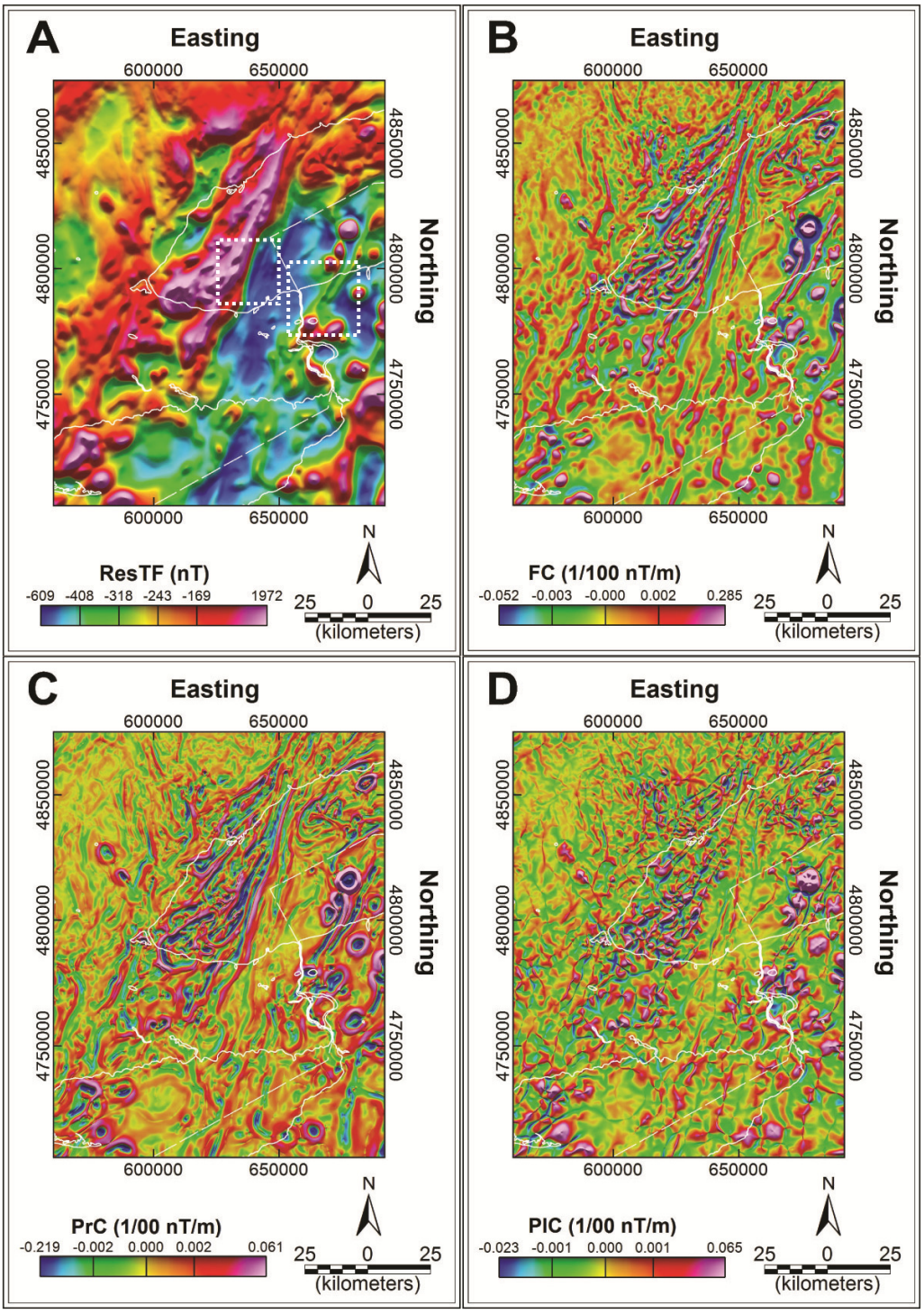

Figure 4.5. The leveled ResTF upward continued to 800m (A). Curvature outputs include FC (B), PrC (C), and PlC (D). All grids are interpolated using minimum curvature and display a normal distribution colour scheme. The geographic boundary between Canada and the United States and hydrology are outlined in white.

Computation of curvature attributes reveals a distinct pattern comprising elongate and near circular features. Elongate patterns are most strongly developed in the PrC (Figure 4.5C); PlC for the same features is less continuous. This is expected since these anomalies represent sheet-like sources in the basement terrain and are near-linear resulting in a low PlC response. Local discontinuities in the PrC pattern serve to accentuate the locus of the boundary between adjacent tectonic domains. For example, there are two cases where fold-like patterns are truncated by linear features (Figure 4.5C – white dotted boxes). Near-circular patterns present in the PrC plot may be associated with plutons in a marble matrix. Their anomalies exhibit strong edges and low curvature in centre. In contrast, PlC for these same features peaks over the top of the anomaly. This suggests these features are homogeneous plutons which have not been deformed along with the basement. In effect combining the attributes of PlC and PrC appears to rapidly separate 3D and 2D sources and to isolate regions of truly coherent 2D (non-interfered) sources.

The most effective way to show these structures is by examining the maximum curvature of PrC and PlC in conjunction with standard geophysical edge and source detection routines. By locating near-zero curvatures identifies source edges. Calculating TDR of the ResTF and contouring the 0° indicates the approximate source edge as per Miller and Singh (1994). The Blakely peaks (Blakely and Simpson, 1986) were calculated from the horizontal gradient of ResTF to indicate the source edges. The Blakely peak detection identified a peak as any grid node with at least two surrounding grid nodes with a smaller value of curvature. This method of Blakely was chosen considering the aim is to identify ridges and not just single point anomalies.

Figure 4.6 shows how maximum negative PrC and maximum positive PlC indicate the location over the source; while maximum positive PrC and maximum negative PlC indicate the edge of the source. Comparison of tilt-derivative and Blakely peaks with maximum PrC and PlC (negative 4.3A and 4.3C; positive 4.3B and 4.3D), we can see the similarities and differences. Both PrC and PlC are able to trace the approximate location of a magnetic source. PlC provides detailed location and strike information of the source while Blakely indicates single sources and struggles with linear or sheet-like sources (Lee et al., 2012a). PrC is far more effective as an edge detector than PlC. PlC does not indicate the edge of the source but likely where magnetic fields of adjacent sources interfere and would therefore be a possible indicator of a complex anomaly.

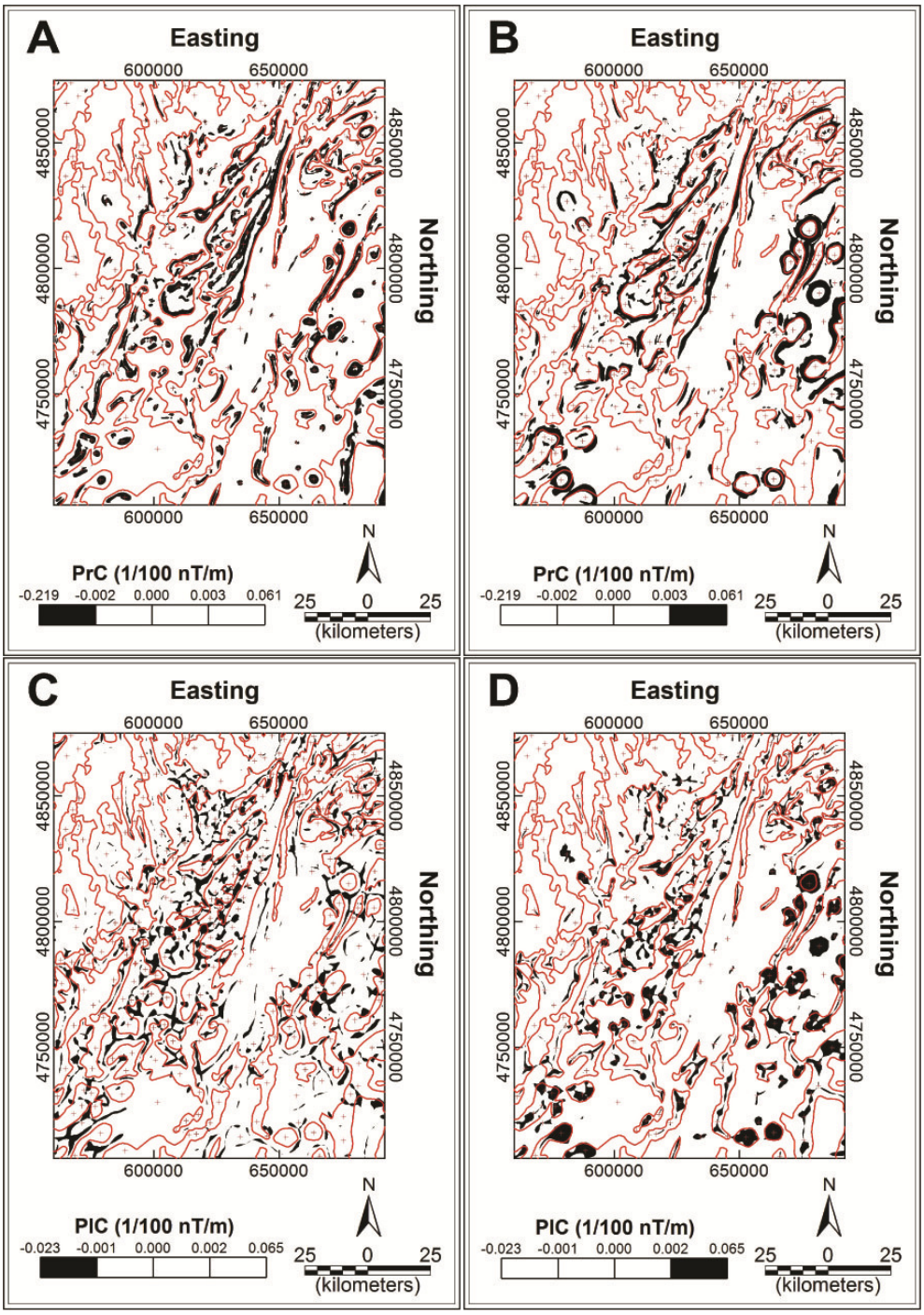

Figure 4.6. Maximum negative (A, C) and positive (B, D) PrC (top) and PlC (bottom). The 0° tilt-derivative contour is indicated by a red line and the Blakely peaks identified by a green +. These two former attributes are indicated to show the approximate source edges and location respectively.

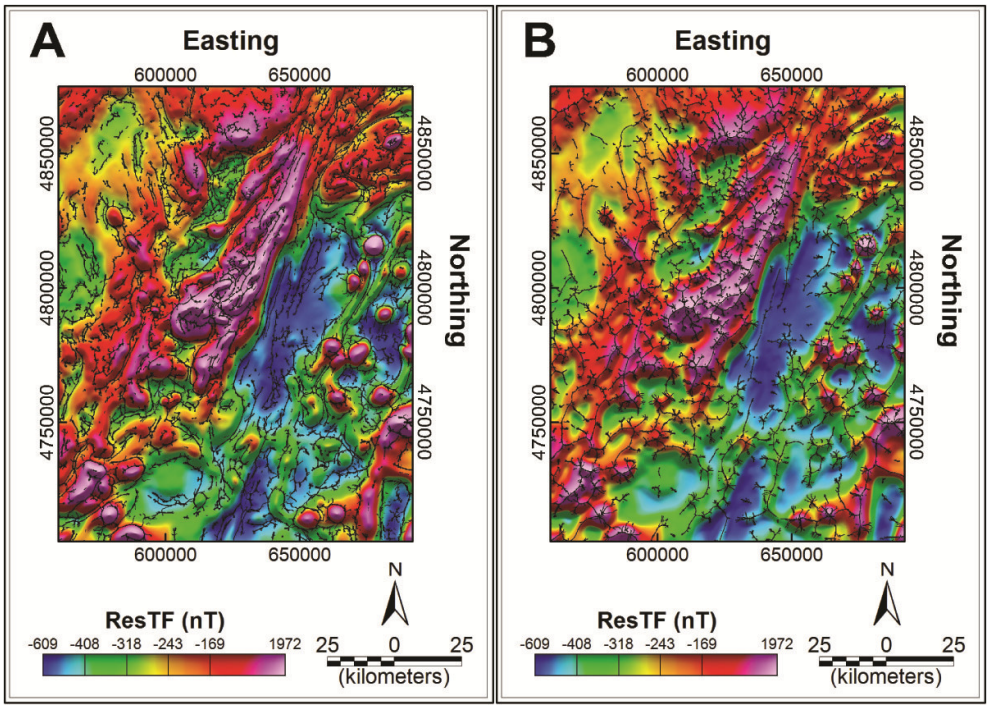

Figure 4.7. Blakely peaks (+) calculated from PrC and PlC grids overlaid on ResTF.

The Blakely peaks were directly calculated from the PrC and PlC grids (Figure 4.7). PrC peaks outline the source boundaries and PlC peaks outline the source locations. These peaks combined as a vector layer provide the essential information required to delineate magnetic sources since *a priori* information states the sources are sub-vertically dipping.

We examine line one flight line (A – A') in the southern section of the study area to work at a refined scale (Figure 4.8). This line was chosen as it does not have high-amplitude anomalies, but is also not magnetically flat: the ResTF amplitude range is 150nT. FC, PrC (Figure 4.8 panel B) and PlC (Figure 4.8 panel C) are also computed. FC produces strictly smooth positive anomalies, while the latter two produce both smooth anomalies and spikes. The spikes occur at the location of a fault (low amplitude ResTF) or an igneous intrusion (high amplitude ResTF). The ResTF Blakely peaks computed are included for comparative purposes. The edges of the sources are defined when all three curvatures are congruent (~ 0 nT/m) and coincide with 0° TDR.

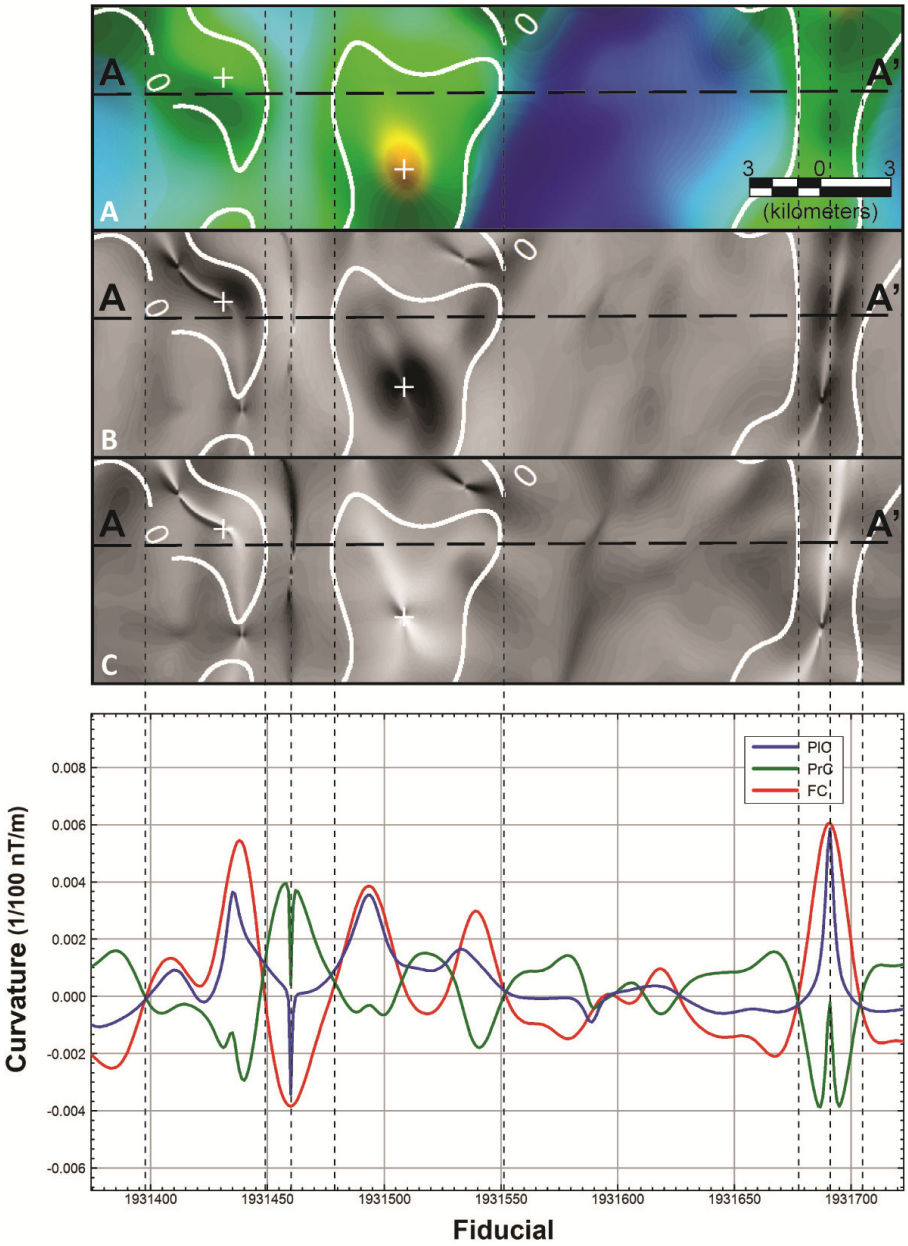

Figure 4.8. Profile analysis along A – A' (black heavy dashed line) showing FC, PrC, and PlC. Panel A shows the ResTF, panels B and C show PrC and PlC respectively. The location of 0° tilt-derivative (heavy white line) and Blakely peaks (white +) are included for reference to the source edge and location. The location of pertinent points on the profile plot and their location on the panels are indicated with black dashed lines. The edge of a source corresponds to $FC \approx PrC \approx PlC$ and is ~ 0 nT/m. The location of a sheet-like source corresponds to either a positive or negative spike.

4.7 Discussion

There are notable differences to be discussed. First, each method misses certain anomalies. Either they are identified by both Blakely and tilt-derivative and missed by PrC and PlC, or vice versa. The former is most notable in the northwest quadrant within the CGB where very few curvature anomalies are identified. Meanwhile PrC and PlC provide significantly more detail over sources with greater amplitude. Second, the supposed size of a source (defined by source edges) varies between PrC and PlC. The morphology of the high amplitude circular anomaly along the central eastern perimeter of the survey area differs between in the two images. According to comparison with tilt-derivative, PrC provides almost an identical width, while PlC underestimates the width. A similar scenario is shown by the two circular anomalies in the southeast quadrant. PlC provides a nearly identical width to tilt-derivative, but PrC is an underestimate. The notable difference between all these anomalies is their proximity to other anomalies and their amplitude. Anomalies with high amplitudes are best resolved by PrC, anomalies with mid-amplitudes are better resolved by PlC, and low-amplitude anomalies are not readily resolved by curvature.

PlC works well for discrete anomalies. Geologically this means only a few generations or intersections (e.g. dykes). Previous curvature work was conducted on the Wopmay Orogen, N.T. (Lee et al., 2012b), which comprises multiple generations of dykes, intrusive suites, and faults. Due to the complexity of the geologic environment, PlC did not work as effectively as a source identifier.

4.8 Conclusion

Profile and plan curvature are useful tools to quickly identify both the location and geometry of a magnetic source. Their application may be used for both sheet-like and broad sources. Profile and plan curvature were used on an aeromagnetic data set to identify the location and shape of various sources by identifying the most maximum positive and negative curvature values. The reliability of these results was determined by comparison with the pre-existing source edge detection methods tilt-derivative and Blakely peak from horizontal gradient. In general the results were nearly corroborated by the standard results except in the case of magnetically quiet or flat regions.

4.9 References

Blakely, R.J., and Simpson, R.W., 1986. Approximating edges of source bodies from magnetic and gravity anomalies: *Geophysics*, 51 (7), 1494-1498.

Briggs, I.C., 1974, Machine contouring using minimum curvature: *Geophysics*, 39 (1), 39-48.

Billings, S.D., Beatson, R.K., and Newsam, G.N., 2002, Interpolation of geophysical data using continuous global surfaces: *Geophysics*, 67 (6), 1810-1822, DOI: 10.1190/ 1.1527081.

Cooper, G.R.J, 2009, Balancing images of potential-field data: *Geophysics*, 74 (3), L17-L20.

Cooper, G.R.J, 2010, Enhancing ridges in potential field data: *Exploration Geophysics*, 41, 170-173.

Cooper, G.R.J., and Cowan, D.R., 2008, Edge enhancement of potential field data using normalised statistics: *Geophysics*, 71 (3), H1-H4.

Cordell, L., 1992, A scattered equivalent-source method for interpolation and gridding of potential-field data in three dimensions: *Geophysics*, 57 (4), 629-636.

El Abass, T., Jallouli, C., Albouy, Y., and Diament, M., 1990. A comparison of surface fitting algorithms for geophysical data: *Terra Nova*, 2 (5), 467-475, DOI: 10.1111/j.1365-3121.1990.tb00104.x.

Evans, I.S., 1972, General geomorphometry, derivatives of altitude and descriptive statistics: In Chorley, R. J. (Ed.), *Spatial Analysis in Geomorphology*, p.36, Methuen, London.

Lee, M.D., Morris, W.A., Harris, J., and Leblanc, G., 2012a, An automatic network extraction algorithm applied to magnetic survey data for the identification and extraction of geologic lineaments: *The Leading Edge*, 31, 26-32, DOI:10.1190/1.3679324.

Lee, M.D., Morris, W.A., Leblanc, G., and Harris, J., 2012b, Curvature analysis to differentiate magnetic sources for geologic mapping: *Geophysical Prospecting*, in press.

Li, X., and Götze, H., 1999, Comparison of some gridding methods: *The Leading Edge*, 898-900.

Mikhailov, V., Pajot, G., Diament, M., and Price A., 2007, Tensor deconvolution: A method to locate equivalent sources from full tensor gravity data: *Geophysics*, 72 (5), 161-169.

Miller, H.G., and Singh, V., 1994, Potential field tilt-a new concept for location of potential field sources: *Journal of Applied Geophysics*, 32 (2-3), 213-217, DOI:10.1016/0926-9851(94)90022-1.

Phillips, J.D., Hansen, R.O., and Blakely, R.J., 2007, The use of curvature in potential field interpretation: *Exploration Geophysics*, 38, 111-119.

Roberts, A., 2001, Curvature attributes and their application to 3D interpreted horizons: *First Break*, 19.2, 85-100.

Sanford, B.V., Thompson, F.J., and McFall, G.H., 1985, Plate Tectonics – a possible controlling mechanism in the development of hydrocarbon traps in southwestern Ontario: *Bulletin of Canadian Petroleum Geology*, 33 (1), 52-76.

Smith, R.S., and O'Connell, M.D., 2005 Interpretation and gridding of aliased geophysical data using constrained anisotropic diffusion to enhance trends: *Geophysics*, 70 (5), V121-127.

Zevenbergen, L.W., and Thorne, C.R., 1987, Quantitative analysis of land surface topography: *Earth surface processes and landforms*, 12, 47-56.

5.0 An automatic network extraction algorithm applied to magnetic survey data for the identification and extraction of geologic lineaments

Lee, M.D., Morris, W.A., Harris, J., and Leblanc, G., 2012, An automatic network extraction algorithm applied to magnetic survey data for the identification and extraction of geologic lineaments: *The Leading Edge*, 31, 26-32, DOI:10.1190/1.3679324

5.1 Abstract

Lineament analysis is commonly undertaken by interpreting a wide range of geoscientific data to delineate geologic structures. These structures include faults, fractures, dykes and lithological contacts, which provide information for geologic mapping and mineral and energy exploration. We offer a simple automatic lineament analysis method combining the principals of peak identification algorithms typically used in geophysical data interpretation and a GIS drainage 'network extraction' algorithm commonly applied to a topographic surface. We apply this network extraction process to a magnetic surface (grid) rather than a topographic one. The GIS approach calculates the curvature of a surface to determine whether a specific coordinate is at a minimum (trough). A simple quadratic surface is computed for a moving 3 x 3 window to determine if the local surface has the form of a dipping plane (or a trough). Continuity of troughs between adjacent kernels defines lineaments typically corresponding to streamflow pathways when analysis is carried out on a topographic surface. On a magnetic anomaly map surface network extraction identifies magnetic lows representing faults having undergone magnetite (depletion) alteration, or dykes with predominantly reversed polarity remanence. As network extraction is designed to locate troughs it is possible to isolate normally magnetized dykes by inverting the values of a magnetic data set by to produce ridges. This modified ridge analysis method is successfully applied to three synthetic data sets. Network extraction offers the principal benefits of continuity in solutions to produce polylines over isolated ridge solutions, automation for consistency and reliability, and optional amplitude thresholding.

5.1 Introduction

A geologic lineament is a linear zone of weakness in the Earth's crust owing its origin to tectonic or glacial causes and often represents geologic features such as faults, dykes, lithological contacts, and structural form lines. However, geologic interpretation is often required to differentiate tectonic from glacial lineaments. With respect to any geoscientific data set, a lineament will appear as a 'line' (2D structure) in a planar view. 'Lineament analysis' has been applied to various geoscientific data for a variety of applications including geologic mapping, resource exploration and disaster management (e.g. landslide prediction). Natural resource exploration utilizes lineament analysis to identify potential structural conduits for mineralized fluids and hydrocarbon traps, while geological mapping utilizes lineament analysis to delineate the regional tectonic structure and assist in the relative dating of structural events (Lalor, 1987; O'Driscoll, 1980; Woodall, 1994; Chernicoff et al., 2002; Crafford and Grauch, 2002; Twidale, 2007; Woodall, 2007). Accordingly, there are various methods in which lineament analysis may be applied.

Lineament analysis is undertaken through simple visual analysis of enhanced geoscientific data (Harris et al., 2008) or by utilizing semi-automated (quantitative) algorithms (Masuda et al., 1991; Raghavan et al., 1993; Karnieli et al., 1996). Visual inspection of aerial photography, satellite imagery, and geophysical data is very effective but depends on the experience and biases of the interpreter. The visual interpretation process, although subjective, does incorporate the geologist's knowledge and the various interpreted lineaments can be screened (e.g. geologically calibrated) in real time during the interpretation process. Automated methods offer advantages over visual interpretation in terms of speed, efficiency and objectivity in the lineament identification and extraction process.

In geophysics, these automated algorithms use the potential field (whether it be magnetics or gravity) defined by the geologic source to provide information about its location, geometry (edges), depth, and various physical properties (Spector and Grant, 1970). Accordingly there are routines specifically designed for each of these end goals although some may be able to determine multiple parameters; e.g. tilt-depth method to determine both source edge and depth (Salem et al., 2007) or Euler deconvolution to determine source location and depth (Reid et al., 1990). To map these source edges also requires pre-processing of the magnetic data (Pilkington and Keating, 2004; Pilkington, 2007; Pilkington and Keating, 2009).

We are strictly interested in identifying the location of sheet-like sources (e.g. lineaments such as fractures, faults, and dykes), which are best resolved through source peak (profile view) or ridge (grid view) identification of total magnetic field data. Peak detection can be simplified by the calculation of curvature. Geophysical data most often interpreted as an interpolated surface (grid) despite collected as point data. Every point on this grid will have a specific curvature defined by the interpolated surface and the causative source. Peaks or ridges (and conversely, troughs) will be grid points having an increased degree of curvature compared to the norm of the data set, which may be calculated through various categories of curvature analysis (Shary, 1995; Roberts, 2001; Florinsky, 2005; Hansen and deRidder, 2006; Phillips et al., 2007; Cooper, 2010).

The Blakely-Simpson algorithm identifies peaks in a gridded surface using a moving window (kernel) to compare the magnitude of the central cell to the surrounding eight cells (Blakely and Simpson, 1986). If the surrounding cells are lower, the central cell is deemed a peak. The user may define 'isolated peaks' where all surrounding eight grid cells are lower than the central cell or 'all peaks' where only the grid cells in one direction from the central cell are lower. Pre-processing of the observed data using horizontal and vertical derivatives are also standard tools used for source peak and edge detection (Pilkington and Keating, 2004; Pilkington, 2007; Pilkington and Keating, 2009). With respect to peak detection, the analytic signal (Nabighian, 1972) is defined through the horizontal and vertical derivatives of a total magnetic field and is equivalent to the total gradient. Analytic signal works effectively as it produces a symmetrical anomaly reaching maximum directly over the source (Roest et al., 1992) and is used for various semi-automated methods, including the depth estimation Euler deconvolution routine (Reid et al., 1990).

We are interested in sheet-like sources which have a distinct ridge anomaly in grid view (compared to the single peak anomaly typical of a kimberlite in grid view). The Geographic Information System (GIS)-based algorithm drainage feature extraction, implements a source location routine, but actually identifies troughs rather than ridges. Drainage feature extraction is typically applied to a Digital Elevation Model (DEM) and is an important step in drainage basin analysis (Evans, 1972; Zevenbergen and Thorne, 1987; Moore et al., 1988; Moore et al., 1991). The method calculates the curvature of a topographic surface to delineate stream location, flow impact, and flow direction by identifying localized, continuous topographic lows. Drainage feature extraction implements a general curvature analysis. Two commonly computed curvature outputs, *profile* and *planform* (plan) (Zevenbergen and Thorne, 1987; Cooper and Cowan, 2006; Cooper and Cowan, 2008; Cooper, 2010), play a critical role in basin analysis. Profile

curvature influences the acceleration (and conversely deceleration) of flow, while plan curvature influences the dispersion of flow.

We present a lineament analysis algorithm similar to these geophysical and GIS routines with respect to detecting ridges, where the solutions are defined as lineaments. We apply this automatic lineament 'network extraction' technique to synthetic magnetic datasets to test the robustness of the algorithm and will be applied to a real world data set in future work. This paper will cover:

1. Application of the standard geophysical peak detection routines, the Blakely-Simpson algorithm and analytic signal (Methods 1 and 2);
2. Application of network extraction to synthetic data (Method 3);
3. Compare all three methods for peak/ridge detection efficiency.

5.2 Method

The drainage feature extraction algorithm implemented by the GIS software package Encom Discover™ uses a 3 x 3 moving window applied to the gridded data set to calculate the gradient between the center cell P_0 (x, y) and the surrounding eight cells (Figure 1). This is an assessment of the surficial curvature of the interpolated surface at the coordinate P_0 (x, y) and is defined by a quadratic function (Evans, 1972; Roberts, 2001).

$$z = ax^2 + by^2 + cxy + dx + ey + f \quad (1)$$

Where x and y are horizontal components and a, b, c, d, e, and f are coefficients. These coefficients represent a series of arithmetic equations from which surficial dip degree and dip angle can be calculated (Evans, 1972; Roberts, 2001). Although this routine is carried out by Encom Discover™, the algorithm may be applied to any gridded data set in MATLAB™ or any other code-based software. It is also important to note the user may define which surrounding eight grid cells are implemented for calculating surficial curvature. The eight cells do not have to be those immediately juxtaposed to the central cell, but may be further out (e.g. equivalent to a 5 x 5 or 7 x 7 grid) producing a more 'regional' computed surficial curvature (Figure 5.1).

At every origin P_0 the slope (m) of z from equation 1 is calculated as (Zevenbergen and Thorne, 1987):

$$m = \frac{\partial z}{\partial s} = g\cos\theta + h\sin\theta \quad (2)$$

Where S is in the direction of maximum slope, also known as aspect (θ) and g and h are directional gradient coefficients perpendicular and parallel respectively to the maximum slope (Figure 5.1). The steepest gradient (m) between cells determines the lineament's azimuth. This azimuth is necessary to determine the impact and location of low-lying surficial features and ultimately, the continuity of peak solutions. The principal or full curvature (FC) in any direction (ϕ) at a specific grid point $P_0(x, y)$ is computed using the directional coefficients from equation 1. FC represents the derivative of the slope in equation 2 where the units for curvature are 1/ nT/m. (Zevenbergen and Thorne, 1987):

$$FC = \frac{\partial^2 z}{\partial s^2} = 2(d\cos^2\phi + e\sin^2\phi + f\cos\phi\sin\phi) \quad (3)$$

The routine also implements upper and lower bounds, where a $P_0(x, y)$ with a value above the upper bound or below the lower may be omitted prior to calculation.

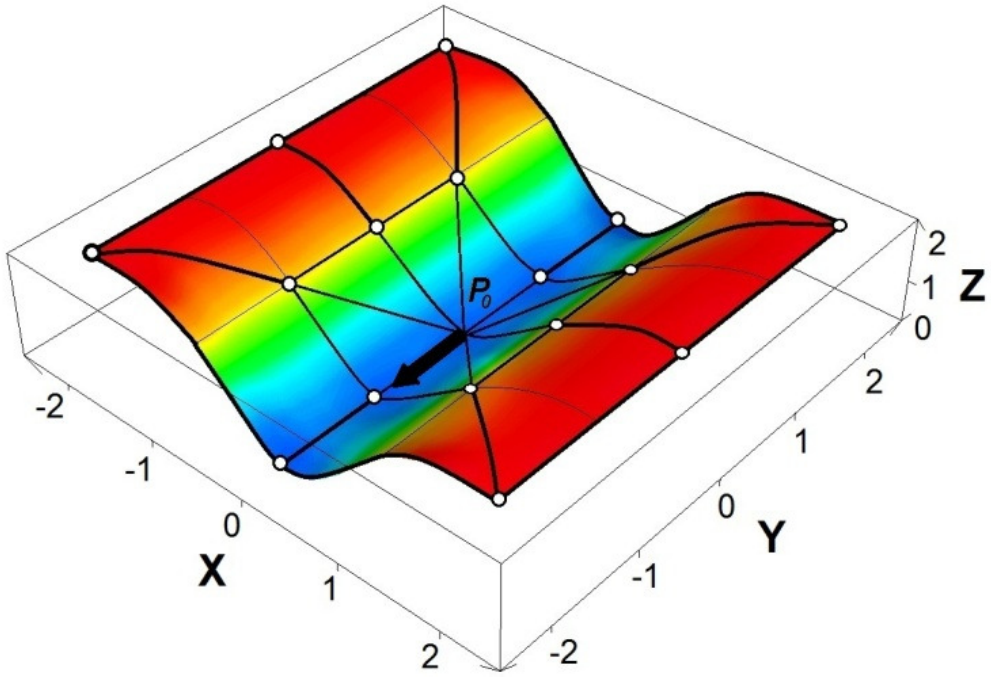

Figure 5.1. A quadratic surface can be fitted to any surrounding eight grid nodes of P_0. The selection of which eight surrounding grid nodes is user defined. The user could select the grid nodes in near proximity (medium weighted lines) or the further grid nodes (heavy weighted lines). The latter would be similar to a 5 x 5 quadratic surface. The direction identified as a lineament is shown by a black arrow, is in the negative y direction and perpendicular to the x axis.

These identified troughs may represent faults and fractures associated with the depletion of magnetite (e.g. alteration through oxidation) or reversed polarity remanently magnetized dykes in a geologic context. Conversely magnetic high anomalies such as normally magnetized dykes with a higher magnetic susceptibility relative to host rock are delineated with the network extraction algorithm by flipping the values of the data set so low values become high (trough becomes a ridge) and vice versa. This is achieved by changing the sign of all data points. In these cases the range is maintained but the scale is inverted. This is acceptable as no computation in this method relies on the magnitude of the values themselves, only their values relative to one another.

5.3 Synthetic data

Three data sets were generated (A, B, C) to which the peak detection comparison was applied. The applied magnetic field for each synthetic data set had an intensity of 59 000 nT, a declination of 0° and inclination of 90°. The simulated survey was acquired along 10 m spaced east-west flight lines, sampled at 10 m spacing along line and at a height of 125 m. Synthetic data set A (Figure 5.2A) comprised of a north-south striking dyke 50 m wide, 2 km in length and 1 km deep with a magnetic susceptibility of 0.4 SI. Synthetic data set B (Figure 5.2B) comprised of the same north-south striking dyke as synthetic data set A, along with a 45° intersecting northwest-southeast striking dyke. This second dyke had a magnetic susceptibility of 0.4 SI and identical geometry to the north-south striking dyke. Synthetic data set C (Figure 5.2C) comprised of the same north-south striking dyke and then a 0.2 SI 45° intersecting northwest-southeast striking dyke. This second dyke had a magnetic susceptibility of 0.4 SI and identical geometry to the north-south striking dyke. In addition, Gaussian noise with a mean of 0 and a standard deviation of 0.479 was added to the simulated magnetic data set.

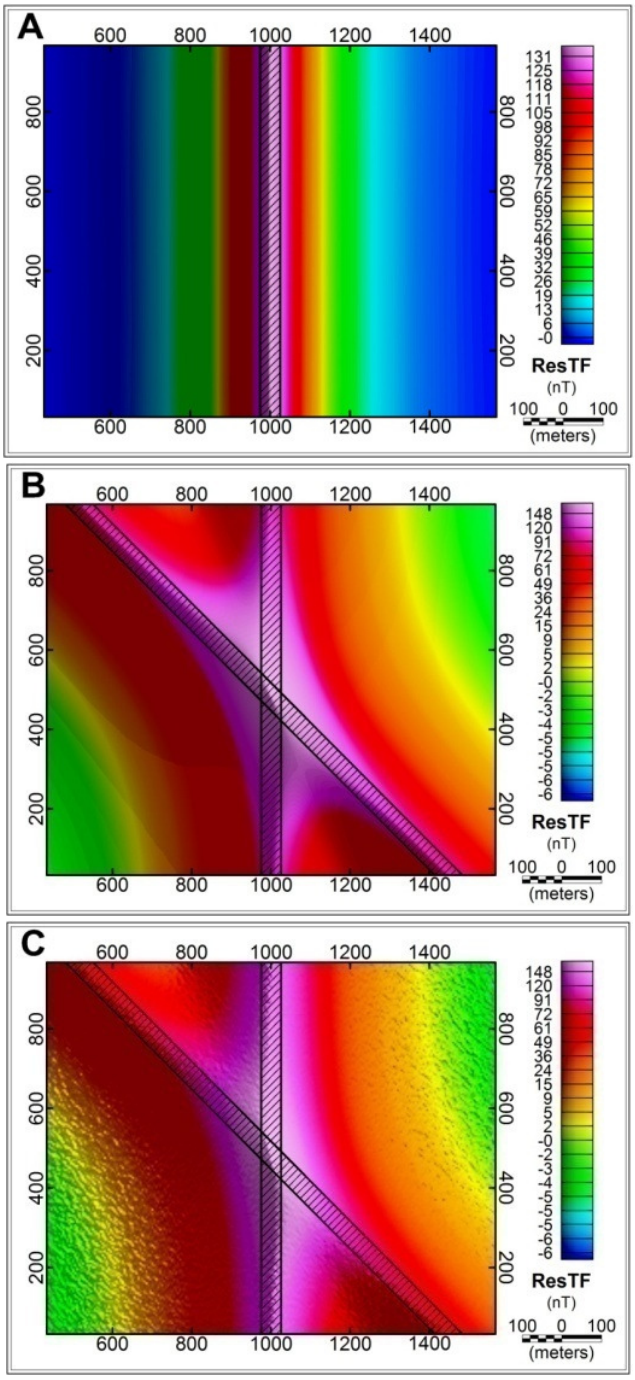

Figure 5.2. The residual total field (ResTF) defined by (A) Synthetic data set A, a N-S non-dipping magnetic dyke (black dashed polygon); (B) Synthetic data set B, intersecting N-S and NW-SE non-dipping magnetic dykes (black dashed polygon); (C) data set C, intersecting N-S and NW-SE non-dipping magnetic dykes with Gaussian noise (black dashed polygon).

5.4 Results

5.4.1 Synthetic data set A

The Blakely-Simpson algorithm defined a peak when all eight surrounding cells to the central cell P_0 are lower ('isolated peak'). This selection produced the most idealistic results (Figure 5.3A) since defining a peak as any central cell with lower cells in only one direction produced too many solutions ('all peaks'). The algorithm ran with the application of a single smoothing filter (Hanning); higher order filters did not produce solutions any better than a single order filter. The analytic signal was determined from the calculated vertical and horizontal derivatives in combination with a single pass Hanning filter. The same peak selection process was used as in Blakely-Simpson (Figure 5.3B). Network extraction was applied to the inverted magnetic data set over a 0.1 km interpretation area. This interpretation area was selected to capture the greatest amount of detail (less than 1% of the grid cells) without being computationally expensive (Figure 5.3C). No filter was applied in network extraction. All methods correctly identified the source peak location and in the case of analytic signal, a source thickness can be approximated.

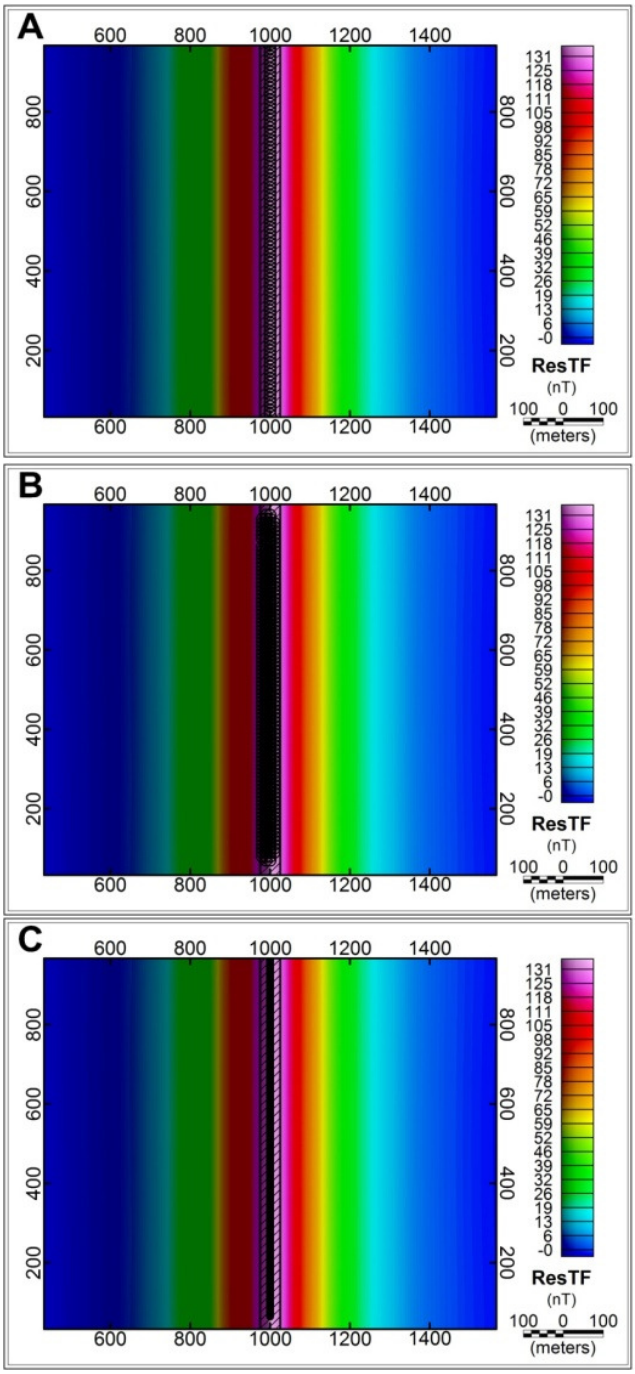

Figure 5.3. Synthetic data set A, a N-S non-dipping magnetic dyke (black dashed polygon); (A) Blakely-Simpson algorithm source peak locations (○); (B) Analytic signal source peak locations (○); (C) Network extraction locations (heavy black line).

5.4.2 Synthetic data set B

The Blakely-Simpson algorithm was applied so 'all peaks' were identified; 'isolated peaks' produced too few solutions and only within proximity of the dyke intersection. A single smoothing filter was once again applied as orders greater than one yielded no significant difference in the solutions (Figure 5.4A). The analytic signal was determined from the calculated derivatives and 'all peaks' were identified with three passes of a smoothing filter to minimize low amplitude variations caused by the interfering magnetic anomalies (Figure 5.4B). The results from the Blakely-Simpson algorithm and analytic signal are very similar. Both methods show a similarity in the distribution of solutions, with the most accurate solutions occuring at the very specific intersection between the dykes and near the extremities of the dykes (edge of study area). Network extraction was again calculated with an interpretation area of 0.1km without a filter (Figure 5.4C). The network extraction shows clean results without any outliers as are visible in both the Blakely-Simpson algorithm and analytic signal solutions. Although the point of intersection determined by network extraction is not as accurate, this miscalculation is due simply to the thickness of the dykes (and therefore an approximate dyke thickness can be determined).

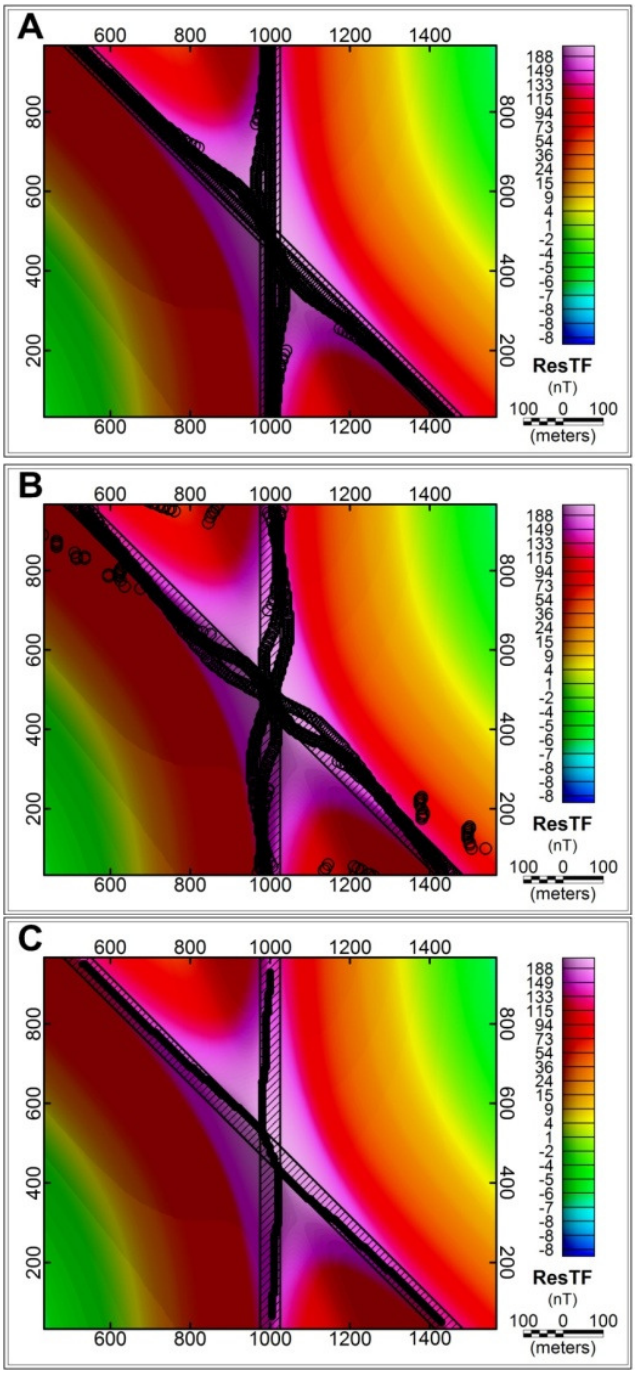

Figure 5.4. Synthetic data set B, intersecting N-S and NW-SE non-dipping magnetic dykes (black dashed polygon); (A) Blakely-Simpson algorithm source peak locations (○); (B) Analytic signal source peak locations (○); (C) Network extraction locations (heavy black line).

5.4.3 Synthetic data set C

Calculating similar parameters as in scenario B, the Blakely-Simpson algorithm identified 'all peaks'. However, this time a high order smoothing filter (20 passes) was required to mitigate the Gaussian noise and even then the noise is still present in the solutions (Figure 5.5A). Extraneous solutions are present over the magnetically 'quiet' areas and along some segments of the dykes even though the solutions produced by the Blakely-Simpson algorithm over the dykes themselves are very accurate. Analytic signal was calculated with a Hanning filter of 20 passes (as with Blakely-Simpson, the noise was still present despite filtering) and 'all peaks' selected (Figure 5.5B). 'Isolated anomaly' selection did not resolve the dykes at all, even after multiple filtering passes. The analytic signal was most susceptible to the noise as a result of the calculated derivatives which amplified the noise. Network extraction was again applied over a 0.1 km interpretation area without a filter (Figure 5.5C). The peak solutions from each method show evidence of the Gaussian noise; however, the network extraction produced the cleanest results and without the application of any pre-processing. The network extraction algorithm did not identify the noise since it is randomly distributed throughout the data set and does not recognize it as signal (a 'lineament'). If we incorporate a lower threshold essentially applying a high-pass filter into the Blakely-Simpson or analytic signal routines then the noise may be diminished and extraneous solutions minimized.

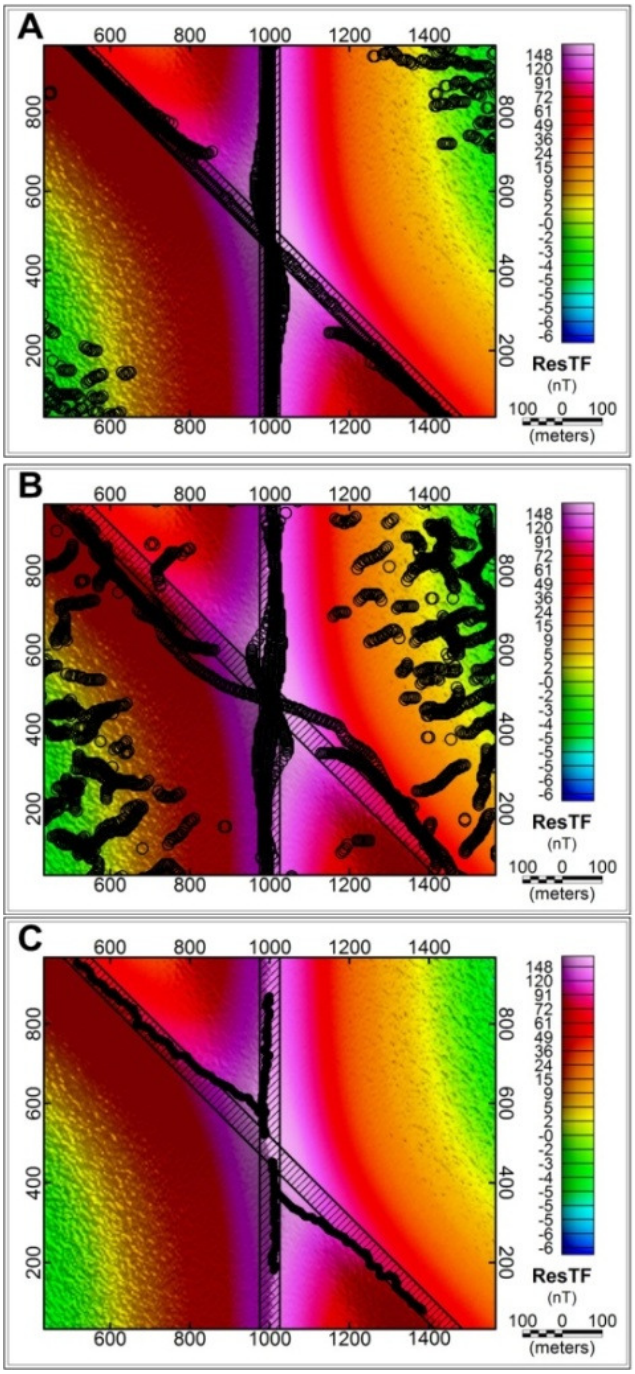

Figure 5.5. Synthetic data set C, intersecting N-S and NW-SE non-dipping magnetic dykes with Gaussian noise (black dashed polygon); (A) Blakely-Simpson algorithm source peak locations (○); (B) Analytic signal source peak locations (○); (C) Network extraction locations (heavy black line).

5.5 Discussion

Based on our work, network extraction offers three advantages over other standard source peak methods:

Continuity: Most source peak methods operate under the assumption of single peak anomalies, while network extraction assumes if central cell P_0 is a ridge and one of the surrounding eight cells was also identified as a ridge then the two ridges are related. This provides two benefits. First the identification of random noise is minimized and second the output is a polyline that may be used as a vector in any geologic or resource assessment map.

Automation: Network extraction is executed automatically on any surface data set (magnetics grid in this work) resulting in a consistent and repeatable methodology. Network extraction does offer though various parameters the experienced user may adjust depending on the data set.

Amplitude cut-off: Network extraction allows the user to enable an amplitude threshold. Although this was not used in the synthetic data sets of this work, this is beneficial for more 'real world' situations. This allows the user to complete analysis over a data range to target specific sources without having to complete a regional-residual separation as a pre-processing step. This amplitude cut-off may also be applied in the Blakely-Simpson and analytic signal methods. The advantage with the presented method is network extraction allows the user to define both an upper and lower bound, whereas the two former methods only offer an upper bound.

5.6 Conclusion

With increased data acquisition (size of the area to be mapped, higher sampling frequency), the prospect of visual interpretation for identifying lineaments becomes more difficult and time consuming. We have compared three peak detection routines using various synthetic data sets. The first two methods, Blakely-Simpson algorithm and analytic signal routine, are standard tools in source location. The third method, network extraction, is a modified routine based on the idea of curvature analysis, drawing properties from the Blakely-Simpson peak detection algorithm and a GIS-derived algorithm typically used on a topographic surface for extracting stream networks. Network extraction offers some benefits over standard source location methods: application to any point data interpolated as a surface (e.g. magnetic data); continuity of features to generate lineament polylines (vector); automatic identification of both negative and positive linear anomalies; and amplitude cut-off for identification of specific

sources. Network extraction may be simple, but is effective as it is a readily available GIS tool enabling a geologist to quickly and automatically identify continuous linear features (lineaments) on any surface. Network extraction does allow though the more experienced user to modify specific parameters by implementing the algorithm in any code-based software. The vector outputs may also be used as an additional layer in any geoscientific map, including bedrock geology and mineral resource assessments. In the end network extraction, used in combination with other standard peak detection routines, allows the interpreter to extract the greatest amount of information from a data set. This modified network extraction method was successfully applied to three synthetic scenarios mimicking idealistic real-world situations involving normally-magnetized dykes. The next step is application of the network extraction algorithm to real-world data to see if the method properly identifies geologic features under less-than ideal parameters.

5.7 References

Blakely, R., and Simpson, R., 1986, Approximating edges of source bodies from magnetic or gravity anomalies: *Geophysics ,* 51 (7), 1494-1498.

Chernicoff, C., Richards, J., and Zappettini, E., 2002, Crustal lineament control on magmatism and mineralization in northwestern Argentina: geological, geophysical, and remote sensing evidence: *Ore Geology Reviews*, 21 (3-4),127-155.

Crafford, A., and Grauch, V., 2002, Geologic and geophysical evidence for the influence of deep crustal structures on Paleozoic tectonics and the alignment of world-class desposits, north-central Nevada, USA: *Ore Geology Reviews*, 21 (3-4) 157-184, DOI: 10.1016/S0169-1368(02)00088-4.

Cooper, G.R.J., 2010, Enhancing ridges in potential field data: *Exploration Geophysics*, 41, 170-173.

Cooper, G.R.J., and Cowan, D.R., 2006, Enhancing potential field data using filters based on the local phase: *Computers and Geosciences*, 32 (10), 1585-1591.

Cooper, G.R.J., and Cowan, D.R., 2008, Edge enhancement of potential field data using normalised statistics: *Geophysics*, 71 (3), H1-H4.

Evans, I.S., 1972, General geomorphometry, derivatives of altitude and descriptive statistics: In Chorley, R. J. (Ed.), *Spatial Analysis in Geomorphology*, p.36, Methuen, London.

Florinsky, I.V., 2005, Artificial Lineaments in Digital Terrain Modeling: Can Operators of Topographic Variables Cause Them?: *Mathematical Geology*, 37 (4), 357-372.

Hansen, R.O., and deRidder, E., 2006, Linear feature analysis for aeromagnetic data: *Geophysics,* 71 (6), L61-L67.

Harris, J.R. (Ed.), 2008, Remote Predictive Mapping: An Aid for Northern Mapping: *Geological Survey of Canada Open File 5643*, CD release.

Karnieli, A., Melsels, A., Fisher, L., and Arkin, Y., 1996, Automatic extraction and evaluation of geologic linear features from digital remote sensing data using a Hough Transform: *Photogrammetric Engineering and Remote Sensing*, 62 (5), 525 -531.

Lalor, J., 1987, The Olympic Dam copper-uranium-gold-silver deposit, South Australia: *4th Circum-Pacific Energy and Mineral Resources Conference*, 561-567, Singapore: Horn, MK (Ed.) .

Masuda, S., Tokuo, T., Ichinose, T., Otani, K., and Uchi, T., 1991, Expert System for lineament extraction from optical sensor data: *Geoinformatics*, 2, 195 -200.

Moore, I.D., Burch, G.J., Mackenzie D.H., 1988, Topographic effects on the distribution of surface soil, water, and the location of Ephemeral gullies: *American Society of Agricultural and Biological Engineers*, 31 (4), 1098-1107.

Moore, I.D., Grayson, R.B., and Landson, A.R., 1991, Digital Terrain Modeling: A Review of Hydrological, Geomorphological, and Biological Applications: *Hydrological Processes*, 5, 3-30.

Nabighian, M.N., 1972, The analytic signal of two-dimensional magnetic bodies with polygonal cross-section: its properties and use for automated anomaly interpretation: *Geophysics*, 37 (3), 507-517.

O'Driscoll, 1980, The double helix in global tectonics: *Tectonophysics*, 63, 397-417.

Phillips, J., Hansen, R., and Blakely, R., 2007, The use of curvature in potential-field interpretation: *Exploration Geophysics,* 38, 111-119.

Pilkington, M., 2007, Locating geologic contacts with magnitude transforms of magnetic data: *Journal of Applied Geophysics*, 63, 80-89.

Pilkington, M., and Keating, P., 2004, Contact mapping from gridded magnetic data – a comparison of techniques: *Exploration Geophysics*, 35, 306-311.

Pilkington, M., and Keating, P., 2009, The utility of potential field enhancements for remote predictive mapping: *Canadian Journal of Remote Sensing*, 35, S1-S11.

Raghavan V., Wadatsum, K., and Masumoto, S., 1993, Automatic extraction of lineament information of satellite images using digital elevation data: *Nonrenewable Resources*, 2 (2), 148–155.

Roberts, A., 2001, Curvature attributes and their application to 3D interpreted horizons. *First Break,* 19.2, 85-100.

Reid, A., Allsop, J., Granser, H., Millett, A., and Somerton, I., 1990, Magnetic interpretation in three dimensions using Euler deconvolution: *Geophysics*, 55 (1), 80-89.

Roest, W.R, Verhoef, J. and Pilkington, M., 1992, Magnetic interpretation of the 3-D analytic signal: *Geophysics*, 57 (1), 116-125.

Salem, A., Williams, S., Fairhead, D., Ravat, D., and Smith, R., 2007, Tilt-depth method: A simple depth estimation method using first-order magnetic derivatives: *The Leading Edge*, 26 (12), 1502-1505.

Shary, P.A., 1995, Land surface in gravity points classification by complete system of curvatures: *Mathematical Geology*, 27 (3), 373-390.

Spector, A., and Grant, F.S., 1970, Statistical models for interpreting aeromagnetic data. *Geophysics*, 35, 293-302.

Twidale, C.R. 2007. E. S. T. O'Driscoll, lineaments and ring structures: In Bourne J. A. and Twidale C. R. (Ed.), *Crustal Structures and Mineral Deposits*, p.15, Rosenburg, Australia.

Woodall, R., 1994, Empiricism and concept in successful mineral exploration: *Australian Journal of Earth Sciences,* 41 (1), 1-10.

Woodall, R., 2007, From Broken Hill to Olympic Dam: E. S. T. O'Driscoll's lifelong study of the structural setting of mineral deposits: In Bourne J. A. and Twidale C. R. (Ed.), *Crustal Structures and Mineral Deposits*, p.15, Rosenburg, Australia.

Zevenbergen, L.W., and Thorne, C.R., 1987, Quantitative analysis of land surface topography: *Earth surface processes and landforms*, 12, 47-56.

6.0 A network extraction tool for mineral exploration: A case study from the Wopmay Orogen, Northwest Territories, Canada

Lee, M.D., Morris, W.A., Harris, J., and Leblanc, G., 2012, A network extraction tool for mineral exploration: a case study from the Wopmay Orogen, Northwest Territories, Canada: *Exploration Geophysics*, DOI: 10.1071/EG11045.

6.1 Abstract

Many mineral exploration initiatives target regional- and local-scale lineaments (e.g. fault systems and dyke swarms) as they may act as conduits for mineralized fluids. In this work, we apply an automatic lineament 'network extraction' method drawing on similar processes as the Blakely-Simpson peak detection algorithm and a stream network extraction algorithm commonly used in the mapping of drainage patterns from a topographic surface (e.g. DEM, DTM) within a Geographic Information System (GIS) environment. We apply the network extraction algorithm to a magnetic surface (grid) rather than a topographic surface. The method uses a simple quadratic surface across a 3 x 3 window to determine the degree of surface slope and if the centre cell of the window represents a localized low point in the surface. This routine is particularly effective at identifying magnetic lows representing faults, which have undergone magnetite depletion (e.g. hematization). These lineament solutions provide insight into mineral exploration vectors through the computation of rose diagrams, fracture density plots and intersection locations. These diagrams, plots, and locations are used in conjunction with other geophysical layers (e.g. radiometrics) to help identify potential mineral exploration targets. We successfully applied this algorithm to an aeromagnetic data set from the Wopmay Orogen in Northwestern Canada. This area is characterised by extensive regional and localized fault systems and dyke swarms, along with promising polymetallic hydrothermal mineral occurrences. Key areas for follow up exploration are identified through a combined study of geophysical grids and lineament analysis.

6.2 Introduction

Lineament analysis has assisted in the identification of many oil and mineral deposits (Lalor, 1986; O'Driscoll, 1986; Woodall, 1994; Chernicoff et al., 2002, Crafford and Grauch, 2002; Woodall, 2007). A geologic lineament is a linear crustal weakness (micro-, meso- and macroscale) that may have a tectonic, lithological or glacial origin and typically represents faults systems and dyke swarms. Lineaments may act as conduits for mineralized fluids and gasses from the mantle. This provides favourable physical and chemical conditions to alter the surrounding wall rocks making lineaments vectors for mineral exploration (Twidale, 2007). With respect to global tectonics, four major lineament directions have been shown to occur: WNW, NNW, NNE, and ENE (Florinsky, 2006; Twidale, 2007) based mainly on the interpretation of LANDSAT and gravity data sets. The intersection points of these global lineaments are associated with geophysical anomalies, such as gravity and magnetics (O'Driscoll, 1980). Mineral deposits and major basin patterns often occur within lineament corridors – a set of lineaments with similar azimuth and/or occur at the junction points of these lineament corridors (Twidale, 2007). Thus lineament analysis can be an effective mineral exploration tool by objectively extracting potential mineralized zones from geoscientific data sets including magnetics - the focus of this work.

Lineament analysis may be conducted in either a visual (qualitative) (Harris et al., 2008) or an automated (quantitative) manner (Masuda et al., 1991; Raghavan et al., 1993; Karnieli et al., 1996). Visual extraction of lineaments is completed through the inspection of various geoscientific data: aerial photography, satellite imagery, and geophysical data. Visual extraction can be very effective as it incorporates the geologist's prior knowledge and as such the extracted lineaments can be screened (e.g. geologically calibrated) in real time (Harris et al., 2008). Visual extraction is subjective though and depends on the experience and biases of the interpreter. Automated lineament extraction methods offer the advantages of speed, efficiency and objectivity in the lineament identification and extraction process. Geophysics offers a suite of automated methods that may be used for delineating lineaments. Geophysical data sets although collected as point data, are typically analyzed as a surface in grid form. With respect to a magnetic surface, it will have a specific curvature at each interpolated data point and this curvature can provide insight on the causative source at that specific geographic location (Spector and Grant, 1970; Roberts, 2001). Curvature analysis of an aeromagnetic grid allows the interpreter to extract lineaments from a magnetic data set and to approximate whether the lineaments are more likely to represent lithological contacts, dykes, or faults by examining the statistics of various types of curvature.

'Network extraction' is a lineament analysis algorithm (Lee et al., 2012) based in curvature analysis and draws on principals from existing peak detection routines like the Blakely-Simpson algorithm (Blakely and Simpson, 1986). The Blakely-Simpson algorithm utilizes a 3 x 3 moving window (kernel) to deduce whether the central cell is a peak (maximum curvature) relative to the surrounding eight cells. The application of a moving window to deduce gradients (and therefore surficial curvature) between cells is a common tool in Geographic Information System (GIS) software packages as well (Encom Discover). Drainage feature extraction utilizes digital elevation models (DEM) and is an important part of drainage basin analysis (Evans, 1972; Zevenbergen and Thorne, 1987; Moore et al., 1988; Moore et al., 1991). Drainage feature extraction calculates the curvature of a topographic surface to delineate stream location, flow impact, and flow direction by identifying localized topographic low points (trough) and their continuity on a topographic surface. Like Blakely-Simpson, this GIS drainage basin analysis method also uses the principal of a simple quadratic surface for a 3 x 3 moving window (kernel) to determine the degree of surface slope and whether the centre cell of the window represents a localized low point in the surface. In this paper, instead of topographic lows the network extraction method identifies troughs on a magnetic surface that may represent faults and fractures associated with the depletion of magnetite (e.g. alteration through oxidation - hematization) or remanently magnetized dykes (Lee et al., 2010).

Once lineaments are extracted from the magnetic data set they can be (geologically) comparatively assessed with information extracted from other complementary data sets such as topography, radiometrics, electromagnetics, and geological field mapping (O'Driscoll, 1980; O'Driscoll, 1986; Shives et al., 1997; Smith, 2002; Woodall, 2007). Geologic terranes often have a dominant fracture or fabric orientation which may be reflective of their deformation history. By isolating specific lineament azimuths we can resolve different geologic terranes, lithologies, or phases. Ore deposits commonly occur along fracture systems acting as conduits for metal enriched hydrothermal and magmatic fluids (O'Driscoll, 1986; Twidale, 2007; Woodall, 2007) as previously mentioned. When multiple fractures culminate at a common intersection, the probability of an ore deposit increases (O'Driscoll, 1986; Twidale, 2007; Woodall, 2007). Mapping of lineament density and intersections in concurrence with geophysical grids may indicate potential exploration areas (vectors). The computation of azimuth, fracture density, and intersection locations can be conducted on any lineament data set regardless of the initial computation method. These applications simply broaden the breadth of information derived.

This paper applies the network extraction method with a suite of secondary studies to a high-resolution aeromagnetic data set flown over a portion of the Wopmay Orogen, Northwest Territories, Canada to delineate geological structure and potential zones of mineralization.

6.3 Method

Network extraction uses a 3 x 3 moving window applied to the gridded data set to calculate the gradient in all directions between the center cell P_0 (x, y) and the surrounding eight cells. This computation is completed using a simple quadratic function and determines whether P_0 (x, y) is a trough (Evans, 1972; Roberts, 2001).

$$z = ax^2 + by^2 + cxy + dx + ey + f \quad (1)$$

Where x and y are horizontal components and a, b, c, d, e, and f are coefficients representing arithmetic equations from which one may determine the dip degree and angle of the surface (Evans, 1972; Roberts, 2001). The scale of interpretation may be controlled though the selection of the eight grid nodes. By selecting grid nodes further from P_0 (x, y), an interpretation area equivalent to 5 x 5 or 7 x 7 for example (or via a coarser grid cell size), regional gradients may be calculated. Although the routine is designed to identify surficial lows, by inverting (multiply each data point by -1) the values of the magnetic data set, positive linear anomalies (ridges) are identified. These ridges may represent normally magnetized dykes for example. This is acceptable as the routine only relies on the relative magnitude of the cells, not the value of the cell itself. This means 'normal' lineament solutions represent low magnetic anomalies (troughs) and 'inverted' solutions represent high magnetic anomalies (ridges).

The network extraction method offers three benefits over conventional peak location methods (Lee et al., 2012). First, the output of a network analysis is a series of polylines. The algorithm seeks laterally continuous troughs by identifying at minimum two consecutive lows. This varies from other methods like the Blakely-Simpson algorithm which produces single point solutions from which a trend needs to be manually interpreted. Second, network extraction is automated which allows the solutions to be repeatable and objective; however, parameters may be modified by a more experienced user if necessary. Thirdly, network extraction offers an amplitude thresholding (an upper and lower bound) which enables interpretation to be conducted over a specific data range. This threshold is useful for isolated targeting as an alternative to regional-residual separation or when a priori knowledge is available. Other semi-automated methods including the Blakely-Simpson algorithm offer an amplitude cut-off, however network

extraction allows a maximum and minimum threshold while most traditional methods only enable an upper bound.

Secondary applications applied to the network extracted lineaments include direction analysis, fracture density plots, and intersection location. Direction analysis is applied to the extracted lineaments by calculating the azimuth of each lineament and displayed as a rose diagram. Each azimuth bin (5°) has been allotted a colourization based on the following (modified from RockWorks^{TM}):

I. **Background (light grey):** $|x| < \mu_{\%} + \sigma$
II. **Moderately Anomalous (dark grey):** $\mu_{\%} + \sigma < |x| < \mu_{\%} + (2\sigma)$
III. **Highly Anomalous (black):** $\mu_{\%} + (2\sigma) < |x| < \mu_{\%} + (3\sigma)$

Where $|x|$ is magnitude of the residual magnetic field, σ is standard deviation, and $\mu_{\%}$ is mean percentage.

As the number of lineaments within a specified area increases so does the probability for alteration and mineralization. The frequency of lineaments within each grid cell across the study area is calculated to determine fracture density over a defined area. The grid cell size will be a function of the computed surface, typically ¼ of the flight line spacing. Any grid cell with a fracture density greater than one represents a possible lineament intersection location. The computation of a buffer zone around these intersections objectively isolates possible exploration target areas that can be overlaid on additional geophysical data, like magnetics and radiometrics. The size of the buffer zone depends on the geologic environment under investigation, as the scale of mineralization and alteration will vary by deposit type.

Specific ore deposits can be associated with characteristic geophysical signatures, such as magnetic highs due to enhanced magnetite alteration, gravity highs due to the positive density contrast of ore and alteration minerals, or radiometric highs due to potassium and uranium enrichment. These lineament analysis outputs (fracture density and lineament intersections) are combined with the response between various geophysical image types to identify key areas for future exploration studies. For example, an association between lineament intersection points and magnetic anomaly highs might be indicative of a region characterised by increased fracture density and increased magnetic mineral content.

6.4 Example data set

Network extraction was applied to a portion of a high resolution (for large scale exploration) aeromagnetic data set from the Wopmay Orogen, Northwest Territories, Canada (Figure 6.1A). The total field magnetics data (along with radiometrics) set was commissioned by the Northwest Territories Geoscience Office for geological mapping and mineral potential assessment. The flight lines were flown east-west at 400 m intervals along a terrain-draped surface with an average elevation of 150 m ± 22.8.

The Wopmay Orogen is a 2.6 to 1.85 Ga Paleoproterozoic orogenic belt composed of four geologic domains: Coronation margin (Archean and Paleoproterozoic metasedimentary rocks and plutons); the 1.87 to 1.85 Ga Great Bear magmatic zone (GBmz); the Wopmay fault zone (divisional fault between Coronation margin and GBmz); and the >1.89 Ga Hottah terrane which extends eastward as the basement for much of the GBmz. Discussion on the geology and geologic history of the Wopmay Orogen can be found in Hildebrand et al. (1987, 1990, 2010a, b), Bowring and Grotzinger (1992); Gandhi (1994), Cook et al. (1999), Gandhi et al. (2001), Cook and Erdmer (2005); Spratt et al. (2009), Oueity and Clowes (2010), Hoffman et al. (2011), Jackson and Ootes (2011). The study area for this work covers portions of the GBmz, the Wopmay fault zone, and the Coronation margin (Figure 6.1B).

The GBmz area has been of recent economic interest due to the recognition of extensive hydrothermal iron oxide copper-gold (IOCG) type alteration with mineralized prospects and deposits (Goad et al., 2000; Mumin, 2002; Corriveau and Mumin, 2008; Corriveau et al., 2008; Mumin et al., 2009). The primary examples are NICO (Co-Au-Bi) and Sue-Dianne (Cu-Ag) deposits (Figure 6.1A), which were discovered as a result of geophysical anomalies (Smith, 2002). Iron oxide copper-gold deposits in Australia, such as Olympic Dam and those in the Cloncurry district (Williams and Skirrow, 2000; Fu et al., 2003; Baker et al., 2008) occur along structural lineament corridors coincident with magnetite, potassium, and uranium enriched granite (Lalor, 1986; Smith, 2002; Twidale, 2007; Woodall, 2007). Therefore lineament analysis is an ideal method to apply within the GBmz as a possible vector for mineralization.

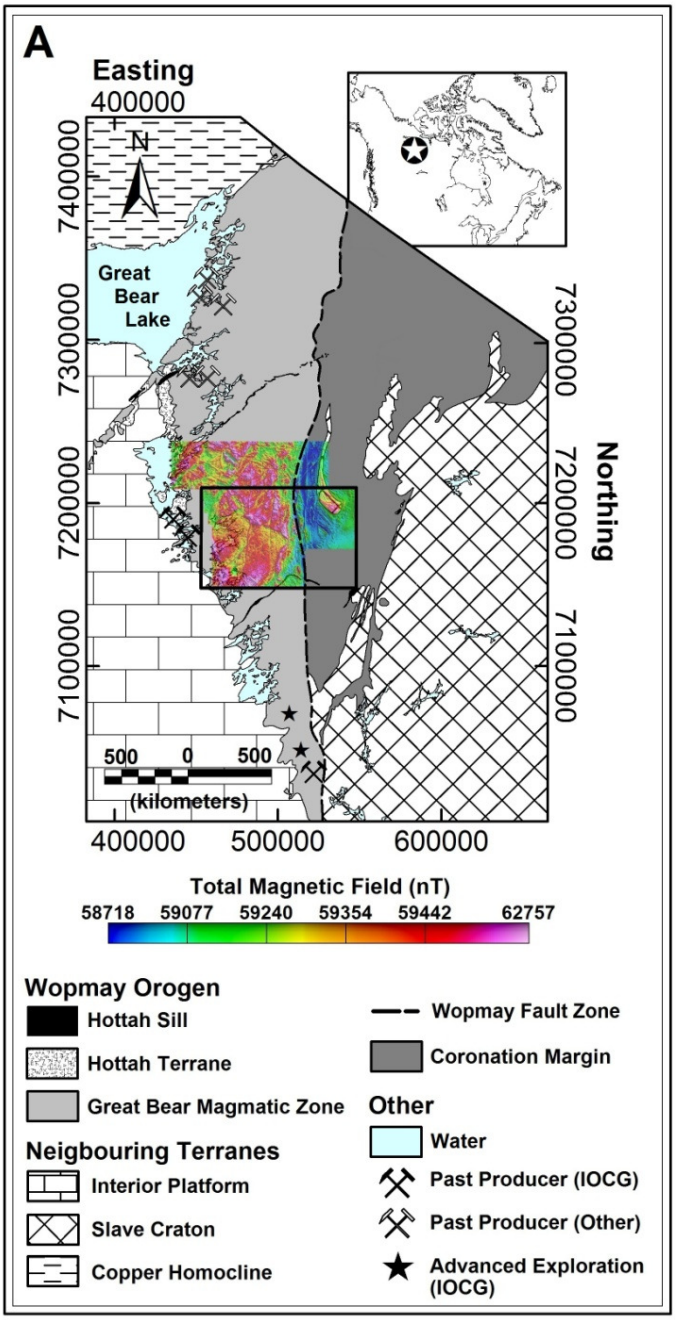

Figure 6.1A. Geologic setting of the Wopmay Orogen (after Hoffman and Hall, 1993) and its location in northwestern Canada (top right inset map). The area of this study is indicated by the black box and partly coincides with the footprint of a combined radiometric and total magnetic field airborne survey flown in 2007. Mineral resources are indicated after NORMIN.db, http://www.nwtgeoscience.ca/normin/. The two black stars represent Sue-Dianne (north) and NICO (south).

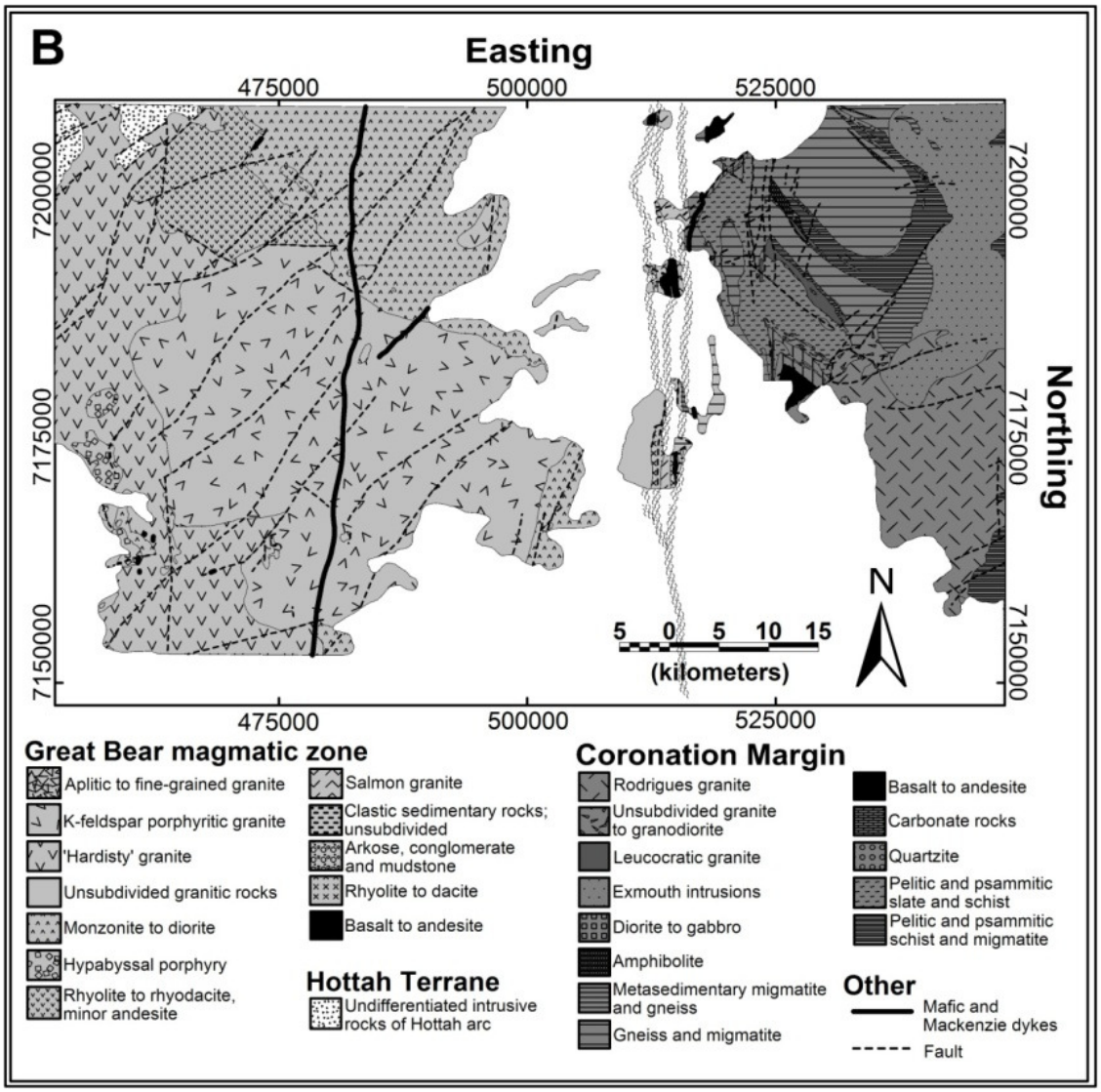

Figure 6.1B. Detailed geological map over study area (after Jackson and Ootes, 2011). The general area of the Wopmay Fault zone (after Hoffman and Hall, 1993) has been indicated with black hashes dividing the Great Bear magmatic zone and the Coronation Margin.

6.5 Results

6.5.1 Lineament extraction

Network extraction was applied to the Residual Total Field (ResTF) (Figure 6.2) to compute the normal (Figure 6.3A) and inverted (Figure 6.3B) lineaments.

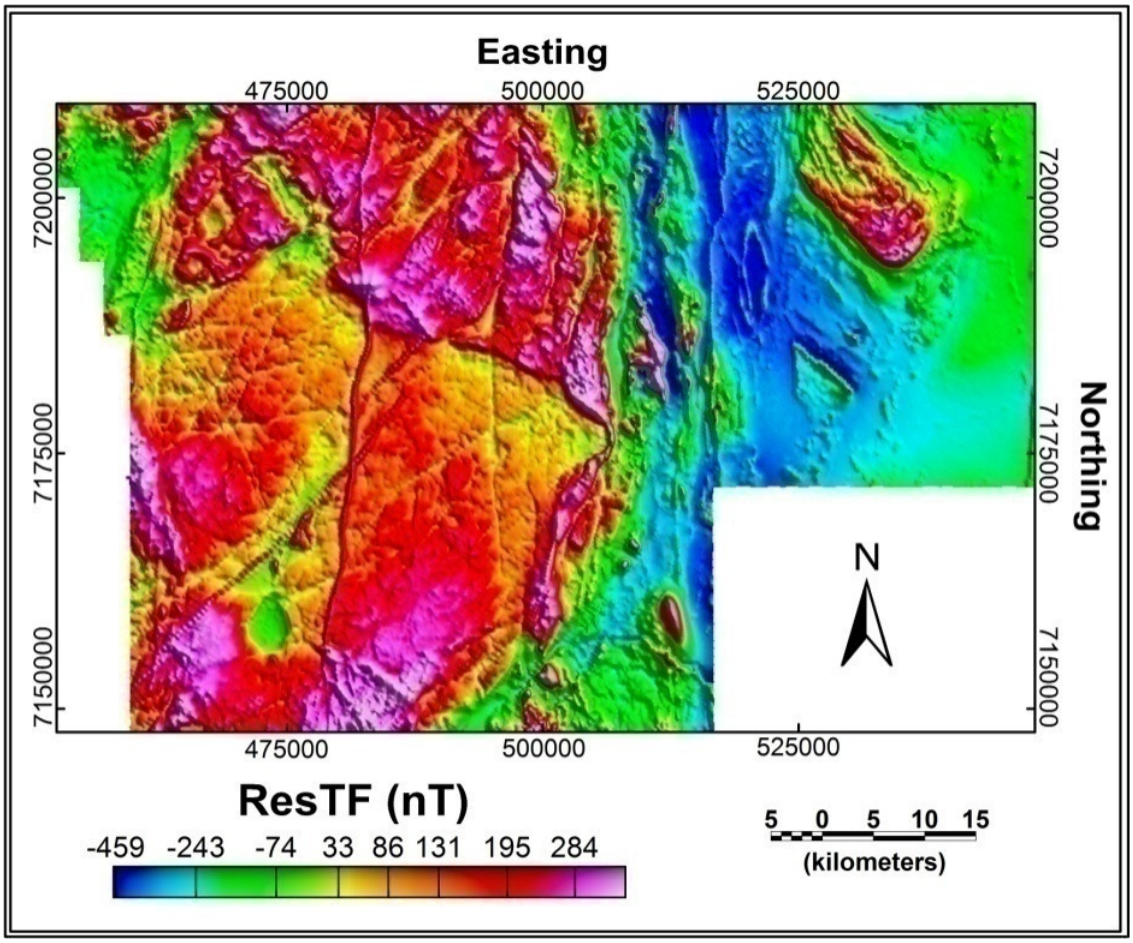

Figure 6.2. Residual Total Field (ResTF) over study area.

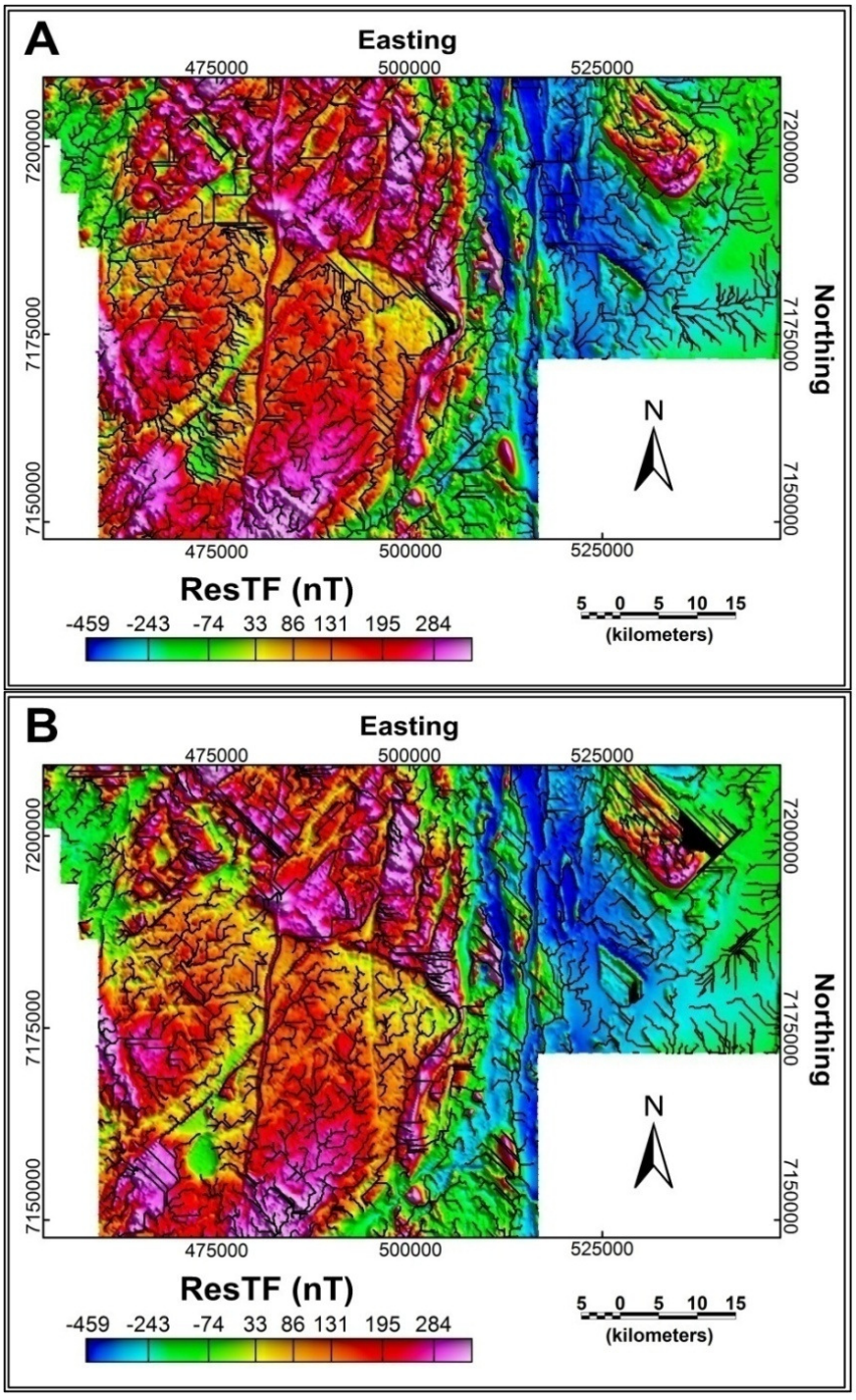

Figure 6.3. ResTF data with network extraction solutions. The normal (A) and inverted (B) lineament solutions are indicated with heavy black lines. Normal solutions represent troughs (faults, fractures, and reverse-polarity dykes) and inverted solutions represent ridges (normal-polarity dykes).

6.5.2 Lineament directions

Direction analysis of the normal and inverted lineament analysis solutions resolved background, moderately anomalous, and highly anomalous populations. Our observation of both rose diagrams in Figure 6.4 reveals three primary populations of lineaments in the magnetic data set. The dominant geologic fabrics are 0°-5° (N), 45°-50° (NE), and 135°-140° (SE). These populations represent geologic lineaments since the analysis is computed on magnetic field data not affected by vegetation or water bodies like other remotely sensed data (e.g. LANDSAT). The study area has been recently mapped (Jackson and Ootes, 2011) at a scale sufficient to support the conclusion majority of the lineaments represent geological features.

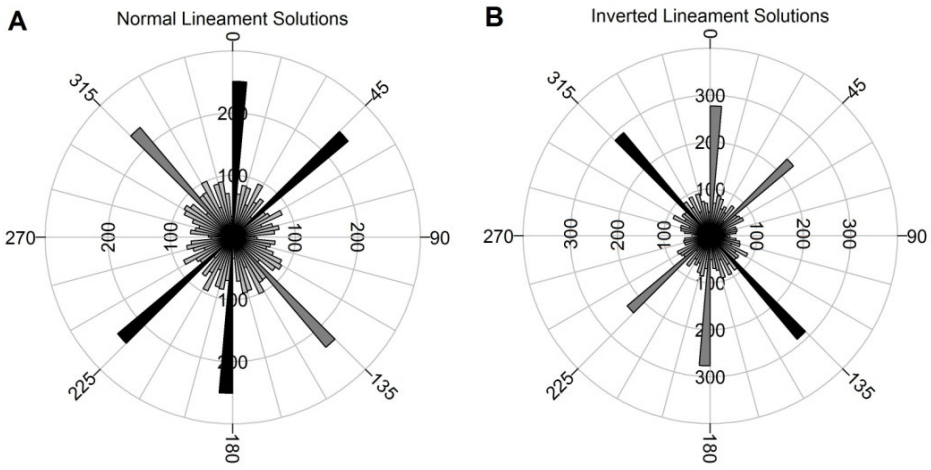

Figure 6.4. Rose diagrams of normal (A) and inverted (B) magnetic lineament directions. Dominant geologic fabrics are 0°-5° (N), 45°-50° (NE), 135-140° (SE). Background, moderately anomalous, and highly anomalous populations are indicated in light grey, dark grey, and black respectively.

These lineament results corroborate previous lineament studies conducted on aerial photographs, topography, and geophysical derivatives over the GBmz (Hildebrand et al., 1987; Goad et al., 2000; Mumin et al., 2009), which indicate strong NE and SE fracture configurations within the Wopmay Orogen. The NE lineaments correspond to mapped faults and fractures (Figure 6.1B) in the GBmz (Hildebrand et al., 1987; Jackson, 2008; Jackson and Ootes., 2011), which merge with the Wopmay fault zone. Subsequent events have used these zones of weakness for magma and hydrothermal fluid injection into the crust, including giant quartz veins and stockworks (Byron, 2010) and diabase dykes associated with Hottah mafic intrusions (Harlan et al., 2003; Sandeman et al., 2007). The aeromagnetic data shows the presence of the NW-trending 1740 Ma Cleaver diabase dyke swarm with an azimuth of 280°-310° immediately north of the study area (Ross and

Eaton, 1997; Irving et al., 2004). The SE lineaments in Figure 6.4 may be related to this dyke swarm based on similar azimuth and proximity.

The N lineaments correspond to the Wopmay fault zone and Mackenzie dykes. The Wopmay fault zone defines a regional deformation and metamorphic boundary between the GBmz and the Coronation margin (Hildebrand et al., 1990; Ghandi et al., 2001; Jackson and Ootes, 2011). The radiating 1260 Ma Mackenzie dyke swarm (LeCheminant and Heaman, 1989) cuts the study area along a north-south trend over this portion of the Canadian Shield (Figure 6.1B). The Mackenzie dykes are mafic in composition and exhibit a magnetic fabric due to late-crystallizing magnetite (Ernst and Baragar, 1992), and represented as positive magnetic lineaments.

Since radiometric surveys can only marginally penetrate water and measurements over water are typically used for calibration of atmospheric radon levels (Grasty and Minty, 1995), any radiometric readings conducted over water are considered noise and omitted (Figure 6.5 – white areas). However, some remnant noise due to shallow water bodies and swamps surrounding lakes and rivers can be seen as areas of blue in Figure 6.5B. The comparison of water bodies with the radioelement grids also ensures any radioelement enrichment due to glacial till (and other clays) accumulation along topographic corridors is not interpreted to be mineral-related. The radioelements (potassium – %K, uranium – eU, and thorium – eTh) were compared to the extracted lineaments representing magnetic lows (normal non-inverted magnetic data set), which likely represent later faults and fracture systems (Figure 6.5). Potassium and uranium enrichment appear as alteration halos around mineral deposits (Shives et al., 1997). Normal lithologic potassium variation can be differentiated from potassium anomalies associated with mineralization through the statistical or qualitative analysis of the characteristic Th/K ratio. Potassic alteration is often accompanied by depletion in Th, since Th is typically immobile when potassium-rich fluids produce hydrothermal alteration zones.

Displayed extracted normal magnetic lineaments (assumed to be faults and fractures) over top of the radiometric ratio layers indicate both potassium enrichment and depletion correlate with zones of increased fracture density (Figure 6.5A). This is particularly evident in the monzonite to diorite rocks of the GBmz in the northern portion of the study area and the abundant tonalite-granodiorite, and the sediments from which they are derived, of the Coronation margin in the eastern portion of the study area (Figure 6.1B). Thorium enrichment is apparent near the lithological boundary between two phases of GBmz granite in the central part of the study area. The spatial correlation is not as apparent with respect to uranium enrichment or depletion. There is correlation though

between increased fractures and uranium enrichment along north-south lineaments in the eastern portion of the GBmz proximal to the Wopmay fault zone.

6.5.3 Fracture density and lineament intersections

The fracture density plot in Figure 6.6 indicates areas with a high probability for alteration and mineralization as those grid cells intersected by a high number of lineaments (warm colours). The lineament frequency was calculated for each grid cell, which was 100 m in size (¼ the flight-line spacing). The maximum number of lineaments in a grid cell was seven, occurring in the southwestern quadrant of the inverted lineaments data set (Figure 6.6B). Increased fractionation results in the intersection of lineaments. Intersection locations for normal and inverted lineaments were overlaid on existing geophysical grids – ResTF (Figure 6.7) and radiometrics (Figure 6.8). We are interested in alteration on a kilometre scale so we have chosen to isolate intersection locations with a 1km buffer.

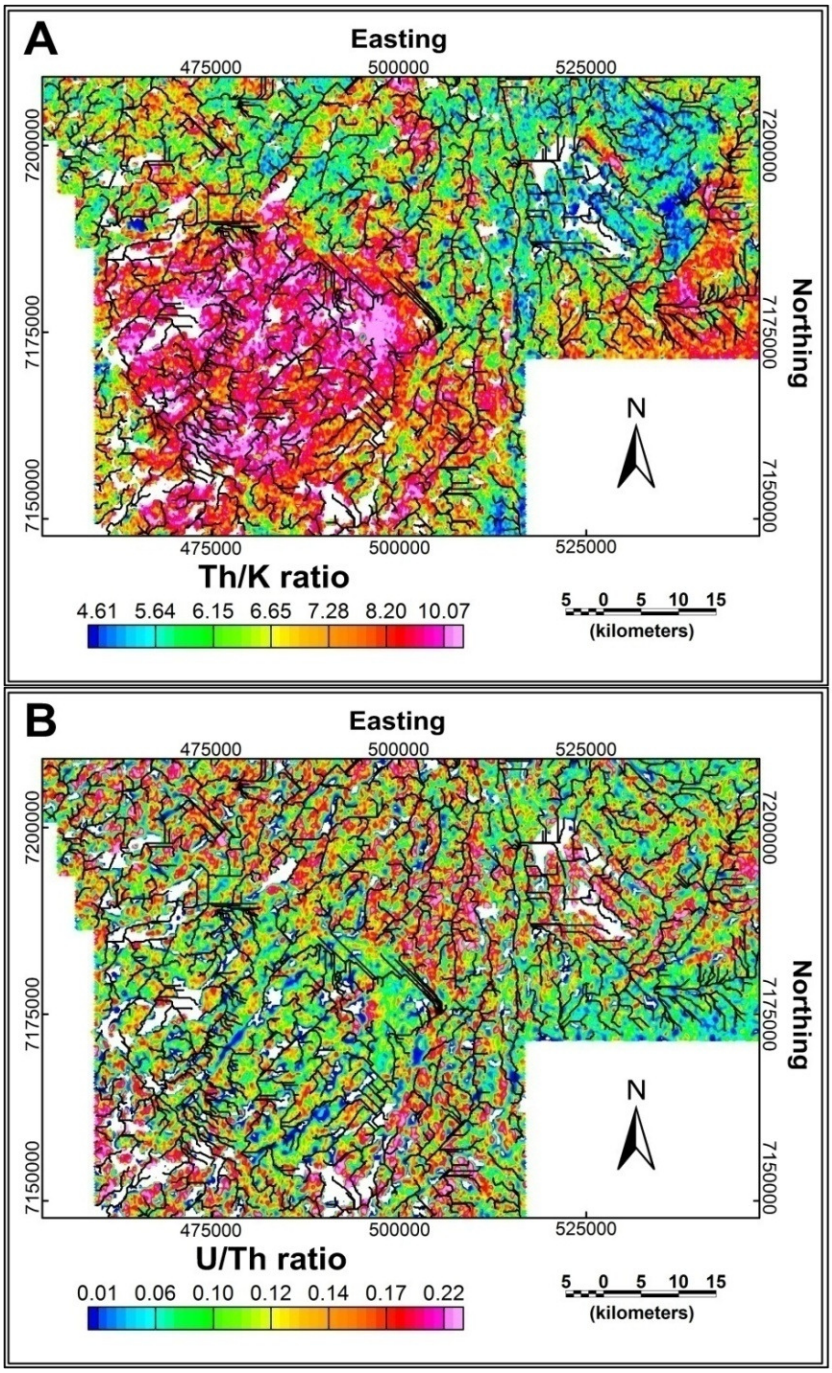

Figure 6.5. Radioelement ratios Th/K (A) and U/Th (B) compared with normal magnetic lineaments (fault systems). The lineaments extracted from the magnetic data show a strong correlation with potassium depletion, especially in the eastern portion of the study area within the Coronation margin. Correlation between uranium enrichment and north-south faulting is apparent in proximity of the Wopmay fault zone. Water bodies have been omitted (white), however remanent effects can be seen in blue.

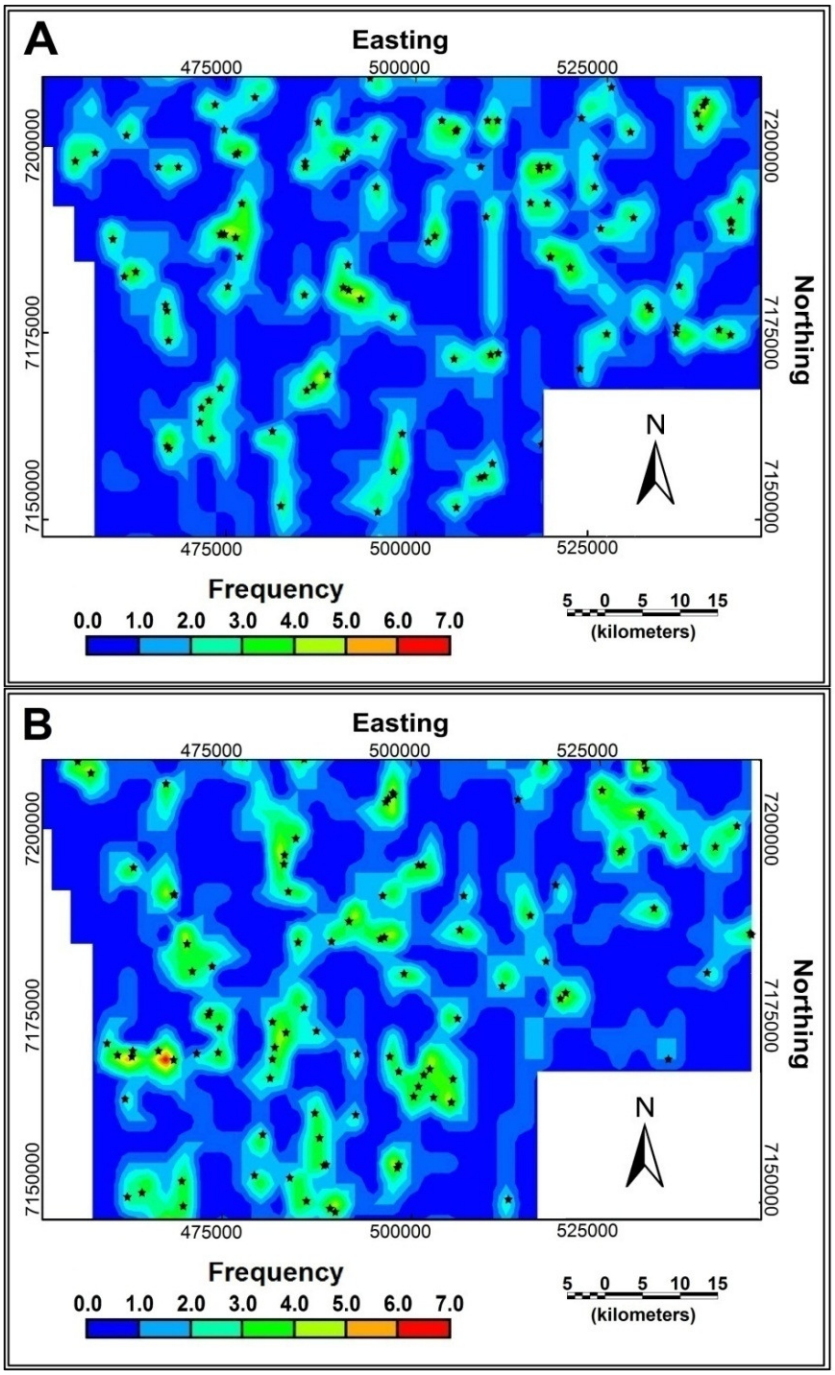

Figure 6.6. Frequency of normal (A) and inverted (B) lineaments with intersection points (□). The greatest frequency of lineaments solutions (seven) occurs in the inverted data set (B).

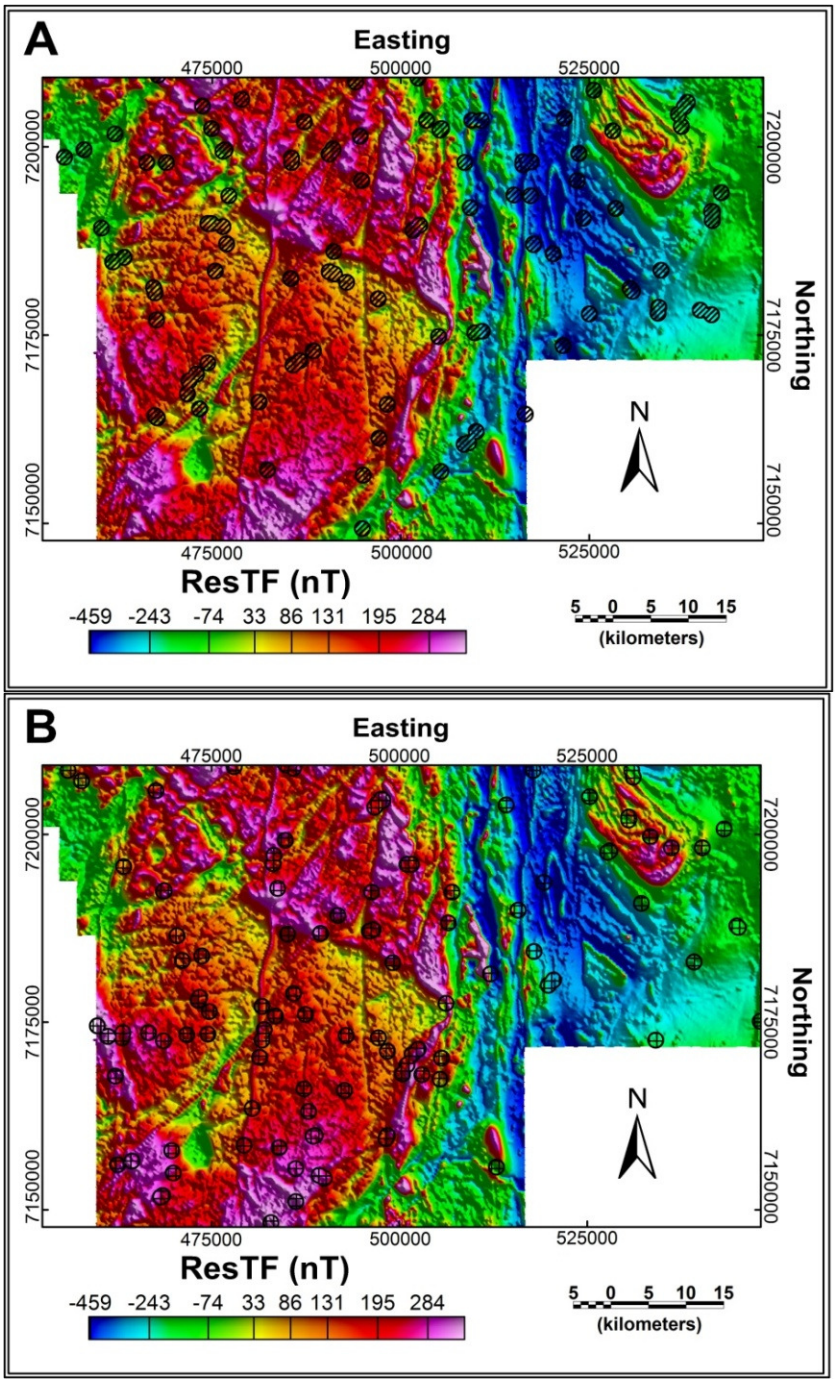

Figure 6.7. Buffer zones (the hatched area within circle) of 1 km have been placed around the intersection coordinate of normal (A) and inverted (B) lineaments and overlaid on ResTF. These buffer areas indicate potential mineral exploration targets.

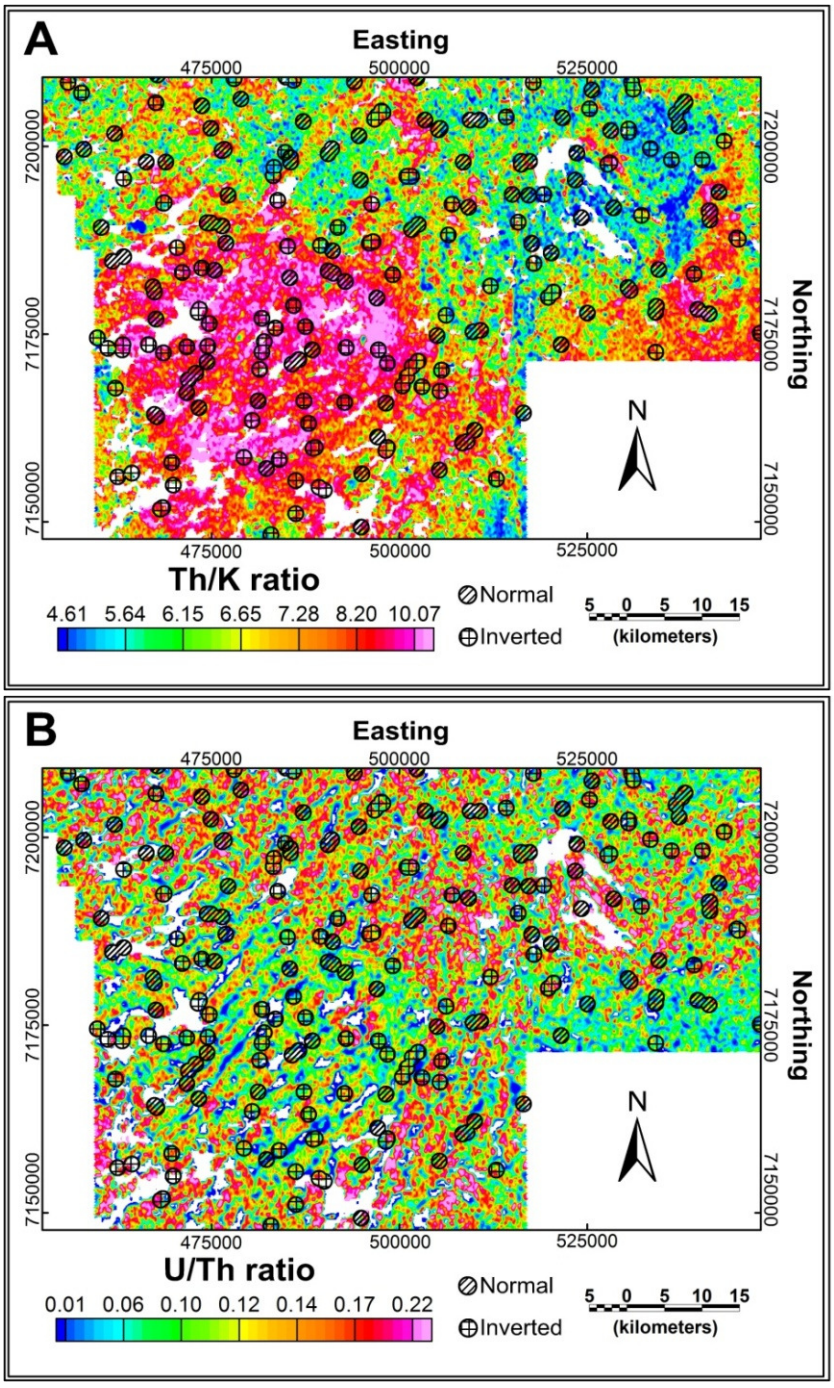

Figure 6.8. Buffer zones (the hatched area within circle) of 1 km have been placed around the intersection coordinate of normal and inverted magnetic lineaments and overlaid on Th/K (A) and U/Th (B) maps. These buffer areas indicate potential mineral exploration targets.

Combining the lineament analysis solutions with the magnetic and radioelement grids, an 'areas of interest' map was generated. This involved converting the ResTF grid, the U/Th, and inverted Th/K (increased potassium appear as highs rather than lows) grids into 0-255 scale images. These grids were added to generate one summation grid (also a 0-255 scale image) where values closest to 255 indicate areas with positive anomalies for all three geophysical quantities. We assume each data set has an equal contribution to the overall probability of mineralization. Limiting the summation grid to the 1 km buffer zones from Figure 6.7 indicated where magnetite and radioelement enrichment are occurring within areas of increased fractionation (Figure 6.9). Promising exploration targets in the final map are mainly located within the GBmz, along the contact with the Wopmay fault zone and between various granitoid phases. If we consider the highest priority area based on the Exploration Target scale (grid value closest to 255) from Figure 6.9 (red box), this location hosts a known (unclassified) magnetite-rich mineral occurrence (white triangle) with elevated uranium, copper, and iron (Gandhi, 2007).

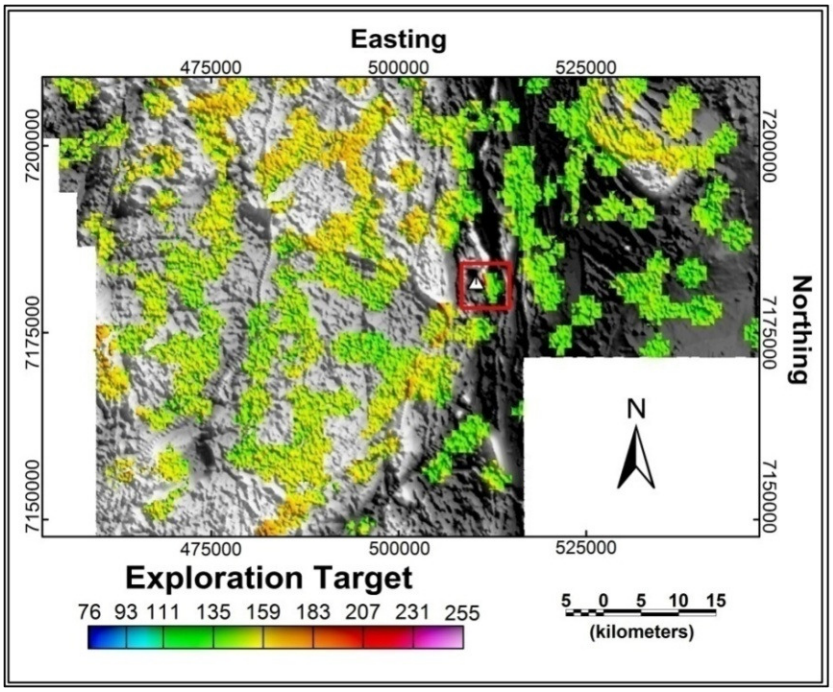

Figure 6.9. Map with areas of interest. The background is a greyscale image of ResTF to give a geological context with a 255 scale 'areas of interest' grid overlaid on top. Warm colours indicate areas with magnetic anomaly highs, and radioelement enrichment (potassium and uranium). The 'areas of interest' grid has been limited to the 1 km buffer zones seen in Figure 6.7. The area of greatest interest (red square) is concurrent with a known magnetite-U showing (white triangle).

6.6 Conclusion

With increased data acquisition and larger mapping areas, the prospect of visual interpretation for delineating lineaments becomes difficult and time consuming. This makes automatic lineament extraction an attractive alternative. We have presented a simple automated method, network extraction, for delineating linear anomalies in a magnetic data set. The method is based on curvature analysis principals used in the Blakely-Simpson algorithm and the GIS-derived drainage basin algorithm. The lineament solutions produced by network extraction may be defined in greater detail through the secondary analyses of lineament azimuth and intersections. These may be used as an additional vector layer in mineral resource assessment maps. Network extraction, lineament direction and intersection studies were successfully applied to a high-resolution aeromagnetic data set from the Northwest Territories, Canada. Three sets of lineaments were resolved by the rose diagrams, each associated with mapped geology (Jackson, 2008; Jackson and Ootes, 2011). Regional geologic terranes were resolved in addition to regional and local scale dykes, shear zones, and fracture systems. A final exploration map was generated by adding the geophysical grids (magnetics and radioelements) into a single summation grid clipped to areas of greatest lineament density.

6.7Acknowledgements

The authors wish to thank V. Jackson, L. Ootes from the Northwest Territories Geoscience Office and L. Corriveau of the Geological Survey of Canada for their support and assistance on bedrock geology, petrology, and helpful discussion of the manuscript. This work was in part funded by numerous programs: the IOCG-Great Bear (00410) and Remote Predictive Mapping (GKM005) projects of the Geomapping for Energy and Minerals program through Natural Resources Canada; the South Wopmay Bedrock Mapping project of the Northwest Territories Geoscience Office through Aboriginal Affairs and Northern Development Canada; and the Polar Continental Shelf Program (50709). The project was conducted through various collaborative agreements between Natural Resources Canada, the Northwest Territories Geoscience Office, the Community Government of Gamètì, and Fortune Minerals Limited. The authors would also like to acknowledge the contribution by the Editor, Associated Editor, and Reviewers for their recommended revisions.

6.8 References

Baker, T., Mustard, R., Fu, B., Williams, P.J., Dong, G., Fisher, L., Mark, G. and Ryan, C.G., 2008, Mixed messages in iron oxide–copper–gold systems of the Cloncurry district, Australia: insights from PIXE analysis of halogens and copper in fluid inclusions: *Mineralium Deposita*, 43, 599-608.

Blakely, R. and Simpson, R., 1986, Approximating edges of source bodies from magnetic or gravity anomalies: *Geophysics*, 51 (7), 1494-1498.

Bowring, S.A. and Grotzinger, J.P., 1992, Implications of new chronostratigraphy for tectonic evolution of Wopmay Orogen, Northwest Canadian Shield: *American Journal of Science*, 292, 1-20.

Byron, S.J., 2010, *Giant Quartz Veins of the Great Bear Magmatic Zone, Northwest Territories, Canada*: M.Sc. thesis (unpublished), University of Alberta, 146 p.

Chernicoff, C., Richards, J. and Zappettini, E., 2002, Crustal lineament control on magmatism and mineralization in northwestern Argentina: geological, geophysical, and remote sensing evidence: *Ore Geology Reviews*, 127-155.

Cook, F.A. and Erdmer, P., 2005, An 1800 km cross section of the lithosphere through the northwestern North American plate: lessons from 4.0 billion years of Earth's history: *Canadian Journal of Earth Sciences*, 42 (6), 1295-1311.

Cook, F.A., van der Velden, A.J., Hall, K.W. and Roberts, B.J., 1999, Frozen subduction in Canada's Northwest Territories: Lithoprobe deep lithospheric reflection profiling of the western Canadian Shield: *Tectonics*, 18(1), 1-24.

Corriveau, L. and Mumin, A.H., 2008, Exploring for Iron Oxide Copper-Gold Deposits - The Need for Case Studies, Classifications and Exploration Vectors: in Corriveau, L. and Mumin, H. (eds.), *Exploring for Iron Oxide Copper-Gold Deposits: Canada and Global Analogues*: Mineral Deposits Division, Geological Association of Canada and Geological Survey of Canada, Short Course, *20*, 1-10.

Corriveau, L., Williams, P.J. and Mumin, H., 2008, Alteration Vectors to IOCG Mineralization - From Uncharted Terranes to Deposits: in Corriveau, L. and Mumin, H. (eds.), *Exploring for Iron Oxide Copper-Gold Deposits: Canada and Global Analogues*: Mineral Deposits Division, Geological Association of Canada and Geological Survey of Canada, Short Course, *20*, 87-106.

Crafford, A. and Grauch, V., 2002, Geologic and geophysical evidence for the influence of deep crustal structures on Paleozoic tectonics and the alignment of world-class desposits, north-central Nevada, USA: *Ore Geology Reviews*, 157-184.

Evans, I.S., 1972, General geomorphometry, derivatives of altitude and descriptive statistics: in Chorley, R. J. (Ed.), *Spatial Analysis in Geomorphology*, 17-90.

Ernst, R.E. and Barager, W.R.A., 1992, Evidence from magnetic fabric for the flow pattern of magma in the Mackenzie giant radiating dyke swarm: *Nature*, 356, 511-513.

Fu, B., Williams, P.J., Oliver, N.H.S., Dong, G., Pollard, P.J. and Mark, G.M., 2003, Fluid mixing versus unmixing as an ore forming process in the Cloncurry Fe-oxide-Cu-Au district, NW Queensland, Australia: evidence from fluid inclusions: *Journal of Geochemical Exploration*, 78-79, 617-622.

Florinsky, I.V., 2006, Global Lineaments and Ring Structures: Application of Digital Terrain Modeling: in *Proceedings of International Symposium on Terrain Analysis and Digital Terrain Modeling*, 1-17.

Gandhi, S., 1994, Geological setting and genetic aspects of mineral occurrences in the southern Great Bear magmatic zone, Northwest Territories: *Geological Survey of Canada Bulletin*, 475, 63-96.

Gandhi, S. (comp.), 2007, World Distribution of Fe Oxide ± Cu-Au-U (IOCG) Deposits: *Geological Survey of Canada*, unpublished.

Gandhi, S. S., Mortensen, J. K., Prasad, N. and van Breeman, O., 2001, Magmatic evolution of the southern Great Bear continetal arc, northwestern Canadian Shield: Geochronological constraints: *Canadian Journal of Earth Sciences*, 38, 767-785.

Goad, R.E., Mumin, A.H., Duke, N.A., Neale, K.L., Mulligan, D.L. and Camier, W.J., 2000, The NICO and Sue-Dianne Proterozoic, Iron Oxide-hosted, Polymetallic Deposits, Northwest Territories: Application of the Olympic Dam Model in Exploration: *Exploration and Mining Geology*, 9 (2), 123-140.

Grasty, R. and Minty, B.R.S., 1995, A guide to the technical specifications for airborne gamma-ray surveys: *Australian Geological Survey Organization*, Record 1995/60, 1-89.

Harlan, S.S., Heaman, L., LeCheminant, A.N. and Premo, W.R., 2003, Gunbarrel mafic magmatic event: A key 780 Ma time marker for Rodinia plate reconstructions, 31, 1053-1056.

Harris J.R. (Ed.), 2008, Remote Predictive Mapping: *An Aid for Northern Mapping*, Geological Survey of Canada Open File 5643, CD release.

Hildebrand, R.S, Hoffman, P.F. and Bowring, S.A., 1987, Tectono-magmatic evolution of the 1.9-Ga Great Bear magmatic zone, Wopmay Orogen, northwestern Canada: *Journal of Volcanology and Geothermal Research*, 32, 99-118.

Hildebrand, R.S., Bowring, S.A. and Housh, T., 1990, The medial zone of Wopmay Orogen, District of Mackenzie: In *Current research, Part C*, Geological Survey of Canada, Paper 90-1C, 167-176.

Hildebrand, R.S, Hoffman, P.F. and Bowring, S.A., 2010a, The Calderian orogeny in Wopmay Orogen (1.9 Ga), northwestern Canadian Shield: *Geological Society of America Bulletin*, 122 (5-6), 794-814.

Hildebrand, R.S., Hoffman, P.F., Housh, T. and Bowring, S.A., 2010b, The nature of volcano-plutonic relations and the shapes of epizonal plutons of continental arcs as revealed in the Great Bear magmatic zone, northwester Canada: *Geosphere*, 6 (6), 812-839.

Hoffman, P.F. and Hall, L., 1993, Geology, Slave craton and environs, District of Mackenzie, Northwest Territories. Geological Survey of Canada Open File 2559, 1 map scale 1:1,000,000.

Hoffman, P.F., Bowring, S.A., Buchwaldt, R. and Hildebrand, R.S., 2011, Birthdate for the Coronation paleocean: age of initial rifting in Wopmay Orogen, Canada: Canadian Journal of Earth Sciences, 48 (2), 281-293.

Irving, E., Baker, J., Hamilton, M. and Wynne, P.J., 2004, Early Proterozoic geomagnetic field in western Laurentia: implications for paleolatitudes, local rotations and stratigraphy. Precambrian Research, 129 (3-4), 251-270.

Jackson, V.A., 2008, Preliminary geologic map of part of the Southern Wopmay Orogen (parts of NTS 86B and 86C; 2007 updates); Northwest Territories Geoscience Office, NWT Open Report 2008-007. 1 map, scale 1:100,000, and accompanying report, 51 p.

Jackson, V.A. and Ootes, L., 2011, Preliminary Geologic Map of the South-Central Wopmay Orogen (parts of NTS 86B, 86C, and 86D); results from 2009 and 2010; Northwest Territories Geoscience Office, NWT Open Report 2011-007. 1 map, scale 1:100,000, and accompanying report, 41 p.

LeCheminant, A.N. and Heaman, L.M., 1989, Mackenzie igneous events, Canada: middle Proterozoic hotspot magmatism associated with ocean opening: *Earth and Planetary Science Letters*, 96 (1-2), 38-48.

Lee, M.D., Morris, W.A., Harris, J. and Leblanc, G., 2012, An automatic network extraction algorithm applied to magnetic survey data for the identification and extraction of geologic lineaments: *The Leading Edge*, 31, 26-31.

Lee, M.D., Morris, W.A. and Ugalde, H.A., 2010, Mapping of apparent magnetic susceptibility and the identification of fractures: A case study from the Eye-Dashwa Lakes pluton, Atikokan, Ontario: *Geophysics*, 75 (3), B147-B156.

Karnieli, A., Melsels, A., Fisher, L. and Arkin, Y., 1996, Automatic extraction and evaluation of geologic linear features from digital remote sensing data using a Hough Transform: *Photogrammetric Engineering and Remote Sensing*, 62 (5), 525 -531.

Lalor, J., 1986, The Olympic Dam copper-uranium-gold-silver deposit, South Australia: in M.K. (Ed.), *4th Circum-Pacific Energy and Mineral Resources Conference*, 561-567.

Masuda, S., Tokuo, T., Ichinose, T., Otani, K. and Uchi, T., 1991, Expert System for lineament extraction from optical sensor data: *Geoinformatics*, 2, 195 -200.

Mitchell, R.N., Hoffman, P.F. and Evans, D.A.D., 2010, Coronation loop resurrected: Oscillatory apparent polar wander of Orosirian (2.05-1.8 Ga) palaeomagnetic poles from Salve craton: *Precambrian Research*, 179, 121-134.

Moore, I.D., Burch G.J. and Mackenzie, D.H., 1988, Topographic effects on the distribution of surface soil, water, and the location of Ephemeral gullies: *American Society of Agricultural and Biological Engineers*, 31 (4), 1098-1107.

Moore I.D., Grayson, R.B. and Landson A.R., 1991, Digital Terrain Modeling: A Review of Hydrological, Geomorphological, and Biological Applications: *Hydrological Processes*, 5, 3-30.

Mumin, A.H., 2002, Scoping study for hydrothermal iron-oxide copper-gold deposits (Olympic Dam–type), Manitoba: *Report of Activities 2002*, Manitoba Industry, Trade and Mines, Manitoba Geological Survey, 303-308.

Mumin, A.H., Somarin, A.K., Jones, B., Corriveau, L., Ootes, L. and Camier, J., 2009, The IOCG-porphyry-epithermal continuum of deposits types in the Great Bear Magmatic Zone, Northwest Territories, Canada, Exploring for iron oxide copper-gold deposits:

Canada and global analogues: *Geological Association of Canada Short Course Notes*, 20, 59-78.

O'Driscoll, E.S.T., 1980, The double helix in global tectonics: *Tectonophysics*, 63, 397-417.

O'Driscoll, E.S.T., 1986, Observation of the lineament-ore relation: Philosophical Transactions of the Royal Society, 317 (1539), 195-218.

Oueity, J. and Clowes, R.M., 2010, Paleoproterozoic subduction in northwestern Canada from near-vertical and wide-angle seismic reflection data: *Canadian Journal of Earth Sciences*, 47, 35-52.

Raghavan V., Wadatsum, K. and Masumoto, S., 1993, Automatic extraction of lineament information of satellite images using digital elevation data: *Nonrenewable Resources*, 2 (2), 148–155.

Roberts A., 2001, Curvature attributes and their application to 3D interpreted horizons: *First Break*, 19 (2), 85-100.

Ross, G.M. and Eaton, D.W., 1997, Winagami reflection sequence: Seismic evidence for postcollisional magmatism in the Proterozoic of western Canada: *Geology*, 25, 199-202.

Sandeman, H.A.I, Ootes, L. and V. Jackson, 2007. Field petrographic, and petrochemical data for the Faber Sill: insights into the petrogenesis of a Gunbarrel event intrusion in the Wopmay Orogen, NWT, Canada; Northwest territories Geoscience Office, NWT Open File Report 2007-007, 25p.

Shives, R.B.K., Charbonneau, B.W. and Ford, K.L., 1997, The detection of Potassic Alteration by Gamma-Ray Spectrometry – Recognition of Alteration Related to Mineralization: In Gubins, A.G. (Ed.), *Proceedings of Exploration 97: Fourth Decennial International Conference on Mineral Exploration*, 1997, 741-752.

Smith, R.J., 2002, Geophysics of Iron Oxide Copper-Gold Deposits: in Porter, T.M. (Ed.), *Hydrothermal Iron Oxide Copper-Gold & Related Deposits: A Global Perspective*, 2, 357-367.

Spector, A. and Grant, F.S., 1970, Statistical models for interpreting aeromagnetic data: *Geophysics*, 35, 293-302.

Spratt, J.E., Jones, A.G., Jackson, V.A., Collins, L. and Avdeeva, A., 2009, Lithospheric geometry of the Wopmay Orogen from a Slave craton to Bear Province magnetotelluric transect: *Journal of Geophysical Research*, 114, B01101.

Twidale, C.R., 2007, E. S.T. O'Driscoll, lineaments and ring structures: in Bourne, J. A. and Twidale, C.R. (Eds.), *Crustal Structures and Mineral Deposits*, 11-21.

Williams, P.J. and Skirrow, R.G., 2000, Overview of Iron Oxide-Copper-Gold Deposits in the Curnomona Province and Cloncurry District (Eastern Mount Isa Block), Australia: In Porter, T.M. (Ed.), *Hydrothermal Iron Oxide Copper-Gold & Related Deposits: A Global Perspective*, 1, 105-122.

Woodall, R., 1994, Empiricism and concept in successful mineral exploration: *Australian Journal of Earth Sciences* , 41 (1), 1-10.

Woodall, R., 2007, From Broken Hill to Olympic Dam: E.S.T. O'Driscoll's lifelong study of the structural setting of mineral deposits: In Bourne, J. A. and Twidale, C. R. (eds.), *Crustal Structures and Mineral Deposits*, 117-127.

Zevenbergen, L.W., and Thorne C.R., 1987, Quantitative analysis of land surface topography: *Earth surface processes and landforms*, 12, 47-56.

7.0 Quality assurance of aeromagnetic data using lineament analysis

Lee, M.D., and Morris, W.A., 2013, Quality assurance of aeromagnetic data using lineament analysis: *Exploration Geophysics*, DOI: 10.1071/EG12034.

7.1 Abstract

Lineament analysis is typically applied to geoscientific data to identify lithological contacts, faults, fractures, and dyke swarms. In this work we implement lineament analysis as a method for quantifying the adequacy of pre-processing of airborne magnetic dataset. This accomplished through the identification of noise due to inappropriate levelling. Lineament analysis involves the extraction of linear features from a data set using visual and/or automatic interpretation techniques and the statistical and directional analyses of these extracted lineaments. We apply lineament analysis to a leveled high resolution aeromagnetic data set from the Northwest Territories, Canada, to assess the levelling quality. *A priori* knowledge will include geology defining regional tectonic trends such as fault systems and dyke swarms. Analysis of a lineament's azimuth separates assumed geologic sources and noise associated with data acquisition or processing artefacts. The lineament azimuths are assessed as rose diagrams. This is an alternative method to standard computation of 2D radially averaged power spectrums in the frequency domain and sunshading orthogonal to flight path. The rose diagrams are compared with the 2D power spectrums, which both provide quantitative directional information; however, the power spectrum provides spectral frequency content and rose diagrams provide frequency of occurrence. Calculation of the number of lineaments along a particular azimuth before and after pre-processing quantifies the degree to which flight-line variations have been suppressed and geological signal more apparent.

7.2 Introduction

Aeromagnetic survey data is collected along oriented and differentially spaced flight lines with the aim of maximizing signal and suppressing noise. Accordingly, flight lines are commonly flown orthogonal to the dominant geologic and structural trend to capture the greatest amount of signal. Levelling procedures in an aeromagnetic survey are carried out to minimize the effects of line-to-line variations caused by diurnal or instrument drift and navigational errors. Typically, navigational errors due to variations in ground speed and survey height are higher than drift effects; especially for mineral exploration surveys (Green, 1983). Signal amplitude artefacts associated with flight line variations will manifest as either a herringbone effect or corrugation bands parallel to the flight direction (Flis and Cowen, 2000). The principal behind levelling potential field data is identifying and then minimizing the presence of any erroneous signal to ensure the resulting signal image best reflects geology-related physical property variations. Usually all flight lines

are corrected and by using a stationary base-station or orthogonal tie-lines (Green, 1983; Luyendyk, 1997; Mauring et. al, 2000). The conventional means for correcting line-to-line variations is statistically-based using a polynomial fit along-line (Yarger et. al, 1978; Beiki et al., 2010). Similarly, Mauring and Kihle (2006) use a differential median filter along line as well. Conversely, Nelson (1994), Hardwick (1999), and Reford (2006) implement horizontal gradients computed from original survey gridded data. This is particularly useful in cases where the survey area is too large to justify a base station and too costly to justify tie-lines. Microlevelling (Minty, 1991) typically follows standard levelling to minimize level shifts between lines and are in the sub-nanotesla range. Microlevelling typically involves the computation of 1D or 2D FFT in grid format (Minty, 1991; Ferracioli et. al, 1998). Although their discussion focuses primarily on survey-draping techniques to offset terrain effects, Flis and Cowen (2000) and Pilkington and Thurston (2001) address the issue of profile- versus grid-processing. Grid-based approachs may over correct for height effects and remove more signal not parallel to flight line direction. While on the other hand, grid-based approaches consider the sources to be 3D. Although both papers recommend along-line or a combination, neither directly offers a means to assess which lines are erroneous (i.e. insufficiently leveled) in a data set and should undergo correction.

Occasionally, a geophysicist will receive a magnetic data set with very little meta-data associated with the survey describing the various acquisition parameters. This is often the case when a consultant or client receives a processed data set from a contractor who has used their own algorithms to manipulate the data and cannot release processing details for proprietary reasons (Billings and Richards, 2000). At this point the client may not be able to evaluate whether the data set has been sufficiently leveled for flight line variations or have the capability to measure the effects of various pre-processing procedures applied to the data.

The standard method to assess levelling is through the calculation of the second vertical derivative. This is achieved visually leveled through the inspection of a sunshaded grid image, where the azimuth and direction (declination) of luminosity of a three dimensional grid is orthogonal to the flight line direction (Cooper, 2003). Although this method is quick, it may be susceptible to noise (a form of high-pass filter) and offers little to no quantitative information. Analysis of the 2D radial power spectrum offers more quantitative insight. The 2D power spectrum displays the spectral content of the data set along with the azimuth (real world spatial trend) of the sources at all frequencies. The frequency of line noise will depend on the direction of analysis. Although 2D power spectrums and sunshaded images show the user whether remanent artefacts remain in the

data, it is difficult to quantify the degree of levelling. Power spectrums reveal no quantitative information on the number of sources with a particular frequency. More so, it reveals no quantitative information on the spatial distribution (source azimuth), which is the principal benefit to quality assessment in grid format. We present lineament analysis as a tool offering both quantitative and spatial information on the quality of levelling.

Lineament analysis is often applied to various geoscientific data including aerial photography, topography, remotely-sensed images and to a lesser degree geophysics. The purpose of lineament analysis is to identify linear features commonly representing lithological contacts, faults, fractures, and dyke swarms. Geological terranes will often have a dominant structural pattern defined by the orientation and density of lineaments reflecting a terrane's unique geologic and tectonic history (O'Driscoll, 1980; O'Driscoll, 1986; Woodall, 1994; Twidale, 2007; Woodall, 2007). This dominant structural pattern is often revealed through lineament analysis. However, as discussed, linear artefacts associated with data acquisition (navigational and diurnal) will also be identified through lineament analysis. Lineament analysis can be carried out either on a visual (Harris et al., 2008) or quantitative basis (Masuda et al., 1991; Raghavan et al., 1993; Karnieli et al., 1996). Often, quantitative methods are chosen over visual-based methods to save time and ensure consistency. However, automation still requires geologic calibration and screening of the extracted lineaments by an expert who often applies visual interpretation methods to undertake this process. Accordingly, the user needs to be able to effectively isolate which lineaments are geologic in origin and others which may be artefacts and to do so in a consistent and timely fashion.

We introduce a novel method using lineament analysis to assess data quality. The method can make use of a priori geologic information if available to the interpreter, however is not mandatory. Lineament analysis is conducted on a high-resolution magnetic survey data set from the Wopmay Orogen in Northwestern Canada, which includes the extraction of lineaments and analysis of their azimuths through rose diagrams. Since lineaments of geologic origin and those defined by artefacts (flight lines) have distinct azimuths we can, in turn, isolate artefacts and assess image/data quality. To more clearly illustrate the need for quality assessment a small sub-set of the magnetic data is identified displaying more sensitivity to levelling issues.

7.3 Survey data

The aeromagnetic data set under investigation commissioned by the Northwest Territories Geoscience Office was flown in 2007 over the Wopmay Orogen, Northwest Territories, Canada. Flight lines were flown east-west at 400m intervals and along a terrain-draped surface of 150 m ± 22.8. The Paleoproterozoic Wopmay Orogen is composed of various geologic domains and is host to numerous dyke swarms and fault systems making the data set ideal for lineament analysis (Figure 7.1). A detailed discussion of the geology and geologic history of the Wopmay Orogen can be found in Hildebrand et al., 1987; Gandhi, 1994; and Gandhi et al., 2001.

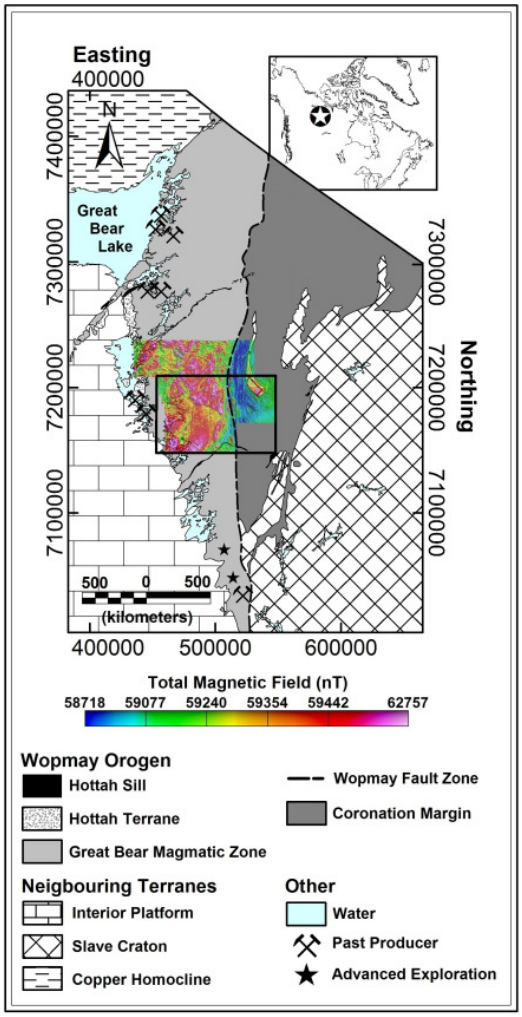

Figure 7.1. Geologic setting of the Wopmay Orogen and its location in northwestern Canada (inset map) after Lee et al. (2012b). The area of this study is indicated by the black box and partly coincides with the footprint of a magnetic airborne survey flown in 2007.

7.4 Method

All of our analyses are conducted on grids where the data are initially gridded using a minimum curvature algorithm at ¼ the flight-line spacing (100m). Standard geophysical processing includes analysis of the power spectrum generated by a Fourier transform to determine dominant spatial frequencies within a magnetic data set. As such, we compute the 2D power spectrums for the raw total magnetic field (TF) and the leveled (lagged, compensated, IGRF-corrected and tie-line leveled - ResTF) aeromagnetic data sets to assess whether survey acquisition artefacts are apparent. Both the raw and leveled aeromagnetic datasets must be of 2^n by 2^n for the 2D power spectrums to be representative of the true spectral content and no padding is necessary. The original grid was cropped to be 512 x 512 grid nodes. The 2D power spectrums were computed for 16 equal blocks of the original magnetic grid where each subset comprised of 128 grid nodes. To highlight anomalous short wavelength directional features, all power spectrums underwent a Butterworth filter to remove regional trends represented by extensive lithology.

Subsequently, the 'network extraction algorithm' (Lee et al., 2012a; Lee et al., 2012b) is applied to identify lineaments from both data sets. This automatic extraction algorithm detects continuous troughs (lows) along a surface which, in this study, are defined by magnetic responses. These troughs are dictated by the surficial curvature of the grid, where each grid node is analyzed with a 3 x 3 window to assess maximum dip direction. Conversely, we may also identify continuous magnetic highs (ridges) by inverting the sign of the data set (multiply by negative one). It is important to note we are not concerned with the lineament extraction method, only the data being analyzed. As such, any automated lineament extraction method may be implemented. The extracted lineament azimuths are plotted on rose diagrams to identify dominant lineament orientations that may reflect an origin due to geological/tectonic processes and/or noise artefacts. These rose diagrams are compared with the computed 2D power spectrums to identify both the frequency content and number of occurrences of the magnetic sources at each orientation. As a comparison we also extracted lineaments over the 128 x 128 subset blocks computed and the azimuths displayed as rose diagrams. Both the power spectrums and rose diagrams are oriented north-upwards, with the rose petals width representing 5° increments and the length representing percentage of total population.

A GIS based buffer analysis procedure is employed to spatially locate lineaments representing artefacts due to insufficient levelling. The buffer locates east-west lineaments situated within 50m of a flight line where both sides result in a buffer area of 100m equivalent to the grid cell size.

7.5 Results

The magnetic grids of the raw and leveled magnetic data were sunshaded from 0° at an inclination of 30° to qualitatively exhibit the differences produced by standard pre-processing routines (Figure 7.2). The lineaments automatically extracted from both grids are shown in Figure 7.3 showing the extracted lineaments are different for the raw and leveled magnetic data. These differences are particularly evident in the magnetically quiet regions within the eastern portion of the study area, where the raw data set (Figure 3A) exhibits strong east-west trends. This region of the study area is characterised by low- to non-magnetized sedimentary and meta-sedimentary rocks.

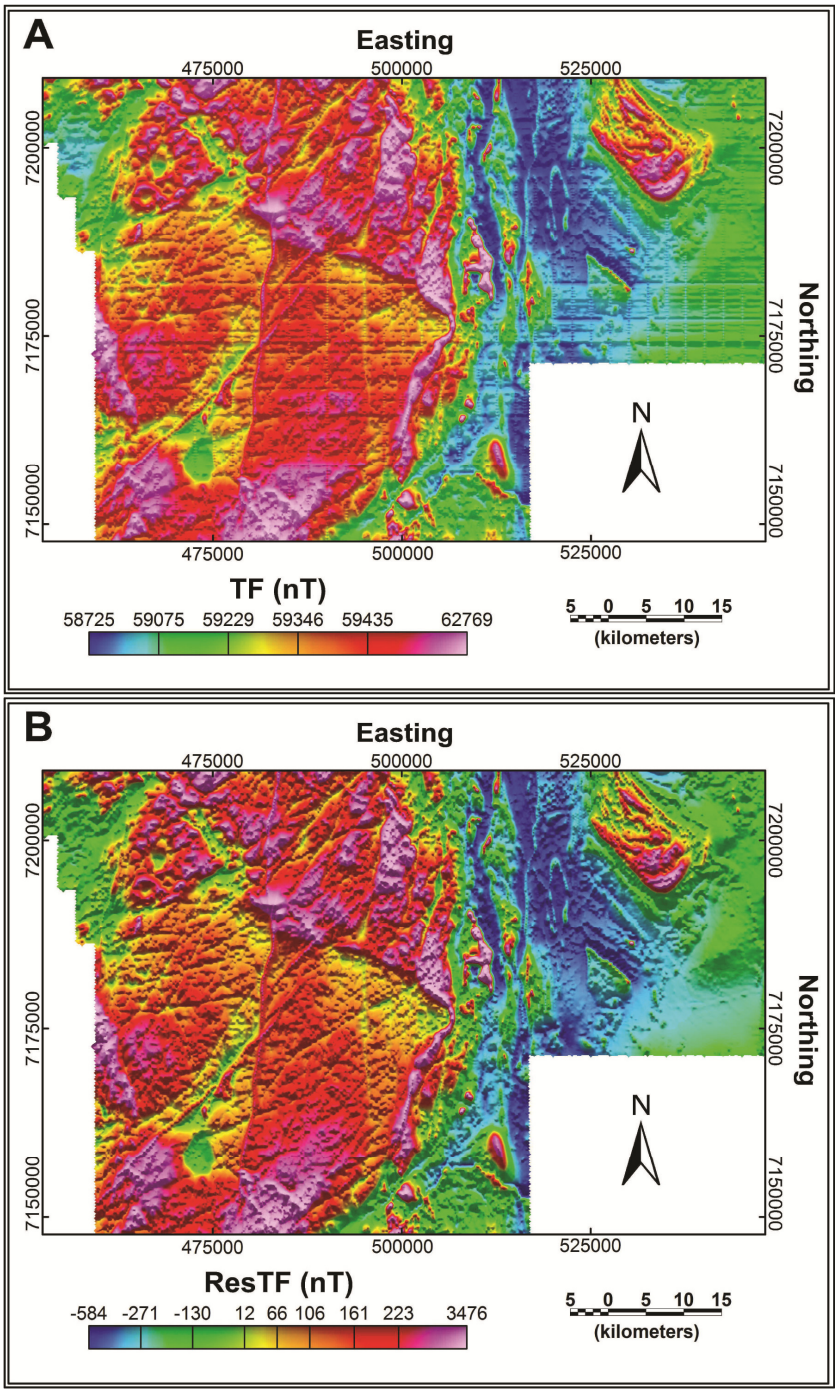

Figure 7.2. The raw (A) and leveled (B) magnetic field data. Both are gridded using a 100 m grid cell size (1/4 flight line spacing) and a minimum curvature interpolation algorithm. Images are sunshaded from a declination of 0° (orthogonal to flight line direction) and inclination of 30°. The raw magnetic data set has been corrected for IGRF and tie-line leveled to produce the leveled clean data set.

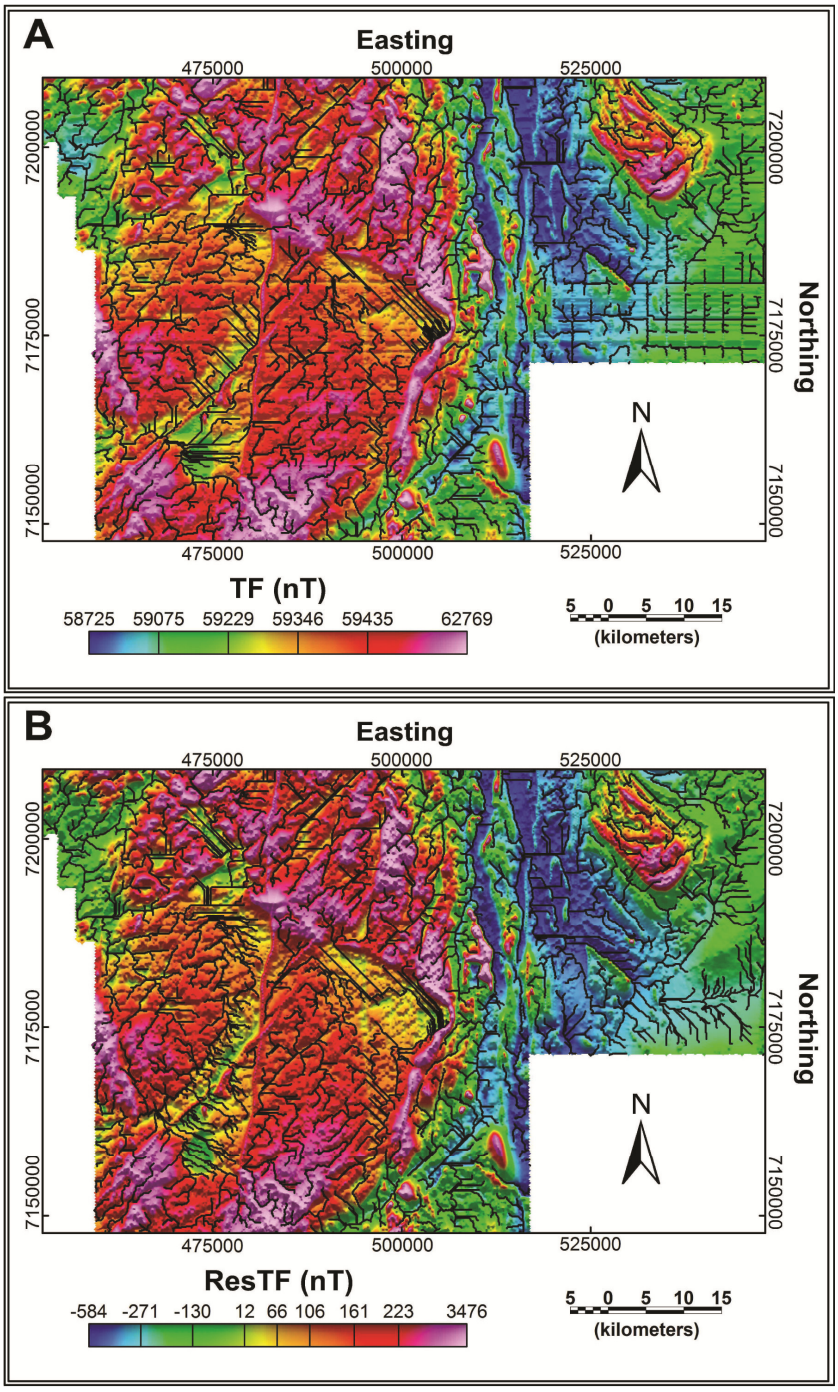

Figure 7.3. The raw (A) and leveled (B) magnetic field data with network extraction solutions (bold black lines) overlaid on the total magnetic field grids from Figure 7.2.

The automatic network extraction algorithm identified a total of 3515 lineaments on the raw magnetic data and 3446 lineaments on the leveled magnetic data, which shows there is only a 2% difference in the total number of lineament solutions. The raw TF and leveled ResTF results are shown in Figures 7.4 and 7.5 respectively, where Figures 7.4A and 7.5A show the subset blocks. Both the power spectrums (Figures 7.4B, 7.4C, 7.5B, and 5C) and the rose diagrams (Figures 7.4D, 7.4E, 7.5D, and 7.5E) indicate principal trends along north-south, east-west, northwest-southeast and northeast-southwest. Based on existing geologic maps, the north-south, northwest-southeast, northeast-southwest lineament may represent the dominant fabric patterns for fault systems and dyke swarms. Cutting through the study area is the large scale Wopmay Fault zone with the same trend (0°) as the tie-lines, which are included in the minimum curvature gridding algorithm. Accordingly, there is a higher probability the north-south trending features may be erroneous. By calculating the associated statistics, processing and levelling procedures reduced these north-south features are reduced by 1.1%, as they represent 11.4% in the raw data set and 10.5% in the processed data set.

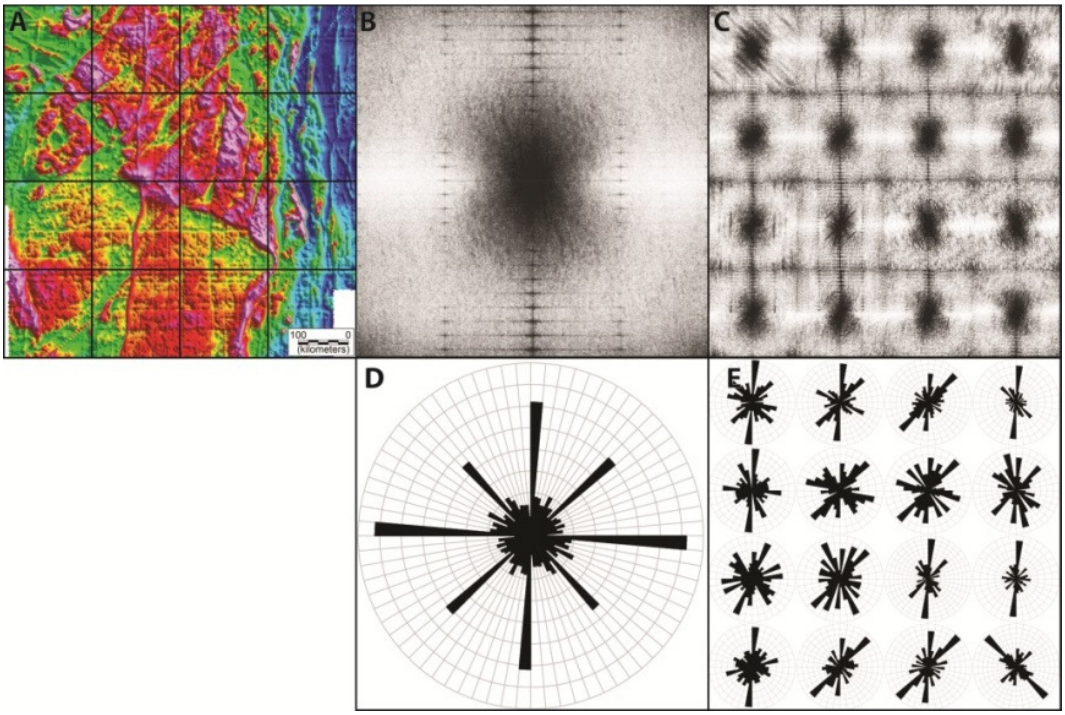

Figure 7.4. (A) Subset of the raw total magnetic field. Each block represents 128 x 128 grid nodes; (B) The 2D power spectrum of the raw TF; (C) The 2D power spectrum over each 128x128 subset in A; (D) The rose diagram of the raw TF; (E) The rose diagrams over each 128x128 subset in A. All plots are oriented with north upwards and the rose diagrams are displayed with rays and petals of 5°.

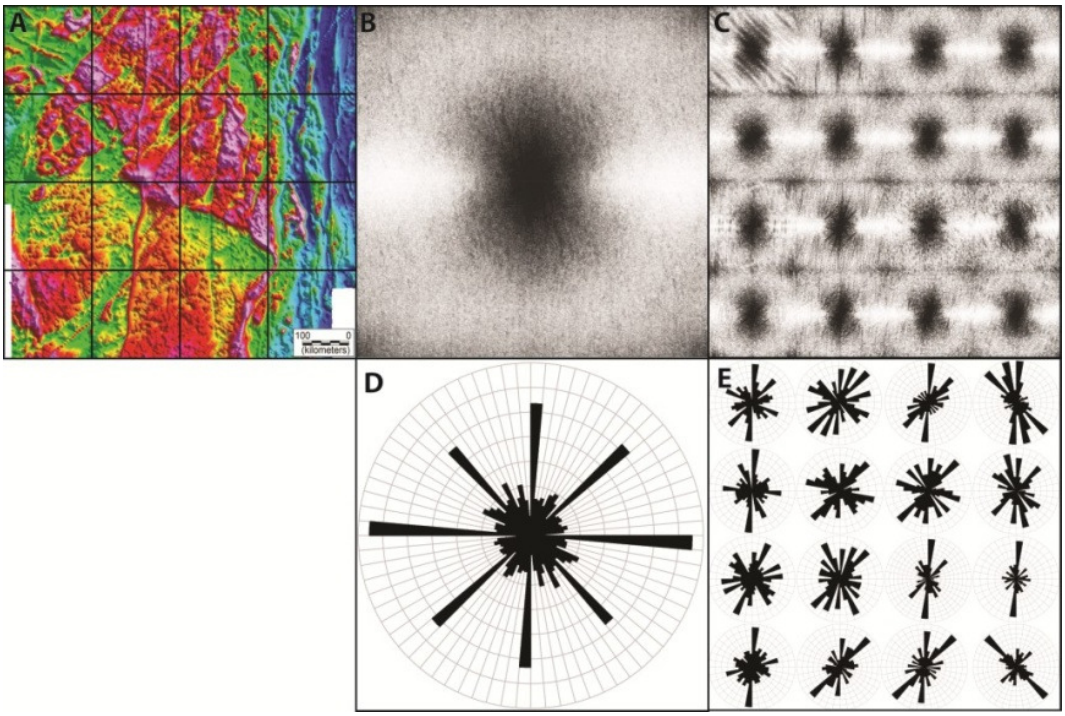

Figure 7.5. (A) Subset of the leveled magnetic field. Each block represents 128 x 128 grid nodes; (B) The 2D power spectrum of the leveled ResTF; (C) The 2D power spectrum over each 128x128 subset in A; (D) The rose diagram of the leveled ResTF; (E) The rose diagrams over each 128x128 subset in A. All plots are oriented with north upwards and the rose diagrams are displayed with rays and petals of 5°.

Magnetic sources with an azimuth of east-west are apparent in the full-scale power spectrums of the raw data (4B and 4C) and occur typically at short wavelengths. Figure 7.4B shows distinct east-west features caused by levelling problems not evident in the processed data of Figure 7.5B and 7.5C. By assessing the lineament statistics these east-west features are quantitatively defined. The computed lineament azimuths indicate east-west trending (90°/270° ± 5°) lineaments account for 13.3% of the total lineament population extracted from the raw data set, while the east-west lineaments account for 12.2% of the total lineament population extracted from the processed data. This indicates a reduction of 1.1 % in east-west lineaments. Since the east-west lineaments represent a small portion of the total lineament population extracted set they may be considered geologically insignificant and are difficult to identify in the rose diagrams (based on number of occurrences) of Figure 7.5D and 7.5E.

To visually identify these inherent and processing artefacts in the magnetic data, difference plots between the raw and processed power spectrums (Figures 7.6A - 7.6C) and rose diagrams (Figures 7.6D – 7.6F) are generated. As can be seen in Figure 7.6F, the processing procedure reduced the number of east-west and north-south trending lineaments (blue petals), while it increased the number of lineaments along most other azimuths (red petals). This rose diagram shows similar directional information as the difference power spectrum in Figure 7.6C however the former provides quantitative information on the difference. These highlighted trends represent geologic features and therefore a greater content of the signal is captured by the lineament analysis post-levelling.

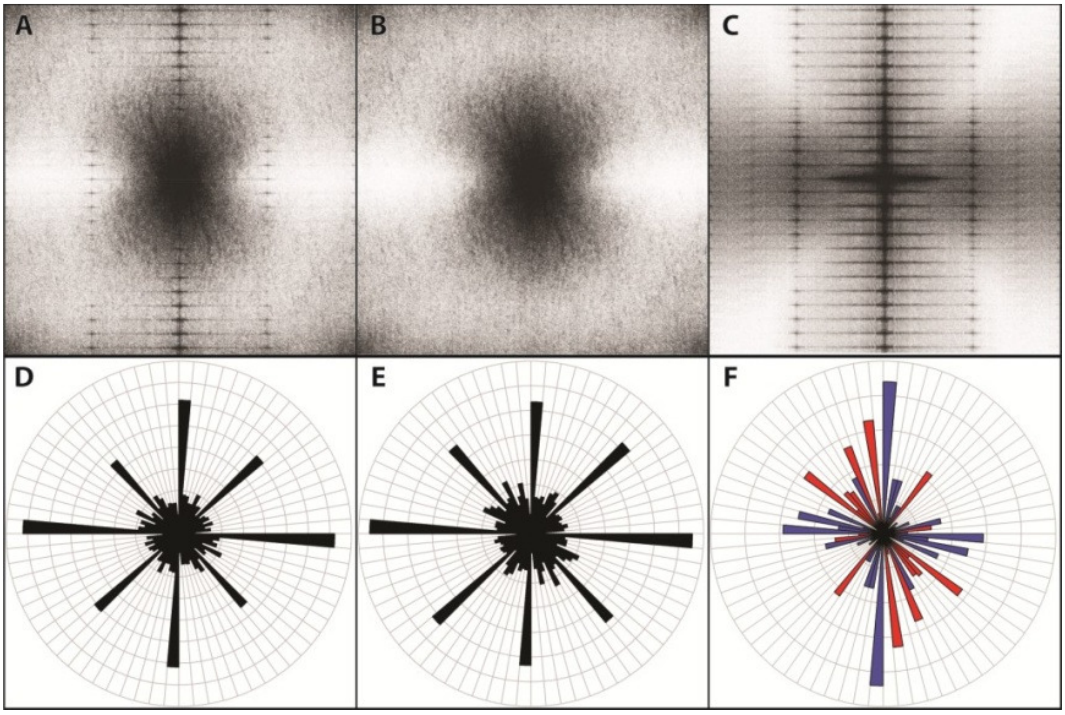

Figure 7.6. Comparison of the raw (A, D) and leveled (B, E) magnetic field 2D power spectrums (top) and rose diagrams (bottom). The respective differences between the raw and leveled data are shown in C and F. All plots are oriented with north upwards and the rose diagrams are displayed with rays and petals of 5° increments. The difference rose diagram (F) indicates an increase (red) or decrease (blue) in lineaments along various azimuths.

Figure 7.3 suggests these east-west lineaments pose a greater problem in regions of low amplitude magnetic anomalies. We compute the 2D power spectrums and conduct a lineament analysis over a magnetically quiet subset of the data set with a dynamic range only 20% of original (Figure 7.7). The 2D power spectrums (Figure 7.8A and 7.8B) both show similar dominant frequencies for the raw and leveled data, however there is evidence for potential noise due to flight-line variations as strong repeating east-west features in the raw data (Figure 7.8A). Computation of the difference between the raw and leveled 2D power spectrums (Figure 7.8C) shows east-west magnetic sources have been removed; however we have no spatial or quantitative information on these sources.

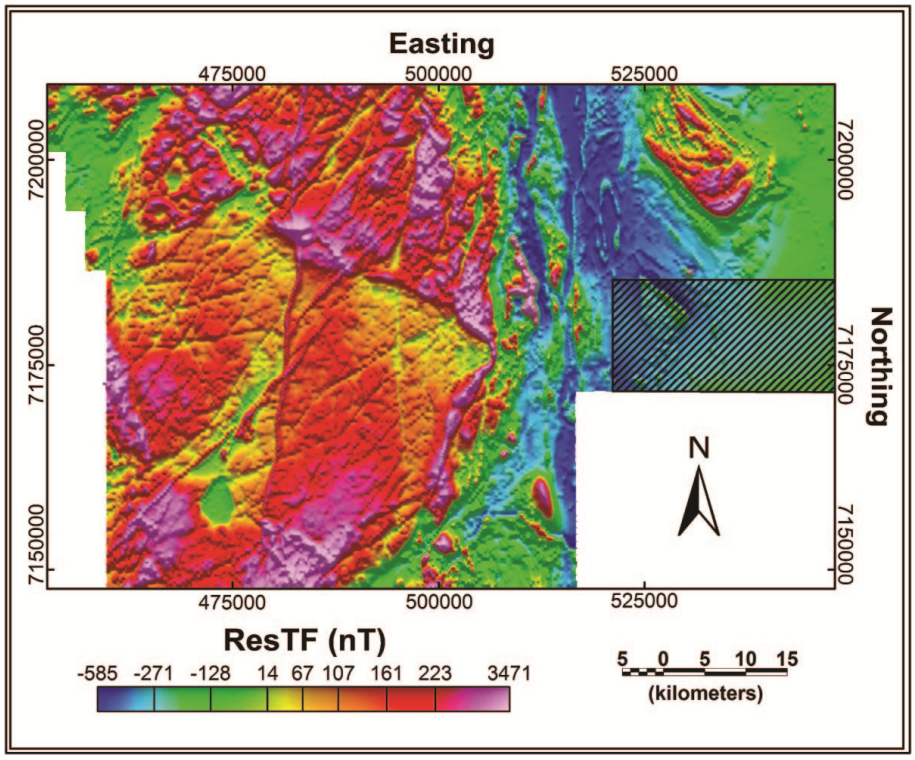

Figure 7.7. Subset magnetic field data set in black hatched box.

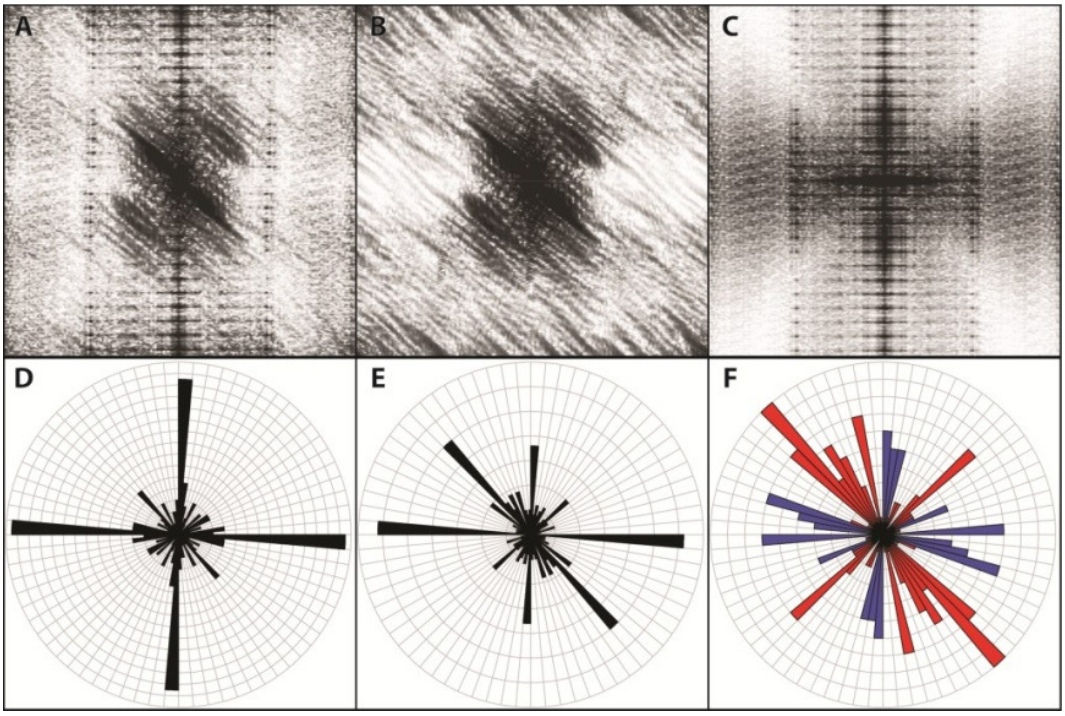

Figure 7.8. Comparison of the raw (A, D) and leveled (B, E) magnetic field 2D power spectrums (top) and rose diagrams (bottom). The respective differences between the raw and leveled data are shown in C and F. All plots are oriented with north upwards and the rose diagrams are displayed with rays and petals of 5° increments. The difference rose diagram (F) indicates an increase (red) or decrease (blue) in lineaments along various azimuths.

One hundred and ninety lineaments were extracted from the raw magnetic data set and 213 lineaments from the leveled data set (Figure 7.8D and 7.8E). Of these solutions, east-west lineaments accounted for 22.6% of the total lineament population extracted from the raw data, while east-west lineaments accounted for only 7.6% of the total lineament population in the leveled data set, representing a 15.0% reduction in levelling errors in the subset area. The north-south lineaments were reduced by 6.1% through the processing and levelling. This quantifies the amount of correction applied without the knowledge of what pre-processing corrections have been done.

Inspection of the difference rose diagram (Figure 7.8F) corroborates where primarily east-west trending lineaments have been removed, along with north-south and a few northeast-southwest lineaments. Again, lineaments along almost all azimuths are captured post-levelling. Lineaments trending northwest-southeast (135°/315° ± 5°) increased by 17.8%. These northwest-southeast trending lineaments reflect (Figure 7.2B) mafic intrusions which follow the regional tectonic fabric of the area. This shows that not only is noise (acquisition artefacts) being removed, but signal associated with geology is more properly identified. A full summary of statistics for both the full data set and subset data set are found in Table 7.1.

	Frequency (% of population)		
Azimuth	**TF**	**ResTF**	**Difference (%)**
0° /180° ±5°	11.5	10.5	1.0
90° /270° ±5°	13.3	12.2	1.1
0° /180° ±5° (subset)	17.4	11.3	6.1
90° /270° ±5° (subset)	22.6	7.6	15

Table 7.1: Summary statistics for lineament extraction. Statistics indicate the levelling process decreases the frequency of lineaments associated with acquisition errors.

One needs to compare the flight path and the data image to identify the lineaments most likely associated with acquisition artefacts. We used a GIS based approach of placing a buffer of 50m was placed around each flight line. This means a total buffer area of 100m equal to the grid cell size was placed along each east-west flight line. Any extracted lineaments occurring entirely within this buffer were considered to be anomalous features. Figure 7.9A shows numerous east-west segments associated with line-to-line variations (white lines). As noted above, the most prominent lineaments occur over magnetically quiet areas in the eastern portion of the study area (sedimentary and meta-sedimentary rocks). Figure 7.9B shows that after levelling the number of east-west lineaments has been reduced but there are a few remanent east-west lineaments associated with insufficient levelling. This is especially true over the magnetically flat areas. Many of these remanent east-west lineaments though could also represent genuine signal defined by geologic structure. Lineaments defining fractures (black rectangles) and a few representing acquisition and pre-processing artefacts (black ovals) are located on the northwest corner of the study area (Figure 7.10). This is the point in the analysis where a hands-on approach by a knowledgeable user is necessary to separate lineaments defined by signal and those defined by noise.

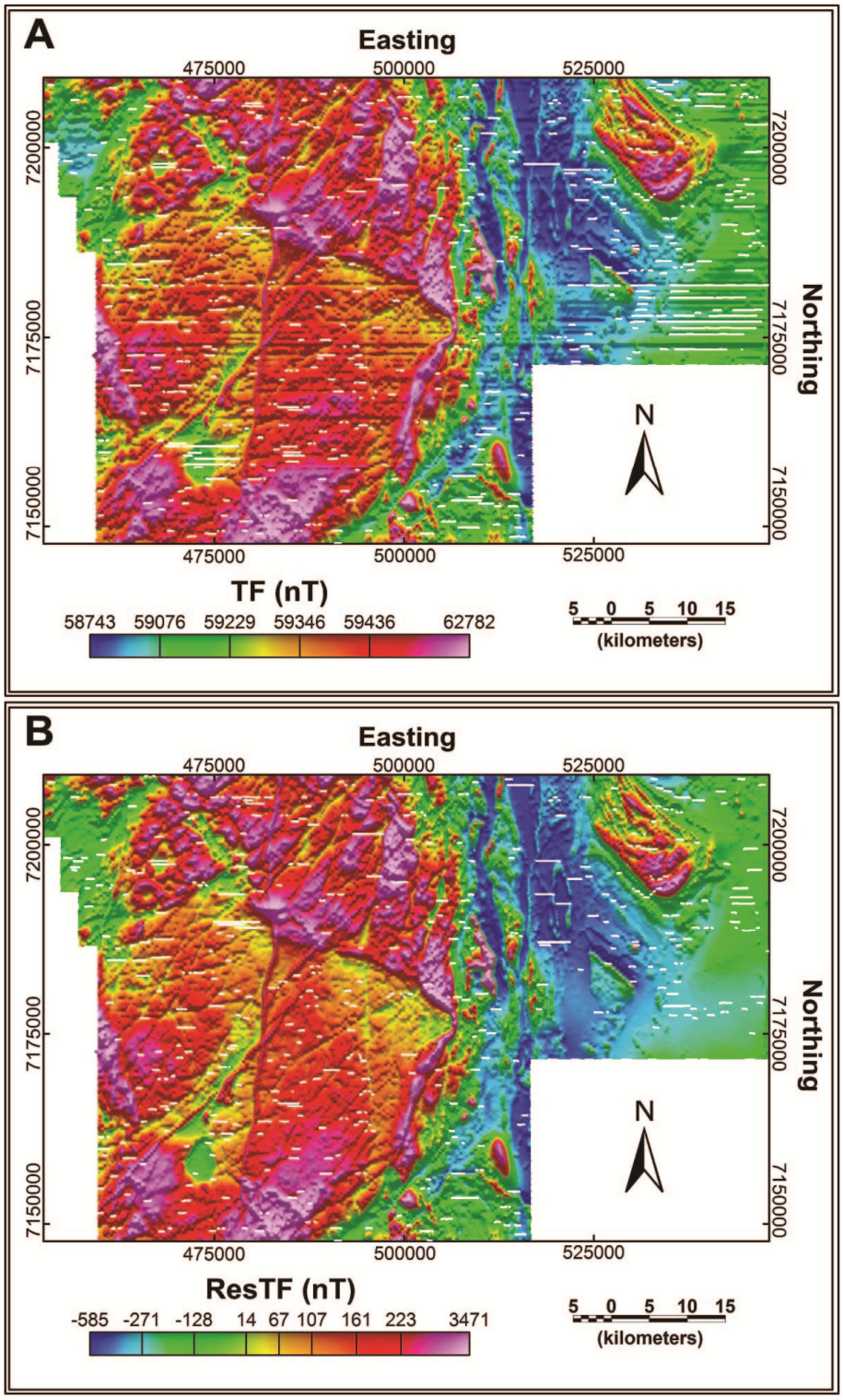

Figure 7.9. Location of all extracted lineaments from the raw (A) and leveled (B) magnetic field data located within 50m of a flight line.

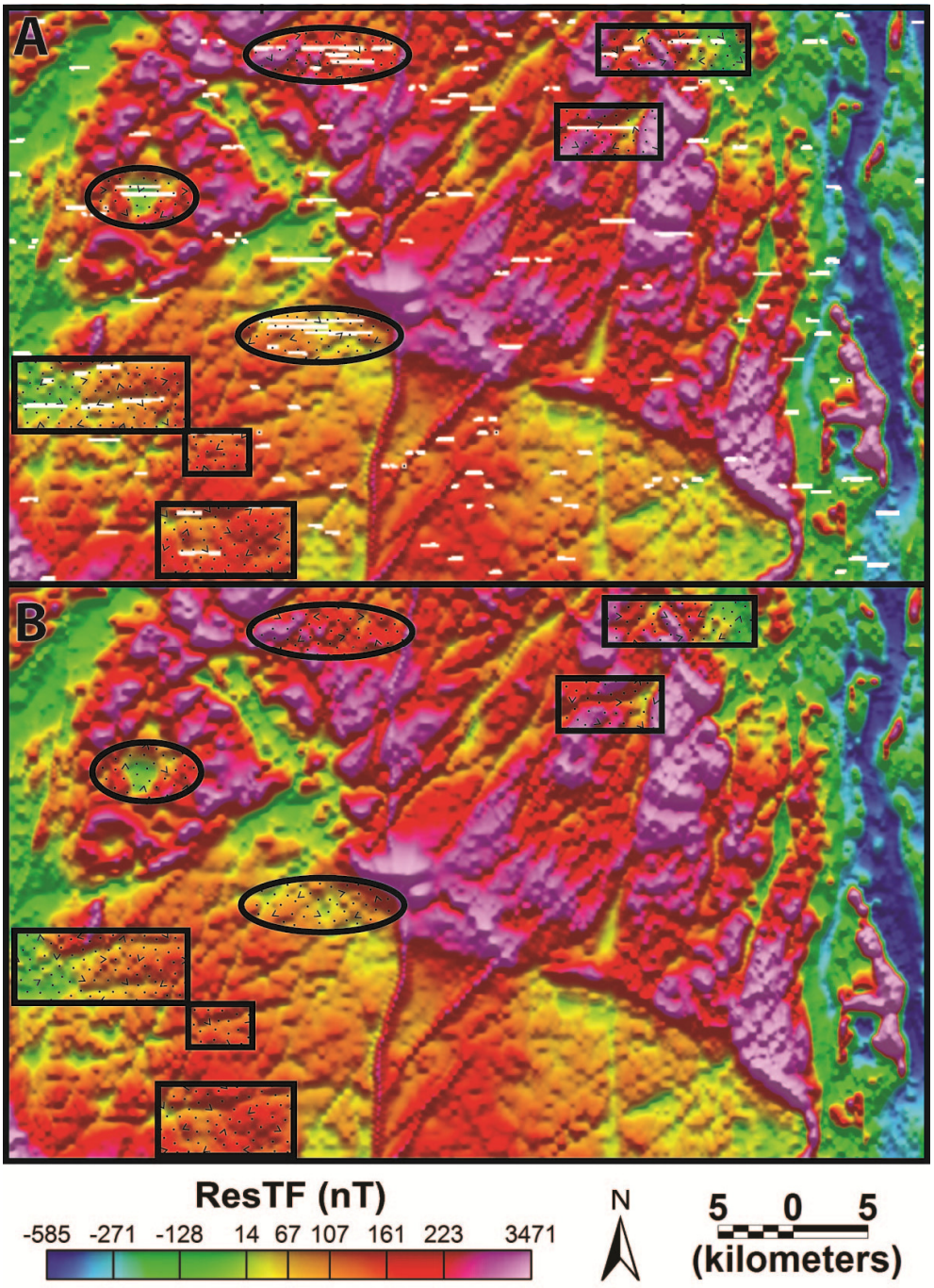

Figure 7.10. Extracted lineaments from the northwest corner of the ResTF occurring within the 100m flight line buffer overlaid on ResTF (A). For example purposes lineaments maybe defined by geologic structure are identified by a black rectangle. Lineaments maybe defined by insufficient levelling or some other artefacts are indicated by a black oval. For comparison the same image is shown without lineaments in (B).

7.6 Conclusion

Assessment of data quality prior to processing and interpretation is compulsory. However, this cannot be adequately quantified with respect to sufficient levelling through the standard methods of radial power spectrums and sunshading alone. We have shown a robust assessment on the data quality and specifically levelling may be accomplished through the application of lineament analysis. Analyzing lineament azimuths in the form of rose diagrams and their associated statistics from both the raw and leveled data set allow for a quantitative measurement to be placed on the corrections. Rose diagrams aid in identifying populations similar to a 2D radially-averaged power spectrum, but rather than frequency we analyze strictly the azimuth. A GIS buffer analysis of flight line and potential field grid image provides spatial constraints on erroneous line segments. It is important to note the raw data set does not have to be available to use lineament analysis to identify regions of insufficient levelling. Having access to the raw data does enable though a more detailed discussion. In either scenario, lineament analysis of a data set still allows the user to assess the signal to noise ratio in a data set so long as *a priori* knowledge (i.e. geology and geologic structure) is available.

7.7 Acknowledgements

The authors wish to thank V. Jackson, L. Ootes from the Northwest Territories Geoscience Office and L. Corriveau of the Geological Survey of Canada for their support and assistance on bedrock geology, petrology. This work was in part funded by numerous programs: the IOCG-Great Bear (00410) and Remote Predictive Mapping (GKM005) projects of the Geomapping for Energy and Minerals program through Natural Resources Canada; the South Wopmay Bedrock Mapping project of the Northwest Territories Geoscience Office through Aboriginal Affairs and Northern Development Canada; and the Polar Continental Shelf Program (50709). The project was conducted through various collaborative agreements between Natural Resources Canada, the Northwest Territories Geoscience Office, the Community Government of Gamètì, and Fortune Minerals Limited. Appreciation is given to the support provided by the Flight Research Laboratory of the National Research Council. The authors would also like to acknowledge the contribution by the Editor, Associated Editor, and Reviewers for their recommended revisions.

7.8 References

Beiki, M., Bastani, M., and Pederson, L.B., 2010, Levelling HEM and aeromagnetic data using differential polynomial fitting: *Geophysics*, 75 (1), L13-L23, DOI: 10.1190/ 1.3279792.

Billings, S., and Richards, D., 2000, Quality control of gridded aeromagnetic data: *Exploration Geophysics*, 31 (4), 611-616, DOI: 10.1071/EG00611.

Cooper, G., 2003, Feature detection using sun shading: *Computers and Geosciences*, 29 (8), 941-948, DOI:10.1016/S0098-3004(03)00091-8.

Ferraccioli, F., Gambetta, M., and Bozzo, E., 1998, Microlevelling procedures applied to regional aeromagnetic data: an example from the Transantarctic Mountains Antarctica: *Geophysical Prospecting*, 46, 177-196, DOI: 10.1046/j.1365-2478.1998.00080.x.

Flis, M.F., and Cowan, D.R., 2000, Aeromagnetic drape corrections to the Turner Syncline, Hamersley Basin: *Exploration Geophysics*, 31 (2), 84-88, DOI: 10.1071/EG00084.

Gandhi, S., 1994, Geological setting and genetic aspects of mineral occurrences in the southern Great Bear magmatic zone, Northwest Territories: *Geological Survey of Canada Bulletin,* 475, 63-96.

Gandhi, S. S., Mortensen J. K., Prasad N., and van Breeman O., 2001, Magmatic evolution of the southern Great Bear continetal arc, northwestern Canadian Shield: Geochronological constraints: *Canadian Journal of Earth Sciences,* 38, 767-785.

Green, A.A., 1983, A comparison of adjustment procedures for levelling aeromagnetic survey data: *Geophysics*, 48 (6), 745-753, 10.1190/1.1441504.

Hardwick, C.D., 1999, Gradient-enhanced total field gridding: *SEG Annual Meeting*, October 31-November 5, Houston, Texas.

Harris J.R. (Ed.), 2008, Remote Predictive Mapping: *An Aid for Northern Mapping*, Geological Survey of Canada Open File 5643, CD release.

Hildebrand, R., Hoffman P., and Bowring, S., 1987, Tectono-magmatic evolution of the 1.9-Ga Great Bear magmatic zone, Wopmay Orogen, northwestern Canada: *Journal of Volcanology and Geothermal Research,* 32, 99-118, DOI: 10.1016/0377-0273(87)90039-4.

Karnieli, A., Melsels, A., Fisher, L., and Arkin, Y., 1996, Automatic extraction and evaluation of geologic linear features from digital remote sensing data using a Hough Transform: *Photogrammetric Engineering and Remote Sensing*, 62 (5), 525 -531.

Lee, M.D., Morris, W.A., Harris, J., and Leblanc, G., 2012a, An automatic network extraction algorithm applied to magnetic survey data for the identification and extraction of geologic lineaments: *The Leading Edge*, 31, 26-32, DOI:10.1190/1.3679324.

Lee, M.D., Morris, W.A., Harris, J., and Leblanc, G., 2012b, A network extraction tool for mineral exploration: a case study from the Wopmay Orogen, Northwest Territories, Canada: *Exploration Geophysics*, DOI:10.1071/EG11045.

Luyendyk, A. P., 1997, Processing of airborne magnetic data: *Journal of Australian Geology and Geophysics*, 17 (2), 31-38.

Mauring, E., and Kihle, O., 2006, Levelling aerogeophysical data using a moving differential median filter: *Geophysics*, 71 (1), L5-L11, DOI: 10.1190/1.2163912.

Mauring, E., Beard, L.P., Kihle, O., and Smethurst, M.A., 2002, A comparison of aeromagnetic levelling techniques with an introduction to median levelling: *Geophysical Prospecting*, 50 (1), 43-54, DOI: 10.1046/j.1365-2478.2002.00300.x.

Masuda, S., Tokuo, T., Ichinose, T., Otani, K., and Uchi, T., 1991, Expert System for lineament extraction from optical sensor data: *Geoinformatics*, 2, 195 -200.

Minty, B. R., 1991, Simple micro-levelling for aeromagnetic data: *Exploration Geophysics , 22*, 591-592, DOI: 10.1071/EG991591.

Nelson, B., 1994, Levelling total-field aeromagnetic data with measured horizontal gradients: *Geophysics,* 59 (8), 1166-1170, DOI: 10.1190/1.1443673.

O'Driscoll, E.S.T., 1980, The double helix in global tectonics: *Tectonophysics*, 63, 397-417.

O'Driscoll, E.S.T., 1986, Observation of the lineament-ore relation: Philosophical Transactions of the Royal Society, 317 (1539), 195-218.

Pilkington, M., and Thurston, J. B, 2001. Draping corrections for aeromagnetic data: line- versus grid-based approaches: *Exploration Geophysics*, 32, 095-101, DOI: 10.1071/EG01095.

Raghavan V., Wadatsum, K., and Masumoto, S., 1993, Automatic extraction of lineament information of satellite images using digital elevation data: *Nonrenewable Resources*, 2 (2), 148–155, DOI: 10.1007/BF02272811.

Reford, S., 2006, Gradient enhancement of the total magnetic field. *The Leading Edge*, 25 (1), 59-66, DOI: 10.1190/1.2164757.

Twidale, C.R., 2007, E. S.T. O'Driscoll, lineaments and ring structures: In Bourne J. A. and Twidale C.R. (Ed.), Crustal Structures and Mineral Deposits, p.15, Rosenburg, Australia.

Woodall, R., 1994, Empiricism and concept in successful mineral exploration: *Australian Journal of Earth Sciences* , 41 (1), 1-10, DOI: 10.1080/08120099408728107.

Woodall, R., 2007. From Broken Hill to Olympic Dam: E.S.T. O'Driscoll's lifelong study of the structural setting of mineral deposits: in Bourne J. A. and Twidale C. R. (*Ed*), Crustal Structures and Mineral Deposits, p.15, Rosenburg, Australia.

Yarger, H.L., Robertson, R.R., and Wentland, R.L., 1978, Diurnal drift removal from aeromagnetic data using least squares: *Geophysics*, 46 (6), 1148-1156, DOI: 10.1190/ 1.1440884.

Zevenbergen, L.W., and Thorne C.R., 1987, Quantitative analysis of land surface topography: *Earth surface processes and landforms*, 12, 47-56, DOI: 10.1002/esp.3290120107.

8.0 Quality assessment of lineament analysis solutions derived from aeromagnetic data grids

Lee, M.D., and Morris, W.A., 2012, Quality assessment of lineament analysis solutions derived from aeromagnetic data grids: *Pure and Applied Geophysics*, submitted (accepted with major revisions).

8.1 Abstract

The typical application of lineament analysis on aeromagnetic data is to extract fault systems and dyke swarms. However, prior to applying a lineament extraction algorithm the data is subjected to a series of processing steps that could potentially produce artificial features which may have an effect on the lineament analysis outputs. Therefore quality assessment of any lineament analysis is essential for accurate exploration and mapping. Our central thesis is that genuine lineaments associated with inherent signal will be invariant to any data rotation while spurious lineaments generated by the lineament extraction routine will be dependent on data rotation. The simplest approach to quantitatively assess lineaments is through their azimuth in the form of rose diagrams. Artificial solutions not apparent in the rotation analysis due to a low frequency count, may also be identified through length analysis. It is also important to assess the impact of various gridding algorithms and filters on the output solution set. We analytically assess extracted lineaments from an aeromagnetic data set over the Wopmay Orogen, Northwest Territories to determine whether they represent signal, defined by geology, or noise, defined by processing artefacts.

8.2 Introduction

Lineament analysis locates linear features within a geoscientific data set such as aerial photography, satellite imagery, topography, and geophysics. These lineaments commonly represent geological features characterised by a linear geometry. For example lithological contacts, fault and fracture configurations, and dyke swarms. With respect to geophysical interpretation these geological features are designated as signal, while lineaments associated with non-geologic origins are defined as noise. Artificial lineaments may be generated as a result of numerous acquisition and processing steps: flight line variations height, incorrect heading and lag corrections, insufficient levelling, or the use of an inappropriate gridding algorithm. The lineament extraction method often computed using a space-domain filter algorithm, may also result in the production of artificial lineaments. When employing the output of these analyses in a later mineral exploration prediction procedure the user needs to be able to effectively differentiate lineament solutions defined by signal and noise in a consistent and timely fashion. The accurate description of surficial attributes is an important discussion and has been thoroughly discussed in a geomorphology context in a series of papers by Florinsky, 1996; Florinsky, 1998a; Florinsky, 1998b; Florinsky, 2002; and Florinsky, 2005. Lineament extraction is a commonly applied tool in geophysical interpretation; however there is limited discussion on the validation of lineaments derived from a potential field survey. We focus strictly on artificial lineaments occurring after the pre-processing (e.g. levelling, microlevelling) of an aeromagnetic data set.

Lineament analysis is carried out visually or quantitatively; however both methods suffer from advantages and disadvantages. Visual interpretation permits a user-defined set of solutions, which makes the method subjective and highly dependent on the interpreter's skill level. On the other hand quantitative methods typically offer consistent and impartial results. Since the methods are systematic there is no discrimination between a lineament caused by a dyke with a similar trend to the flight path and one caused by a misfit flight line.

Geological terranes will often have a dominant structure pattern representing their unique geologic and tectonic history. This dominant structure pattern should become apparent through lineament analysis. When a quantitative lineament analysis is applied to a spatially rotated data set the intrinsic lineament structures should still be readily apparent in the rotated reference frame. This means geologically valid lineaments will be independent of any rotation of the data. Valid lineaments computed by a lineament extraction algorithm should have the same spatial pattern in the rotated data reference frame.(anisotropic vs. isotropic). In this study we examine the lineament solution set

generated after a data set has been subjected to a series of controlled rotations. After each rotation of the data a grid surface is computed using a surface interpolation algorithm. Lineaments are computed from the grid surface using a space domain filter. Both the data gridding and the subsequent lineament extraction require the operator to define a search "window". With respect to gridding the window is controlled by the grid cell size, or pixel resolution of the output grid, which is in turn linked to the original sample flight survey specifications (Luyendyk, 1997). With respect to the lineament extraction the window is controlled by the size of the grid node matrix (Lee et al., 2012). It must be remembered that when using a pixelised data set and a space domain filter there will always be a preferred alignment of axes defined by the 9 pixels in a 3 x 3 matrix.

Magnetic data is acquired as individual point observations, regardless of how small the sample spacing is. As such the data must undergo interpolation to produce a smooth image surface (i.e. grid) for subsequent processing and interpretation. There are many different gridding procedures that may be implemented but the user must consider some fundamental issues: defining a continuous function intercepting all data points; is representative of the data's nature; how the gridding algorithm addresses values in poorly constrained areas; addressing what points should be included; and the global properties of a solution (Smith and Wessel, 1990). Each gridding algorithm imposes its own signature on a magnetic data set (Billings and Richards, 2000, Billings et al., 2002). It is essential the user understand the impact of a specific interpolation algorithm on their data set when using the resultant magnetic anomaly grid for detailed geological mapping. Abbass et al. (1990) and Billings and Richards (2000) presented a comparative analyses of the effect of various interpolation algorithms on geophysical data. Geosoft® (Oasis Montaj) implements six methods for data interpolation where the four most commonly used interpolation methods are: minimum curvature, bidirectional splining, kriging, tinning. The minimum curvature routine originally developed by Briggs (1974) as modified by Swain (1976) and Smith and Wessel (1990), is the most commonly used due to its wide applicability, time efficiency, and robust nature. Minimum curvature is ideal for random data, smooth data or in cases where the data has tie-lines. Bi-directional gridding is ideal for situations where data is collected along roughly parallel lines and when the along-line sampling interval is significantly smaller than the between line spacing; however it is unable to accommodate tie-lines. Kriging is best used for randomly distributed data since its variance model approach is best able to cope with sparse and clustered data points. Kriging considers the spatial distribution of the data using a weighted moving function (kernel). Tinning is typically used for highly irregular data but may also be used in circumstances when the data is an equal grid (N x N sampling rather than M x N). The impact of the gridding algorithm on data interpretation is an important discussion.

However, this is not the major focus of this work. Rather it is our intent to show that different interpolation schemes will produce localized changes in the location of a computed lineament and that these differences represent limits in the resolution of any given data set.

Magnetic data may undergo various image enhancement techniques to accentuate high frequency features. Standard practice is the computation of derivatives, specifically vertical and tilt derivative (Miller and Singh, 1991). These derivatives perform as high pass filters. The vertical gradient calculates the rate of change of the magnetic field in the *z* direction at some specific height. In the case of an aeromagnetic survey the vertical gradient represents the residual magnetic field (nT/m). Tilt derivative (degrees) is the arctangent of the ratio of the horizontal to vertical derivatives. Tilt-derivative may also be considered an Automatic Gain Control (AGC) technique (Rajagopalan and Milligan, 1995). AGC is often used in association with lineament mapping from aeromagnetic data to make weakly-magnetic features more prominent for interpretation (Rajagoplan 1987, Mudge 1991, Rajagopalan and Milligan, 1995, Boyce and Morris, 2002). The AGC procedure systematically applies a moving window across a data set where the amplitude of the signal variance within each window is adjusted to a predefined uniform gain function. Application of this uniform gain function amplifies weak signals and suppresses strong signals so all anomalies have the same amplitude. As discussed by Rajagopalan and Milligan (1995) no ideal gain function or window size may be implemented to appropriately capture all anomalies since the aeromagnetic data set will have a large range of input frequencies. A good choice for the window size should be representative of the average wavelength. A smaller window results in a faster computation if time efficiency is to be considered (Rajagoplan, 1987). Since tilt-derivative does affect the amplitude of a magnetic signal, it may be considered a form of automatic gain control.

To differentiate between lineament noise and lineament signal as proposed by Florinsky (2005) is achieved by controlled rotation of a data set. In detail this could achieved in two ways: a) rotation of the data followed by gridding of the rotated data in the new reference frame, or b) gridding of the data in the original reference frame followed by rotation and resampling of the computed grid. The difference between these two scenarios is a measure of the imprint of that the individual interpolation algorithm imposes on the resulting grid. Lineament noise can therefore arise from the interpolation algorithm and / or the grid rotation resampling which also involves an interpolation step. In this work we verify lineament solutions for a synthetic data set and an aeromagnetic data set from northwestern Canada. Quality assessment of lineaments is carried out with systematic

rotation of the data, the application of image enhancements, and assorted gridding algorithms.

8.3 Synthetic models

A simple, synthetic magnetic anomaly model was designed similar to that presented by Lee et al. (2012a). The model included two non-dipping sheets; one north-south trending and one northwest-southeast trending. Both sheets were 50m thick, 200m long, and 2km deep. The depth extent was chosen to approximate infinite and remove depth to bottom effects. The magnetization of both sheets was 0.04SI. A vertical ambient field with a strength of 59 000nT was applied and sample spacing was 10m along and across line.

The method produces three grids: g_0, original grid of non-rotated data; g_1, grid of rotated (rotation of n°) data; g_2, back-rotated (rotation -n°) grid of g_1. The point data was gridded using four interpolation algorithms: minimum curvature, bi-directional, kriging, and tinning (g_0). A grid cell size of 5m was selected for the first three algorithms. Minimum curvature implemented no internal tension. Akima splining was used along- and across-line for bi-directional gridding. Kriging used a variogram power of one model since no sill or nugget is required. A natural neighbour approach was selected for tinning and no grid cell size was required. The data was rotated around the fixed location (0, 0) at 5°, 45°, 60°, and 90°. The rotated data was gridded using the same four interpolation algorithms (g_1) as g_0. Network extraction (Lee et al., 2012a) was performed on each g_1 grid to delineate the N-S and NW-SE sheets. A catchment area of 200m was chosen. Artificial lineaments along the survey edge were extracted when a smaller window was selected. The g_1 grids are then back-rotated (g_2) to their original location and network extraction is repeated on the back-rotated grids. The difference between the extracted lineaments for g_1 and g_2 will reflect the artefacts generated by the gridding algorithm.

8.3.1 N-S sheet

All four gridding lineament solutions from g_1 produced the same location for 0° and 90° rotation (Figure 8.1 and 8.2D). The location of the minimum curvature and kriging lineaments were identical for a rotation of 5°, 45° and 60° (Figure 8.2A, 8.2B, 8.2C). This was also true for bi-directional gridding and tinning. The distance between the two pairs of lineaments was approximately 13m. This is very similar to the original survey sample spacing of 10m. An interesting phenomenon occurs after 45° rotation; minimum curvature and kriging delineate an artefact along the northeast edge of the body that bi-directional and tinning do not identify. Back-rotation was only completed on 45° and 60° rotations to investigate whether the spatial difference for the gridding lineaments and the

eastern edge anomaly were due to the gridding algorithm or the network extraction routine (Figure 8.3). The back-rotated gridding lineaments from g_2 exhibited a similar phenomenon. The spatial occurrence for the minimum curvature and kriging results were nearly identical. The same held true for bi-directional gridding and tinning. As with g_1 the lineament pairs were separated by approximately 13m. The spatial discrepancy is due to how the gridding algorithm handles data points not oriented N-S or E-W. When the data is rotated the gridding algorithm's selection process of 'nearest value' changes and is unique to each gridding algorithm. The eastern edge anomaly is no longer present after back-rotation indicating it was a consequence of the extraction routine.

8.3.2 NW-SE sheet

All four gridding lineaments had the same location after 0°, 5°, 45°, 60°, and 90° rotations (Figure 8.2). At 0° a lineament artefact was extracted along the northeastern edge of the anomaly. The location of this artificial lineament is identical to the artefact generated by the N-S sheet rotated 45°. These artificial lineaments are associated with the network extraction routine and oriented along the axis of interpretation. The back-rotated grid lineaments had the same location (Figure 8.3). This indicates the gridding algorithm treated the NW-SE sheet the same.

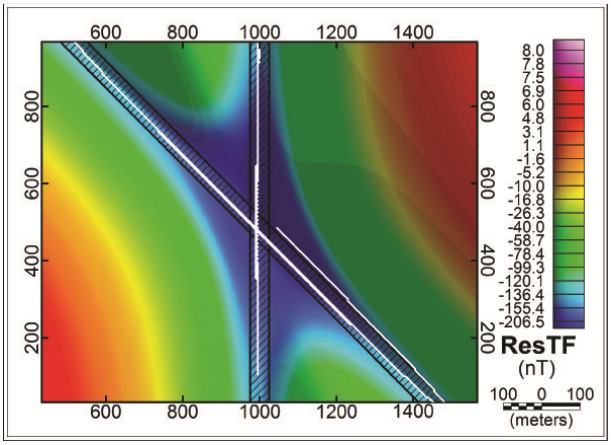

Figure 8.1. Location of modelled sheets in black hashes overlaid on minimum curvature ResTF. Extracted lineaments (g_0) computed from minimum curvature, bi-directional, kriging, and tinning are shown in white. The locations for all lineaments are coincident. The artefact along the eastern edge of the northwest-southeast sheet is associated with the minimum curvature grid.

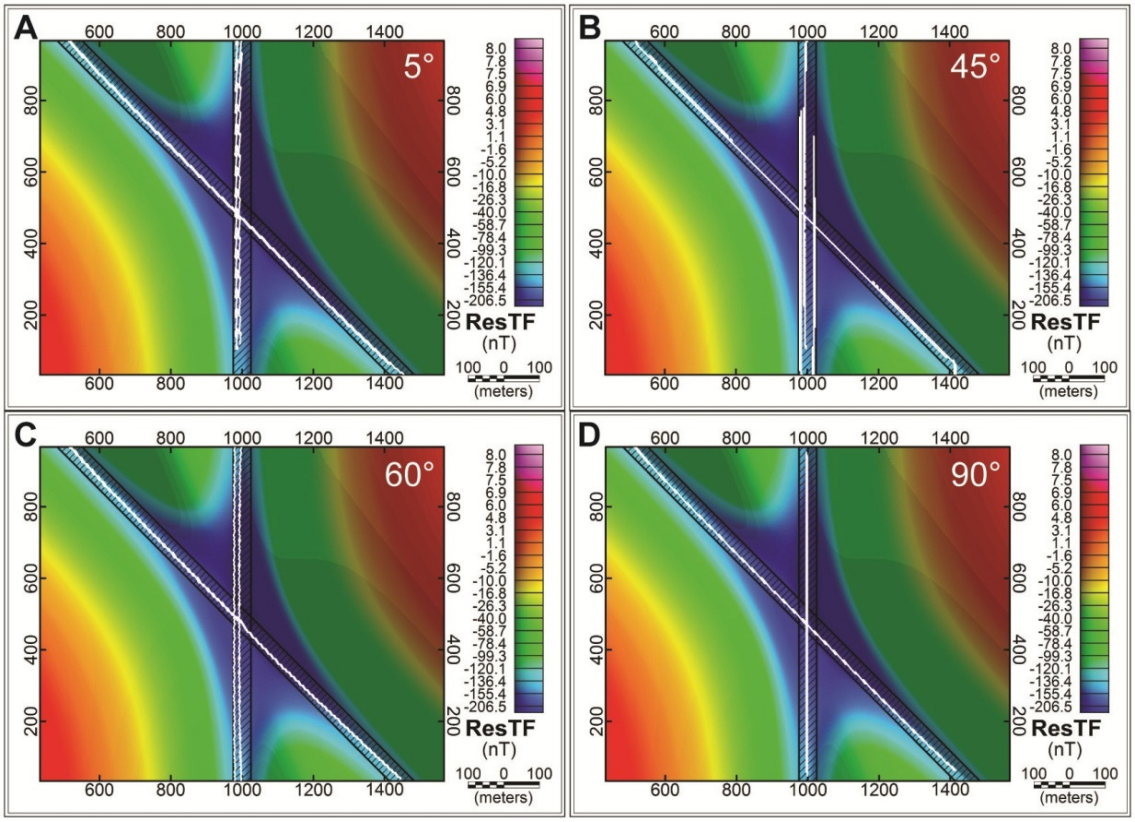

Figure 8.2. Each data set was rotated 5° (A), 45° (B), 60° (C), and 90° (D) and gridded using minimum curvature, bi-directional, kriging, and tinning. The extracted lineaments (g_1) were computed (white) from each grid and overlaid on ResTF. The lineaments are coincident for all rotations of the NW-SE sheet. Artefacts are apparent along the N-S sheet for 45° rotation. There is a spatial separation of ~10m between lineaments for 5° and 60° solutions. Lineaments are coincident for the N-S sheet after 90°.

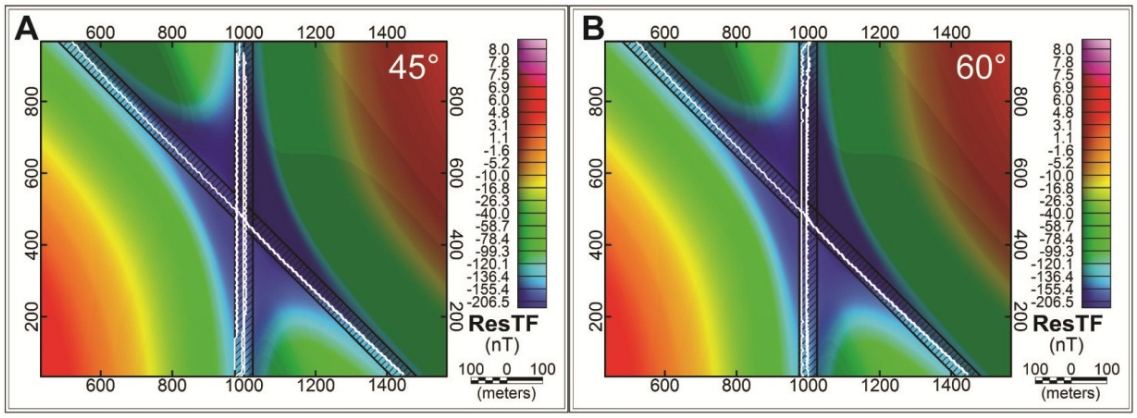

Figure 8.3.The rotated grids for 45° and 60° were back-rotated and lineament extraction computed. The eastern edge anomaly in Figure 2B is no longer presented after back-rotation (A). This indicates it was a result of the extraction algorithm. The separation between the gridding lineaments in Figure 2C is still present after back-rotation (B) and is a consequence of the gridding algorithm. In both (A) and (B) minimum curvature and kriging share the same location; while bi-directional gridding and tinning share the same location. The distance between solutions is approximately 13m.

8.4 Real world example

Lineament analysis is applied to a 2007 aeromagnetic survey covering a section of the 1.88 Ga Paleoproterozoic Wopmay Orogen, Northwest Territories, Canada (Figure 8.4). The data was flown at a constant mean terrain clearance along east-west flight lines with a 400m line separation. Tie-lines were flown orthogonally with a 2500m separation. The geological environment is host to various linear features such as fault systems and dyke swarms. This makes the aeromagnetic data set ideal for a study on the identification of geological and artificial lineaments.

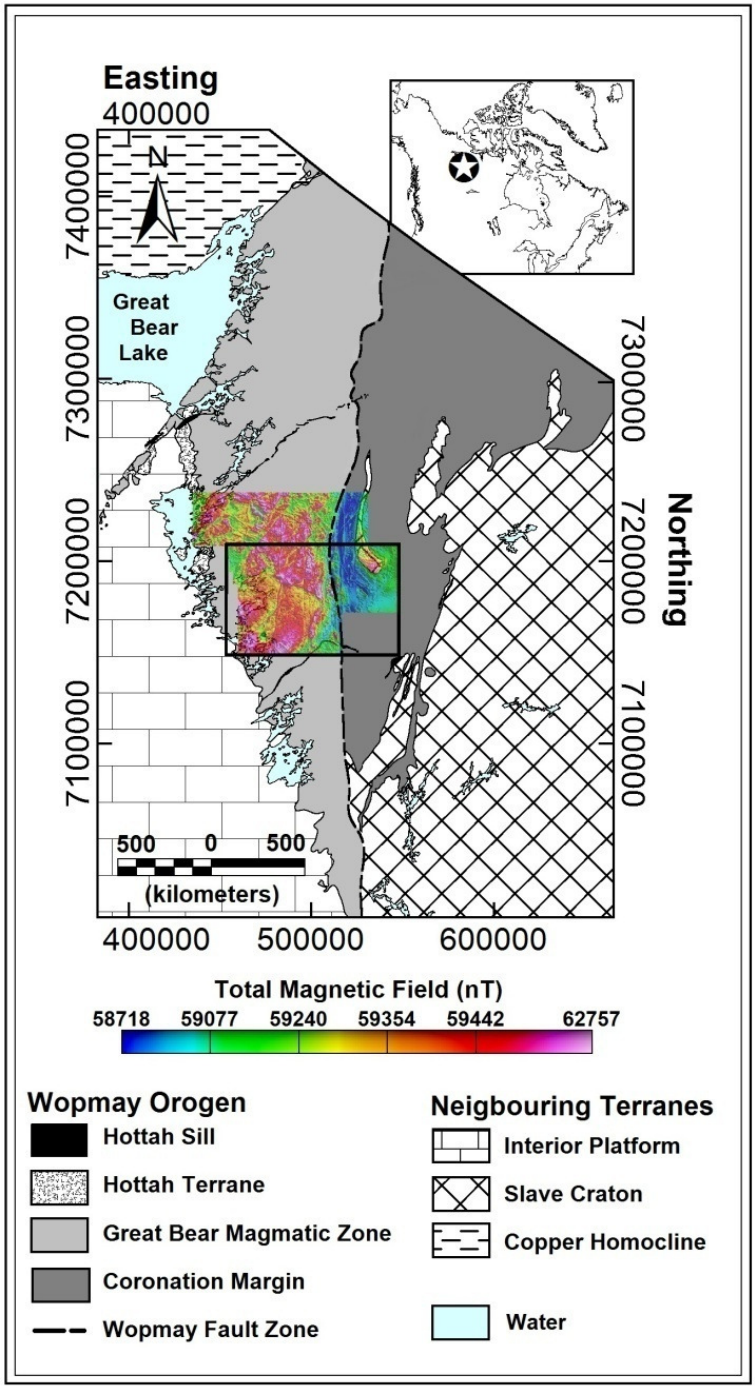

Figure 8.4. Geological provinces within the Wopmay Orogen area and its location within Canada (inset - black star). The Wopmay fault zone represents the suture zone between the Hottah terrane and the Slave craton. This work is focused over a portion of the 2007 aeromagnetic study area indicated by the black box (after Lee et al., 2012b).

Lineament extraction was carried out using the network extraction approach (Lee et al., 2012a) originally designed for topographic analysis. In this study only surficial continuous lows (troughs) were extracted, which represent faults, reverse-polarity dykes and the boundary along either side of a normal polarity dykes. As demonstrated by Lee et al. (2012a) it is equally possible to apply the same approach to locate continuous highs (ridges), which would represent normal polarity dykes. A constant window size of 0.1% of the data set size (~1km) was used for lineament extraction in each scenario. This allowed for delineation of both regional and localized features.

The results are portrayed as rose diagrams for visualization of the lineament solutions. These rose diagrams allow for both a rapid qualitative and quantitative means of representing lineament solutions. All rose diagrams use 5° bins and their petal lengths represent percentage of total population. The lineaments are bidirectional (0°-180°) in magnetic field interpretation. We are not concerned with direction of flow along a lineament as in topographic interpretation where the lineaments are unidirectional (0°-360°).

8.4.1 Artificial versus valid solutions

We define valid lineaments as those defined by geology and structure. Artificial lineaments are those generated by the gridding algorithm or as a consequence of the lineament extraction routine. A valid solution will be dependent on the grid's position in x, y, z space. The orientation of a valid solution varies with incremental rotation of the data. In a geological context this means a N-S trending dyke will have a NW-SE trend after the data has been rotated counterclockwise 45°. Also the location of a valid solution would not change in relation to neighbouring features after rotation. The dyke's original azimuth would fall into a bin of 0° while after rotation its azimuth would fall into a bin of 45°. An artificial lineament will be independent of rotation as the extraction routine will have a preferred analysis direction controlled by the selection window. Artificial solutions repeatedly appear with the same orientation even after the data has been rotated. This means if the predisposition of the extraction routine is 0° then after repeated rotations there will be a conspicuous surplus of solutions within the 0° bin. Using this observation it is possible to differentiate between valid and artificial solutions by systematically computing lineament patterns for an incrementally rotated data grid.

The residual magnetic field data was rotated prior to gridding by increments of 5° around the southwest corner (0, 0) from 0° to 180°. The lineaments were recalculated on each grid and rose diagrams computed. As valid data are common to all of the rose diagrams irrespective of rotation it is possible to separate the valid from the artificial data by

computing the minimum lineament loading for each histogram bin azimuth. To correctly compute the proper bin loading one must first back rotate each of the rose diagram histogram bins by the same amount as used in the initial grid rotation. After back-rotation of the rose diagram it is possible to discriminate between lineament error and artefact by examining a histogram of the number of lineaments within each histogram bin. Error in computation of the valid signals can be defined by variance around the most common minimum value. Directions associated with a higher probability of being an artefact can be identified by subtracting the minimum common value from each individual bin.

8.4.2 Data interpolation

All grids were calculated with a ¼ line spacing (100m) grid cell size. The Southern Wopmay Orogen aeromagnetic survey was acquired along east-west oriented flight lines of relatively equal spacing. Tie-lines were flown making the optimal gridding algorithm minimum curvature. Tie-lines were omitted for bidirectional gridding and an akima-spline approach was implemented along line. The kriging algorithm used a variogram power model of 1 as computation does not require a defined nugget, range or sill. The tinning method used a natural neighbour approach which identifies the nodes closest to a given coordinate.

8.4.3 Image enhancement

The aim is to enhance magnetic fabric. More specifically narrow, linear, continuous features defined by local faults and dykes. Typically dykes are strongly magnetic and readily apparent in most magnetic data sets. Faults are typically weakly magnetic, which is further complicated as their anomalies are often situated within a large magnetic homogeneous body. For the Southern Wopmay this is true as many faults are located within the Great Bear magmatic zone producing small anomalies within a large one. To accentuate signals associated with faults and diminish signal associated with high amplitude anomalies we computed the first vertical derivative and two AGC filters - tilt derivative and a small filter window (Pilkington and Keating 2004). Image enhancement is applied to the minimum curvature grid since it is deemed the most appropriate gridding algorithm considering the survey configuration. The vertical derivative is simply the change in the z-direction and the tilt-derivative is calculated using the equation defined in Miller and Singh (1994). The AGC filter is calculated using the method defined in Rajagoplan and Milligan (1994). The AGC uses a local amplitude filter with a size of 10m and maximum gain correction of 10 making the filter highly localized.

8.5 Real world results

Prior to modifying the data set itself through interpolation algorithms and image enhancement techniques it is important to first address the quality of the lineament extraction method first. This is accomplished through rotation of the data set in *x*, *y* space around a fixed point. The non-rotated lineament data set computed from the minimum curvature grid (Figure 8.5) indicates dominant populations as any multiple of 45°. These bins have suspiciously high counts as shown in Figure 8.6. The total count of these dominant populations is relatively high with each rotation increment indicating they may represent artificial solutions. That being said there are some mapped NW-SE and NE-SW dyke swarms and faults in the study area that contribute to the higher count. For example purposes in Figure 8.6 the counts for each azimuth are shown for rotations of 0°, 30°, and 150°.

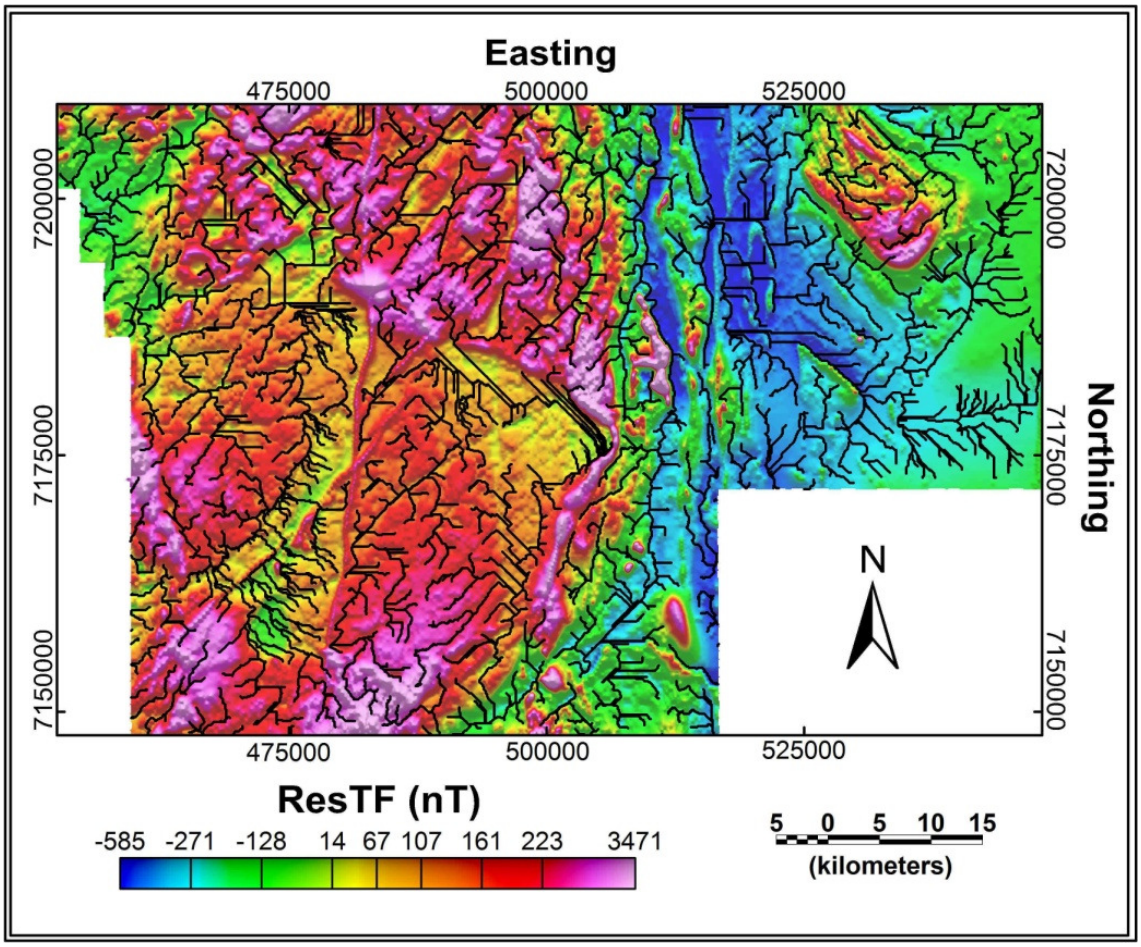

Figure 8.5. Lineaments extracted from a 1km window over the ResTF gridded using a minimum curvature 100m grid cell size.

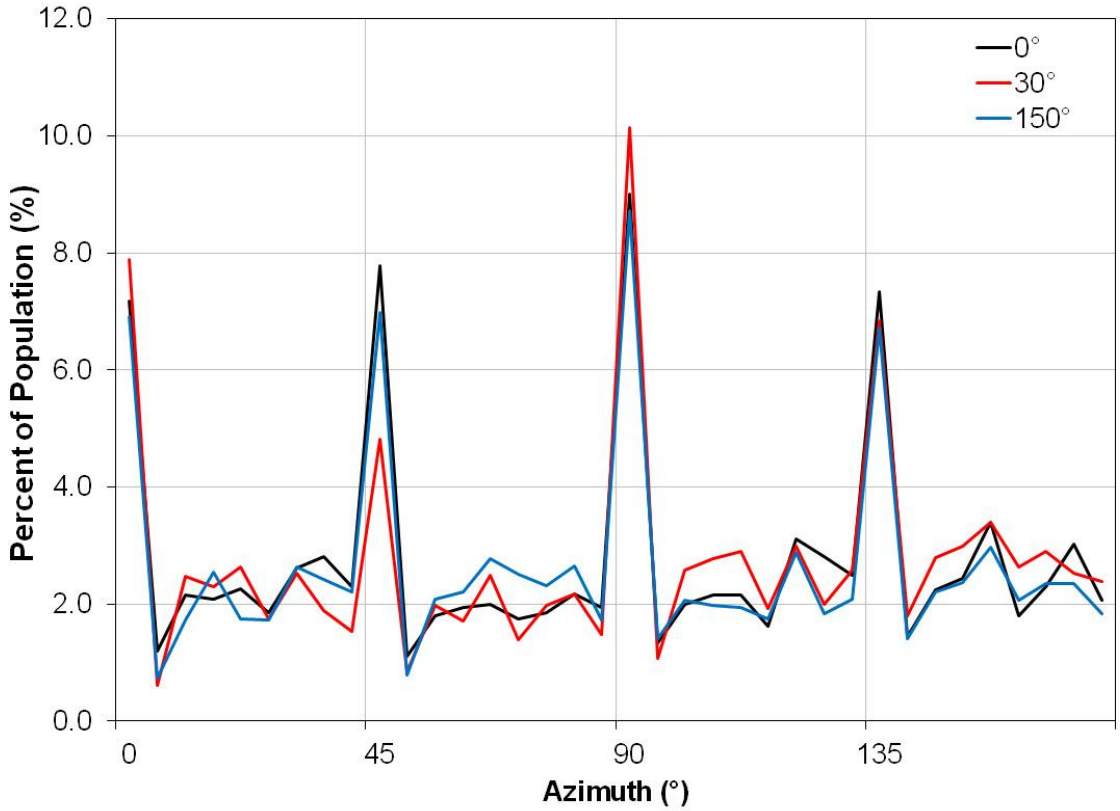

Figure 8.6. Linear plot of percent of population versus azimuth for rotations of 0°, 30°, and 150°. There are anomalous counts for increments of 45° regardless of rotation degree.

Rose diagrams present evidence for a preferred orientation of a specific lineament pattern; they do not contain information about the length of a lineament. As demonstrated by Florinsky (2005) artificial lineaments are often associated with anomalous lengths. It is possible that artefacts in the data will have both an anomalous orientation and length. To investigate this possibility we generated a cross plots between lineament orientation and lineament length (Figure 8.7). For this data set most lineaments shorter than 3km exhibit a systematic pattern relative to the 45° signal. Lineaments with lengths greater than 3km do not exhibit the same pattern. This is shown by the Percent of Population Difference (black line) between the short and long lineaments in Figure 6. This confirms most lineaments along increments of 45° are spurious and generated by the lineament algorithm. These artificial lineaments are especially identifiable over magnetically-flat areas such as the eastern edge of the study area (Figure 8.5).

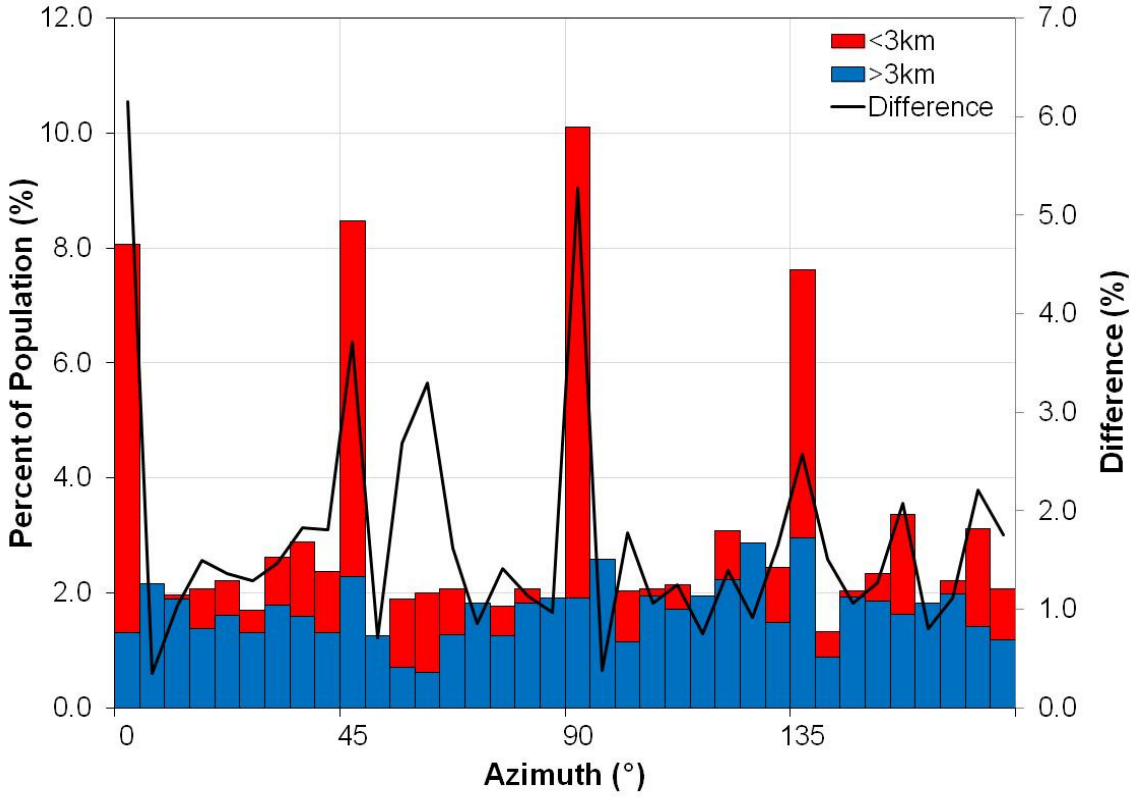

Figure 8.7. Histogram of percent of population versus azimuth divided into two subsets – lineaments that are less than (light grey) and greater than (dark grey) 3km in length. The percent of population difference between the two subsets is represented as a bold black line. The greatest difference occurs at increments of 45° and contrary to standard assumption, the anomalous solutions principally occur at the shortest lengths, less than 3km.

The above results are displayed as rose diagrams in Figure 8.8 where 8.8A exhibits the original rose diagram with the suspiciously populated bins and the latter two rose diagrams have omitted the artificial lineaments from the original solutions set. The latter rose diagrams (Figure 8.8B and 8.8C) indicate distributions more commonly expected from a geological data set. For example the 26 lineaments oriented north-south correspond to the Wopmay fault zone; while the 19 lineaments with an orientation of 150° represent local northeast-southwest mafic dyke swarms.

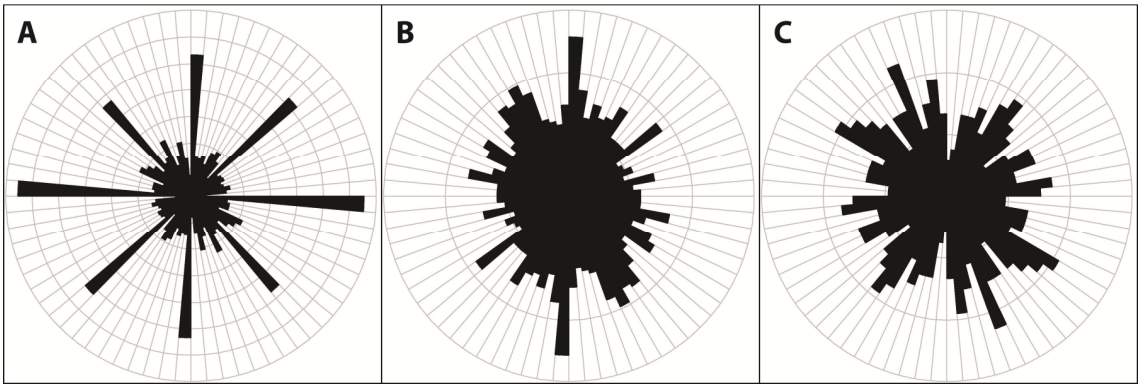

Figure 8.8. Rose diagrams of the lineament solutions. (A) has all lineament solutions while (B) has the rotation artefacts removed, and (C) has the length artefacts removed. Each petal and ray is an increment of 5° while the circles are percentage of total population.

Magnetic anomaly grids are produced through the use of interpolation algorithms on flight line data. Comparison of the lineaments extracted from grids computed using different interpolation algorithms is shown in Figure 8.9. All of the interpolation routines produced artefacts with anomalous values having increments of 45°. These anomalies were removed from Figure 8.9. A linear interpolation scheme was used to determine an appropriate number of occurrences for the 45° bin. In the original minimum curvature data set the erroneous solutions represented 18.1%, while bidirectional, kriging, and tinning had reductions of 23.1%, 20.6%, and 23.0% respectively. This shows that minimum curvature produced the fewest erroneous solutions and is likely the optimal interpolation method when used in conjunction with automated lineament extraction. Bidirectional gridding exhibited the largest reduction in erroneous solutions; however only marginally over tinning. The extracted lineaments should be carefully analyzed prior to acceptance and interpretation in cases where bidirectional gridding is the optimal interpolation method. These results are likely due to the fact that bidirectional gridding introduces a biased through preferential gridding direction and a tin surface is constructed through a series of triangles between points that have discontinuous edges. This is unlike minimum curvature or kriging that construct smooth surfaces.

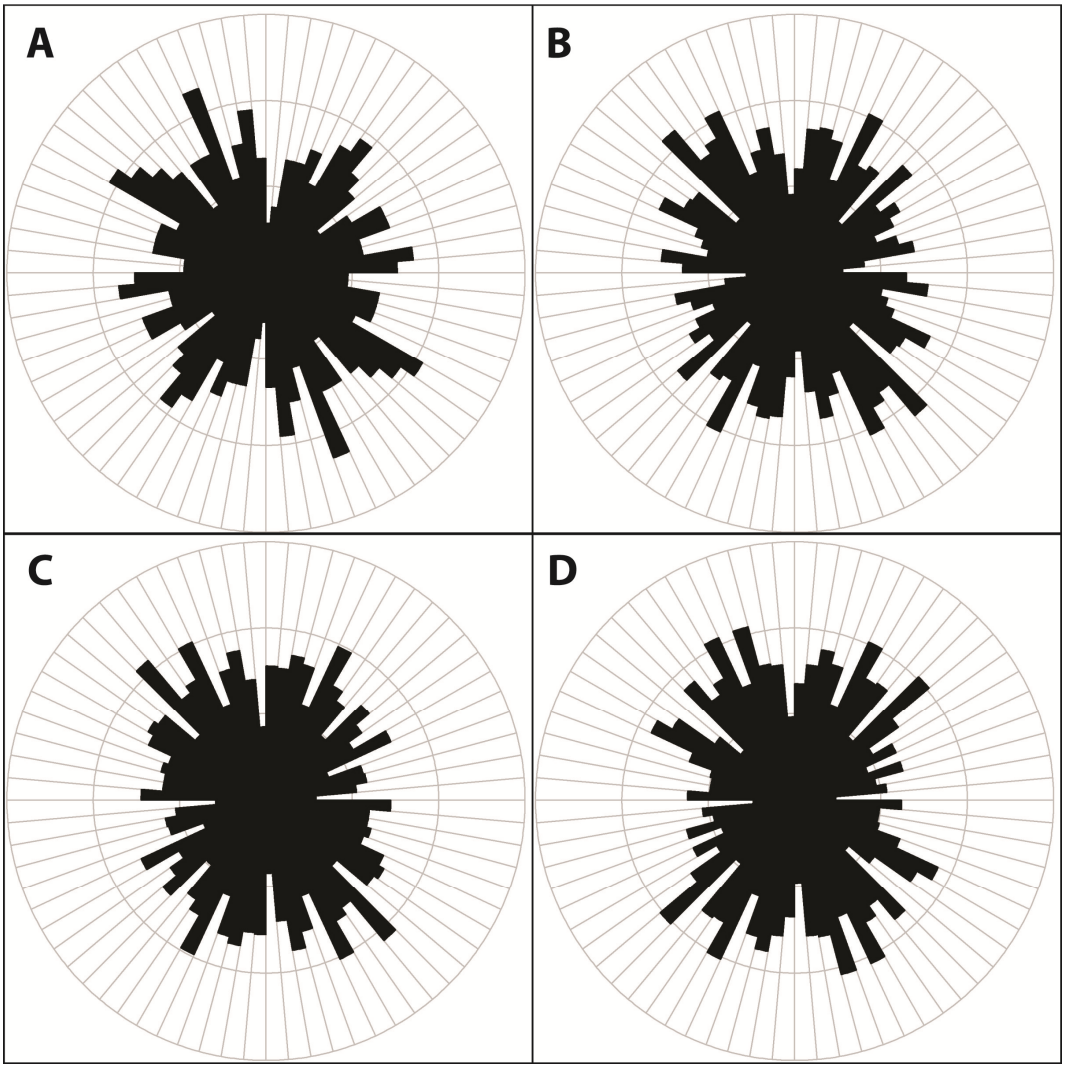

Figure 8.9. Comparison of rose diagrams produced by minimum curvature (A), bi-directional gridding (B), kriging (C), and tinning (D). Anomalous values have been removed so that overall azimuth trends are exemplified.

Figure 8.3 showed that the spatial location of various gridding lineaments is not identical for a synthetic data set. This is an important point to address for the real world data set as well. The extracted lineaments from each gridding routine were overlaid on the Southern Wopmay ResTF to evaluate their relative spatial locations (Figure 8.10). The spatial locations of the lineaments were nearly identical over prominent magnetic linear lows (i – white arrows). These lineaments show irregular patterns more consistent with expected geological trends and are likely valid. The lineaments along the 45° and 0° axis of interpretation are apparent over this area and all four gridding lineaments identify them consistently (ii – white arrows). These are the lineaments identified in the rose diagrams as artificial as they are related to the lineament extraction routine. The differences between the lineament solutions are apparent over magnetically flat areas (iii – white arrows). The extraction routine struggles with these areas due to the fundamental properties of the extraction algorithm. The algorithm utilizes surficial curvature to identify continuous troughs. Curvature struggles to identify features when the curvature value is small since these values are typically associated with either the location over a source or along the edges of a source (Lee et al., 2012a). The interpretation window relies on a 3 x 3 window to identify the nearest cell with a lower value. This fails when multiple nearby cells have nearly identical values – resulting in a low area rather than a low lineament. The extraction method then makes subtle differences between each gridding routine more apparent. This results in a lack of consistency between gridding lineaments over surficially flat areas and highlights the differences in the gridding algorithms.

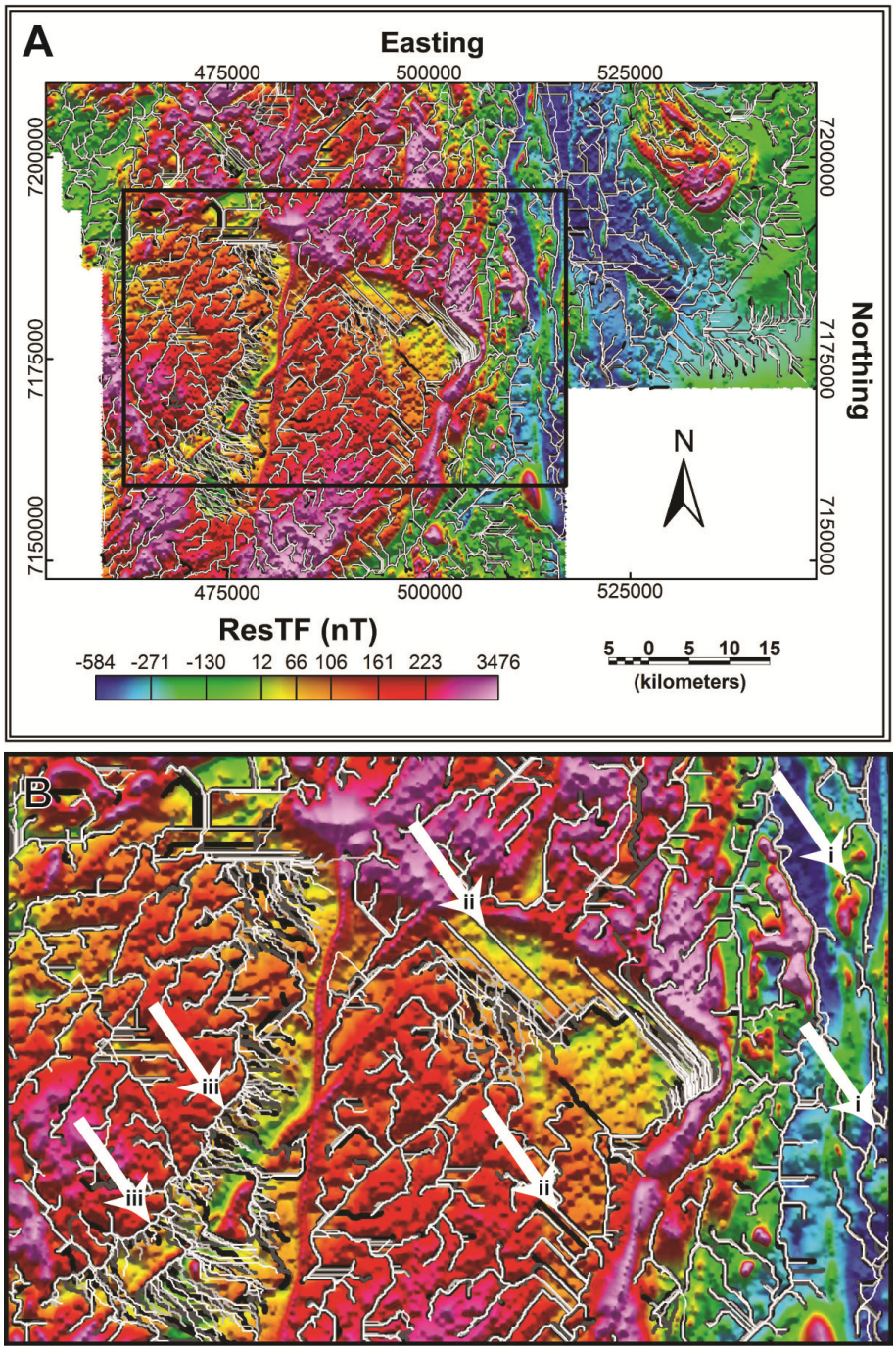

Figure 8.10. Comparison of lineaments produced by minimum curvature (black lines), bi-directional (dark grey lines), kriging (light grey lines), and tinning (white lines). The full lineament solution set overlaid on minimum curvature ResTF (A). A subset of the study area (A – bold black box) was selected to demonstrate valid and artificial lineaments (B).

The image enhancement results are shown in Figure 8.11. Both the derivative and the AGC filter calculations yet again produced lineaments with the same four anomalous dominant directions: 0°, 45°, 90°, and 135°. These were removed using the same omit and interpolate method employed in the grid algorithm section. Principal solutions oriented north-south are readily apparent, while secondary northwest-southeast and northeast-southwest are also extracted. The image enhancement routines amplify weakly-magnetized anomalies, minimizing the area over which the data is magnetically-flat. In this case, magnetically-weak features such as faults within the relatively homogeneous granitoids of the Great Bear magmatic zone become far more apparent following the small AGC filter.

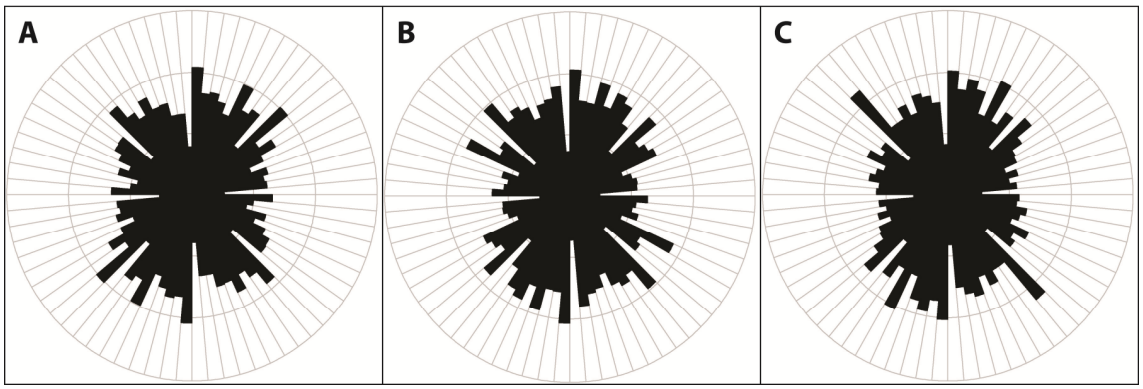

Figure 8.11. Rose diagrams of the lineament solutions produced by image enhancement techniques; First vertical derivative (A), tilt derivative (B), and automatic gain control. The rose diagrams all show similar solutions with high counts along north-south, northwest-southeast, and northeast-southwest. Each petal and ray is an increment of 5° while the circles are percentage of total population.

It is recommended for optimal solutions the data is first interpolated using a suitable gridding algorithm. For the Southern Wopmay data set minimum curvature was the most appropriate gridding algorithm due to the acquisition of tie-lines. Minimum curvature produced similar results to the bidirectional and kriging lineament results but incorporated the full data. Second, the magnetic grid should undergo image enhancement, such as an AGC filter with a small window to amplify weakly-magnetic anomalies. Finally, the interpolated, AGC-filtered grid should undergo systematic rotation and length analysis to identify erroneous solutions produced by the lineament algorithm.

8.6 Conclusion

Transformation of the data sets through systematic rotation and length analysis showed which lineaments were defined by signal (i.e. geology) and which were products of either the lineament extraction routine or gridding algorithm. Lineaments defined as signal were clearly identified and the effects of pre-processing techniques on the final lineament data set by varying the interpolation method and the application of image enhancement techniques. Using a synthetic model the effect of rotating the data and back-rotating the grid allowed for a quick routine to identify lineaments generated by the network extraction process and those generated by the gridding algorithm. In the case of the real world data set from the Southern Wopmay, the lineament extraction routine had the greatest impact on the lineament outputs. These artificial lineaments are most apparent over magnetically-quiet areas. They are readily identified by rotation and length analysis. When attempting to extract lineaments from aeromagnetic data one should fully investigate the veracity of the results by a thorough statistical analysis rather than accepting the output of any algorithm. Application of an AGC filter helped minimize this issue by amplifying weakly-magnetic anomalies. This stresses the importance of the collaboration between automation and user-defined lineament extraction for obtaining a reliable product for map production and resource exploration.

8.7 Acknowledgements

The authors wish to thank V. Jackson, L. Ootes from the Northwest Territories Geoscience Office and L. Corriveau of the Geological Survey of Canada for their support and assistance on bedrock geology, petrology. This work was in part funded by numerous programs: the IOCG-Great Bear (00410) and Remote Predictive Mapping (GKM005) projects of the Geomapping for Energy and Minerals program through Natural Resources Canada; the South Wopmay Bedrock Mapping project of the Northwest Territories Geoscience Office through Aboriginal Affairs and Northern Development Canada; and the Polar Continental Shelf Program (50709). The project was conducted through various collaborative agreements between Natural Resources Canada, the Northwest Territories Geoscience Office, the Community Government of Gamètì, and Fortune Minerals Limited. Appreciation is given to the support provided by the Flight Research Laboratory of the National Research Council. The authors would also like to acknowledge the contribution by the Editor, Associated Editor, and Reviewers for their recommended revisions.

8.8 References

Billings, S.D., and Richards, D., 2000, Quality control of gridded aeromagnetic data: *Exploration Geophysics*, 31 (4), 611-616.

Billings, S.D., Beatson, R.K., and Newsam, G.N., 2002, Interpolation of geophysical data using continuous global surfaces: *Geophysics*, 67 (6), 1810-1822. DOI: 10.1190/ 1.1527081.

Boyce, J.I., and Morris, W.A., 2002, Basement-controlled faulting of Paleozoic strata in southern Ontario, Canada: Evidence from geophysical lineament mapping,: *Tectonophysics*, 353, 151- 171.

Briggs, I.C., 1974, Machine contouring using minimum curvature: *Geophysics*, 39 (1), 39-48. DOI: 10.1190/1.1440410.

El Abbass, E., Jallouli, C., Albouy, Y, and Diament, M. , 1990, A compariosn of surface fitting algorithms for geophysical data: *Terra Nova*, 2 (5), 467-475. DOI: 10.1111/j.1365-3121.1990.tb00104.x.

Florinsky, I., 1996, Quantitative topographic method of fault morphology recognition: *Geomorphology*, 16, 103-119.

Florinsky, I., 1998a, Combined analysis of digital terrain models and remotely sensed data in landscape investigations: *Progress in Physical Geography*, 22 (1), 33-60.

Florinsky, I., 1998b, Accuracy of local topographic variables derived from digital elevation models*: International Journal of Geographical Information Sciences*, 12 (1), 47-61.

Florinsky, I., 2002, Errors of signal processing digital terrain modeling: *International Journal of Geographical Information Sciences*, 16 (5), 475-501.

Florinksy, I., 2005, Artificial lineaments in digital terrain modeling: Can operators of topographic variables cause them?: *Mathematical Geology,* 37, 357-372. DOI: 10.1007/s11004-005-5953-3.

Ghandi, S., 1994, Geological setting and genetic aspects of mineral occurrences in the southern Great Bear magmatic zone, Northwest Territories: *Geological Survey of Canada Bulletin,* 475, 63-96.

Ghandi, S.S., Mortensen J.K., Prasad, N., and van Breeman O., 2001), Magmatic evolution of the southern Great Bear continetal arc, northwestern Canadian Shield: Geochronological constraints: *Canadian Journal of Earth Sciences,* 38, 767-785.

Lee, M.D., Morris, W.A., Harris, J., and Leblanc, G., 2012a, An automatic network extraction algorithm applied to magnetic survey data for the identification and extraction of geologic lineaments: *The Leading Edge*, 31, 26-32, DOI:10.1190/1.3679324.

Lee, M.D., Morris, W.A., Harris, J., and Leblanc, G., 2012b, A network extraction tool for mineral exploration: a case study from the Wopmay Orogen, Northwest Territories, Canada: *Exploration Geophysics*, 43, 116-124, DOI:10.1071/EG11045.

Pilkington, M., and Keating, P., 2004, Contact mapping from gridded magnetic data – A comparison of techniques: *Exploration Geophysics*, 35, 306-311, DOI: 10.1071/EG04306.

Smith, W.H.F., and Wessel, P., 1990, Gridding with continuous curvature splines in tension: *Geophysics*, 55 (3), 293-305.

Rajagopalan, S., 1987, The use of 'Automatic Gain Control' to display vertical magnetic gradient data: *Exploration Geophysics*, 18, 166–169, DOI: 10.1071/EG987166.

Rajagopalan, S., and Miligan. R., 1995, Image Enhancement of Aeromagnetic Data using Automatic Gain Control: *Exploration Geophysics*, 25, 173-178, DOI:10.1071/EG994173.

Swain, C.J., 1976, A Fortran IV program for interpolating irregularly spaced data using the difference equations for minimum curvature: *Computers and Geosciences*, 1, 231-240.

9.0 Conclusion and future outlook

9.1 Key results

Curvature analysis is a powerful technique for magnetic data interpretation Each chapter discussed an aspect of curvature analysis: Curvature fundamentals; a statistical approach; profile versus plan curvature for magnetic field interpretation; automated lineament extraction; lineament analysis for geologic structural and lithological mapping; lineament analysis for quality control of systematic survey data; and quality control of extracted lineaments.

Curvature analysis starts with the application of a 3 x 3 moving window to a magnetic grid. The window calculates gradients along nine different directions at each grid node which are used as coefficients in fundamental equations to calculate full, profile, and plan curvature. These curvatures are used to conduct statistical and lineament analyses to ultimately separate signal and noise. Curvature may be quantitatively described using statistical analyses. The calculated curvature data set's kurtosis describes the magnetic frequency content and the curvature's skew describes the sign, dip and magnitude of the magnetic data when compared with the mean. These attributes are represented graphically as multivariate scatterplots, histograms and probability plots. These visual representations of the curvature data distribution may be used as a rapid means for assessing bulk frequency content. Curvature may also be described qualitatively as continuous ridges and troughs forming surficial lineaments. The lineaments are displayed as rose diagrams for the purpose of identifying groupings based on their orientation. This is an alternative approach to standard power spectrum analysis as it retains directional information and quantitative values in the form of lineament count. These lineament groupings apparent in rose diagrams are dictated by the geologic fabric describing the magnetic field. The linearity and intersection locations of lineaments are important tools for natural resource exploration since many mineral deposits and hydrocarbon reservoirs are structurally controlled. Lineament location in conjunction with mapped alteration and lithology may be used to delineate mineralization vectors and generate exploration target maps.

Undesirable features generated by data processing are defined as artefacts. The data must be assessed for quality prior to commencing interpretation. This is achieved by extracting the surficial lineaments and comparing their location and azimuth with known flight specifications. Coincidence of lineaments with flight path direction through the use of buffers may indicate insufficient levelling. The degree of levelling is quantified through the calculation of these lineaments pre- and post-levelling. This is achieved qualitatively with rose diagrams pre- and post-levelling of the curvature derived lineaments. The user may then determine whether the magnetic data should undergo further processing

depending on the results. Artefacts due to processing besides levelling may also occur. Careful consideration of the interpolation method and projection characteristics is very important since it will dictate the magnetic anomaly in the final magnetic grid. Curvature analysis incorporates both quantitative and qualitative approaches allowing for an interpretation by any geoscientist. The graphical options allow curvature as a raster or vector layer in mapping or exploration. Previous authors have implemented curvature for geophysical investigations and specifically potential fields (Cooper and Cowan, 2006; Phillips et al., 2007; Cooper and Cowan, 2008; Cooper, 2009; Cooper, 2010). What is unique in this apart is the comprehensive procedure developed for each step in the quality control, processing and interpretation of magnetic data.

9.2 Future outlook on research

The development of the statistical approach is important. Current statistical analysis is limited to univariate and bivariate descriptors of variables. For example, scatterplots comparing different attributes of curvature have been shown in this thesis to produce near-linear relationships defined by the simple equation $y = \mathrm{m}x + \mathrm{b}$. Simple least-squares line fitting of the data included herein has shown it is possible to use this information to differentiate broad scale features of the individual data sets. Different source geometry can lead to different curvature attributes. It should theoretically be possible to develop a routine which computed the spatial variation of skew and kurtosis integrated this with local estimates of PrC and PlC to end up with a procedure which could rapidly isolate sole source anomalies whose dip direction and structural index morphology were defined by the curvature.

All of the analysis presented in this study is based on the examination of data relative to a single observational surface. In order to locate source bodies using magnetic data a number of recent studies (Keating, 2009; Smith et al., 2012) compare the response signal from a series of upward continued surfaces. Smith et al. (2012) showed the relationship between the response of an isolated anomaly on sequential surfaces follows a simple power law. Moving forward, it is possible to conceive of applications of curvature analysis where one could generate a multi-dimensional space plot populated by curvature attributes computed at a series of increasing upward continuation levels. In this conceptual space it may be possible to differentiate source geometries and depths through searches for clusters, lineations and planar features. This will necessitate development of a plotting framework which permits the incorporation of source signal alignment and amplitude along with curvature. The Fourier transform radial power spectrum provides a basis for the type of approach one might expect. However, implementation of this type of approach for curvature studies is beyond the scope of this thesis. Once such an N-dimensional data scheme has been produced to locate features in this data space one could

easily adapt procedures currently employed in hyperspectral remote sensing. Curvature analysis has only been applied to magnetic data however the method may be refined for other geophysical surfaces. Gravity is also a potential field and many methods applied in magnetic interpretation are also applied in gravity (Blakely and Simpson, 1986; Reid et al., 1990; Miller and Singh, 1994; Zhang et al., 2000; Fitzgerald et al., 2004). Gravity data may be described with respect to amplitude and frequency content. The principle difference is density is used rather than magnetic susceptibility as the described physical property. Application of a statistical approach using kurtosis and skew would serve as a way to identify density contrasts. A deep or extensive source will be defined by a low frequency while a near surface source will be defined by a high frequency. This means the use of kurtosis as a means for frequency content analysis remains the same. Skew on the other hand will not describe gravity data the same as magnetic data. A dipping magnetic source or a magnetic source in an inclined field will generate an asymmetric dipole anomaly. This is not the same for a gravity anomaly. The gravity anomaly associated with a single source may have a positive or negative value but it will always be a monopole. This actually simplifies the use of skew since a right skew will indicate a preference for less-dense materials and a left skew will indicate a preference for denser materials. Information on dip is not contained in the curvature data set.

In any geophysical interpretation having access to *a priori* data makes the final outcome more reliable. Included in Appendix B and C are a full database of magnetic, electrical, and radiometric properties from the Southern Wopmay Orogen, N.T. These include: mineralogy; Curie Temperature; skeletal density; volume corrected magnetic susceptibility; natural remanent magnetization; chargeability; resistivity; hysteresis parameters; and radiometric ratios. These physical properties of the lithology fine tune initial interpretations produced by the curvature and lineament analysis. This geoscientific data integration will aid in bedrock mapping and mineralization studies already in progress. Appendix C includes numerous figures exhibiting these various properties for both in-situ measurements and rock samples. These properties may be correlated to existing studies within the study area. This includes mineralization vectors for multiple metals. For example, the area is known for Iron-Ore Copper Gold deposits, which are associated with elevated magnetite, hematite, and radiometric elements (potassium and uranium enrichment). These figures along with the preliminary map products generated in previous chapters will help form a story on the geology as well as potential zone of mineralization.

In the end, to make curvature analysis a common geophysical tool involves integrating all steps as outlined in Figure 1.1 into one program or code. At present each component is divided between different software, thus diminishing efficiency. As such, amalgamating

the steps into one interface is important to make the analysis more user-friendly by any geoscientist.

9.3 References

Blakely, R., and Simpson, R., 1986, Approximating edges of source bodies from magnetic or gravity anomalies: *Geophysics*, 51, 1494–1498, DOI: 10.1190/1.1442197.

Fitzgerald, D., Reid, A., and McInerney, P., 2004, New discrimination techniques for Euler deconvolution: *Computers and Geosciences*, 30 (5), 461-469, DOI: 10.1016.

Keating, P., 2009, Improved use of the local wavenumber in potential-field interpretation: *Geophysics*, 74 (6), L75-L85.

Miller, H.G. and Singh, V., 1994, Potential field tilt – a new concept for location of potential field sources: *Journal of Applied Geophysics*, 32, 213-217.

Reid, A., Allsop, J., Granser, H., Millett A., and Somerton I., 1990, Magnetic interpretation in three dimensions using Euler deconvolution: *Geophysics,* 55, 80-91.

Smith, R.S, Thurston, J.B., Salem, A., and Reid, A.B., 2012, A grid implementation of the SLUTH algorithm for visualizing the depth and structural index of magnetic sources: *Computers and Geosciences*, 44, 100-108, DOI: 10.1016/j.cageo.2012.03.004.

Zhang, C., Mushyandebvu, M.F., Reid, R.B., Fairhead, J.D., and Odegard, M.E., 2000, Euler deconvolution of gravity tensor gradient data: *Geophysics*, 65 (2), 512-520, DOI: 10.1190/1.1444745.

APPENDICES

A. Comparison of magnetic susceptibility meters using rock samples from the Wopmay Orogen, Northwest Territories, Canada

Lee, M.D., and W.A. Morris, 2012, Comparison of magnetic susceptibility meters using rock samples from the Wopmay Orogen, Northwest Territories, Canada: *Current Research* , Submitted

A.1 Abstract

Fifty one rock specimens from the Wopmay orogen, N.T., Canada were cut and their magnetic susceptibility measured using three different meters (KT10, MS2E, and SM-30) to quantify any variability between instruments. The three meters are all hand-held instruments designed for taking measurements on outcrop, core, or hand specimens. Each instrument calculates magnetic susceptibility from a frequency change produced in an EM circuit in the presence of a magnetic source. The three instruments differ in three ways; a) the frequency of the inductive EM signal, b) the size and geometry of the source coil, and c) the strength of the applied field. The fifty one rock specimens ranged in magnetic susceptibility from 0.02 SIx10-3 to 192.82 SIx10-3. After measuring each specimen with all three instruments we compared the response of each instrument by computing the best fit least squares line to log10 cross plots. The slope and intercept of the best fit line provides an estimate of the relative gain and offset between instruments. The SM-30 and the KT-10 produce very similar response. The MS2E gave results that were systematically higher than the SM-30 and the KT-10. It is possible that this might be associated with the differing frequency of the applied field: the MS2E uses a much lower frequency input signal than the KT-10 and the SM-30. Repeat measurements of a sample provide a measure of signal noise and the detection of within sample susceptibility variations. The MS2E exhibited the largest within sample signal standard deviation. In summary, the larger coil size used by the KT-10 and SM-30 instruments averages susceptibilities over a broader surface area, while the smaller coil of the MS2E is capable of detecting smaller scale susceptibility fluctuations. For the purposes of acquiring susceptibility data for use in magnetic modeling there is no effective difference between the KT-10 and the SM30. Using the MS2E one needs to make many more individual measurements.

A.2 Introduction

In-situ magnetic susceptibility measurements are one of the most commonly used physical rock property measurements. A magnetic susceptibility reading provides a rapid means of estimating the magnetic mineral content of a rock. As demonstrated by Henkel (1991) a comparison between magnetic susceptibility and density readings can provide insight into the mineralogy of the magnetic mineral content. Magnetic susceptibility then provides key information in linking geophysical observations to geological models. Prior knowledge of the magnetic susceptibility of representative rock units provides a critical constraint in any geophysical modeling exercise using aeromagnetic data. All magnetic anomaly inversion models are compromised by the trade-off that exists between source geometry, source depth and physical property contrast. This issue is commonly described by the phrase "non-unique" solution. Having access to susceptibility data permits the interpreter to impose some limitations on the range of solutions that are mathematically viable. Of course the quality of these inversions and forward models are significantly influenced by the veracity of the susceptibility data that are used in the model definition. There are a number of magnetic susceptibility meters available on the market. However, a review of instrument specifications shows that there are significant differences between individual instruments which may affect the reported magnetic susceptibility value. Instrument design variations include factors such as: dimension and position of the sensor coil and the frequency of the current used to activate the coil. In this study, we compare the magnetic susceptibility values reported by three commonly used meters on hand rock specimens from the Wopmay orogen, Northwest Territories, Canada to establish if there are any systematic differences which could impact magnetic model outcomes.

A.3 Data

The Wopmay orogen is a 2.6 to 1.85 Ga Paleoproterozoic orogenic belt that has been of economic interest because it hosts various mineralized prospects and deposits. A total of fifty one rock samples were selected from the Wopmay orogen, collected in 2009 and 2010 (Figure A.1). The primary rock types present in the samples include monzonite, diorite, leucogranite, rhyodacite and mafic dykes. Samples were also obtained from five known mineral occurrences: Sue-Dianne, NICO, Damp, Fab Lake, and Ron Lake.

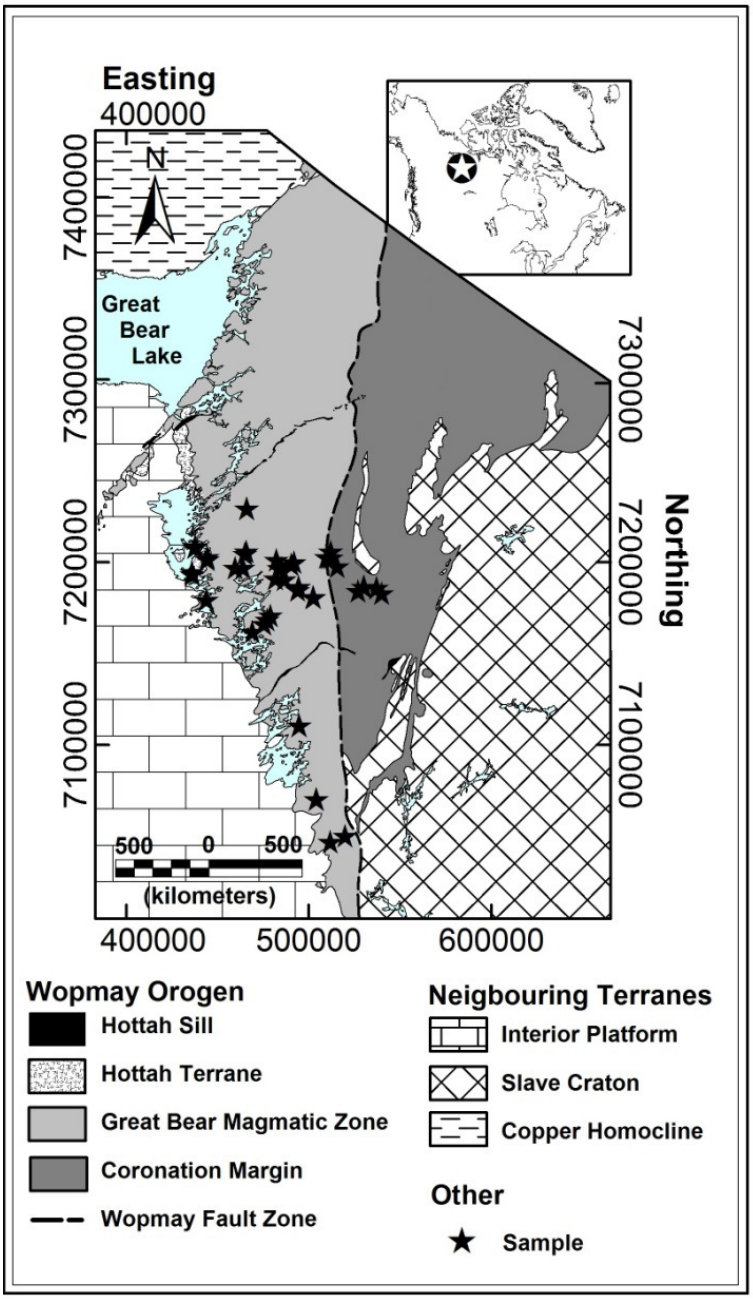

Figure A.1. General geology of the Wopmay Orogen (after Hoffman and Hall, 1993). Locations of samples are indicated with a black star.

A.4 Method

A.4.1 Instruments

Bartington MS2E (Bartington Ltd.)

The MS2 magnetic susceptibility meter manufactured by Bartington Instruments Ltd. is a portable meter that may be used with rechargeable batteries or a main power supply. The Bartington tool comprises two elements: a) the MS2 meter; and b) a sensor package that is linked by a cable to the meter. This design approach allows for a variety of sensor configurations. Variations in the geometry and dimensions of the sensor coil permit the user to tailor a measurement to a specific application. Specific sensor and coil geometries are offered for each of the following types of specimens, soil or rock samples, larger diameter drill cores, soil surfaces, rock outcrops and even for down auger holes. In this study we used the MS2E laboratory sensor. The sensor only weighs 0.22kg, while the meter weighs 1.2kg. The sensor element, which is located within a ceramic cylinder, is a rectangular coil (3.8 mm x 10.5 mm) which corresponds to a total sensing area of 39.9 sq. mm. The small size of the sensor means that it is possible to precisely locate the coil over localised variations within an outcrop. . The operating frequency for the coil is 2 kHz. The MS2E incorporates a standard correction for volume giving it a sensitivity of 1x10-5 SI (volume specific) or 1x10-8 SI (mass specific). Instrument calibration is provided by reference to a 15mm x 33mm Fe304 in alumina and epoxy resin provided by the manufacturer.

Heritage Geophysics SM-30 (Heritage Geophysics Inc.)

The SM-30 magnetic susceptibility meter by Heritage Geophysics Inc. is a small compact hand-held field meter that weighs only 0.180 kg, ideal for outcrop measurements. This instrument has a 50mm diameter detector coil, corresponding to a sensing area of 1964 sq. mm. that is incorporated in the body of the meter. The exact location of the sensor coil in the body of the meter is not exactly known and there is no external measurement trigger (pin) as in the KT-10. The sensor coil has an operating frequency of 9 kHz and a sensitivity of 1x10-7 SI units. The instrument output does not include any correction for sample volume, or mass.

Terraplus KT-10 (Terraplus Inc.)

The KT-10 magnetic susceptibility meter by Terraplus Inc. is a hand-held field meter also designed for measurements on outcrops, drill cores, and rock samples. The KT-10 is much bigger than the SM-30 and at 0.30kg weighs almost twice as much. The inductive coil of the KT-10, which has a diameter of 65mm corresponding to a total sensor area of 3318 sq. mm., is located at the end of the instrument. The KT-10 is designed to be used either with the standard pad that is equivalent in diameter to the inductor coil or an

attachable pin that holds the meter parallel to the rock surface to increase accuracy over uneven samples. This meter utilises an operating frequency of 10 kHz with a sensitivity of 1x10-6 SI units. No volume or mass correction is performed by the operational software. Unlike other units the KT-10 does include a GPS sensor which allows the user to tie a measurement to an observation location.

A.4.2 Measurements

Superficially, measurement of magnetic susceptibility might seem to be a simple procedure; that is one holds the instrument in contact with a rock surface for a specific period of time while the instrument measures the change in frequency of the input signal caused by the presence of magnetic material. In practice there are a number of operational complexities that need to be considered. First, when taking a measurement in the field it is imperative that one choose a flat surface to ensure optimum coupling between the inductive coil and the rock surface. The MS2E having a smaller coil can acquire readings on surfaces that are more curved than the other two instruments. In contrast the KT-10 which has the largest coil diameter includes a "pin" option which is intended to help guide the user in finding the best coupling between the rock surface and the coil. Second, in a natural setting the mineralogy in the immediate near surface of a rock outcrop may have been modified by weathering. Often that weathering might include alteration of magnetite to less magnetic hematite. The depth extent of the weathering rind is dependent on rock type, and the location of the observation point. The number of magnetic grains examined in a measurement is controlled by two factors: the frequency of the current driving the sensor coil and the size of the coil. Third, magnetic susceptibility as measured using an inductive circuit is dependent on the frequency of the input signal. Bartington, for example, offer a coil, MS2B, designed for measuring core samples which can take measurements at two frequencies, 0.465 kHz and 4.65 kHz The ratio of these two readings, which is defined as "frequency dependent" susceptibility, is related to the grain size distribution of magnetite in the rock sample. This difference arises from "skin depth" effects associated with varying frequency. Fourth, each susceptibility observation is a summation of all magnetic mineral contributions that are activated by the inducing coil. Varying the size of the inducing coil means that susceptibility is averaged over different volumes of material. Given multiple measurements of susceptibility on any given rock surface the observed value will depend on the homogeneity of the rock with respect to the dimension of the sensor coil. That is, the smaller MS2E sensor should detect more detailed variation than the larger KT-10.

Measurements dependent on frequency changes in an inductive coil circuit are known to drift. To obtain reliable magnetic susceptibility readings involves minimisation of instrument drift and absolute calibration of the observed frequency change in terms of susceptibility. Each instrument permits different measurement methods, including interpolation, and scan mode. An interpolation method was used for the KT-10 and SM-30 measurements where a free air measurement is taken, followed by a direct rock sample, and finally a second free air measurement, where the first and third measurements are compensation steps.

The MS2E measurements were determined using a more interpolation mode where a preliminary free air measurement was followed by up to three measurements, before a second free air reading was taken. In all instances absolute calibration was made by repeat measurement of a sample with known susceptibility. This approach only produces a single calibration point. For the common user it is usually assumed that the original manufacturer installed calibration of frequency change versus susceptibility is maintained.

The purpose of this study was to evaluate the relative performance of three different instruments. We achieved this by recording the magnetic susceptibility value of 51 specimens with the three different instruments. Measurements with the KT-10 were made using both the “pin” and standard pad mode

We eliminated two possible sources of error by first preparing flat surfaces on each of the samples. These flat surfaces were larger than the largest inductive coil. No attempt was made to look at variations associated with taking measurements on a curved or partially weathered surface. The average thickness of the samples was 13mm and the magnetic susceptibility measurements were taken right at surface as the average depth of response drops off to 50% at 1mm and 10% 3.5mm. The minimum thickness of a sample would not affect a reading. Second, the susceptibility of each specimen as measured six times. The location of the sensor coil was moved between each individual measurement. Since the instrument was drift corrected between measurements any variation between these six readings represents mineralogical inhomogeneities.

For each sample we computed an average susceptibility and standard deviation of the six readings. Each magnetic susceptibility reading represents one value in a population of values. That is, when estimating the representative magnetic susceptibility for a rock unit it is essential that one obtain more than one reading at each sample location. Taking six readings represents the efficient trade-off between acquiring a large number of observations and adequately representing a population. Having obtained the six readings there are two possible approaches to calculating the average susceptibility: a) an arithmetic approach which one uses a simple mean calculation; or b) a geometric approach where the average susceptibility value computed on the log10 value. A number of publications have shown that when looking at the statistics of magnetic susceptibility that a geometric approach is the more appropriate method (Latham et al., 1989). Susceptibility is directly linked to mineralogical contents which it is known exhibit a log10 normal distribution.

As stated above the object of this study was to compare the signal response of three commonly used magnetic susceptibility meters. Any such comparison of sensor technology defaults into three variables: offset (do the instruments give the same result, ideally the offset should be near zero); gain (does the offset between the two instruments vary with signal amplitude); and linearity (does the signal show a linear change of response with signal amplitude). Estimates of these variables are easily derived from computation of the best fit least squares line between equivalent readings taken by two instruments. In this study we computed best fit lines on log10 transformed values (Figure A.2).

A.5 Results

The average magnetic susceptibility of the 51 samples ranged from a low of 2×10^{-5} SI to a high value of 1.9×10^{-1} SI. If each of these three meters used in this study were accurately calibrated and were measuring the same magnetic grains then there should be no difference in the magnetic susceptibility values they report. This is not the case.

The MS2E consistently reports higher magnetic susceptibility values than the other two instruments (Figure A.2). The difference between the instruments is approximately 2×10^{-4} SI. Closer inspection of the table inset in Figure A.2B reveals another problem with the MS2E; the slope of the least squares best fit line is consistently greater than 1.0 suggesting that there is also a difference in detection response between the instruments. This is actually more apparent than real. The five most strongly magnetised samples measured with the MS2E consistently plot above the least-squares best fit line. If these five points are eliminated and the best fit line is recalculated the slope of the line closely

approximates 1.0. This suggests that the MS2E is not properly recording susceptibility for these more strongly magnetic samples.

Comparisons between the SM-30 and the KT-10 indicate that these instruments are producing similar results. The highest level of correlation was found to exist between the KT-10 pad and the SM-30 ($R^2 = 0.9976$). This correlation also suggests that the SM-30 readings are systematically slightly lower than the KT-10 pad values by approximately 5 $x10^{-5}$ SI. The slope of the least squares best fit line between the SM-30 and the KT-10 is less than 1.0 (Figure A.2B). For strongly magnetic rocks, these two instruments would produce slightly different susceptibility values with the SM-30 giving higher values: they would be less than 2% different. As should be expected the comparison between the two styles of measurement using the KT-10 provides a correlation with a slope that most closely approaches 1.0; it is actually 0.9995. The fact that the best fit slope does not pass through the origin, and the R^2 value is less than 1.0 can only be attributed to noise in the individual measurements.

Taking six readings on a sample permits us to examine the repeatability of the susceptibility values. Again the results obtained with the MS2E are quite different from the results obtained with the KT-10 and SM-30 instruments which yield a similar response. The MS2E exhibited a much larger within sample variation of magnetic signal than either the KT-10 or the SM-30. Broadly there appears to be an increase in signal variance with increasing susceptibility value (Figure A.3). This trend is not surprising since a more weakly magnetic sample will not have any stronger magnetic regions. The sensor coil used in the MS2E samples an area two orders of magnitude less than the KT-10 and SM-30. If the MS2E is measuring a heterogeneous coarse grained rock then it is quite possible that small size of the sensor package could detect local “nuggets” with enhanced magnetite concentration. The SM-30 and the KT-10 both show little variance in repeat susceptibility readings especially for more magnetic samples (Figure A.3). This is expected since each of these tools has a larger measurement coil. What was surprising is that all three of these measurements showed a noticeable increase in signal variance for the most weakly magnetic samples (Figure A.3). The SM-30 showed the least variation, followed by the KT-10 pad configuration, with the KT-10 pin configuration showing the largest variance (Figure A.3). The only viable explanation for this observation is that both the SM-30 and especially the KT-10 have limited detection capability for susceptibilities below 10^{-4} SI. Further using the pin activation on a flat surface sample appears to increase signal noise.

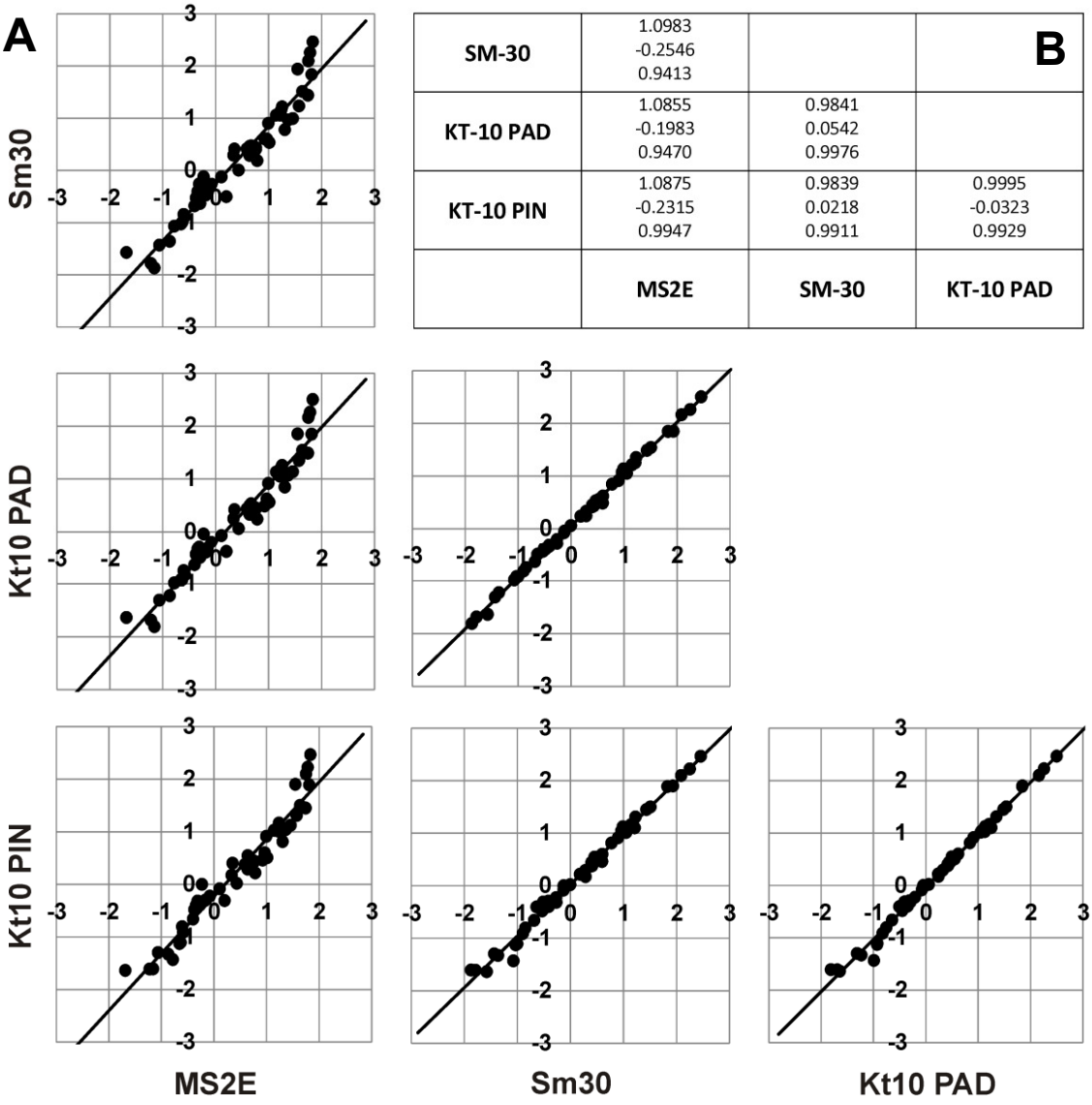

B

SM-30	1.0983 -0.2546 0.9413		
KT-10 PAD	1.0855 -0.1983 0.9470	0.9841 0.0542 0.9976	
KT-10 PIN	1.0875 -0.2315 0.9947	0.9839 0.0218 0.9911	0.9995 -0.0323 0.9929
	MS2E	SM-30	KT-10 PAD

Figure A.2. Results between equivalent readings taken by two instruments and the respective computation of the best fit least squares line (A). Inset table summarizes the value of least squares line and the level of correlation (B).

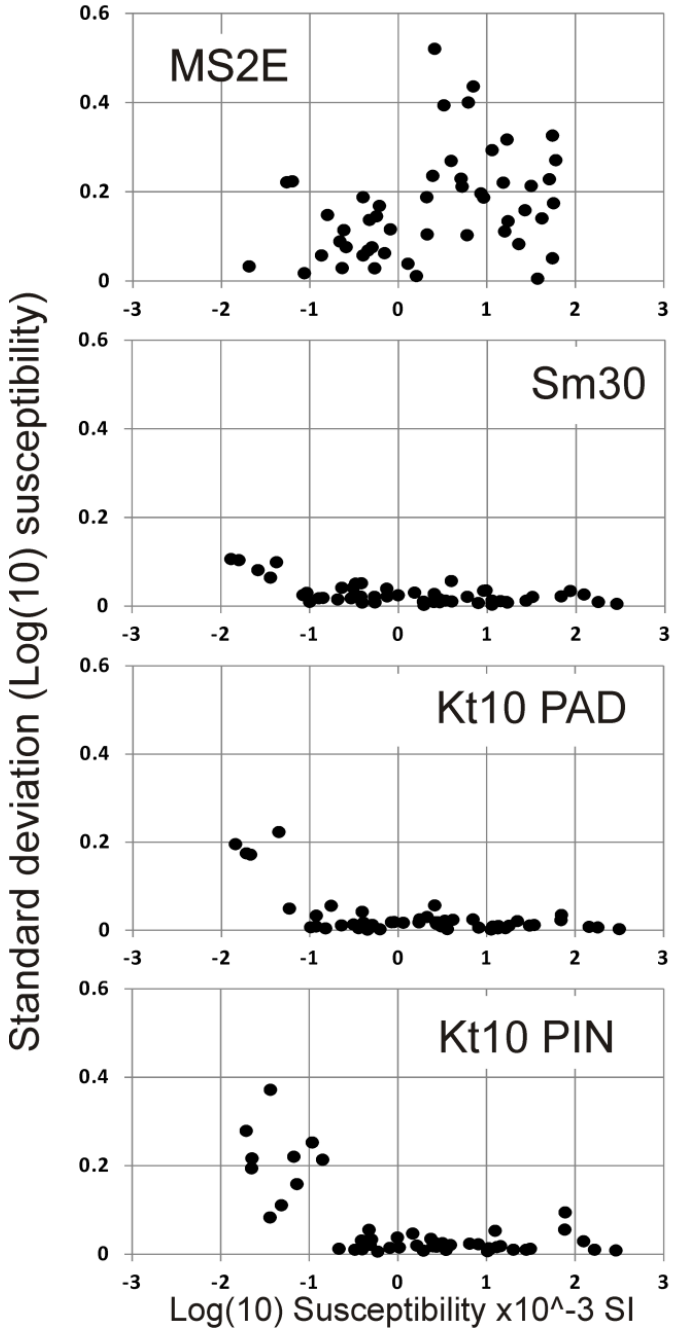

Figure A.3. The standard deviation of measurements between instruments.

A.6 Conclusion

This comparison suggests that there are no meaningful differences in the susceptibility values observed with the KT-10 and SM-30 instruments. When considered in terms of the errors associated with making field measurements on irregular possibly weathered surfaces this difference in susceptibility values has no significance in terms of magnetic anomaly modeling, or geological mapping. Both of these instruments use a similar higher frequency signal in their inductive coil. Both of the instruments also use coils with similar order of magnitude area. The MS2E reported magnetic susceptibility values that were consistently higher than the KT-10 and the SM-30. This difference may be explained by the lower frequency signal used by this sensor. Magnetic susceptibility as measured with an inductive circuit exhibits frequency dependency. It is quite possible that the MS2E is recording the presence of coarser grain size magnetic mineral fraction. Laboratory susceptibility meters which offer a range of signal frequency values are available to take advantage of this factor. For example, the SM100 meter produced by ZH Instruments offers 5 frequency levels and 6 power settings.

Depending on the usage of the instrument this could be detrimental, or advantageous. When used as a general field tool it would require the operator to take more readings at a location in order to minimise impact of local mineralogy effects. The larger coils of the SM-30 and the KT-10 average susceptibility values over a broader area so fewer observations at a point would be required. In contrast, the small coil size of the MS2E would be best suited for taking susceptibility measurements on curved surfaces such as drill core. In this case a significant portion of the larger coils of the SM-30 and the KT-10 are not in effective contact with the rock surface. When attempting to compare susceptibility results obtained by different groups using different instruments the interpreter should ensure that they are only compiling results obtained with the sensors using the same operating frequency.

A.7 References

Bartington Instruments Ltd., Operation Manual for MS2 Magnetic Susceptibility System, Issue 48, Oxford, England.

Henkel, H., 1991, Standard diagrams of magnetic properties and density – a tool for understanding magnetic petrology: *Journal of Applied Geophysics*, 32, 43-53.

Hoffman, P.F. and Hall, L., 1993, Geology, Slave craton and environs, District of Mackenzie, Northwest Territories: *Geological Survey of Canada Open File 2559*, 1 map scale 1:1,000,000.

Latham, A.G., Harding, K.L., Lapointe, P., Morris, W.A., and Balch, S.J., 1989, On the lognormal distribution of oxides in igneous rocks, using magnetic susceptibility as a proxy for oxide mineral concentration: *Geophysical Journal International*, 96 (1), 179 – 184, DOI: 10.1111/j.1365-246X.1989.tb05259.x.

Terraplus Inc., KT-10 Magnetic Susceptibility Meter User's Guide, Revision 1.5, Ontario, Canada.

Heritage Geophysics Inc, Magnetic susceptibility meter SM-30 User's Manual, June 2003.

B. Physical rock property database from Southern Wopmay Orogen

Please refer to attached DVD. This field work was in part funded by numerous programs: the IOCG-Great Bear (00410) and Remote Predictive Mapping (GKM005) projects of the Geomapping for Energy and Minerals program through Natural Resources Canada; the South Wopmay Bedrock Mapping project of the Northwest Territories Geoscience Office through Aboriginal Affairs and Northern Development Canada; and the Polar Continental Shelf Program (50709). The project was conducted through various collaborative agreements between Natural Resources Canada, the Northwest Territories Geoscience Office, the Community Government of Gamètì, and Fortune Minerals Limited. Fieldwork was permitted under the Aurora Research Institute Scientific Research licences 14548 and 14649, Polar Continental Shelf Program and the Government of the Northwest Territories archaeological sites database agreement DR2009-335 and DR2010-390.

C. Preliminary figures of magnetic and electrical properties from Southern Wopmay Orogen rock samples

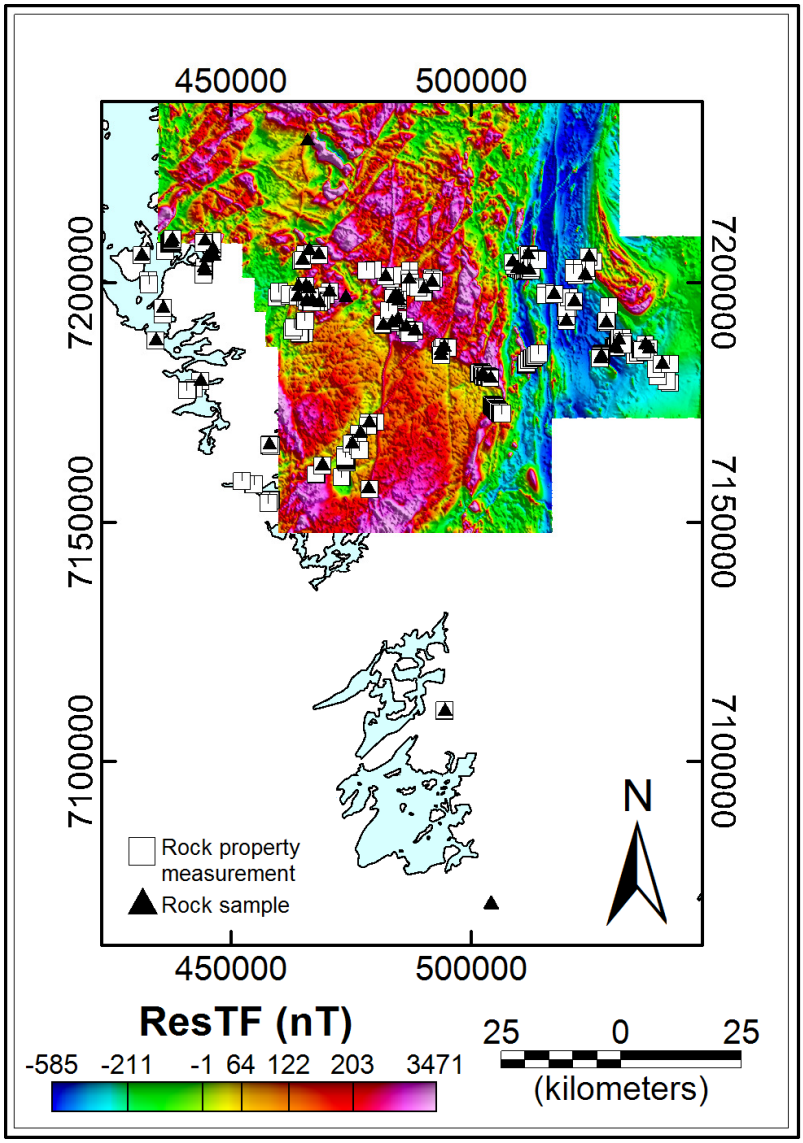

Figure C.1 Location of rock property measurements (magnetic susceptibility and radiometric ratios) and rock samples overlaid on ResTF. Most measurements and samples were collected within the boundary of the 2007 high resolution so they may be incorporated into any geophysical interpretation.

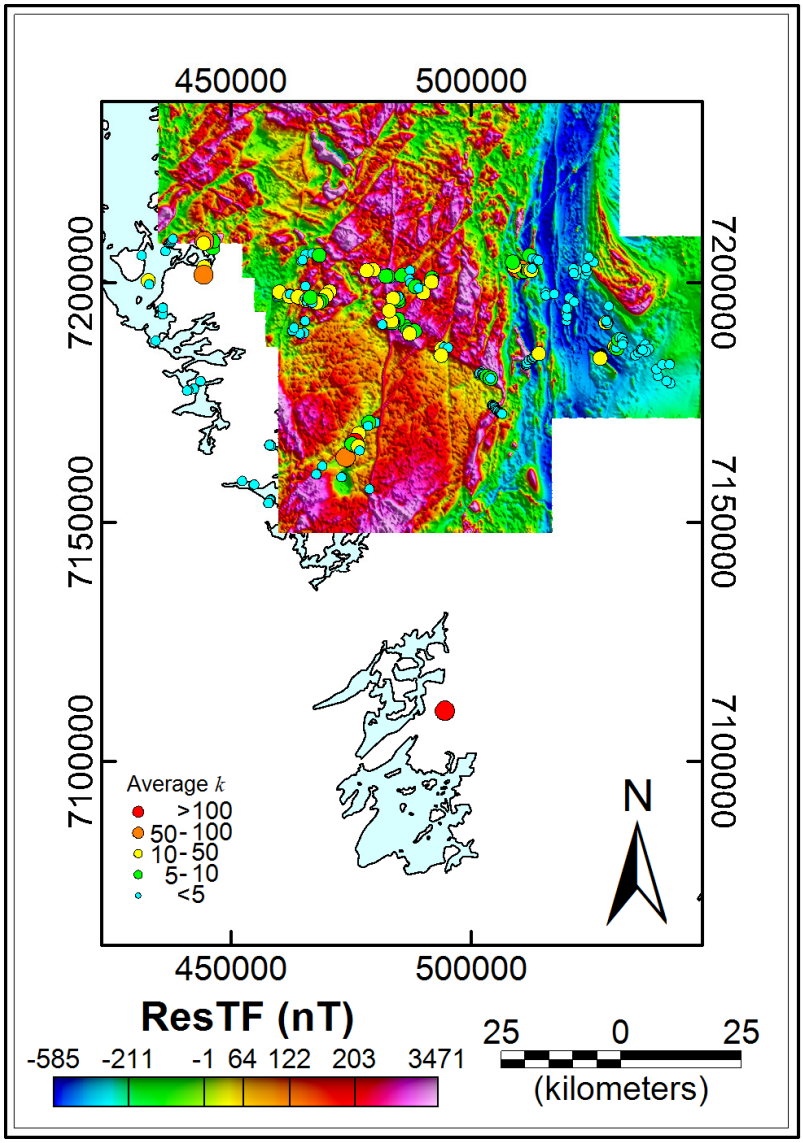

Figure C.2 In-situ magnetic susceptibility average (of three measurements) overlaid on ResTF. Low magnetic susceptibility values are associated with sedimentary and meta-sedimentary rocks within the Coronation Margin (eastern area of survey) and granitoids of the Great Bear magmatic zone. Highest magnetic susceptibility values are associated with areas of banded iron formations (western area of survey), intrusive gabbros, and FAB occurrence.

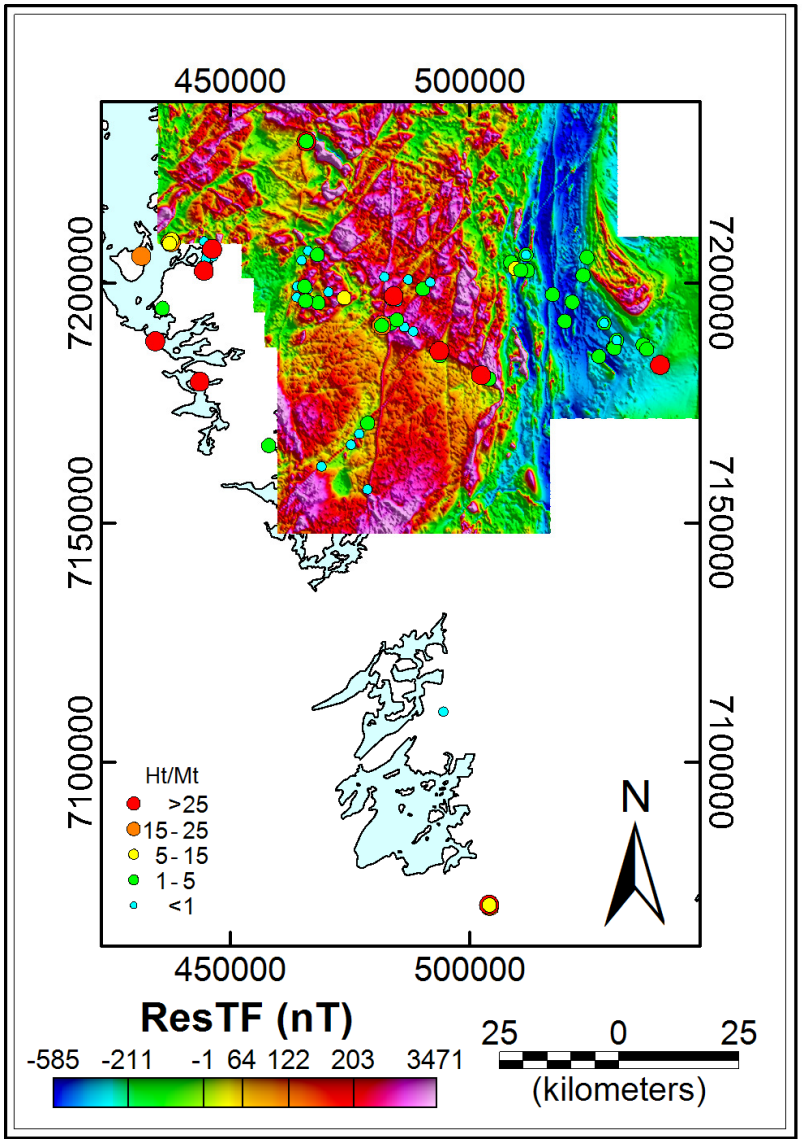

Figure C.3. Ht/Mt ratios for rock samples. Warm colours indicate hematite abundance while cool colours indicate a magnetite abundance. The samples associated with magnetite are related to FAB and magnetite content of GBmz. Elevated hematite is associate with Sue-Dianne deposit and DAMP (similar to Sue-Dianne) and the Beaverlodge unconformity along the Hottah Terrane.

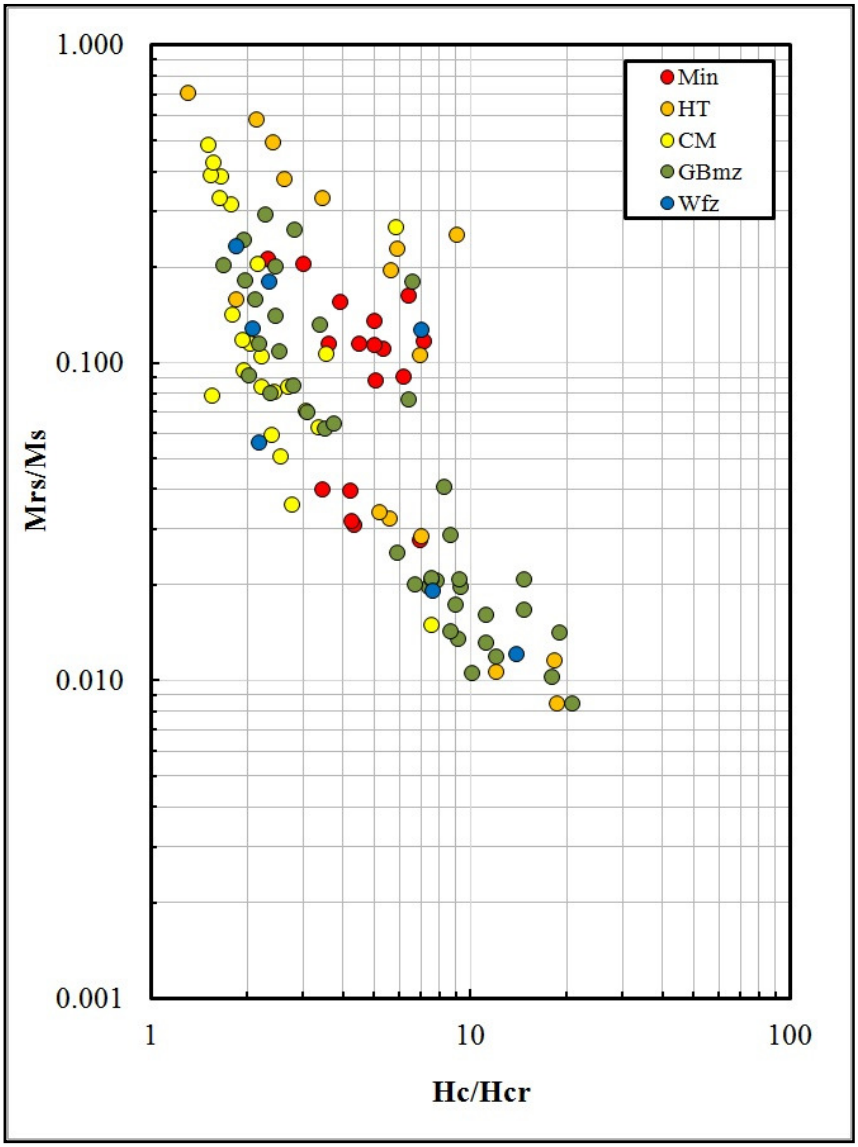

Figure C.4. Dayplot of rock samples from Figure. The samples have been colour-coded based on their approximate location of collection: Min – Known occurrence or deposit; HT – Hottah Terrane; CM – Coronation Margin; GBmz – Great Bear magmatic zone; Wfz – Wopmay fault zone.